SLAC-R-802

Collider Phenomenology of Extra Dimensions

B. H. Lillie

Stanford Linear Accelerator Center
Stanford University
Stanford, CA 94309

SLAC-Report-802

Prepared for the Department of Energy
under contract number DE-AC02-76SF00515

Printed in the United States of America. Available from the National Technical Information Service, U.S. Department of Commerce, 5285 Port Royal Road, Springfield, VA 22161.

COLLIDER PHENOMENOLOGY OF EXTRA DIMENSIONS

A DISSERTATION
SUBMITTED TO THE DEPARTMENT OF PHYSICS
AND THE COMMITTEE ON GRADUATE STUDIES
OF STANFORD UNIVERSITY
IN PARTIAL FULFILLMENT OF THE REQUIREMENTS
FOR THE DEGREE OF
DOCTOR OF PHILOSOPHY

Benjamin Huntington Lillie
August 2005

I certify that I have read this dissertation and that, in my opinion, it is fully adequate in scope and quality as a dissertation for the degree of Doctor of Philosophy.

JoAnne Hewett Principal Adviser

I certify that I have read this dissertation and that, in my opinion, it is fully adequate in scope and quality as a dissertation for the degree of Doctor of Philosophy.

Stanley J. Brodsky

I certify that I have read this dissertation and that, in my opinion, it is fully adequate in scope and quality as a dissertation for the degree of Doctor of Philosophy.

Michael Peskin

Approved for the University Committee on Graduate Studies.

Abstract

In recent years there has been much interest in the possibility that there exist more spacetime dimensions than the usual four. Models of particle physics beyond the Standard Model that incorporate these extra dimensions can solve the gauge hierarchy problem and explain why the fermion masses a spread over many orders of magnitude.

In this thesis we explore several possibilities for models with extra dimensions. First we examine constraints on the proposal of Arkani-Hamed and Schmaltz that the Standard Model fermions are localized to different positions in an extra dimension, thereby generating the hierarchy in fermion masses. We find strong constraints on the compactification scale of such models arising from flavor-changing neutral currents.

Next we investigate the phenomenology of the Randall-Sundrum model, where the hierarchy between the electroweak and Planck scales is generated by the warping in a five-dimensional anti-de Sitter space. In particular, we investigate the "Higgsless" model of electroweak symmetry breaking due to Csaki et. al., where the Higgs has been decoupled from the spectrum by taking its vacuum expectation value to infinity. We find that this model produces many distinctive features at the LHC. However, we also find that it is strongly constrained by precision electroweak observables and the requirement that gauge-boson scattering be perturbative. We then examine the model with a finite vacuum expectation value, and find that there are observable shifts to the Higgs scalar properties.

Finally, in the original large extra dimension scenario of Arkani-Hamed, Dimopoulos, and Dvali, the hierarchy problem is solved by allowing gravity to propagate in a large extra dimensional volume, while the Standard Model fields are confined to 4

dimensions. We consider the case where there are a large number of extra dimensions ($n \sim 20$). This model can solve the hierarchy problem without introducing a exponentially large radii for the extra dimensions, and represents a scenario that is difficult to obtain in string theory. We show that, if this scenario holds, the number of dimensions can be constrained to be larger than the number predicted by critical string theory. Searching for signals of many dimensions is then an important test of whether string theory is a good description of quantum gravity.

Acknowledgements

I would like to thank the many people that helped along the way to make this thesis possible.

Most importantly, I would like to thank my adviser, JoAnne Hewett, for her extraordinary help no only in teaching me physics, but also providing guidance as I begin my career. I also would like to express my tremendous indebtedness to Tom Rizzo for working with me and sharing his vast knowledge of particle phenomena.

I am also very thankful to all the faculty and postdocs, in the theory groups at SLAC and Stanford. In particular I have benefited greatly from discussions with Stan Brodsky, Savas Dimopoulos, Michael Peskin, Lance Dixon, Hooman Davoudiasl, Aaron Pierce, Jay Wacker, Babis Anastasiou, Adam Lewandowski, and Carola Berger.

Thanks very much to Frank Petriello, Marc Schreiber, and Michael Binger for putting up with me as an officemate.

Finally, I would like to express my greatest thanks to my parents for encouraging and supporting me through all my schooling; and to Sara, for putting up with me for the last three years.

Chapters 2 through 6 of this thesis have been published previously as:

- B. Lillie and J. L. Hewett, Phys. Rev. D **68**, 116002 (2003) [arXiv:hep-ph/0306193].
- B. Lillie, JHEP **0312**, 030 (2003) [arXiv:hep-ph/0308091].
- H. Davoudiasl, J. L. Hewett, B. Lillie and T. G. Rizzo, Phys. Rev. D **70**, 015006 (2004) [arXiv:hep-ph/0312193].
- H. Davoudiasl, J. L. Hewett, B. Lillie and T. G. Rizzo, JHEP **0405**, 015 (2004) [arXiv:hep-ph/0403300].
- J. L. Hewett, B. Lillie and T. G. Rizzo, JHEP **0410**, 014 (2004) [arXiv:hep-ph/0407059].

Chapters 7 and 8 have appeared as the preprints

- B. Lillie, arXiv:hep-ph/0505074.
- J. L. Hewett, B. Lillie and T. G. Rizzo, arXiv:hep-ph/0503178.

Contents

List of Tables

List of Figures

Chapter 1

Introduction

The Standard Model (SM) of particle physics is a spectacularly successful description of all current data on high-energy particle collisions [74]. However, if electroweak symmetry is broken by the SM Higgs mechanism, then the potential for the Higgs boson receives quantum corrections that tend to drive the scale of electroweak symmetry breaking (EWSB) up to the highest scale in the theory. This scale is currently thought to be either the GUT scale ($\sim 10^{15}\,\mathrm{GeV}$), or the Planck scale ($\sim 10^{18}\,\mathrm{GeV}$), both of which are far larger then the known scale of EWSB, $\sim 100\,\mathrm{GeV}$. This is known as the gauge hierarchy problem. It is not a fatal problem for the theory, as the initial potential can simply be fine-tuned so that the full potential after the quantum corrections breaks electroweak symmetry at the correct scale. Nevertheless, it would be far more natural for there to be a dynamical reason for the electroweak scale to be so low.

Most of the effort in searching for physics beyond the SM over recent years has focused on solutions to this problem. For most of the history of the SM the leading ideas for the solution to this problem were low energy supersymmetry and technicolor. Recently, it has been probed that the presence of extra spacial dimensions, beyond the usual 3, could also solve this problem. There are two possible approaches. In the first model, of Arkani-Hamed, Dimopoulos, and Dvali the fundamental gravity scale is taken to be near a TeV [20]. There are n extra compactified dimensions with the SM fields localized to a point in those dimensions. The apparent weakness of gravity

is then generated by the fact that the field generated by a gravitational source can expand in the extra dimensions. This generates an effective Planck scale $\bar{M}_{\rm pl}^2 = VM^{2+n}$, where V is the volume of the compactified dimensions. The exponentially large size of V generates the apparent hierarchy.

The second approach is due to Randall and Sundrum [136]. They propose that spacetime is five dimensional with the metric of anti-de Sitter space (AdS_5), $ds^2 = e^{2ky}dx^2 - dy^2$, where k is the AdS curvature and y is the coordinate of the extra dimension. This extra dimension is compactified on an orbifold S^1/Z_2, with a 3-brane localized at each fixed point, producing a slice of the AdS_5. The electroweak symmetry breaking sector is localized on one of the branes (called the TeV brane), with a breaking scale that is naturally of Planckian size. However, in AdS space, all scales are multiplied by powers of the exponential "warp" factor in the metric. Hence, the masses appearing in the Higgs potential will be multiplied by the warp factor evaluated on the TeV brane. In this way, the effective mass scale of EWSB is $v' = ve^{-\pi kr_c}$. With a radius of compactification $r_c \sim 10/k$, this generates the correct weak scale.

In the next few years, the Large Hadron Collider will become operational. We will then have direct access to physics at the scale where electroweak symmetry is broken. Analysis of this data, possibly combined with data from the proposed International Linear Collider, will give important insights into the mechanism of EWSB, and possibly the solution to the hierarchy problem. In light of this, it is very important to explore the phenomenological consequences of the various possibilities for physics beyond the Standard Model.

This thesis will explore some of the observable consequences of having extra space dimensions. In the first two chapters we will examine a sceario of Arkani-Hamed and Schmaltz called "split fermions" [23]. In this class of models the SM fermions are localized to different positions in a flat extra dimension. It is possible that these models could address the question of why the SM fermion masses are spread over many orders of magnitude. In Chapter 2 we find the constraints on these models from flavor changing neutral currents. Chapter 3 proposes a slight readjustment of the model that relaxes these constraints.

Chapters 4 through 7 explore various aspects of a version of the Randall-Sundrum model. In this model, not only gravity, but all gauge fields and fermion fields live the bulk of the AdS_5. Only the Higgs is confined to the TeV-scale brane. Additionally, the gauge group will be expanded from the usual $SU(3) \times SU(2)_L \times U(1)_Y$ to the left-right symmetric $SU(3) \times SU(2)_L \times SU(2)_R \times U(1)_{B-L}$. Csaki et. al. have shown that in this setup the W and Z masses remain finite as the Higgs vacuum expectation value is sent to infinity, and in the same limit the Higgs boson decouples [55]. The leads to the so-called Higgsless model. In chapter 4 we investigate the phenomenology of this model. We find strong constraints from precision electroweak observables, and the requirement that the scattering of longitudinal gauge bosons remains perturbatively unitary up to the cutoff. However, we show that when the model is brought into agreement with current constraints, it must produce distinctive signals at the Large Hadron Collider. Chapter 5 extends this analysis to include kinetic operators for the gauge fields localized on one of the branes. These shift many of the electroweak observables, and can help bring the model into agreement with current data. In Chapter 6 we conclude this analysis by doing a Monte Carlo scan over the entire parameter space. We find that, without adjusting the fermion sector, the model can not simultaneously satisfy the precision electroweak and perturbative unitarity constraints. One possible way of relaxing this tension is explored in chapter 7, where we allow the Higgs vacuum expectation value to be finite. There it is found that the model can be brought into agreement with all known constraints. There is then a physical Higgs scalar in the spectrum, and it's properties are shifted from those of the SM Higgs by amounts that should be measurable at the International Linear Collider.

Finally, in chapter 8 we investigate a very different type of model. We consider an ADD type of scenario where the fundamental gravity scale is small. However, we take the number of extra dimensions to be ~ 20. The hierarchy problem is then solved without introducing exponentially large compactification radii. In addition, this scenario is difficult to obtain in string theory, making experimental searches for it an important test of whether strings provide a good description of quantum gravity. We show that, if this scenario holds, it is possible to exclude the region of parameter

space predicted by critical string theory.

Chapter 2

Flavor constraints on split fermion models

2.1 Introduction

In recent years there has been much interest in the possibility that there may exist compact extra dimensions with sizes far above the Planck length. In particular, the possibility of TeV^{-1}-sized extra dimension arises in braneworld theories [16, 118, 155, 106, 107, 39]. By themselves, they do not allow for a reformulation of the hierarchy problem, but they may be incorporated into a larger structure in which this problem is solved, such as the case of large extra dimensions [20, 17, 21]. In the scenario with TeV^{-1} extra dimensions, the Standard Model (SM) fields are phenomenologically allowed to propagate in the bulk. These models are hence subject to stronger experimental constraints and have distinct experimental signatures from the case where gravity alone is in the bulk.

There are many possibilities for how to place the Standard Model fields in the TeV^{-1} bulk. In the universal extra dimensions scenario all fields see the extra dimensions, giving rise to a conserved parity that relaxes direct production and precision electroweak constraints, and may provide a dark matter candidate [18, 149, 148, 46]. The effects of universal extra dimensions in rare processes have been considered in [33, 34, 6, 44]. It is also possible to localize the fermions without localizing the

bosons, which allows for the gauge fields to propagate freely throughout the bulk. More recently it was noticed by Arkani-Hamed and Schmaltz (AS) that one could localize different fermion species at different points in the TeV^{-1} extra dimensions [23]. These "split fermion" models naturally suppress many dangerous operators, particularly those inducing proton decay. They also can naturally generate large Yukawa hierarchies; and it has been shown by multiple authors that there exist models which can generate the correct spectrum of fermion masses, as well as the correct magnitudes for CKM matrix elements [90, 125, 45, 31, 113, 67]. The most stringent generic limits in this case arise from precision electroweak measurements, which place the compactification radius at $R \lesssim 2 - 4\,\mathrm{TeV}^{-1}$ [144, 123, 122, 102]. The specific fermion locations can be probed in high energy collisions, and at very large energies, cross sections will rapidly vanish since split fermions will completely miss each other in the extra dimensions.[22, 142]

This makes the split fermion scenario an attractive possibility for the origin of the Yukawa hierarchy. However, split fermions (like most models of the fermion spectrum) are also capable of generating large flavor changing neutral currents (FCNC). The magnitude of these currents in the neutral meson sector has been estimated by several groups, and apparently generate strong constraints[45, 68, 3]. In this paper we reexamine these computations to derive more model independent constraints on split fermion models arising from FCNC and show that it is possible to evade the stringent bounds for natural regions of the parameters.

This paper is organized as follows. In Section 2 we set up the split fermion scenario in as much generality as possible and give statistical arguments to demonstrate that they can account for the observed fermion spectrum. We then describe how FCNC are generated in this scenario. In section 3 we calculate the effects on neutral meson oscillation. Section 4 presents the effects on rare B decays, and single top production in e^+e^- collisions, and Section 5 concludes.

2.2 The Model of Split Fermions

Here, we construct a very general model that characterizes the effects of separating the Standard Model fermions in an extra dimension. We start by examining the original model considered by AS.

In the AS model there is one extra dimension, which is taken to be flat. It is possible that this extra dimension is actually a "brane" with a finite width embedded in some other extra-dimensional scenario. For this reason TeV^{-1} dimensions are often called "fat branes", but they need not be tied to other models. Note that if the brane is not a string theory object, but arises from some field theory mechanism, then it *necessarily* has finite extent in the extra dimensions. This makes the study of fat branes essential to building realistic field-theoretic models of extra dimensional scenarios.

In this model the Standard Model fields are localized to the brane. Note that the word *brane* here refers to any mechanism for achieving this localization. It may or may not be the same as the branes encountered in string theory. Initially, all fields are allowed to propagate in the entire dimension. In addition to the fields present in the Standard Model, there is a real scalar field which couples to the fermions, but not to the gauge bosons or the Higgs.

If the scalar has a Z_2-symmetric potential, then it can develop a stable solution which tunnels from one of the vacua to the other, called a kink solution. A mechanism for localizing fermions to a thin but finite width region inside a domain wall has been known for some time [109]. There it was noted that in 1+1 dimensions a massless fermion with a Yukawa coupling to a scalar field that has a kink-profile vacuum expectation will develop a zero mode, with a Gaussian profile centered at the location of the kink. This can be trivially extended to more dimensions by considering a domain wall instead of a soliton and making all zero modes constant in the transverse directions. Note that a five-dimensional fermion field contains two four-dimensional fermions, one of each chirality. If the extra dimension is infinite, then the zero-mode of only one chirality is normalizable. If the extra dimension is finite then something else is needed to produce chirality. A standard procedure is to compactify the dimension

on an S^1/Z_2 orbifold, which projects out the unwanted chirality. A nice side-effect of this is to render the kink absolutely stable.[1]

In contrast to the fermion sector, the gauge bosons are free to propagate throughout the extra dimension. Since the dimension is compact, and flat, the mass spectrum of the Kaluza-Klein gauge states is linear with $M_n^2 = n^2/R^2$, and the orbifold boundary conditions project out the odd solutions, so the wavefunctions along the fifth dimension, y where $0 \leq y \leq R$, are

$$A^{(n)\mu}(x, y) = \sqrt{\frac{2}{R}} \cos(\frac{n\pi y}{R}) A^{\mu}(x) \qquad (n \geq 1), \tag{2.1}$$

where R is the size of the extra dimension. Putting all this together allows investigation of brane world models where there is a single extra-dimension of roughly inverse TeV size with fermions localized in the center and gauge bosons propagating though the entirety.

A more interesting picture can be obtained by thinking about the fermion localization mechanism. There is a simple heuristic for why this should occur. The fermion is Yukawa coupled to a scalar field which develops a non-zero VEV. The ordinary fermion Higgs phenomena should then give the fermion a mass. However, the VEV is position dependent and in particular there is a place where it is zero (the center of the kink). So the fermion has a position dependent mass, which is somewhere zero. Thus, the fermion is easiest to excite near the zero mass, and so most of the probability for the lowest lying state (the zero mode) will live near the center of the kink.

Given that heuristic, it should be reasonable that if the 5D fermion has a mass M, then the center of the Gaussian moves to $y = M/2\mu^2$, where μ is the slope of the kink profile, and v is the scale of the VEV. Indeed, it turns out that this is the case, as was first noted by Arkani-Hamed and Schmaltz [23]. This allows different fermion fields to be localized at different points in the extra dimension. To see why this is desirable, consider an operator, $\mathcal{O}$, that involves fermions separated by a distance d. The effective 4D coupling in the dimensionally reduced theory is proportional to the

[1] It is interesting to think that if one invokes a mechanism to localize the gauge bosons, as in [73], then one could have a fat brane residing in an infinite dimension.

integral over the extra dimensions of the wavefunctions of all fields appearing in $\mathcal{O}$. Since the fermion wavefunctions are Gaussian, this gives a suppression proportional to $e^{-a\mu^2 d^2}$, where a depends on the operator being considered. This has been shown to be very effective at suppressing dangerous higher-dimensional operators, such as proton decay. Additionally, the fact that exponentially different couplings can result from linear separations provides a natural means of explaining the fermion mass hierarchy. Lighter fermions have greater separation between their left and right handed components. In this way Arkani-Hamed and Schmaltz proposed a theory to explain the Yukawa hierarchy without invoking new symmetries, and which is safe from proton decay. Several authors have proposed specific "geographies" that do indeed reproduce the correct fermion masses, as well as the CKM parameters [90, 125, 45].

There are, however, other potentially dangerous effects of the fermion separation which are not suppressed by this mechanism. The gauge bosons will have a Kaluza-Klein (KK) tower of states. The zero modes, which are flat in the extra dimensions, correspond to the SM gauge fields, and have the correct couplings to the fermion zero modes. On the other hand, the excited states have cosine profiles, as given in Eq. (2.1).[2] The coupling strength of these modes to the fermions are scaled by an integral over the overlap of the fermion and gauge wavefunctions. However, since the height of the boson wavefunction will be different at the locations of the different fermions, there will be non-universal couplings of a single gauge KK-state to different fermion species. This leads to the possibility of flavor changing interactions, including tree-level neutral currents, for the KK-modes of the γ, Z, and gluon, as illustrated in Fig 2.1. One then expects large effects to come from the tree-level contributions of the KK gluon states to FCNC processes, in particular to neutral meson oscillation. Calculation of these effects can put limits on the size of the extra dimension. Also, note that while this discussion was motivated by the kink model, these issues will be relevant to any model with split fermions. This is an example of the general principle that any attempt to explain the Yukawa hierarchy will necessarily treat flavors differently, and will tend to generate large flavor-changing effects.

In practice, geography independent constraints have been difficult to obtain due

[2] In general they are exponentials, e^{iny}, but the orbifolding projects out the odd modes.

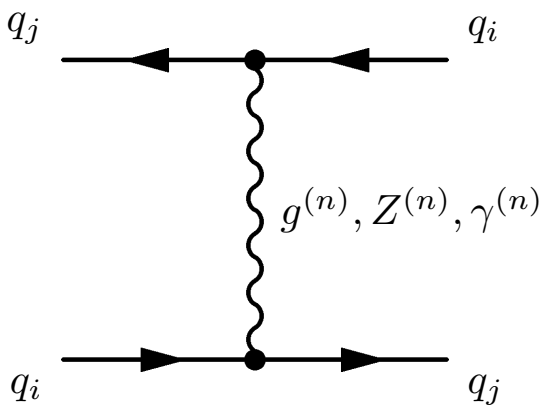

Figure 2.1: Feynman diagram for the tree-level KK gauge exchange mediating neutral meson oscillation.

to the large number of parameters in the model. These are, R, σ, the width of the fermion wavefunctions (which is $1/\mu$ in the kink model), and $(d^n - d)$ positions, where d is the number of extra dimensions and n is the number of independent fermion fields. Previous discussions [45, 68, 3] have put constraints on R only by first obtaining a single set of positions that reproduce the Yukawa couplings of the Standard Model, and calculating the flavor-changing effects in that particular geography. However, one would like a more model-independent way of understanding the magnitude of flavor effects in this class of models.

To accomplish this we consider the problem of FCNC in split fermion models in as much generality as possible. A specific, realistic model exists in string theory [3], as well as the field theory example just presented. In summary, we abstract from these the following points:

1. There exist one or more extra dimensions, compactified with a radius R.[3]

2. Each fermion field, ψ_i has a chiral zero mode that is localized near the center of the dimension at y_i, with Gaussian profiles $\psi \sim e^{-(y-y_i)^2/\sigma^2}$, where the width $\sigma \ll R$. If there is more than one extra dimension they are taken to be isotropic in those dimensions $\psi \sim e^{-(\vec{y}-\vec{y_i})^2/\sigma^2}$.

[3]In one dimension the compactification is S^1/Z_2. In more dimensions we take the compactification to be flat, and orbifolded in such a way that it looks like a simple product of single dimensions.

3. The gauge bosons are free to propagate in the entire "fat brane" part of the extra dimension. (There may be a larger bulk accessible to gravity.)

4. The boundary conditions for the bosons are taken to be such that the wavefunction for the n-th KK-mode is $A \sim \cos(n\pi y/R)$. Note that these are generally the same conditions that allow chiral zero modes for the fermions.

5. The field content (gauge group, number and charge of matter fields) is identical to the Standard Model, plus whatever fields are necessary to localize the fermions.

These assumptions generate an effective four-dimensional Lagrangian that reduces to the Standard Model at low energies. The new features present are the propagating gauge KK-modes, their couplings, and the fact that the Higgs Yukawa couplings are determined by the fermion locations.

We now construct the interaction Lagrangian for this scenario, focusing on the quark sector in this paper. An analogous treatment of the leptonic sector can be performed. Note that there are excited states of the fermion fields in addition to the KK boson states. However, since the fermions are localized with a width smaller than R, the scale of the fermion excitations will be significantly higher than that of the KK gauge states. In addition, the fermion KK modes do not participate in the processes considered here. We therefore only consider the fermion zero modes, while we include the complete KK-tower for the bosons. With one extra dimension the coupling of the n-th KK boson to a flavor localized at the scaled position $\ell = x/R$ is determined by the overlap of wavefunctions

$$\int_0^1 dy \bar{\psi}(y)\psi(y)A^{(n)}(y) \simeq \int_0^1 dy \cos(n\pi y)\, e^{-(y-\ell)^2 R^2/\sigma^2} \simeq \cos(n\pi\ell)\, e^{-n^2\sigma^2/R^2}. \quad (2.2)$$

where y has now been normalized to R. For δ extra TeV^{-1} dimensions this generalizes to

$$c^{(\vec{n})}(\ell) \equiv \left(\prod_{k=1}^{\delta} \cos(n_k \pi \ell_k)\right) e^{-\vec{n}^2\sigma^2/R^2}. \quad (2.3)$$

The gauge coupling of the gluons, for instance, can then be written in flavor space as

$$\mathcal{L}_{\rm int} = \sqrt{2} g_s G^A_{(n)\mu} \left(\bar{\mathbf{d}}_L \gamma^\mu T^A C^{(n)}_L \mathbf{d}_L + \bar{\mathbf{d}}_R \gamma^\mu T^A C^{(n)}_R \mathbf{d}_R \right) + (\mathbf{d} \to \mathbf{u}) + \text{h.c.}. \tag{2.4}$$

Here $\mathbf{d}_{L(R)}$ is the vector of left (right) handed down-type quarks, $\bar{\mathbf{d}} = (d\ s\ b)$, g_s is the SU(3) coupling constant, and $G^{(n)\mu}$ is the n-th KK gluon field. The diagonal matrices $C^{(n)}_i$ are the wavefunction overlaps given by Eq. (2.2). The factor of $\sqrt{2}$ arises from the rescaling of the gauge kinetic terms to the canonically normalized value for all n.

Now, the Higgs zero mode, which is the Standard Model Higgs, is flat in the extra dimension, $H^0 \propto 1/R$. Then the Yukawa couplings to the 4D Higgs field are given by

$$R\lambda_5 \int_0^1 dy H^0 \bar{q}_L q_R \simeq \lambda_5 \int_0^1 dy\ e^{-(y-y_i)^2/\sigma^2} e^{-(y-y_j)^2/\sigma^2} \simeq \lambda_5 e^{-(y_i-y_j)^2/\sigma^2}. \tag{2.5}$$

Here λ_5 is an overall 5D coupling constant that is fixed to be $\mathcal{O}(1)$ by the top quark mass. We write the 4D Yukawa couplings to (for instance) the down-type quarks in the flavor basis as

$$\mathcal{L}_{\rm Yukawa} = \bar{d} V^{(d)\dagger}_R M_d V^{(d)}_L d \tag{2.6}$$

Where $V^{(d)\dagger}_R M_d V^{(d)}_L$ is the matrix of Yukawa couplings with elements given by Eq. (2.5), and M_d is the diagonal mass matrix.

We can now write the relevant terms of the Lagrangian as

$$\begin{aligned} \mathcal{L} = \bar{\mathbf{d}}_L V^{(d)\dagger}_R M_d V^{(d)}_L \mathbf{d}_R + \bar{\mathbf{u}}_L V^{(u)\dagger}_R M_u V^{(u)}_L \mathbf{u}_R + \frac{g}{\sqrt{2}} W^{(0)}_\mu \bar{\mathbf{u}}_L \gamma^\mu \mathbf{d}_L \\ + \sum_{n=1}^{\infty} \left[\sqrt{2} g_s G^{(n)A}_\mu \left(\bar{\mathbf{d}}_L \gamma^\mu T^A C^{(n)}_L \mathbf{d}_L + \bar{\mathbf{d}}_R \gamma^\mu T^A C^{(n)}_R \mathbf{d}_R \right) + (\mathbf{d} \to \mathbf{u}) \right] + \text{h.c.} \end{aligned} \tag{2.7}$$

After the usual transformation to the mass basis, the CKM-matrix is clearly the product $V^{(u)\dagger}_L V^{(d)}_L$. Note, however, the presence of non-universal couplings prevents the products $U^{q(n)}_i \equiv V^{(q)\dagger}_i C^{(n)}_i V^{(q)}_i$ from being trivial, so there are flavor-changing interactions in the KK-gluon sector. These also occur in the excited photon and Z couplings. However, those are suppressed relative to the gluons by a factor of g/g_s,

so we expect that the KK-gluons will dominate any process to which they contribute.

Before examining the numerical impact of the tree-level FCNC interaction in rare processes, it will first be useful to get a handle on how far the fermions need to be separated. It has been shown by Grossman and Perez [90] that there exists at least one set of positions that correctly reproduces the observed fermion spectrum and magnitude of the CKM elements. They found that, subject to a certain set of naturalness assumptions, there was a single solution. A different solution was found in [45] by choosing different up and down-type Yukawa coupling constants in the 5D theory. Typical separations in these solutions are from $1 - 20$ units of the fermion width. In what follows, we parameterize the separation between 2 fermions in units of the width, i.e. $\Delta y = y_i - y_j = \alpha_{ij}\sigma$, and treat α_{ij} as phenomenological parameters. In addition, we find it useful to define $\rho = \sigma/R$.

As a counterpoint to the studies in [90] and [45] we have performed a simple Monte-Carlo analysis in an attempt to see how large of a hierarchy is generated naturally for fermions randomly distributed on an interval. To do this we randomly draw fermion positions from a distribution flat on the interval $[0, \alpha_{\max}]$, and use these to compute the Yukawa matrices from Eq. (2.5). We then compute the singular values of these matrices, which are the fermion masses. We can get a sense of the hierarchy by taking a particular Yukawa matrix (say the up-type) and finding the ratio of the largest to smallest singular value. In Fig 2.2 we show a histogram of the log of this ratio for $\alpha_{\max} = 15$. For comparison we have computed the same value for a "null hypothesis" where instead of the split fermion scenario, the entries of the Yukawa matrices themselves are drawn directly from a distribution flat on the interval $[0, 1]$. As expected, the case of split fermions clearly generates a much larger hierarchy. What is surprising is that one needs to set $\alpha_{\max} \approx 10 - 15$ before a hierarchy of six orders of magnitude becomes common, while in [23] it was claimed this hierarchy could result from $\alpha_{\max} \approx 5$. The discrepancy is due to the fact that, while a separation of $\alpha = 5$ will indeed generate a matrix element of order 10^{-6}, the singular values (which are the actual masses) of a full Yukawa matrix with separations no larger than 5 will tend to be too large. We note that the full fermion spectrum can be generated by ρ as large as $1/15$, i.e. without introducing a new large hierarchy

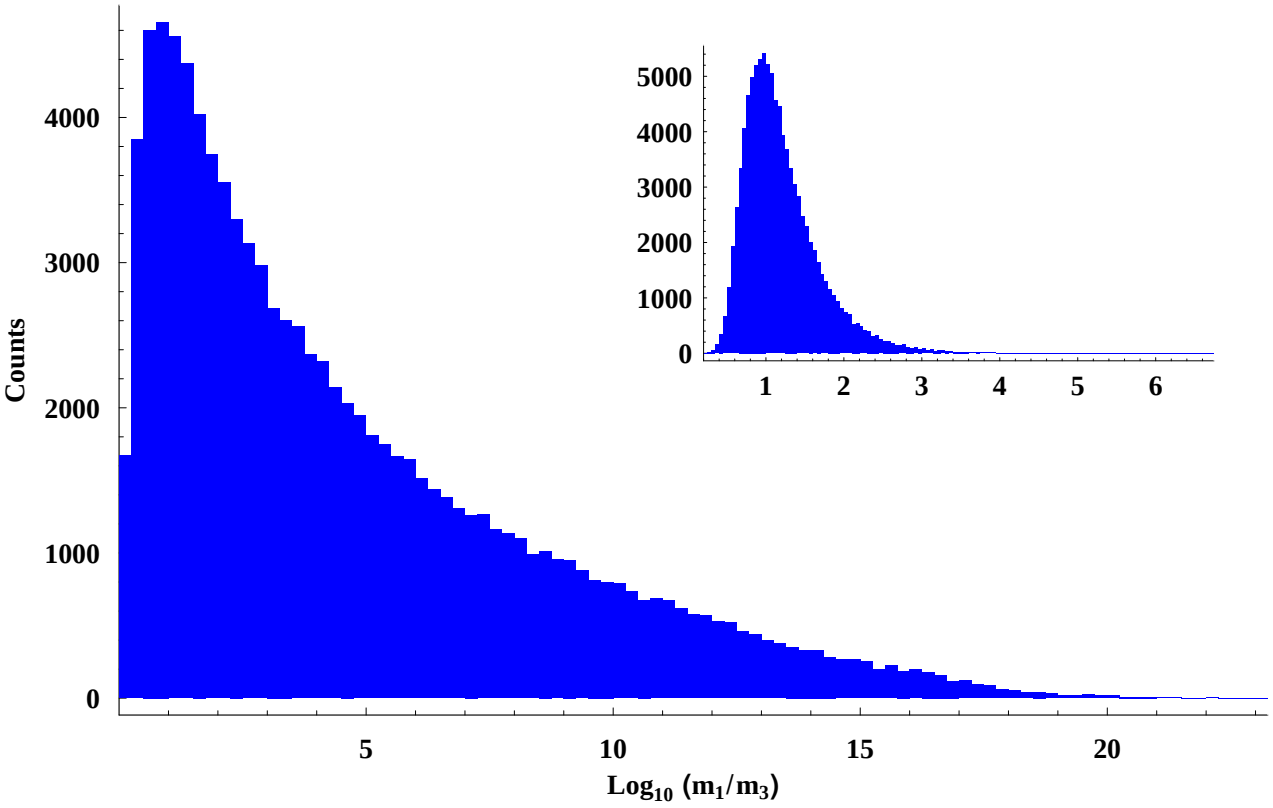

Figure 2.2: Histograms of 10^5 random trials of the size of the fermion hierarchy, $\log(m_1/m_3)$, where m_1 is the largest and m_3 the smallest mass for a single Yukawa matrix. Main graph: In the split fermion model where the positions are randomly drawn on the interval $[0, 15]$ in units of the fermion width. Inset: In a "null hypothesis" where the Yukawa matrix elements are randomly drawn from the interval $[0, 1]$.

between the compactification and fermion localization scales. Also note that $\alpha_{\max}$ represents the part of the extra dimension in which the fermions can be localized and need not be the same as $1/\rho$, which is the size of the dimension through which the gauge bosons can propagate.

2.3 Constraints from Neutral Meson Oscillation

Significant effects from the flavor-changing gluonic couplings should show up in neutral meson oscillations. We start by examining the effects on Kaon mixing. The

$\Delta S = 2$ effective Lagrangian from the single KK-gluon exchange depicted in Fig. 2.1 is

$$\begin{aligned}\mathcal{L}_{\rm eff}^{\Delta S=2} &= \frac{2}{3} g_s^2 \sum_{\vec{n}=1}^{\infty} \frac{1}{M_n^2} \sum_{i,j=L,R} U_{i(sd)}^{d(n)*} U_{j(ds)}^{d(n)} \bar{d}_i \gamma^\mu s_i \bar{d}_j \gamma_\mu s_j \\ &= \frac{2}{3} g_s^2 \Bigg(\sum_{i,j=L,R} V_{i(11)}^{d} V_{i(12)}^{d*} V_{j(11)}^{d*} V_{j(12)}^{d} \\ &\times \ \times \sum_{n=1}^{\infty} \frac{(\cos(n\pi x_{d_i}) - \cos(n\pi x_{s_i}))(\cos(n\pi x_{d_j}) - \cos(n\pi x_{s_j}))}{M_n^2} e^{-\rho^2 n^2} \Bigg). \end{aligned} \tag{2.8}$$

Here, the x_i are the positions of the d quark fields, y_i of the s quark, and we have used the unitarity of the V's (here, we have approximated this with 2×2 unitarity, we discuss the third-generation effects below). We are especially interested in the form of the sum over the KK-modes. While KK-sums are usually divergent in more than one extra dimension and require a cutoff, ours contains a natural cutoff arising from the finite width of the fermion zero mode, and hence is convergent for a number of extra dimensions $\delta \geq 1$. This is simple to understand physically. The cutoff sets in when the wavelength of the KK-mode is of order the fermion width, which occurs at $R/n_{\rm max} = \sigma$. At higher momenta the wavefunction of the boson is oscillating many times within the fermion allowing it to resolve the fermion's wavefunction, and exponentially decouples. The fact that this cutoff arises naturally in the field theory model is an attractive feature of that particular mechanism for fermion localization.

In one additional dimension the sum converges even without the exponential suppression. In this case it is insensitive to the value of ρ and can be computed analytically by ignoring the exponential factor. To do this we need to evaluate

$$F(x,y) \equiv \sum_{n=1}^{\infty} \frac{(\cos(n\pi x) - \cos(n\pi y))^2}{n^2}, \tag{2.9}$$

and

$$G(x,y) \equiv \sum_{n=1}^{\infty} \frac{(\cos(n\pi x_1) - \cos(n\pi y_1))(\cos(n\pi x_2) - \cos(n\pi y_2))}{n^2}. \tag{2.10}$$

The computations for these sums are presented in the appendix. The final result is

$$F(x,y) = \frac{\pi^2}{2}|x-y|, \tag{2.11}$$

and

$$G(x_1,y_1,x_2,y_2) = \frac{\pi^2}{2}(|x_1-x_2|+|y_1-y_2|-|x_1-y_2|-|x_2-y_1|). \tag{2.12}$$

This tells us that the flavor changing effects depend, as expected, on any nonzero separation between fermion fields.

The hadronic matrix elements for the gluonic contributions to Kaon mixing are given by (computed in the vacuum insertion approximation)[78]:

$$\begin{aligned}\langle\bar{K}^0|\bar{d}_L\gamma^\mu s_L\bar{d}_L\gamma_\mu s_L|K^0\rangle &= \frac{1}{3}f_K^2 m_k \\ \langle\bar{K}^0|\bar{d}_L\gamma^\mu s_L\bar{d}_R\gamma_\mu s_R|K^0\rangle &= f_K^2 m_k\left(\frac{1}{12}+\frac{1}{4}\left(\frac{m_K^2}{m_d^2+m_s^2}\right)\right)\end{aligned} \tag{2.13}$$

as well as those with $(L \leftrightarrow R)$, which have the same evaluation. Written out in full, the contribution to Δm_K is then

$$\begin{aligned}\Delta m_K =& \mathcal{R}e\,\langle\bar{K}^0|\mathcal{L}^{\Delta S=2}|K^0\rangle \\ =& \frac{2}{3}g_s^2R^2\Big(\ |V^d_{L\ 11}V^{d*}_{L\ 12}|^2F(x_{d_L},x_{s_L})\langle\bar{K}^0|\bar{d}_L\gamma^\mu s_L\bar{d}_L\gamma_\mu s_L|K^0\rangle \\ &+|V^d_{R\ 11}V^{d*}_{R\ 12}|^2F(x_{s_R},x_{s_R})\langle\bar{K}^0|\bar{d}_R\gamma^\mu s_R\bar{d}_R\gamma_\mu s_R|K^0\rangle \\ &+(V^d_{L\ 11}V^{d*}_{L\ 12}V^{d*}_{R\ 11}V^d_{R\ 12})G(x_{d_L},x_{s_L},x_{d_R},x_{s_R})\langle\bar{K}^0|\bar{d}_L\gamma^\mu s_L\bar{d}_R\gamma_\mu s_R|K^0\rangle \\ &+(V^d_{R\ 11}V^{*d}_{R\ 12}V^{*d}_{L\ 11}V^d_{L\ 12})G(x_{d_L},x_{s_L},x_{d_R},x_{s_R})\langle\bar{K}^0|\bar{d}_R\gamma^\mu s_R\bar{d}_L\gamma_\mu s_L|K^0\rangle\ \Big),\end{aligned} \tag{2.14}$$

where $x_{d_{L,R}}$ are the positions of the d field, and the $x_{s_{L,R}}$ of the s. Note that all possible separations (between quark fields) are present, but some enter with different signs. In principle then, the gluonic contribution could be made small for any values of R and ρ by placing the quarks at appropriate places. However, the terms involving only right or left handed fields occur with the same sign. So, to achieve significant

reduction, cancellations must occur between those terms and the terms which involve both chiralities. This involves tuning the quark positions to the values of different hadronic matrix elements, which introduces a fine-tuning problem. Otherwise, it would imply that the UV physics that localizes the quarks has information about the IR behavior of QCD! We can therefore expect that cancellations will be $\mathcal{O}(1)$ at most. This is seen clearly in the Monte Carlo trials, where the random positions have no relation to the hadronic matrix elements and no significant cancellation occurs.

In light of this we can explore the magnitude of the flavor effects just by looking at a single term in (2.14); for convenience we choose the first. We can then describe the contributions with only three parameters: the radius R, the scale ratio ρ, and the separation between one pair of fermions, α. The sum over KK-modes is then calculable in terms of these parameters. Since R enters only in the mass in the KK propagator, we can write the contribution in the simple form

$$\Delta m_K = \frac{2}{9} g_s^2 f_K^2 m_K R^2 V_{\mathrm{ds,ds}}^4 F_\rho(\rho\alpha) \tag{2.15}$$

where $V_{ds,ds}^4$ stands for the appropriate product of 4 elements of the $V_{L,R}^{u,d}$ matrices, two at each vertex, and, as shown in (2.11), $F(x,y)$ only depends on the difference of it's arguments, so we can write it as a function of only a single variable, given by the product $\rho\alpha$. The subscript on F reminds us that in two dimensions or more F also depends on ρ directly as the cutoff parameter, in which case it must be computed numerically. If we demand that this contribution to Δm_K be no larger than the measured value (a conservative assumption from the point of view of constraining the model) we get

$$\frac{1}{R} \geq \beta_K \sqrt{V_{ds,ds}^4 F_\rho(\rho\alpha)}, \tag{2.16}$$

where β_K is a coefficient of dimension 1, which depends on the meson parameters. This expression immediately generalizes to other neutral meson systems by using the appropriate coefficient β, and the appropriate matrix elements of V. Table 2.1 shows the values of β for cases of interest, along with representative values of $F_\rho(\rho\alpha)$.

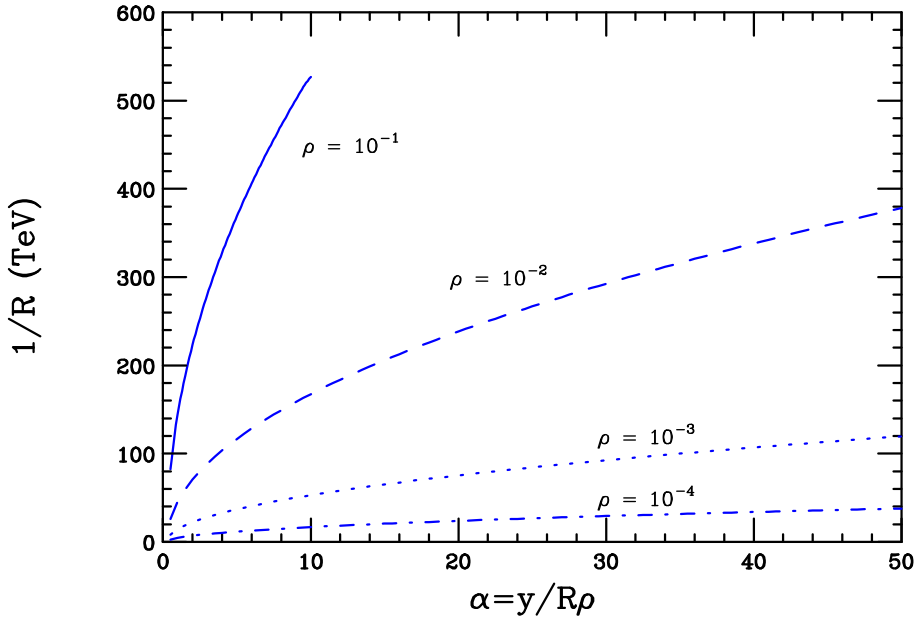

Figure 2.3: The behavior of the constraint on $1/R$ with α for various values of ρ. The area below the curves is excluded. Note that the size of the additional dimension in units of the fermion width is $1/\rho$, so the curve for $\rho = 1/10$ ends at a maximal separation of $\alpha = 10$.

The resulting constraints are shown in Fig. 2.3 and 2.4, for 1 and 2 extra dimensions respectively, using the value of β and $V^4_{ds,ds}$ appropriate for the Kaon sector, and assuming that the V are CKM-like in magnitude (we discuss that assumption in detail below). There are two features of note. First, with one extra dimension the constraint is a simple square-root function, as can be seen from Eq. (2.11). This means that the flavor-changing effects can be made arbitrarily small by reducing ρ. That is, by increasing the hierarchy between fermion and boson scales. Second, in two dimensions the effect seems to be roughly constant in ρ, and flattens off at large α. We know that the sum over the KK states is diverging logarithmically before it reaches the cutoff, and so it should be getting larger as ρ decreases. However, shrinking ρ brings the fermions closer together making the flavor effects smaller. In two dimensions these two effects are seen to roughly cancel. In three or more dimensions, the divergence of the sum wins completely, and the bounds on R^{-1} are huge, effectively removing these cases from consideration as realistic models.

In Figs. 2.5 and 2.6 we display our results for all meson mass differences, taking

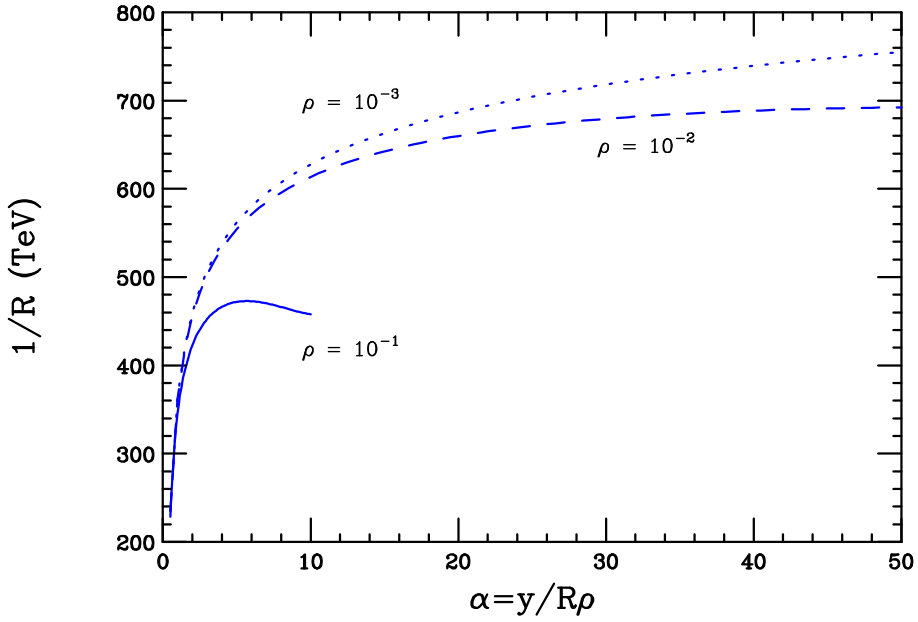

Figure 2.4: Constraints on $1/R$ from Kaon mixing for two extra dimensions; the area below the curves is excluded.

$\rho = 1/100$. For mixing in the Kaon sector and B_d^0 sector, the bound is set by demanding that the new physics produce an effect which is no larger than the observed value. For D^0 mixing, the effect is restricted to lie below the current experimental bound. There is no experimental upper bound on B_s^0 mixing, so we assume two values, one the size expected in the Standard Model, the other about 4 times larger, corresponding to the curves labeled small and large, respectively. Note that the most stringent constraints come from mixings involving the first and second generation.

This pattern suggests a loop-hole in the otherwise stringent constraints. Namely, the V matrices need not be CKM-like. Since the CKM matrix is the product $V_L^{(u)\dagger} V_L^{(d)}$, the observed CKM hierarchical structure could result from a completely different structure at the level of the V^i. If there is small first to second generation mixing the Kaon and D^0 constraints will be relaxed, and all constraints would then be of order a few TeV, even for large values of ρ.

However, in the previous calculation we ignored the third generation when imposing the unitarity condition in Eq. (2.8). Transitions between two 4D mass eigenstates will involve all three generations in the localization (flavor) basis. In this case the

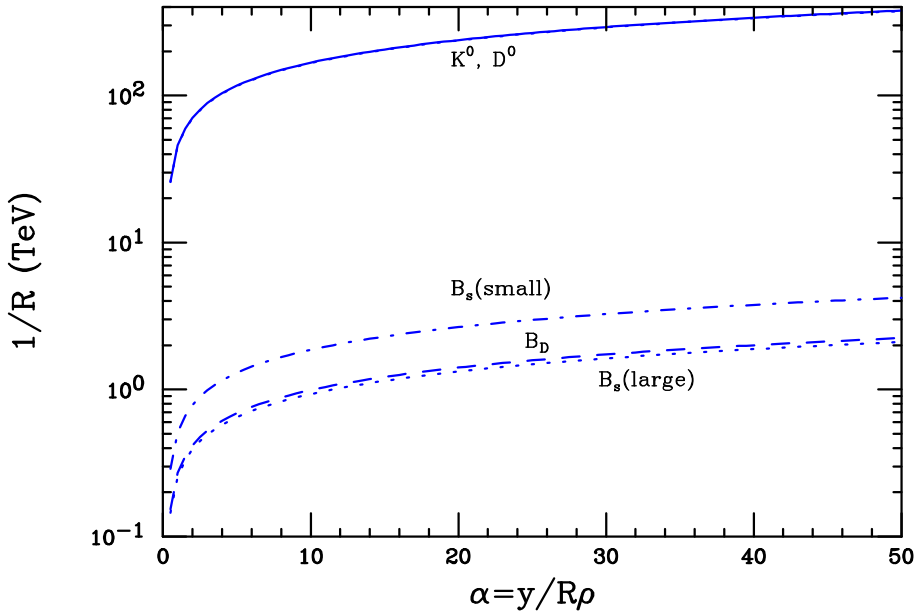

Figure 2.5: Constraints from all species of neutral meson mixings for one extra dimension, taking $\rho = 1/100$. See text for a description of the experimental values used. Note that the K^0 and D^0 results are separate lines that overlap due to a numerical coincidence.

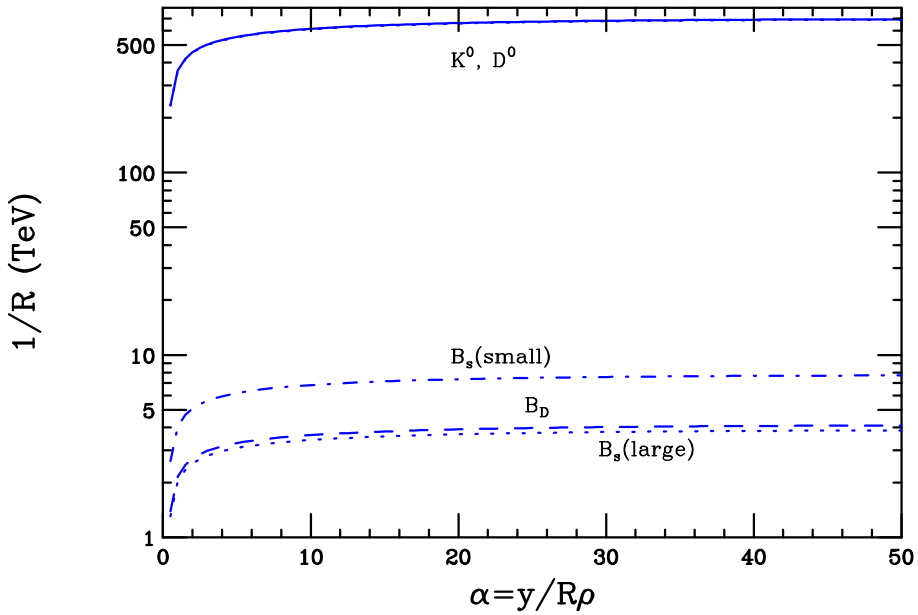

Figure 2.6: Neutral meson constraints for two extra dimensions. The area below the curves is excluded.

ρ	$\alpha = 1$	$\alpha = 5$	$\alpha = 10$	$\alpha = 20$	$\alpha = 50$
1D					
10^{-1}	1.15	2.33	4.76	NA	NA
10^{-2}	0.036	0.23	0.48	1.00	2.45
10^{-3}	0.0012	0.023	0.048	0.097	0.25
2D					
10^{-1}	2.05	3.82	3.59	NA	NA
10^{-2}	2.25	5.27	6.46	7.47	8.22
10^{-3}	2.27	5.41	6.67	8.08	9.78

Meson	β(MeV)
K^0	1125.86
B_d^0	478.01
B_s^0	67.4346
D^0	1124.23

Table 2.1: Left: Representative values of the sum $F_\rho(\rho\alpha)$ for one and two extra dimensions. Right: Multiplicative β factors for mass splittings of the neutral mesons; $1/R \geq \beta\sqrt{V^4 F_\rho(\rho\alpha)}$.

matrices $U_i^{(n)}$ will contain the positions of all three generations of quarks, and the unitarity conditions on the V matrices will be changed. For instance, for the term in Eq. (2.14) with both left-handed chiralities (and dropping the L index), in place of $|V^d_{L\ 11} V^{d*}_{L\ 12}|^2 F(x_d, x_s)$ we should have

$$\begin{aligned} &|V_{11}|^2 V_{12} V_{13}^* F(x_d, x_s) + V_{11}^* V_{12} V_{32}^* V_{31} G(x_d, x_s, x_b, x_s) \\ &+ V_{31}^* V_{32} V_{13}^* V_{11} G(x_b, x_s, x_d, x_s) + |V_{31}|^2 |V_{32}|^2 F(x_b, x_s) \end{aligned} \tag{2.17}$$

These additional terms (including the ones not displayed above corresponding to right and mixed chiralities) will insure that in any mass splitting observable many mixing angles and fermion separations will enter. It then becomes non-trivial to reduce Δm_K by adjusting mixings alone. However, it is still possible to reduce the Kaon and D^0 constraints by noticing that the new terms contain fewer diagonal elements. Hence, if the weak and mass eigenbases are not too badly misaligned, i.e. the V^i have large diagonal elements and smaller off-diagonal elements, then the strongest constraints may be relaxed somewhat. To get a better sense of what is typically possible, we again run Monte Carlo simulations. From these we learn that a typical suppression factor is 10^{-1} for the factors multiplying β in Eq. (2.16), 10^{-2} is not uncommon, and 10^{-4} is obtainable, but rare, even for the fairly large value $\alpha_{\max} = 15$. This is illustrated in Fig. 2.7.

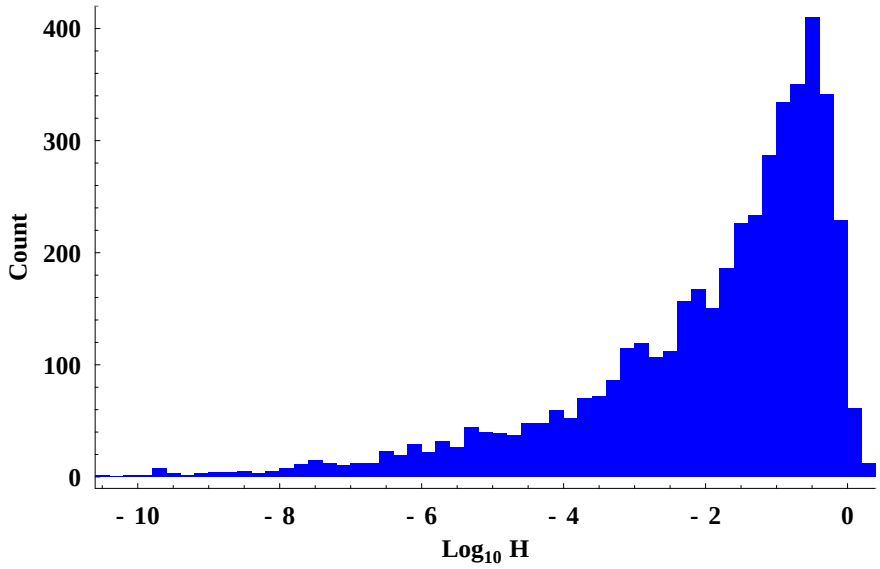

Figure 2.7: Histogram of values of the factor $H = \sqrt{\sum V^4 F(x,y)}$ summed over the appropriate fermion positions and V matrix elements.

All of these considerations together show that once the parameter space is thoroughly explored, it is possible to evade the large constraints from meson mixing for natural regions of the parameters.

2.4 Rare Decays

We also consider processes involving only a single flavor-changing vertex. The best examples of this type which receive contributions from KK gluon exchange are rare B decays, such as $B \to \psi K_S$ and $B \to \phi K_S$. The most interesting aspects of these decays are, of course, their associated CP-violating asymmetries. However, since we have no control of the phases present in split fermion models, we can't address the new contributions to CP-violating observables in a model independent fashion. Nonetheless, there are tree-level strong coupling contributions to these decays, so we can expect significant contributions to the branching fractions in split fermion models.

The effective Lagrangian for a process with a single flavor change is given by

$$\mathcal{L}_{\text{eff}}^{\Delta b=1} = \frac{2}{3} g_s^2 \sum_{n=1}^{\infty} \frac{1}{M_n^2} \sum_{i,j=L,R} U_{i(qb)}^{d(n)} \bar{q}_i \gamma^\mu b_i \bar{q}_j \gamma^\mu q_j. \tag{2.18}$$

Since one vertex is flavor diagonal, the sum depends on the absolute position of the fermions. For instance, the analog of Eq3. (2.9-2.11) is

$$\begin{aligned} F'(x,y,z) &= \sum_{n=1}^{\infty} \frac{\cos(n\pi z)(\cos(n\pi x) - \cos(n\pi y))}{n^2} \\ &= -\frac{\pi^2}{4} \left(|z+x| + |z-x| - |z+y| - |z-y| + \pi x^2 - \pi y^2 \right). \end{aligned} \tag{2.19}$$

where z corresponds to the location of the quark at the flavor conserving vertex. This additional complication turns out to be minor, as the actual magnitude of the sum is similar to that in the previous case and does not vary much over the parameter space, as can be seen from Fig. 2.8.

We consider the decay amplitude

$$\mathcal{A}(B \to \phi K_S) = \frac{2}{3} g_s^2 R^2 \sum_{i,j=L,R} F'(x_{b_i}, x_{s_i}, x_{s_j}) \langle \phi K_S | (\bar{s}_i \gamma^\mu b_i)(\bar{s}_j \gamma_\mu s_j) | B^0 \rangle \tag{2.20}$$

The relevant matrix elements are [28]

$$\begin{aligned} \langle \phi K_S | (\bar{s}_L \gamma^\mu b_L)(\bar{s}_L \gamma_\mu s_L) | B^0 \rangle &= \frac{1}{3} H \\ \langle \phi K_S | (\bar{s}_{L,i} \gamma^\mu b_{L,j})(\bar{s}_{L,j} \gamma_\mu s_{L,i}) | B^0 \rangle &= \frac{1}{3} H \\ \langle \phi K_S | (\bar{s}_L \gamma^\mu b_L)(\bar{s}_R \gamma_\mu s_R) | B^0 \rangle &= \frac{1}{4} H \\ \langle \phi K_S | (\bar{s}_{L,i} \gamma^\mu b_{L,j})(\bar{s}_{R,j} \gamma_\mu s_{R,i}) | B^0 \rangle &= \frac{1}{12} H. \end{aligned} \tag{2.21}$$

Here, i, j are color indices, displayed explicitly in the non-singlet terms which now

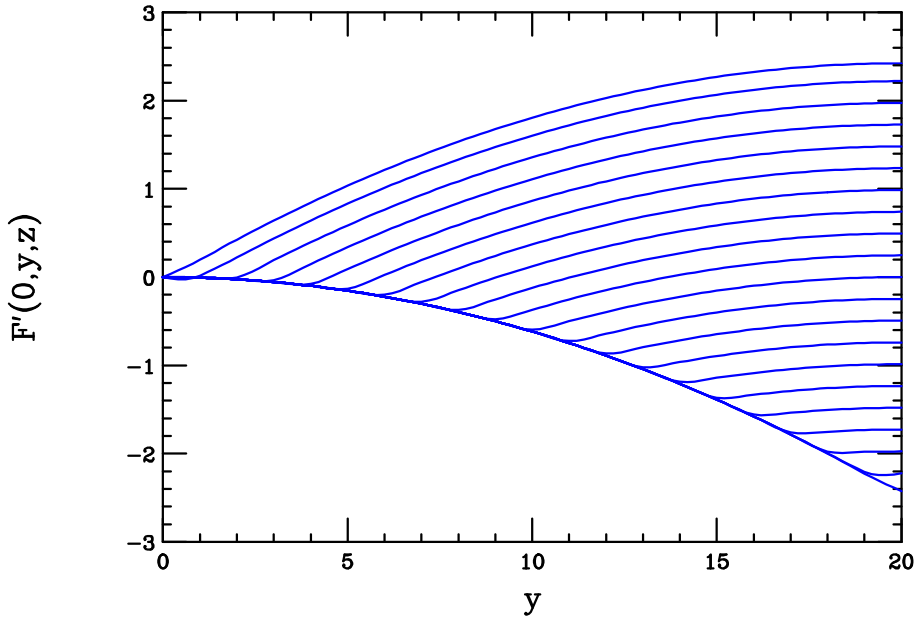

Figure 2.8: KK sum for processes involving a single flavor changing vertex as a function of one of the fermion positions, corresponding to the case where one of the fermions is localized at the orbifold fixed point. The position of the third (flavor conserved) fermion, z, is varied in steps of one unit, with $z = 0$ corresponding to the top curve and $z = 20$ to the bottom. The sum is done for a single extra dimension of size 20 units.

contribute. The common factor is

$$H = 2(\epsilon_\phi \cdot p_B) f_\phi m_\phi^2 F_+(m_\phi^2), \tag{2.22}$$

where ϵ_ϕ represents the polarization vector of the phi meson, and $F_+(q^2)$ is the form factor for this decay. There are an additional four matrix elements obtained by taking $(L \leftrightarrow R)$. We use the values $f_\phi = 233\,\mathrm{MeV}$ [94], $F_+(m_\phi^2) = 0.38$ [154], and $m_\phi = 1020\,\mathrm{MeV}$ [95].

For the branching fraction we obtain (ignoring the O(1) differences among matrix

elements)

$$\mathcal{B}(B \to \phi K_S) = \frac{1}{64\pi m_B \Gamma_B} f_\phi^2 m_\phi^4 F_+^2(m_\phi^2) \left(\sum_{n=1}^{\infty} \frac{U^{d\dagger}_{L(ss)} U^d_{L(bs)}}{n^2} \right)^2 \tag{2.23}$$

$$\approx 9.1 \times 10^{-6} \left(\frac{V^4_{sb,ss}}{0.04} \right)^2 \left(\frac{R}{1\,\mathrm{TeV}^{-1}} \right)^4 \left(\sum_{i,j=L,R} F'(x_{b_i}, x_{s_i}, x_{s_j}) \right)^2 ,$$

and similarly

$$\mathcal{B}(B \to \psi K_S) \approx 5.6 \times 10^{-5} \left(\frac{V^4_{sb,cc}}{0.04} \right)^2 \left(\frac{R}{1\,\mathrm{TeV}^{-1}} \right)^4 \left(\sum_{i,j=L,R} F'(x_{b_i}, x_{s_i}, x_{c_j}) \right)^2 . \tag{2.24}$$

Demanding that this not be larger than the observed rate gives the approximate constraints $1/R \geq 1.0$ TeV from $B \to \phi K_S$ and $1/R \geq 0.5$ TeV from $B \to \psi K_S$. These are not competitive with those from B_d and B_s meson oscillation, and provide a good consistency check. It is interesting to note that if a way can be found to reduce the constraints from the Kaon sector to the few TeV scale without disturbing the b-quark couplings (say by arranging the mixing angles), then this contribution to $B \to \psi K_S, \phi K_S$ is of roughly the same order as that of the Standard Model. Any new phases in this scenario will thus contribute to the CP-violating observables with equal effects in each decay channel.

We have also estimated the ree-level KK contribution to single top quark production at LEP, $e^+e^- \to \bar{t}q + t\bar{q}$ (with $q = u, c$) which proceeds via KK $\gamma^{(n)}$ and $Z^{(n)}$ exchange. Using the parameterization in [96] we find an effective anomalous flavor-changing vector coupling v_Z given in this case by

$$v_{Z\mathrm{eff}} = \left(\sqrt{2} + 2\sin\theta_W Q \right) M_W^2 R^2 \sum_{i,j=L,R} \sum_{n=1}^{\infty} \frac{U^u_{i(tc)} U^l_{j(ee)}}{n^2} \tag{2.25}$$

$$\approx 6.9 \times 10^{-4} \left(\frac{R}{1\,\mathrm{TeV}^{-1}} \right)^2 \sum_{i,j=L,R} \left(\frac{V^4_{ut,ee}}{0.04} \right) \left(\sum_{i,j=L,R} F'(x_{c_i}, x_{t_i}, x_{e_j}) \right) , \tag{2.26}$$

where we have used only the $c \to t$ since it dominates the $u \to t$ by a factor of 10. The current constraint on this effective flavor changing coupling from LEP data is $v_Z \leq 0.75$ [4], and so split fermions in the up-quark sector are not significantly constrained.

Lastly, we examine the potential gauge KK contributions to the purely leptonic decay of neutral B mesons, $B_q^0 \to \ell^+\ell^-$, with $q = d, s$. This process proceeds through tree-level $\gamma^{(n)}$ and $Z^{(n)}$ KK exchange, and could ,in principle, probes fermion splitting in the leptonic sector as well as in the quark sector. Here, for simplicity, we will assume that the leptonic fields are all localized at the same point in the extra dimension and will ignore any possible flavor changing leptonic interactions. The $\Delta b = 1$ Lagragian describing this decay is then

$$\mathcal{L}_{\rm eff}^{\Delta b=1} = \sum_{\alpha=\gamma,Z} 2G_\alpha^2 \sum_{\vec{n}=1}^{\infty} \frac{1}{M_n^2} \sum_{i=L,R} U_{i(qb)}^{d(n)} g_{i,\alpha}^b \bar{q}_i \gamma^\mu b_i \, g_{i,\alpha}^\ell \bar{\ell}_i \gamma_\mu \ell_i \,, \tag{2.27}$$

where $G_\gamma = e$ and $G_Z = g/\cos\theta_w$. The hadronic matrix element governing this decay is given by

$$\langle 0|g_{L,\gamma/Z}^b U_L^{d(n)} \bar{q}_L \gamma^\mu b_L + g_{R,\gamma/Z}^b U_R^{d(n)} \bar{q}_R \gamma^\mu b_R | B_q^0 \rangle = i f_b p_B^\mu [g_{L,\gamma/Z}^b U_L^{d(n)} - g_{R,\gamma/Z}^b U_R^{d(n)}] \,, \tag{2.28}$$

where p_B^μ represents the momentum of the B^0 meson. Due to parity, only the axial-vector current contributes to this matrix element. In the case of photon KK exchange, such contributions are generated when the left- and right-handed fermions are localized at separate points. Here, we will ignore this possibility and consider the case where only the $Z^{(n)}$ exchange mediates this decay. The branching fraction is then

$$\begin{aligned} \mathcal{B}(B_s \to \mu^+\mu^-) &= \frac{4G_F^2 M_W^4 f_B^2 m_\ell^2 m_B}{\pi c_w^4} \tau_B R^4 \left[1 - \frac{4m_\ell^2}{m_B^2}\right]^{1/2} \Big| \sum_n \frac{g_{L,Z}^b U_L^{d(n)} - g_{R,Z}^b U_R^{d(n)}}{n^2} \Big|^2 \\ &= 1.15 \times 10^{-6} \left(\frac{R}{1\,\text{TeV}^{-1}}\right) \frac{V_{db,\mu\mu}^4}{(0.04)^2} \\ &\quad \times \Big| g_{L,Z} F'(x_{b_L}, x_{q_L}, x_{\ell_L}) - g_{R,Z} F'(x_{b_R}, x_{q_R}, x_{\ell_R}) \Big|^2 , \end{aligned} \tag{2.29}$$

where we have chosen $q = s$ and used $f_B = 200$ MeV. The function F' is as given in Eq. (19) and has a value in the range -2 to $+2$ as shown in Fig. 8. Taking values of this function which maximizes the sum over the KK states, *i.e.*, $F' = 2$, yields a value of unity for the sum, resulting in a branching fraction of 1.15×10^{-6} for $R = 1\,\mathrm{TeV}^{-1}$. This is a significant enhancement over the Standard Model value[32] of $\mathcal{B}(B_s \to \mu^+\mu^-) \simeq 4.0 \times 10^{-9}$. The experimental bound on this decay, $\mathcal{B}(B_s \to \mu^+\mu^-) < 2.6 \times 10^{-6}$, as determined by CDF[2], sets the limit $R^{-1} > 815$ GeV when the sum over the KK states takes on its maximal value. The sensitivity of this decay mode in probing the size of the additional dimension is thus comparable to that of B_s mixing and will improve with Run II data at the Tevatron[15].

2.5 Conclusions

Models where the Standard Model fermions are localized at specific points along a compact extra dimension offer an attractive means for constructing the fermion mass hierarchy and suppressing dangerous operators such as proton decay. In these scenarios, the fermions obtain narrow Gaussian wavefunctions in the additional dimension with a width much smaller than the compactification scale. The fermion Yukawa couplings are then generated by the overlap of the localized wavefunctions for the left- and right-handed fermions. Lighter fermions are thus more widely separated than heavier ones.

The gauge fields are free to propagate throughout the bulk in these scenarios and their KK excitations develop tree-level flavor changing interactions which are proportional to the overlap of their wavefunctions with those of the localized fermions. Gluons, as well as the electroweak gauge bosons, then mediate flavor changing neutral current processes at dangerous levels. Previously, it was thought that the only way to avoid stringent bounds on the size of the compact dimensions was to minimize the separation of the fermion fields, thus endangering the scenario's natural explanation of the fermion hierarchy.

In this paper, we have reinvestigated these new FCNC interactions and have performed a general, systematic, model independent analysis. Our results hold for

any such model of the fermion hierarchy with specific fermion geographies. We have employed a model parameterization which contains only three parameters: the size of the extra dimension R, the scaled width of the localized fermion $\rho = \sigma/R$, and the fermion separation distance expressed in units of the width, $\Delta x = \alpha\sigma$. We performed a simple Monte Carlo analysis and determined that the fermion mass hierarchy can be reproduced in our parameterization for natural values of the parameters.

We then evaluated the KK gluon tree-level flavor changing contributions to neutral meson oscillations. We found that the sum over the KK states is exponentially damped for higher KK gauge states as the KK states can then resolve the finite size of the fermion wavefunction. This allows us to perform the KK sum in a scenario with more than one extra dimension. We then evaluated the constraints from Kaon mixing in the case of one extra dimension and confirmed previous results that $1/R \gtrsim 100$'s TeV for larger values of ρ unless the separation was very small. However, the constraint shrinks to $1/R \gtrsim$ few TeV for smaller values of ρ, even for widely separated fermions, at the expense of introducing a new hierarchy between the compactification and fermion localization scales. The constraints from B_d and B_s mixing were found to be much less restrictive. We also performed the evaluation for the case of two or more additional dimensions and found that the FCNC constraints were much more difficult to evade.

We next studied the dependence of our constraints on the fermion mass mixing matrices, and found that with a realignment of the matrix elements our bounds could be reduced further by factors of 10-100.

In addition, we examined the rare meson decays $B_d \to \psi K_S, \phi K_S$, as well as single top-quark production in e^+e^- collisions, and found weaker limits of the size of the extra dimension of order TeV^{-1}. We note that the KK gluon contributions to these rare decays are significant enough to generate interesting effects in the related CP violation observables.

In summary, we have shown that once the parameter space is systematically explored, it is possible to evade the stringent bounds from FCNC in split fermion models for natural values of the parameters and without the introduction of any additional hierarchies. Lastly, we note that the introduction of brane localized kinetic terms are

known to significantly reduce the couplings of gauge KK states [42, 66] and may help to even further reduce the constraints from FCNC in these scenarios.

Appendix

Here we present a cute way to perform the sum over KK modes analytically in one dimension, and see that the sum is exactly linearly proportional to the separation.[52] The functions that we need are

$$F(x,y) \equiv \sum_{n=1}^{\infty} \frac{(\cos(n\pi x) - \cos(n\pi y))^2}{n^2}, \tag{2.30}$$

and

$$G(x_1,x_2,y_1,y_2) \equiv \sum_{n=1}^{\infty} \frac{(\cos(n\pi x_1) - \cos(n\pi y_1))(\cos(n\pi x_2) - \cos(n\pi y_2))}{n^2}. \tag{2.31}$$

We can do both of these by evaluating

$$f(x) \equiv \sum_{n=1}^{\infty} \frac{\cos(nx)}{n^2}. \tag{2.32}$$

So that

$$F(x,y) = \frac{1}{2}(f(2\pi x) + f(2\pi y) + \frac{\pi^2}{3} - 2f(\pi x + \pi y) - 2f(\pi x - \pi y)) \tag{2.33}$$

$$\begin{aligned} G(x_1,x_2,y_1,y_2) = \Big[& f(\pi x_1 + \pi x_2) + f(\pi x_1 - \pi x_2) + f(\pi y_1 + \pi y_2) + f(\pi y_1 - \pi y_2) \\ & - f(\pi x_1 + \pi y_2) - f(\pi x_1 - \pi y_2) - f(\pi y_1 + \pi x_2) - f(\pi y_1 - \pi x_2) \Big] \end{aligned} \tag{2.34}$$

Writing the $\cos(nx)$ as two exponentials and combining the sums we have

$$f(x) = \frac{1}{2} \sum_{n \neq 0} \frac{e^{inx}}{n^2}. \tag{2.35}$$

The function f is then the solution of the differential equation

$$f''(x) = -\frac{1}{2}\sum_{n\neq 0} e^{inx} = -\frac{1}{2}\sum_{n=-\infty}^{\infty} e^{inx} + \frac{1}{2} \tag{2.36}$$

$$= -\frac{1}{2}\left(2\pi \sum_{k=-\infty}^{\infty} \delta(x - 2\pi k) - 1\right). \tag{2.37}$$

This is solved by

$$H(x) = -\frac{1}{2}\left(\pi|x| - \frac{x^2}{2} - \frac{\pi^2}{3}\right), \tag{2.38}$$

where H is defined on the interval $[-\pi, \pi]$ and is 2π-periodic for other values (this takes care of the sum over delta functions). We then have

$$f(x) = H(x) + \alpha x + \beta. \tag{2.39}$$

Looking at the original function we see that we must have $\int_{-\pi}^{\pi} f = 0$ which gives $\beta = 0$. Also, since f is an even function $\alpha = 0$.

We can then use Eq. (2.39) in (2.33) and (2.34) and use the physical condition that all arguments are positive to get the final result

$$F(x, y) = \frac{\pi^2}{2}|x - y|, \tag{2.40}$$

and

$$G(x_1, x_2, y_1, y_2) = -\frac{\pi^2}{4}\left(|x_1 - x_2| + |y_1 - y_2| - |x_1 - y_2| - |y_1 - y_2|\right). \tag{2.41}$$

Chapter 3

Yukawa hierarchies from extra dimensions with Small FCNC

3.1 Introduction

Recently there has been much interest in the possibility that there exist extra dimensions much larger than the Planck scale [16, 118, 155, 106, 107, 39]. There are many reasons for this excitement, particularly the fact that having large dimensions accessible to gravity may allow a solution of the hierarchy problem associated with the Higgs mass [20, 17, 21, 136, 135]. However, extra dimensions may also be able to address other puzzles left unexplained in the Standard Model, such as why there are three families [70], or the origin of dark matter [18, 149, 148, 46].

In particular, it was noticed by Arkani-Hamed and Schmaltz (AS) that localizing the standard model fermion fields in an extra dimension could solve the other serious hierarchy problem, that of the relative size of the fermion masses [23]. This is accomplished by assigning a universal Yukawa coupling in the higher dimensional theory, but separating the left and right handed components of the effective 4D fermions in the additional dimension. This is accomplished by localizing the zero modes to Gaussian profiles, and separating the centers of the Gaussians. The 4D Yukawa couplings, and hence fermion masses, are proportional to integrals of products of these zero modes over the compact dimension. They are thus suppressed by exponentially small

wavefunction overlaps. Realizations of this model that match the Standard Model masses and mixing parameters have been produced [90, 125, 45, 67, 113, 31]. There also exist possibilities for observing the effects of this localization at future colliders, such as the production of Kaluza-Klein excitations of the Standard Model particles. Current results from the direct production of KK states. and precision electro-weak measurements restrict the size of dimensions accessible to Standard Model fields to be $R \lesssim \text{few}\,\text{TeV}^{-1}$ [144, 123, 122, 102]. The separation between fields also allows for detection of some novel effects [22, 142].

However, split fermion models also generate tree-level flavor-changing neutral currents (FCNC). Strict bounds from these are hard to obtain due to the large number of model parameters, but in general one finds $R \lesssim 400\,\text{TeV}^{-1}$ [45, 68, 3, 115]. Without miraculous cancellations, this can be evaded only by making very small the ratio $\rho = \sigma/R$, where σ is the width of the localized fermions, thus introducing a new hierarchy.

In this paper we present a different model based on similar ideas. Instead of fixed width fermions localized at different points, we consider variable width fermions localized at the same point. We will show that this model can produce the observed fermion mass hierarchy and mixing angles, including the CP violating phase while generating much smaller FCNC. This model has the additional virtue suppressing any proton decay operators. The resulting constraints on the compactification scale turn out to be a factor of 30 smaller than similar constraints on the AS model, and can be as low as $1/R \geq 2\,\text{TeV}$. This is low enough to raise the exciting possibility that they could be within reach of the next generation of colliders, and that the model could be embedded in a more encompassing one that also solves the Higgs mass hierarchy problem. This is similar to the proposal of Kaplan and Tait [113], although they still required the left and right handed fermions to be separated from each other. This idea is also similar to a model studied in the case of a warped extra dimension [108].

This paper is organized as follows. In section 3.2 we show how variable widths can explain the Yukawa hierarchy. A specific set of model parameters that reproduce the observed fermion masses and mixing angles is shown in section 3.3. In section 3.4 we consider the constraints from FCNC. Section 3.5 discusses possible mechanisms

for implementing the model, and section 3.6 concludes.

3.2 Yukawa Hierarchies

We propose the configuration where different fermion flavors are localized in the extra-dimensional bulk as exponentially localized wavefunctions with different widths, as illustrated in Fig. 3.1. For most of this paper we consider this to be a phenomenological ansätz. A discussion of what types of models may produce this picture is given in section 3.5. This paper will focus on models with a single compact extra dimension, which we take to be the interval $[0, R]$, with the edges of the additional dimension being defined either by a brane configuration or by an orbifolding condition.

We begin with a general configuration that allows each fermion species to be localized with different widths to a specific point. A fermion is taken to be localized at x_0 with width σ if it has a profile $\psi \propto e^{-|x-x_0|^a/\sigma^a}$. The power a is determined by the localization mechanism, and represents a phenomenological parameterization of the unknown mechanism. In the AS model, for instance, fermions are localized with Gaussian profiles, so $a = 2$; in the Randall-Sundrum (RS) scenario, or in brane-worlds with bulk mass terms, fermions are localized to exponentials, so $a = 1$. For simplicity, we take the localization point to be $x_0 = 0$. The normalized wavefunction for the i-th fermion is

$$\psi_i = \frac{2^{1/2a}}{\sqrt{\sigma_i}} \frac{1}{\sqrt{\alpha_a(R, \sigma)}} e^{-y^a/\sigma_i^a}, \tag{3.1}$$

where we have defined

$$\alpha_a(R, \sigma) = \int_0^{\frac{R}{\sigma}} dz \; e^{-z^a}. \tag{3.2}$$

This integral will cancel to good approximation in the following computations of the coupling constants.

The gauge boson wavefunctions will also generally depend on the model details. For the moment the only important point is that the Higgs zero mode be flat in the

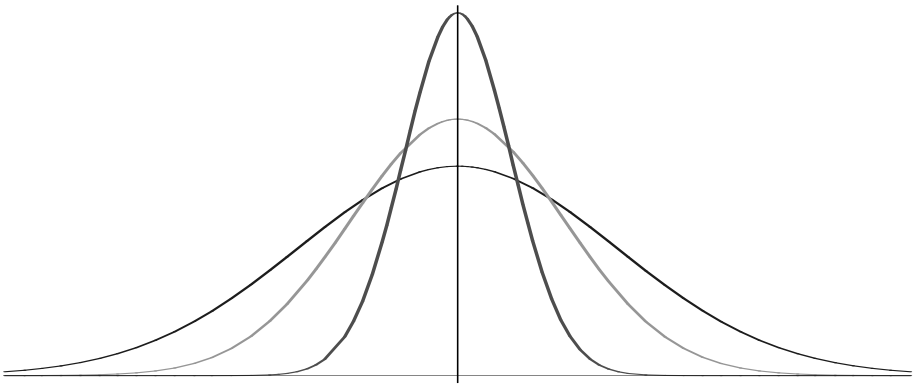

Figure 3.1: Illustration of the idea of variable width fermions localized to a single point.

extra dimension, so $h^{(0)}(y) = 1/\sqrt{R}$, where h is the Higgs field and $h^{(0)}$ is the zero mode of the Kaluza-Klein expansion. This zero mode corresponds to the Standard Model Higgs, the vev of which is responsible for electro-weak symmetry breaking and generating 4D fermion masses. The 5D Yukawa couplings for the fermions carry mass dimension $-1/2$. In the dimensionally reduced theory this scale is given by the compactification scale R. We therefore write the 5D Yukawa terms as

$$\mathcal{L}^{5D}_{\text{Yukawa}} = \lambda_{5,ij}\sqrt{R}\, h\bar{\psi}_i\psi_j. \tag{3.3}$$

The dimensionally reduced 4D Lagrangian is obtained by integrating over the compact dimension. The 4D Yukawa couplings are then given, in the physically appropriate approximation that R is much larger than any of the widths, by

$$\begin{aligned}\lambda_{4,ij} &= \lambda_{5,ij}\sqrt{R}\int_0^R dy\ h^{(0)}(y)\ \bar{\psi}_i(y)\ \psi_j(y) \\ &= \lambda_{5,ij}\sqrt{R}\left(\frac{2^{1/a}\sqrt{\sigma_i\sigma_j}}{(\sigma_i^a+\sigma_j^a)^{1/a}}\right).\end{aligned} \tag{3.4}$$

This can be rewritten as

$$\lambda_{4,ij} = \lambda_{5,ij}\sqrt{R}\left(2^{1/a}\left(\left(\frac{\sigma_i}{\sigma_j}\right)^{a/2}+\left(\frac{\sigma_j}{\sigma_i}\right)^{a/2}\right)^{-1/a}\right). \tag{3.5}$$

The factor in parenthesis is determined by the wavefunction overlap. It is unity when $\sigma_i = \sigma_j$, and does not change dramatically as the widths vary. If we take all the 5D Yukawa couplings to be the same, $\lambda_{5,ij} = \lambda_5$ we expect this model to have 4D Yukawa matrix elements given by $\lambda_{4,ij} \approx \lambda_5$, and essentially equal with small differences due to the different widths. This is a realization of the "democratic" scenario of fermion mass generation [77]. This scenario relies on the observation of the singular values of the matrix

$$A = \begin{pmatrix} 1 & 1 & 1 \\ 1 & 1 & 1 \\ 1 & 1 & 1 \end{pmatrix} \xrightarrow{\text{diag}} \begin{pmatrix} 3 & 0 & 0 \\ 0 & 0 & 0 \\ 0 & 0 & 0 \end{pmatrix}. \tag{3.6}$$

That is, there is one large singular value and two vanishing ones. If one then perturbs the values of the elements in A, the two zero diagonal values become finite, but small. When A is a Yukawa matrix this gives a natural hierarchy in the resulting masses. This is in stark contrast to the AS scenario, where the hierarchy is generated by small elements directly in the Yukawa matrices.

We have studied the expected size of the resulting Yukawa hierarchy by performing random trials. We drew six widths for the 5D fermion wavefunctions from the interval $[1, 3]$ and computed the physical mass spectrum for the case $a = 2$. The interval was chosen so that all widths are of the same order of magnitude; the overall scale is irrelevant. The size of the hierarchy is taken to be $\log_{10}(m_1/m_3)$, where m_1 is the largest mass, and m_3 the smallest. Fig. 3.2 shows a histogram of the resulting hierarchies for 10^5 random trials. We see that hierarchies of size 3 to 5 are generic.

It is important to note that Fig 3.2 shows the hierarchy between the masses resulting from a single Yukawa matrix; *i.e.*, between fermions with the same quantum numbers. In this democratic scheme the largest singular value (and hence mass) is always of the same order of magnitude. Therefore it is impossible to generate the the large ratios m_t/m_b or m_t/m_τ simply by varying the widths. We speculate on how to obtain these ratios within the model in section 3.5; for now we simply take the five dimensional Yukawa couplings λ_5^u, λ_5^d, λ_5^e to be different.

Finally, note that while Fig. 3.2 was computed for $a = 2$, similar results hold

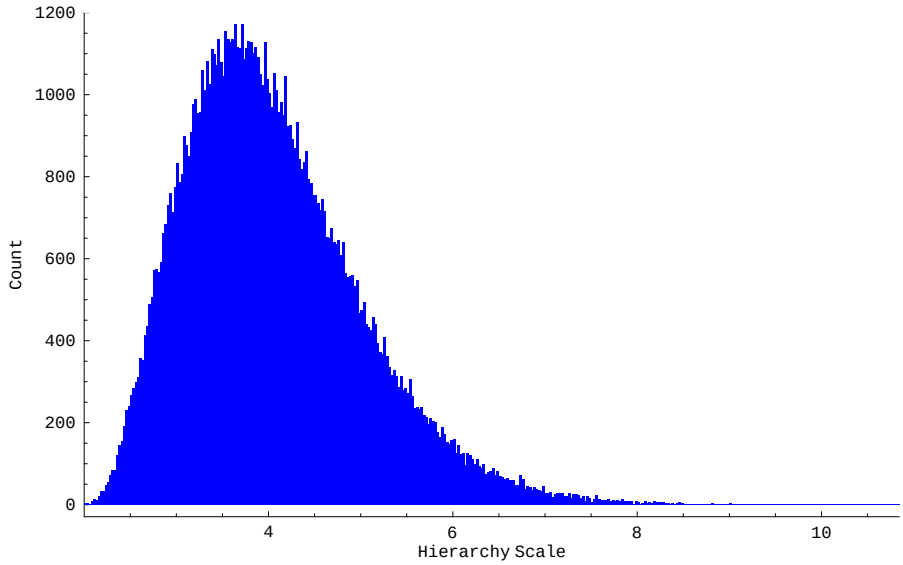

Figure 3.2: Histogram of the expected size of the Yukawa hierarchy for 10^5 random configurations of fermion widths, with the widths drawn from the interval $[1, 3]$. The hierarchy scale is defined as $\log_{10}(m_1/m_3)$, where $m_1(m_3)$ is the largest (smallest) mass resulting from that configuration.

for any value of a. The important point is that the mass matrix is almost universal, and that small perturbations are generated by slightly different zero mode profiles. In addition, the Higgs profile need not be perfectly flat. As long as the variation in the Higgs 5D wavefunction is slow across the width of the fermions the same pattern will emerge.

3.3 Standard Model parameters

For illustration, we will now obtain a set of model parameters that generates the observed fermion masses and mixings of the Standard Model to within experimental accuracy. For now, our model contains the following: There is the localization mechanism parameter a, which will be fixed to 2 in this section. There are the three Yukawa couplings λ_5^u, λ_5^d, λ_5^e. For the quark sector, there are nine widths, one each for the three left handed quark doublets, Q_i, the three right handed up singlets, $\bar{u}_i$,

and the three right handed down singlets, $\bar{d}_i$. Only eight of the widths are independent because the Yukawa matrix elements from Eq. 3.4 only depend on the ratios of widths. For the lepton sector there are at least another six widths, for the doublets L_i, and the charged singlets e_i^+. There are possibly three more depending on whether right-handed neutrinos are included. For the purposes of this paper we ignore the neutrinos and only match the charged lepton masses to their observed values. Finally, it is necessary to include two arbitrary, but small, phases in one of the quark Yukawa matrices to be able to match all the CKM mixing angles and incorporate CP violation.

As a proof of principle, we have performed a search of the parameter space and located a configuration that reproduces the Standard Model parameters. For this search we used the values of quark masses and mixing angles from [95]. The fermion masses were evaluated at the common scale m_t using factors given in [125]. The values of the three five dimensional Yukawa couplings were obtained by matching to the large third generation masses (so $\lambda_5^u = \sqrt{2}m_t/v$, etc. where v is the Higgs vev). The smaller fermion masses are then obtained by diagonalizing the Yukawa matrices generated from Eq. (3.4). The mixing angles can then be obtained from the relation

$$V_{\rm ckm} = V_L^{(u)\dagger} V_L^{(d)}, \tag{3.7}$$

where the $V_L^{(u,d)}$ are the unitary matrices that rotate the left-handed (u, d) quark fields to diagonalize the Yukawa matrices. The real part of the CKM matrix was parameterized by matching to the magnitude of the three entries above the diagonal, V_{us}, V_{ub}, and V_{cb}. Finally, to match the observed CP phenomenology we included two arbitrary phases, ϕ_1, in in $\lambda_{dd}^{(d)}$ and ϕ_2 in $\lambda_{ss}^{(d)}$, and computed the Jarlskog invariant

$$J = \mathcal{I}m\left(V_{us} V_{cb} V_{ub}^* V_{cs}^*\right) \tag{3.8}$$

and required it to be near the Standard Model expectation $J \approx 3 \times 10^{-5}$. The search was performed by Monte Carlo sampling of the parameter space to find a reasonably close match.

In the lepton sector we are only matching three masses with five parameters, so

solutions are essentially trivial to come by. For illustration, one such set is

$$L_i = \begin{pmatrix} 6.118 \\ 5.815 \\ 2.360 \end{pmatrix}, \quad e^+ = \begin{pmatrix} 2.696 \\ 3.443 \\ 5.576 \end{pmatrix}, \tag{3.9}$$

which produces $m_e = 0.511\,\mathrm{MeV}$ and $m_\mu = 105\,\mathrm{MeV}$ from matching the coupling to $m_\tau = 1777\,\mathrm{MeV}$. There are many others that will match the leptonic masses just as well.

In the quark sector there are many more constraints. It is possible that there are many configurations that match the Standard Model, but since this search was for illustrative purposes only the search was stopped after a solution was obtained. This configuration is

$$Q_i = \begin{pmatrix} 8.132 \\ 2.365 \\ 6.235 \end{pmatrix}, \quad \bar{u} = \begin{pmatrix} 9.865 \\ 9.279 \\ 9.404 \end{pmatrix}, \quad \bar{d} = \begin{pmatrix} 7.218 \\ 6.463 \\ 8.073 \end{pmatrix}, \qquad \phi_1 = -0.0140, \qquad \phi_2 = -0.0633. \tag{3.10}$$

These produce the values

$$\begin{aligned} m_t &= 175\,\mathrm{GeV} & m_b &= 4.30\,\mathrm{GeV} \\ m_c &= 1.31\,\mathrm{GeV} & m_s &= 107\,\mathrm{MeV} \\ m_u &= 2.00\,\mathrm{MeV} & m_d &= 8.02\,\mathrm{MeV}. \end{aligned} \tag{3.11}$$

The absolute values of the resulting CKM matrix are

$$|V_{\mathrm{CKM}}| = \begin{pmatrix} 0.975 & 0.224 & 0.00482 \\ 0.224 & 0.974 & 0.0439 \\ 0.00590 & 0.0438 & 0.999 \end{pmatrix}. \tag{3.12}$$

The Jarslkog invariant is $J = 2 \times 10^{-5}$. Another way of estimating the magnitude of CP violation is to calculate $\sin 2\beta$. Doing this we find $\sin 2\beta = 0.627$, which is less

than 2σ away from the current world average $\sin 2\beta = 0.734 \pm 0.055$.[137] Interestingly, under the substitution $\phi_{1,2} \to -\phi_{1,2}$ all masses and absolute values of CKM elements remain the same, and J and $\sin 2\beta$ switch sign, picking up the alternate solution that results from the sign ambiguity in β. Both of J and $\sin(2\beta)$ are slightly smaller then the experimental values. However, since this is only an illustrative configuration, and there may be others that work as well, the significance is not in exact agreement, but rather in the fact that they are very close. We note for completeness that this configuration predicts $\alpha = 2.37$ and $\gamma = 0.430$.

There are a few points to note about this configuration. First, the largest ratio of widths is $9.865/2.365 \approx 4$, so the widths of all the fermion fields are of the same order of magnitude, with $\mathcal{O}(1)$ differences between them. Second, the phases required are very small. That small phases are required can be easily understood by noting that the mechanism for generating the hierarchy depends on the singularity of the Yukawa matrices. A large phase would ruin that singularity. It is thus significant that these very small phases are enough to generate the observed CP-violation.

3.4 Flavor Changing Processes

The above discussion of the generation of the Yukawa hierarchy made no mention of the overall scale of the fermion widths. This is can be understood from the fact that the Yukawa couplings in Eq. (3.4) involve only ratios of widths, and hence are independent of any overall scale.

Effects that depend on the scale will come from interactions with the Kaluza-Klein (KK) excitations of the gauge bosons. These will turn out to depend explicitly on R, as well as on the ratio $\rho = \sigma/R$. Here σ is taken to be the generic scale of the fermion widths, with $\sigma_i = \gamma_i \sigma$ where γ_i is of order unity, and we further define $\rho_i = \sigma_i/R$ for later convenience. We see that ρ is a measure of the separation between the energy scales of the fermions (the localization energy) and the bosons (the compactification scale).

For simplicity at this point we take the extra dimension to be flat. The bosons are allowed to propagate in the entire bulk, which has size R. The wavefunctions are

then

$$A^{(n)}(y) = \frac{1}{\sqrt{R}} e^{\frac{in\pi y}{R}}. \tag{3.13}$$

In most models half of these will be projected out by boundary conditions. We retain only the cosine modes, to preserve the zero modes (n=0) which correspond to the Standard Model bosons. The gauge couplings are then

$$\begin{aligned} g_i^{(n)} &= g_5 \int_0^R dy\ A^{(n)}(y)\bar{\psi}_i(y)\psi_i(y) \\ &= \sqrt{2} g_4 \frac{\left[1 - e^{-\frac{1}{\rho_i}}\right]}{1 + \frac{n^2\pi^2\rho_i^2}{4}}, \qquad n \geq 1, \end{aligned} \tag{3.14}$$

for $a = 1$, and

$$g_i^{(n)} = \sqrt{2} g_4 e^{-\frac{1}{8}n^2\rho_i^2}, \qquad n \geq 1, \tag{3.15}$$

for $a = 2$.

These couplings depend on the fermion species. To see that this results in flavor-changing currents, consider the phenomenological 4D Lagrangian for the quarks, $\boldsymbol{d}_L = (d_L, s_L, b_L)^\dagger$ and similarly for $\mathbf{d}_R$, $\mathbf{u}_L$, $\mathbf{u}_R$, all coupled to the gluon field G:

$$\begin{aligned} \mathcal{L} =& \mathcal{L}_{\text{kinetic}} + g G_\mu^0 \sum_{i=L,R} \left(\bar{\boldsymbol{d}}_i \gamma^\mu \boldsymbol{d}_i + \bar{\boldsymbol{u}}_i \gamma^\mu \boldsymbol{u}_i\right) + \sqrt{2} g \sum_{n=1}^{\infty} G_\mu^{(n)} \sum_{i=L,R} \left(\bar{\boldsymbol{d}}_i C_i^{d(n)} \gamma^\mu \boldsymbol{d}_i + \bar{\boldsymbol{u}}_i C_i^{u(n)} \gamma^\mu \boldsymbol{u}_i\right) \\ &+ \boldsymbol{d}_L V_L^{d\dagger} M_d V_R^d \boldsymbol{d}_R. + \boldsymbol{u}_L V_L^{u\dagger} M_u V_R^u \boldsymbol{u}_R, \end{aligned} \tag{3.16}$$

where $M_{u,d}$ are the diagonal mass matrices, the $V_{L,R}^{(u,d)}$ are the unitary matrices that accomplish the diagonalization, the $G^{(n)}$ are the Kaluza-Klein excitations of the gluons, and we have ignored all but the zero modes for the fermions, since the fermion KK modes will not enter the processes considered here. The couplings to the KK gluons are contained in the diagonal matrices $C_{L,R}^{u,d(n)}$, with the i-th coupling given by Eqs. (3.14) and (3.15). When we transform to the mass basis the gauge couplings

will be the elements of the matrices

$$U_{L,R}^{u,d(n)} \equiv V_{L,R}^{u,d\dagger} C_{L,R}^{u,d(n)} V_{L,R}^{u,d}. \tag{3.17}$$

Since the C matrices are not the identity, these couplings are not diagonal in flavor space, and hence there will be flavor-changing currents in the KK gauge sector. In particular there will be tree-level FCNC mediated by the KK gluon states.

Processes that involve these tree-level FCNC are the source of the strong constraints on split fermion models. However, if one compares the FCNC effects in our model to the split fermion models, for the same value of the ρ parameter, the magnitude turns out to be much smaller. We can measure the magnitude of the FCNC with the difference of couplings between two fermion species $g_i^{(n)} - g_j^{(n)}$, since the FCNC will vanish if this difference does. Figure 3.3 shows the difference of couplings as a function of the KK number n, of two fermion species; in the first case two fermions of the same width and $\rho = 1/10$ separated by 4σ; in the second two fermions at the same location, one with $\rho_i = 1/10$, the other with $\rho_j = 1/20$. The total effect is the sum over n, or roughly the integral of the curves. Clearly the effect is much smaller in the variable width case.

The reason for this suppression can be understood quite simply. When the fermion species are directly on top of one another and with the same width the flavor changing currents are zero. When they are separated the non-universality of the couplings comes from the different heights of the KK wavefunctions at the location of the fermions. So every KK state, starting from $n = 1$, can resolve the difference, up to the cutoff $n \approx 1/\rho$. When the fermions are localized to the same point and the widths are changed the non-universality can only start to be resolved when the KK wavefunctions oscillate fast enough to resolve the widths. In this case the first few KK states will have nearly universal couplings, and the large flavor difference won't start until roughly $n \approx 1/\rho_>$, where $\rho_>$ is the larger of the two widths, and will only last until $n \approx 1/\rho_<$. Additionally, if there is only one extra dimension, the mass in the KK propagator provides a $1/n^2$ suppression in the sum, further suppressing the FCNC from variable widths, while leaving the FCNC from the first few KK modes from

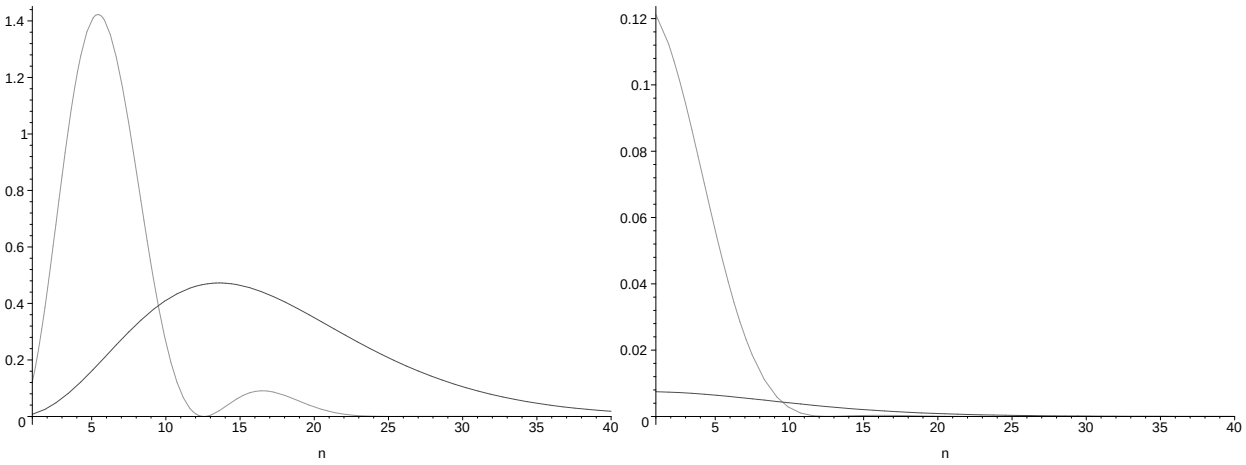

Figure 3.3: Comparison of the flavor-changing effects of models with split fermions (upper curve) and different widths with $a = 2$ (lower), for the same hierarchy of scales, $\sigma/R = 1/10$. Left: the difference of couplings as a function of n. Right: the same difference multiplied by $1/n^2$, as it would appear in the KK sum. Flavor changing currents are proportional to the sum over n of the right curves.

split fermions large. Note that this argument does not depend crucially on the shape of the fermion wavefunctions. The key points are the slow variation of the gauge wavefunctions for small n over the size of the fermions, and the $1/n^2$ suppression in the propagator. Thus the argument holds for any value of a, and indeed would hold for very different, potentially very irregular, shapes of the fermions. The only requirement is that they all fall off exponentially or faster from the same point on length scales of order the first KK mass.

The most stringent specific constraint comes from the mass splitting in the neutral kaon sector, Δm_K. The calculation of Δm_K here is identical with that in the split fermion case, except for the form of the sum over KK-modes. In [115] it was found

that

$$\begin{aligned}\Delta m_K =& \mathcal{R}e\,\langle \bar{K}^0|\mathcal{L}^{\Delta S=2}|K^0\rangle \\ = \frac{2}{3}R^2 f_K^2 m_K \mathcal{R}e\,\Bigg(& |V^d_{L\ 11}V^{d*}_{L\ 12}|^2\zeta_1\sum_{n=1}^{\infty}\frac{(g_{d_L}-g_{s_L})^2}{n^2} + |V^d_{R\ 11}V^{d*}_{R\ 12}|^2\zeta_1\sum_{n=1}^{\infty}\frac{(g_{d_R}-g_{s_R})^2}{n^2} \\ & + (V^d_{L\ 11}V^{d*}_{L\ 12}V^{d*}_{R\ 11}V^d_{R\ 12})\zeta_2\sum_{n=1}^{\infty}\frac{(g_{d_L}-g_{s_L})(g_{d_R}-g_{s_R})}{n^2} \\ & + (V^d_{R\ 11}V^{*d}_{R\ 12}V^{*d}_{L\ 11}V^d_{L\ 12})\zeta_2\sum_{n=1}^{\infty}\frac{(g_{d_L}-g_{s_L})(g_{d_R}-g_{s_R})}{n^2}\Bigg),\end{aligned} \tag{3.18}$$

where the ζ_i are the dimensionless part of the hadronic matrix elements and are given by

$$\begin{aligned}\zeta_1 &= \frac{1}{3}, \\ \zeta_2 &= \left(\frac{1}{12}+\frac{1}{4}\left(\frac{m_K^2}{m_d^2+m_s^2}\right)\right),\end{aligned} \tag{3.19}$$

when computed in the vacuum insertion approximation [78]. Requiring this to not be larger than the observed value produces a constraint on $1/R$, given a value of ρ,

$$\frac{1}{R} \geq 1960\,\text{TeV}\sqrt{\mathcal{R}e\left(\zeta_1\sum(\text{LL}+\text{RR})+\zeta_2\sum(\text{LR}+\text{RL})\right)}, \tag{3.20}$$

where LL is the left-left term in Eq. (3.18), etc..

We have calculated Δm_K for the configuration given in section 3.3. Fig. 3.4 shows the constraint for a range of ρ. This demonstrates clear power-law behavior, with $1/R = (73.8\,\text{TeV})\rho^{1/2}$. We see that for very large values, say $\rho = 10^{-1}$, we have large constraints $1/R \geq 30\,\text{TeV}$. One can get down to the direct production constraint of $1/R \geq 2\,\text{TeV}$ by going to $\rho \approx 10^{-3}$. The constraints here turn out to be very close to those obtained for the model of Kaplan and Tait [113], where they localized fermions to exponentials centered at one of two fixed points, much like here, but still produced small Yukawa matrix elements by separating the left and

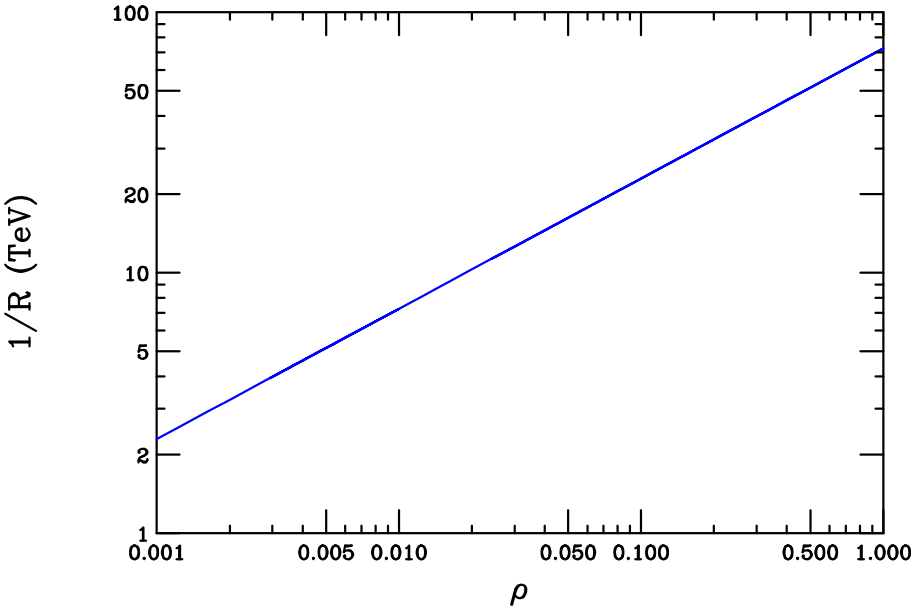

Figure 3.4: Constraints on the compactification scale $1/R$ from Δm_K as a function of $\rho = \sigma/R$, the ratio of the compactification scale to the fermion localization scale. The area below the curve is excluded.

right handed components.[1] Since they presumably have very different $V_{L,R}^{u,d}$ mixing elements, this shows that the flavor constraints on variable width models are quite robust. These constraints are to be contrasted with the similar results for the split fermion case, where $1/R \geq 400\,\text{TeV}$ for $\rho = 10^{-1}$ and $1/R \geq 60\,\text{TeV}$ for $\rho = 10^{-3}$; in those models one must go to $\rho \approx 10^{-5}$ before the flavor constraints are similar to direct production constraints.

Note that in several places it was claimed that the constraint from ϵ_K was even larger than that from Δm_K [68, 3, 113]. This can be seen from the ϵ_K equivalent to Eq. (3.20)

$$\frac{1}{R} \geq 40,900\,\text{TeV}\sqrt{\mathcal{I}m\left(\zeta_1 \sum(\text{LL}+\text{RR}) + \zeta_2 \sum(\text{LR}+\text{RL})\right)} \tag{3.21}$$

However, the imaginary part is, in fact, quite small. For $\rho = 10^{-1}$, the factor in the

[1] The paper [113] presents results for $\rho = 10^{-1}$. The apparent disagreement between the numbers quoted there and here is due to a normalization factor of 2π between their M_c and our $1/R$.

square root is 1.6×10^{-3}, leading to a constraint $1/R \geq 6.6\,\text{TeV}$; this is much smaller than the constraint from Δm_K.

3.5 Discussion

In previous sections we have tried to emphasize the aspects which are independent of the mechanism for the variable width scenario of fermion localization. Here we discuss possible techniques of fermion localization that produce this scenario. The easiest implementation of localized fermions is on a five-dimensional space with the extra dimension compactified on S_1/Z_2. The fermions are then coupled to a scalar field that is odd under the Z_2 action of the orbifold. It can then be shown that the fermions will develop chiral zero modes localized near one of the orbifold fixed points [81]. This Lagrangian is given by

$$\mathcal{L} = \sum_i \bar{\Psi}_i (i \not{\partial} - \gamma^5 \partial_5 - f_i \varphi) \Psi_i + \frac{1}{2} \partial^\mu \varphi \partial_\mu \varphi - \frac{1}{2} \partial_5 \varphi \partial_5 \varphi - \frac{\lambda}{4} (\varphi^2 - v^2)^2, \qquad (3.22)$$

where here we allow each fermion to have a separate coupling, f_i, to φ. Since φ is odd under the orbifolding it must vanish at each of the fixed points, $y = 0$ and $y = \pi R$. However, if λv^2 is large enough φ will develop a y-dependent vev, $h(y)$, that is zero on the fixed points and is non-vanishing elsewhere. The fermions then develop zero modes with profiles

$$\psi_i(y) \propto e^{-f_i \int_0^y dy' \; h(y')}. \qquad (3.23)$$

This is localized near $y = 0$ if $f_i h(y) > 0$, and at $y = R$ otherwise. The class of models parameterized by a in Eq. (3.1) can be constructed by demanding that $h(y)$ behave like $h(y) \approx k y^{a-1}$ near $y = 0$ for some constant k, and picking all the f to have the same sign as $h(y)$, so all fermions are localized to $y = 0$. The fermions are then localized as in Eq. (3.1) with width parameter $\sigma_i = (f_i k)^{-1/a}$.

Note that this construction does not appear to generate any non-trivial phases in the Yukawa matrices with which we could generate $\phi_{1,2}$. However, phases will

be present if one allows the localizer field φ to be complex and imposing boundary conditions on the phase at the orbifold fixed points. For instance we could require that $\arg(\varphi(y=0))=0$ and $\arg(\varphi(y=R))=\pi/2$. The vev then has a profile $ve^{i\frac{\pi}{2}\frac{y}{R}}$. This still results in localized fermions, but the Yukawa matrix elements pick up phases relative to each other, since the phase at each point will be weighted differently due to the distinct widths. For fermions with width ratios of order those given in the solution in section 3.3 with $1/R \approx 5\,\mathrm{TeV}$, we find phase differences of order $\phi = 0.03$, so this looks like a promising way to make a realistic construction of this scenario.

Another interesting example of fermion localization occurs in the RS scenario. In this case, the fermions are localized near a brane with $a = 1$ profiles, and possibly different widths [101]. The gauge boson wavefunctions are Bessel functions rather than cosines, so the flavor analysis in section 3.4 is not strictly applicable. However, since the low KK-number wavefunctions are reasonably flat, the reasoning that the flavor changing currents are small will still hold. This has been seen explicitly in [108].

One would like to embed the variable widths model in a larger scenario that, for instance, solves the Higgs mass hierarchy problem. The fermions and gauge bosons could be localized within a thick brane embedded in a larger dimension of the ADD type. Or the complete manifold could be $AdS_5 \times (S_1/Z_2)$ with the RS scenario playing out in the AdS_5 and the fermion mass generation playing out in the S_1/Z_2 [65]. Unfortunately, with all fermions localized at a single point there is nothing to suppress the proton decay operators that tend to occur in these models, unlike in the original split fermion scenario. However, a simple twist on this scenario can restore this suppression. Instead of a single fixed point, there could be two points, with the quark fields localized on one of them, and the leptons on the other, as shown in Fig. 3.5. Proton decay operators are then suppressed by approximately $e^{-\frac{3}{4}l^2}$, where l is the separation between the two fixed points, in units of the scale of the fermion widths. Note that this changes none of the conclusions above about the generation of the mass hierarchy. In the simple S_1/Z_2 model presented above this could be accomplished by taking the couplings to φ for quarks to be $f_i > 0$ and for leptons $f_i < 0$.

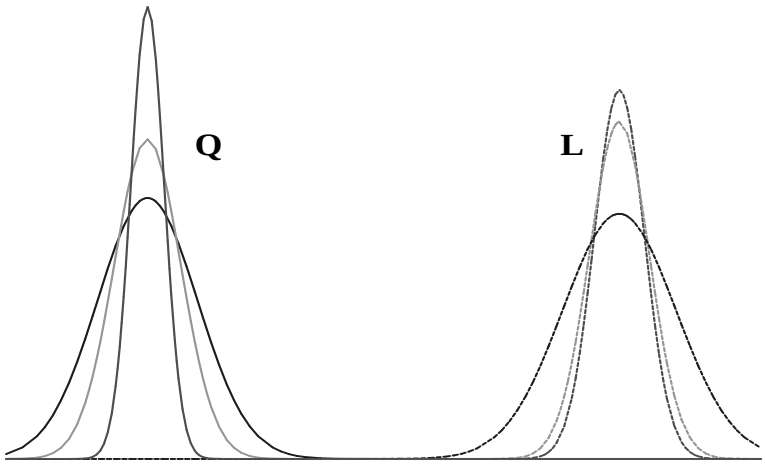

Figure 3.5: Illustration of a configuration that would suppress proton decay while generating the Yukawa hierarchy with variable widths.

We could also try to modify the model in order to generate the ratios λ_5^u/λ_5^d and λ_5^u/λ_5^e, rather than having to put them in by hand. One way to do this would be to make use of the original AS suggestion of separating left and right handed fermions. The up-type singlets, u_i, could be very close to the quark doublets, Q_i. The down-type singlets, d_i, could then be farther away (about 2σ for $a = 2$), and the lepton doublets and charged singlets separated slightly farther than that. This is then a hybrid model where the hierarchies between fermions with the same charge are generated by the different widths, and the hierarchy between those with different charges is generated by the exponentially small overlaps. Combined with separating the lepton wavefunctions to suppress proton decay, one obtains the picture in Fig. 3.6. The whole assembly with $a = 2$ requires about 10σ of length in the additional dimension; most of that is needed to suppress proton decay. Note that as long as all fermions with the same quantum numbers are localized to the same place the suppression of FCNC described above will apply.

3.6 Conclusion

We have proposed a model that localizes fermions with different widths in a single, compact, extra dimensional bulk, and shown that this produces a realization of the

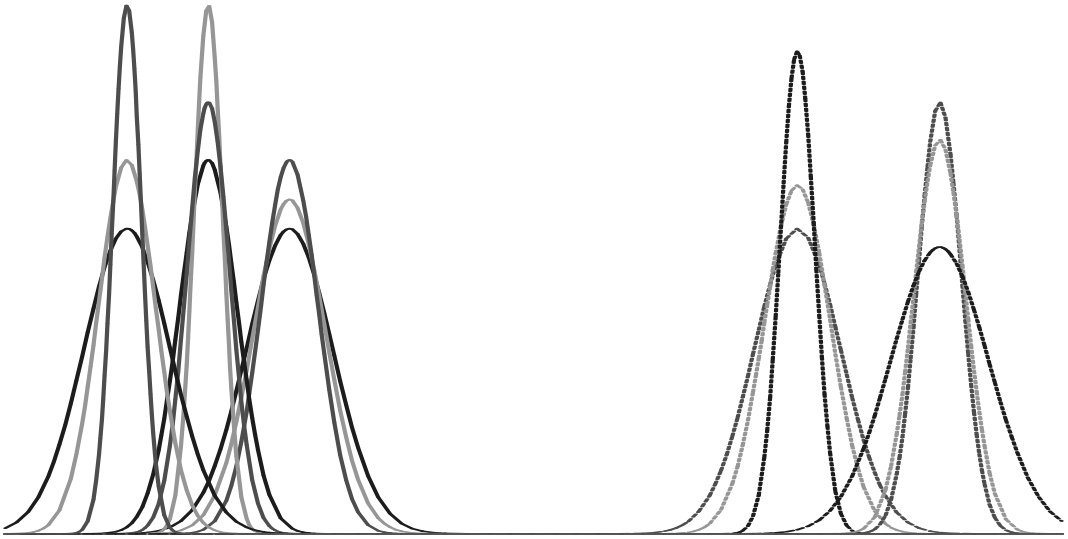

Figure 3.6: Illustration showing a "Swiss Army Knife" configuration. It generates the hierarchy between generations with the variable width method; uses split fermions to generate the hierarchy between the top mass and the bottom and τ masses; and suppresses proton decay by localizing quarks and fermions to different fixed points.

democratic scenario of fermion mass matrices. Ratios of the fermions widths that are $\mathcal{O}(1)$ can produce the observed fermion masses and mixing angles. With the inclusion of additional small phases one can reproduce all Standard Model parameters in the fermion sector, including the CP-violating CKM phase. This is not a reduction of parameters, but it does explain the large hierarchy in Yukawa couplings in terms of a simple physical picture. The tree-level FCNC contributions are smaller than in similar models by about a factor of 10 per flavor changing vertex. The resulting constraints on the compactification scale can be as small as $1 - 2\,\text{TeV}$ if one allows the ratio of localization to compactification scales to be $\rho \approx 10^{-3}$. This advantage in reducing FCNC effects comes not so much from the particular mechanism of localization, but rather from the facts that all fermions are localized to the same point, and that the gauge boson KK wavefunctions are very smooth for the first few modes, so they fail to resolve the difference in fermion zero modes. When the KK mode number n is high enough to resolve the differences in fermions the $1/n^2$ suppression is large. It is also interesting that the mechanism for generating the Yukawa hierarchy does not depend on the shape of the fermion wavefunction near the localization point, as long

as it is exponential far away. It only requires $\mathcal{O}(1)$ differences between overlaps of the wavefunctions. As long as they were all appropriately localized, the zero-mode wavefunctions could be extremely irregular and still generate the correct fermion hierarchy while being consistent with the FCNC constraints. It may also be possible to reduce the FCNC constraints further by the inclusion of the effects of brane-localized kinetic terms, which were not considered here [42, 66].

Effects of variable width localization could be observable at future colliders, particularly in flavor-changing processes. Even if direct effects are not seen at the LHC, precision measurements of mass splittings or rare B decays may provide clues. In [22], it was noted that when fermions are separated in an extra dimension, one might be able to observe cross sections that fall exponentially in the center-of-mass energy in certain channels. There it was proposed to look at polarized e^+e^- collisions to search for split fermions. In the scenario presented here this may apply to high energy ep collisions if the quark and lepton separation prevents proton decay.

Note Added: While this paper was being completed a similar paper [151] appeared. There, a specific model for the vev in section 3.5 was made and the Standard Model parameters were obtained.

Chapter 4

Higgsless electroweak symmetry breaking in warped backgrounds: Constraints and signatures

4.1 Introduction

After more than 30 years of experimental investigation, the mechanism for electroweak Symmetry Breaking (EWSB) remains unknown. The simplest picture of EWSB employs a scalar field, the Higgs, whose vacuum expectation value provides masses for the Standard Model (SM) $W^{\pm}$, Z bosons, as well as for the fermions. Experiments have yet to find this particle, even though generic expectations place it within the reach of recent searches. Direct searches place the lower limit on the Higgs mass of $m_h \gtrsim 114$ TeV, whereas a global fit to the precision electroweak data set [91] places the indirect upper bound of $m_h < 219$ GeV at 95% CL.

On a more theoretical level, a weak scale Higgs scalar seems unnatural, as its mass is typically expected to receive large radiative corrections from UV physics. Thus, a hierarchy problem arises, as there seem to be much higher scales present in Nature, such as the Planck scale of gravity, $\overline{M}_{Pl} \sim 10^{18}$ GeV. This problem may be resolved by the addition of new physics at the weak scale, such as Higgs compositeness, strong dynamics (technicolor), or supersymmetry. None of these proposals have been

experimentally verified, and they also suffer from various phenomenological problems.

Over the past few years, the possibility of extra spatial dimensions has been exploited to address the hierarchy conundrum. In particular, the warped 5-dimensional (5-d) Randall-Sundrum (RS) model [136], which is based on a truncated AdS_5 space-time, offers a natural geometric setup for explaining the size of the weak scale. In this model, the weak scale is generated exponentially from the curvature of the extra dimensional space. The AdS/CFT conjecture in string theory [120] suggests that the RS model is dual to a 4-d strongly interacting field theory. The Higgs in the 5-d picture is then identified with a dual 4-d composite scalar.

It has been recently proposed [55] that one could use the boundary conditions of a 5-d flat space $\mathrm{SU}(2)_L\times\ \mathrm{SU}(2)_R\times\ \mathrm{U}(1)_{B-L}$ theory to generate masses for $W^{\pm}$ and Z bosons of the SM, in the absence of a Higgs scalar. This proposal predicted unacceptably large deviations from precision EW data and seemed to be excluded. However in Ref.[56], this Higgsless approach to EWSB was studied in the context of the RS geometry, and agreement with data was much improved. This can be understood from the fact that the model contains a custodial SU(2) symmetry, as noted in Ref. [9] which is broken only by terms of size of order the spatial variance of the bulk W and Z wavefunctions. In the warped geometry, these wavefunctions are nearly flat over most of the bulk, as opposed to the $\mathcal{O}(1)$ spatial variance in the case of flat space.

Using the AdS/CFT correspondence [120], one may think of this proposal as a technicolor model without a Higgs scalar. This duality also addresses the improved agreement of the warped model with data, since the global $\mathrm{SU}(2)_L\times\ \mathrm{SU}(2)_R$ symmetry in the bulk provides the equivalent of a 4-d custodial symmetry that suppresses corrections to the EW observables. Here, we note that even though this construct is dual to some strong dynamics, the warped 5-d geometry could in principle provide a computationally controlled theory, with quantitative predictions.

In this paper, we study a 5-d Warped Higgsless Model (WHM), employing a set of parameters that is more general than those used in the original model of Ref.[56]. In particular, we allow for independent bulk gauge couplings to the L and R gauge sectors, which is crucial in getting good agreement with the precision EW data. We

also include the effects of UV boundary gauge kinetic terms, assuming that they are radiatively generated [128]. We do not specify a mechanism for fermion mass generation, but adopt a simple parametrization that could accommodate a large class of possible scenarios.[1] In addition, our analysis incorporates all higher order corrections from the curvature of the 5-d space that were ignored in the initial work[56].

We will demonstrate that with typical values for the model parameters, good agreement with the precision EW data can be achieved. However, we have found that perturbative unitarity in $W_L^+W_L^-$ gauge boson scattering is violated throughout the entire model parameter space. In particular, for the region where the good agreement with precision measurements is obtained, we find that unitarity is violated at $\sqrt{s} \approx 2$ TeV, which is below the mass of the new states studied by Csaki *et al.* [55]. We thus find that this model is not reliably predictive in its present form. However, assuming that unitarity can be restored by an appropriate modification of this scenario, *e.g.*, with the inclusion of additional non-Higgs states, we then consider the collider signatures which should be present in any generic WHM. In particular, we find that the gauge boson Kaluza Klein (KK) excitations of the strong and electroweak sectors are observable at the LHC. However, it is unlikely that the LHC experiments will be able to detect the spin-2 graviton KK resonances which constitute the most distinct signature of the conventional RS-based models.

In the next section, we introduce our formalism and notation. We then determine the couplings of the various KK towers to the SM fields in Section 3. Our predictions for the EW observables and the resulting parameter space constraints are given in Section 4. Unitarity is examined in Section 5 and the collider signatures of the model are discussed in section 6. Concluding remarks are given in Section 7.

4.2 Formalism and Notation

In the analysis that follows, we will, for the most part, follow the notation of Csaki *et al.*[56] with some modifications that are necessary to make contact with our previous

[1] We note that a recent paper [54] has proposed a mechanism for generating the fermion masses geometrically by also employing boundary conditions from the WHM configuration.

work [63, 134, 60, 41]. For this reason we now review the RS metric in both notations. In the original RS scheme (employed in our earlier work), the 5-d metric is given by

$$ds^2 = g_{MN}dx^M dx^N = e^{-2\sigma}\eta_{\mu\nu}dx^\mu dx^\nu - dy^2\,, \tag{4.1}$$

with uppercase Roman indices extending over 5-dimensional space-time and Greek indices corresponding to 4-d. Here, $\sigma = k|y| = kr_c|\phi|$, with r_c being the compactification radius, k is the curvature scale associated with the 5-d space, and $-\pi \leq \phi \leq \pi$ with ϕ parameterizing the 5th coordinate. For numerical purposes we will take $kr_c = 11.27$ throughout our analysis. The geometrical setup contains 2 branes, one residing at $\phi = 0$ (known as the Planck brane) and one at $\phi = \pi$ (the TeV brane), *i.e.*, the branes are located at the boundaries of the 5-dimensional Anti-de Sitter space. We define the quantity $\Lambda_\pi \equiv \overline{M}_{Pl}e^{-\pi kr_c}$, which represents the scale of physical processes on the TeV brane. In the scheme used in Ref. [56], this metric is rewritten as

$$ds^2 = \left(\frac{R}{z}\right)^2(\eta_{\mu\nu}dx^\mu dx^\nu - dz^2)\,, \tag{4.2}$$

with $R \leq z \leq R'$. Here, we see that the relationships $k = R^{-1}$, $R' = Re^{\pi kr_c}$, and $z = e^{ky}/k$ converts one form of the metric to the other. In this convention, the Planck (TeV) brane resides at $z = R\,(R')$. It is important to note that the range $R \leq z \leq R'$ maps onto only *half* of the $-\pi \leq \phi \leq \pi$ interval. When employing the Csaki *et al.* notation in what follows, we will normalize our wavefunctions over twice the $R \leq z \leq R'$ interval for consistency with our earlier work.

In the WHM, the gauge theory in the bulk is $\mathrm{SU}(3)_C \times \mathrm{SU}(2)_L \times \mathrm{SU}(2)_R \times \mathrm{U}(1)_{B-L}$ for which the bulk action is given by

$$S = \int d^4x dy\,\sqrt{-g}\sum_i \frac{-1}{4g_{5i}^2}F^i_{AB}F_i^{AB}\,, \tag{4.3}$$

where we have suppressed the group indices, $-g \equiv det(g_{MN})$, the sum extends over the four gauge groups, and g_{5i} are the appropriate 5-d coupling constants. Note that for generality, we allow for the possibility of $g_{5L} \neq g_{5R}$ in our analysis below. The boundary conditions are chosen such that the gauge symmetry breaking chain

$\mathrm{SU}(2)_R\times\ \mathrm{U}(1)_{B-L} \to \mathrm{U}(1)_Y$ occurs at the Planck scale and subsequently the gauge symmetry breaking $\mathrm{SU}(2)_L\times\ \mathrm{U}(1)_Y \to \mathrm{U}(1)_{QED}$ takes place at the TeV scale. This hierarchical two-step breaking scheme is analogous to that of the usual breaking pattern of the conventional Left-Right Symmetric Model [126]. After the gauge symmetry is broken at the Planck scale, a global $\mathrm{SU}(2)_R\times\ \mathrm{SU}(2)_L$ symmetry remains in the brane picture. This global symmetry is broken on the TeV brane to a diagonal group, $\mathrm{SU}(2)_D$, which corresponds to the SU(2) custodial symmetry present in the SM. It is the presence of this custodial symmetry which essentially preserves the tree-level value of unity for the ρ parameter in this model. Of the 7 generators present in the high-scale electroweak sector, 3 are broken near $\bar{M}_{Pl}$, 3 are broken near the TeV scale, leaving one generator for $\mathrm{U}(1)_{QED}$ as in the SM. $\mathrm{SU}(3)_C$, of course, remains unbroken and is simply the 5-d analog of QCD.

In addition to the bulk action above, significant boundary (brane) terms can exist in this scenario [128] which can be generated via quantum contributions[2] [80]. The only sizable effects arise at $y = 0$, *i.e.*, on the Planck brane, due to the renormalization group evolution (RGE) between the physical scales associated with the two branes, $\sim k$ and $\sim ke^{-\pi kr_c}$. Since the gauge group below the scale k is simply $\mathrm{SU}(3)_C\times$ $\mathrm{SU}(2)_L\times\ \mathrm{U}(1)_Y$, only these gauge fields will have brane localized kinetic terms, which we may write as

$$S_{brane} = \int d^4x dy\, \sqrt{-g}\, \delta(y) \left\{ -\frac{1}{4\tilde{g}_L^2} F_L^{\mu\nu} F^L_{\mu\nu} - \frac{1}{4\tilde{g}_Y^2} F_Y^{\mu\nu} F^Y_{\mu\nu} - \frac{1}{4\tilde{g}_s^2} F_C^{\mu\nu} F^C_{\mu\nu} \right\} , \qquad (4.4)$$

where

$$\frac{1}{\tilde{g}_i^2} = \frac{\beta_i}{8\pi^2} \ln(\frac{k}{ke^{-\pi kr_c}}) = \frac{\beta_i}{8\pi^2} \pi k r_c \,, \qquad (4.5)$$

for $i = L\,, Y\,, s$ and β_i being the appropriate beta function. If only SM fields are present in the model, then $(\beta_L\,, \beta_Y\,, \beta_s) = (-10/3\,, 20/3\,, -7)$; we will assume these values in our numerical analysis. Note that due to the large logarithms, these coefficients can be significant, of $\mathcal{O}(1)$ or larger, and will lead to important effects as will be seen below.

[2]There may be other brane terms in the effective theory that can be important on both the IR and UV branes. In this treatment, we ignore such possible terms.

In our earlier analysis [63], we introduced the notation

$$\frac{g_{5i}^2}{\tilde{g}_i^2} \equiv r_c c_i \equiv \frac{2\delta_i}{k}\,, \qquad\qquad (i = L\,, Y\,, s) \tag{4.6}$$

which is useful for quantifying the size of the brane kinetic terms. Given the above relations for $1/\tilde{g}_i^2$, and the assumption that only SM fields contribute to the beta functions, one can show that δ_Y is not an independent parameter, but is directly calculable. (We will return to the case of 5-d QCD later.) From Eq. (4.5) we have

$$\frac{1}{\tilde{g}_Y^2} = -2\frac{1}{\tilde{g}_L^2}\,, \tag{4.7}$$

where the factor of -2 arises from the ratio β_Y/β_L. This leads to

$$\frac{g_{5Y}^2}{\tilde{g}_Y^2} = -2\frac{g_{5Y}^2}{\tilde{g}_L^2}\,. \tag{4.8}$$

Since $\mathrm{SU}(2)_R\times\ \mathrm{U}(1)_{B-L} \to \mathrm{U}(1)_Y$, we have the relations

$$\frac{1}{g_{5Y}^2} = \frac{1}{g_{5R}^2} + \frac{1}{g_{5B}^2}\,, \tag{4.9}$$

which we can write as

$$\frac{g_{5L}^2}{g_{5Y}^2} = \frac{1}{\kappa^2} + \frac{1}{\lambda^2}\,, \tag{4.10}$$

by introducing the notation

$$\kappa \equiv \frac{g_{5R}}{g_{5L}}\,, \qquad\qquad \lambda \equiv \frac{g_{5B}}{g_{5L}}\,. \tag{4.11}$$

Solving the above for g_{5Y}^2, we obtain

$$\frac{g_{5Y}^2}{\tilde{g}_Y^2} = -2\frac{\lambda^2\kappa^2}{\lambda^2+\kappa^2}\frac{g_{5L}^2}{\tilde{g}_L^2}\,, \tag{4.12}$$

which yields

$$\delta_Y = -2\frac{\lambda^2\kappa^2}{\lambda^2+\kappa^2}\delta_L\,. \tag{4.13}$$

As we will see below, the value of λ will be determined by the $M_{W,Z}$ mass relationship while κ will remain a free parameter confined to a constrained region.

The following set of boundary conditions generate the symmetry breaking pattern discussed above (note that we suppress the Minkowski indices):
On the TeV brane at $z = R'$ $(y = \pi r_c)$ one has

$$\begin{aligned} \partial_z(g_{5R}A_L^a + g_{5L}A_R^a) &= 0\,; \qquad \partial_z A_C^a = 0\,; \\ g_{5L}A_L^a - g_{5R}A_R^a &= 0\,; \qquad \partial_z B = 0\,; \\ g_{5L}A_5^{La} + g_{5R}A_5^{Ra} &= 0\,; \qquad B_5 = 0\,; \\ \partial_z(g_{5R}A_5^{La} - g_{5L}A_5^{Ra}) &= 0\,, \end{aligned} \tag{4.14}$$

with $A_{L(R)}^a$ or A_C^a being one of the $\mathrm{SU}(2)_{L(R)}$ or $\mathrm{SU}(3)_C$ fields with gauge index a, and B being the corresponding $\mathrm{U}(1)_{B-L}$ field.
On the Planck brane at $z = R$ $(y = 0)$ the boundary conditions are

$$\begin{aligned} \partial_z A_L^a &= -\delta_L x_n^2 k\epsilon^2 A_L^a\,; \qquad \partial_z A_C^a = -\delta_s x_n^2 k\epsilon^2 A_C^a\,; \\ A_R^{1,2} &= 0\,; \qquad g_{5B}B - g_{5R}A_R^3 = 0\,; \\ \partial_z[g_{5B}A_R^3 &+ g_{5R}B] = -\delta_Y x_n^2 k\epsilon^2[g_{5B}A_R^3 + g_{5R}B]\,; \\ A_5^{La} &= 0\,; \qquad A_5^{Ra} = 0\,; \qquad B_5 = 0\,, \end{aligned} \tag{4.15}$$

where $\epsilon = e^{-\pi k r_c}$, and $m_n = x_n k\epsilon$ is the mass of the n^{th} gauge KK state. For the remainder of this paper, we will work in the unitary gauge, where the fifth components of the gauge fields are zero.

Recalling the breaking pattern for $\mathrm{SU}(2)_R \times \mathrm{U}(1)_{B-L} \to \mathrm{U}(1)_Y$, we introduce the fields

$$\begin{aligned} Y &= \frac{g_{5R}B + g_{5B}A_R^3}{\sqrt{g_{5R}^2 + g_{5B}^2}}\,, \\ \zeta &= \frac{g_{5B}B - g_{5R}A_R^3}{\sqrt{g_{5R}^2 + g_{5B}^2}}\,, \end{aligned} \tag{4.16}$$

and identify Y with the usual hypercharge field. In that case, the boundary condition

on the third line in Eq. (15) can be written more simply as

$$\partial_z Y = -\delta_Y x_n^2 k\epsilon^2 Y\,. \tag{4.17}$$

The KK decomposition we use is essentially that of Csaki *et al.*, but allowing for $g_{5L} \neq g_{5R}$ and is expanded to include the $\mathrm{SU}(3)_C$ group:

$$\begin{aligned}
B(x,z) &= \alpha_B\gamma(x) + \sum \chi_k^B(z) Z^{(k)}(x)\,,\\
A_L^3(x,z) &= \alpha_L\gamma(x) + \sum \chi_k^{L^3}(z) Z^{(k)}(x)\,,\\
A_R^3(x,z) &= \alpha_R\gamma(x) + \sum \chi_k^{R^3}(z) Z^{(k)}(x)\,,\\
A_L^\pm(x,z) &= \sum \chi_k^{L^\pm}(z) W^{(k)\pm}(x)\,,\\
A_R^\pm(x,z) &= \sum \chi_k^{R^\pm}(z) W^{(k)\pm}(x)\,,\\
A_C(x,z) &= \alpha_g g(x) + \sum \chi_k^g(z) g^{(k)}(x)\,,
\end{aligned} \tag{4.18}$$

where we have again suppressed the Lorentz indices and the sum extends over the KK tower states, $k = 1...\infty$. Here, $\gamma(g)$ is the massless photon(gluon) field and $\alpha_{B,L,R,g}$ are numerical constants which are determined from the boundary conditions. Note that since the photon and gluon zero-mode states are massless, their wavefunctions are z-independent, *i.e.*, they are 'flat' in z. The wavefunctions $\chi_k^A(z)$ take the form

$$\chi_k^A(z) = z(a_A^k J_1(m_k z) + b_A^k Y_1(m_k z))\,, \tag{4.19}$$

with $J_1\,, Y_1$ being first-order Bessel functions with the coefficients $a_A^k\,, b_A^k$ and the KK masses m_k to be determined by the boundary conditions as we now discuss.

Let us first consider the case of the charged gauge boson sector. We first introduce the notation,

$$\begin{aligned}
R_i &\equiv Y_i(x_n^W\epsilon)/J_i(x_n^W\epsilon)\,,\\
\tilde{R}_i &\equiv Y_i(x_n^W)/J_i(x_n^W)\,,
\end{aligned} \tag{4.20}$$

where $x_n^W k\epsilon$ are the masses of the $W^\pm$ KK tower states. Expressions for the coefficients $b_{L,R}^\pm\,, a_R^\pm$ in terms of $a_L^\pm$ can easily be obtained via the boundary conditions; we find (dropping the KK index for convenience)

$$\begin{aligned} b_L^\pm &= -\frac{a_L^\pm}{R_0} X_L\,, \\ b_R^\pm &= -\frac{a_R^\pm}{R_1}\,, \\ a_R^\pm &= -\kappa \frac{(1 - X_L \tilde{R}_0/R_0)}{(1 - \tilde{R}_0/R_1)} a_L^\pm\,, \end{aligned} \tag{4.21}$$

where $a_L^\pm$ will be determined by the wavefunction normalization and

$$X_L \equiv \frac{1 + \delta_L x_n^W \epsilon R_W}{1 + \delta_L x_n^W \epsilon R_1 R_W/R_0}\,, \tag{4.22}$$

with $R_W \equiv J_1(x_n^W\epsilon)/J_0(x_n^W\epsilon)$. The masses of the KK states can then be determined and are explicitly given by the root equation

$$(R_1 - \tilde{R}_0)(R_0 - X_L\tilde{R}_1) + \kappa^2 (R_1 - \tilde{R}_1)(R_0 - X_L \tilde{R}_0) = 0\,. \tag{4.23}$$

Note that for $g_{5L} = g_{5R}$, *i.e.*, $\kappa = 1$, and in the absence of boundary terms ($\delta_L = 0$, $X_L = 1$), this expression reduces to that obtained by Csaki *et al.* [56]. We will return to a study of the roots and corresponding gauge KK masses in the next section.

We now turn to the neutral electroweak sector and first consider the massive tower states. The boundary conditions yield (where $R_i\,, \tilde{R}_i$ are defined as above with

$W \to Z$)

$$\begin{aligned} b_L &= -\frac{a_L X_L}{R_0}\,, \\ b_R &= -a_L \frac{(1 - X_L\tilde{R}_1/R_0) + \kappa^2(1 - X_L\tilde{R}_0/R_0)}{\kappa(\tilde{R}_0 - \tilde{R}_1)}\,, \\ a_R &= -\kappa a_L(1 - X_L\tilde{R}_0/R_0) - b_R\tilde{R}_0\,, \\ b_B &= -\frac{a_B}{\tilde{R}_0}\,, \\ a_B &= -\frac{\lambda a_L(X_Y a_R/a_L + R_0 b_R/a_L)}{\kappa(X_Y - R_0/\tilde{R}_0)}\,, \end{aligned} \tag{4.24}$$

where now a_L is determined via normalization and we have defined

$$X_{L,Y} \equiv \frac{1 + \delta_{L,Y} x_n^Z \epsilon R_Z}{1 + \delta_{L,Y} x_n^Z \epsilon R_Z R_1/R_0}\,, \tag{4.25}$$

with $R_Z \equiv J_1(x_n^Z\epsilon)/J_0(x_n^Z\epsilon)$. The root equation for the neutral KK tower masses is then,

$$\begin{aligned} & -\lambda^2(\tilde{R}_0 - R_1)\Big\{\kappa^2 X_Y(\tilde{R}_0 - \tilde{R}_1)(R_0 - X_L - \tilde{R}_0) + (R_0 - X_L\tilde{R}_1)(R_0 - X_Y\tilde{R}_0) \\ + \;& \kappa^2(R_0 - X_L\tilde{R}_0)(R_0 - X_Y\tilde{R}_0)\Big\} \\ + \;& \kappa^2(R_0 - X_Y\tilde{R}_0)\Big\{\kappa^2(\tilde{R}_0 - \tilde{R}_1)(R_0 - X_L\tilde{R}_0) + (R_1 - \tilde{R}_0)(R_0 - X_L\tilde{R}_1) \\ + \;& \kappa^2(R_0 - X_L\tilde{R}_0)(R_1 - \tilde{R}_0)\Big\} = 0\,. \end{aligned} \tag{4.26}$$

Note that unlike the case where brane terms are neglected, this equation does not factorize into a pair of KK towers associated with the γ and Z. In fact, as we will see below, the γ and Z tower states are highly mixed and do not simply appear to be more massive copies of the SM photon and Z boson.

Turning to the case of the zero-mode photon, the fact that its wavefunction is constant in z trivializes all but two of the boundary conditions from which the coefficients

in Eq. (18) may be obtained:

$$\alpha_R = \alpha_L/\kappa\,, \qquad\qquad \alpha_B = \alpha_L/\lambda\,, \tag{4.27}$$

with α_L to be determined via normalization of the massless photon field.

For the remaining case of $SU(3)_C$, we see that α_g is determined via the normalization of the massless gluon field and the two boundary conditions lead to the single relation

$$b_s = -\frac{a_s X_s}{R_0}\,, \tag{4.28}$$

where X_s is defined from Eq. (22) with $x_n^W \to x_n^g$, $\delta_L \to \delta_s$. The mass spectrum of the gluon excitations are then given by the simple relation

$$R_0 - X_s \tilde{R}_0 = 0\,. \tag{4.29}$$

As before, a_s will be determined via the normalization conditions in the next section.

4.3 Determination of the KK Mass Spectrum and Couplings

In this section, we solve the various root equations to determine the mass spectrum and couplings of the KK sector. A priori, it would seem that the parameters $\kappa\,, \lambda$, and δ_L are completely arbitrary, but as we will see, some of them are determined by data. We first consider the $W^\pm$ KK tower. In this case, the root equation depends on κ and δ_L, and although $1/\tilde{g}_L^2$ is known, the ratio $g_{5L}^2/\tilde{g}_L^2$, which gives δ_L, is not. However, δ_L is not arbitrary and can be determined from the measured value of the Fermi constant in a self-consistent manner as follows. Our approach is: (i) we choose a value of κ and an input value of $\delta_L(=\delta_L^{in})$ and then calculate the roots x_n^W using Eq. (22). Since $m_{W_1} = M_W = x_1^W k\epsilon$ is identified with the physical $W^\pm$ state observed in experiment and is thus known, this fixes $k\epsilon$ so that the masses of all the KK excitations m_{W_n} can be determined. (ii) Now that the values of the x_n^W are known, the coefficients $a_R^\pm\,, b_{L,R}^\pm$

of the wavefunctions are also calculable; this allows us to determine the couplings of the KK states to the SM fermions. These are of the form

$$g_{W_n}^2 = N_n \frac{g_{5L}^2}{2\pi r_c} \,, \tag{4.30}$$

where the coefficients N_n are computed below. (*iii*) We observe that the above equation can be rewritten to give g_{5L}^2 provided that $g_{W_1}^2$, which corresponds to the usual W boson coupling, is known. We find

$$g_{5L}^2 = 2\pi r_c g_{W_1}^2 / N_1 \,, \tag{4.31}$$

so that

$$\delta_L^{out} = \pi k r_c \frac{g_{W_1}^2}{N_1 \tilde{g}_L^2} \,. \tag{4.32}$$

(*iv*) Next we must examine whether $\delta_L^{out} = \delta_L^{in}$ as a test of consistency. We recall from μ-decay that at tree-level,

$$\frac{8G_F}{\sqrt{2}} = \sum_{n=1}^{\infty} \frac{g_{W_n}^2}{m_{W_n}^2} = \frac{g_{W_1}^2}{M_W^2} \sum_{n=1}^{\infty} \frac{N_n}{N_1 (x_n^W / x_1^W)^2} \,, \tag{4.33}$$

with all the quantities in this equation being known except $g_{W_1}^2$. Hence solving for $g_{W_1}^2$ and inserting this result into the previous equation, we obtain a calculable expression for δ_L^{out},

$$\delta_L^{out} = \frac{\pi k r_c}{N_1 \tilde{g}_L^2} \frac{8 G_F M_W^2}{\sqrt{2}} \left[\sum_{n=1}^{\infty} \frac{N_n}{N_1 (x_n / x_1)^2} \right]^{-1} \,. \tag{4.34}$$

If $\delta_L^{out} \neq \delta_L^{in}$ for a fixed value of κ, we perform another search until convergence is obtained. When we have found a consistent solution (*i.e.*, $\delta_L^{in} = \delta_L^{out}$), $g_{W_n}^2$ and g_{5L}^2 are determined absolutely as a function of κ. We would expect δ_L to only weakly depend on κ since this dependence vanishes at zeroth-order in $1/\pi k r_c \simeq 1/35$. Here, we emphasize the importance of the μ-decay constraint in obtaining this result, as G_F determines the absolute strength of the coupling g_{W_1}, thus providing a reference to which all others can be scaled. Fig. 4.1 displays the value of δ_L^{out} versus δ_L^{in} for

$\kappa = 3$, for demonstration, and we see that a unique solution is obtained only when $\delta_L \simeq -7.8$; we find similar results for other values of κ near unity.

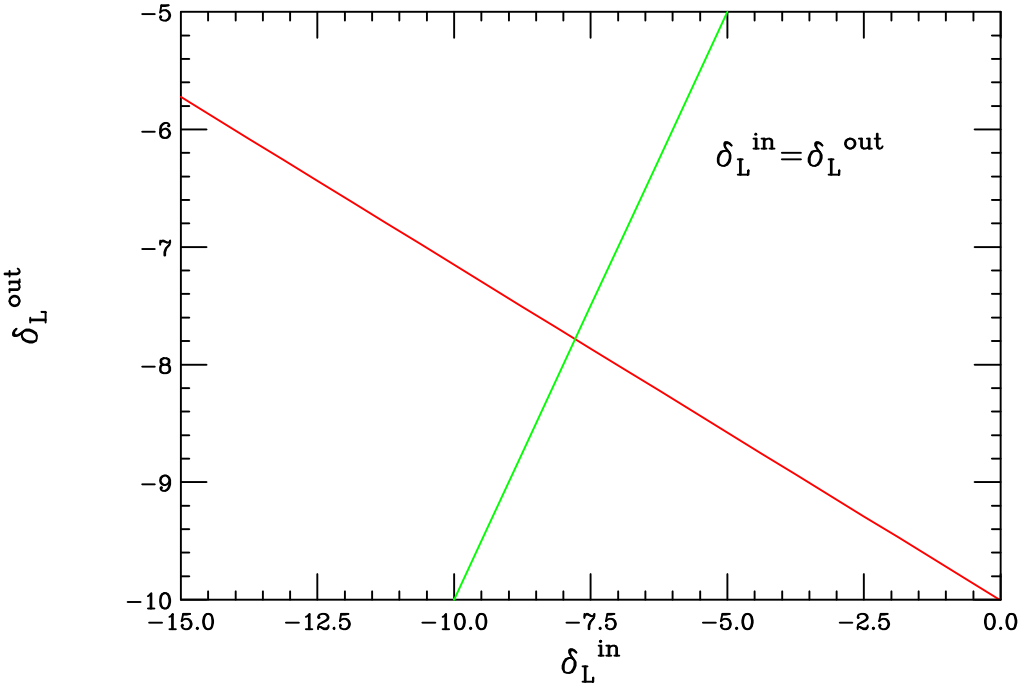

Figure 4.1: The value of $\delta_L (= \delta_L^{out})$ calculated via the procedure described in the text as a function of the input value (red curve). The curve corresponding to $\delta_L^{in} = \delta_L^{out}$ is also shown (green curve); the solution lies at the intersection of the two curves. Here, $\kappa = 3$ is assumed.

The parameter κ is bounded from below as can be seen from Eqs. (10) and (11) of Ref. [128] which apply at lowest order in $1/\pi k r_c$,

$$c_w^{-2} = \frac{M_Z^2}{M_W^2} = \frac{\kappa^2\lambda^2(1+D_L) + (\kappa^2+\lambda^2)(1+D_Y)}{(\kappa^2+\lambda^2)(1+D_Y)}\,, \tag{4.35}$$

where $D_{L,Y} = \delta_{L,Y}/\pi k r_c$, and $c_w = \cos\theta_w$ where θ_w is the weak mixing angle. Solving for λ^2, using $D_Y = -2D_L\kappa^2\lambda^2/(\kappa^2+\lambda^2)$, and demanding that $\lambda^2 > 0$, we obtain the bound

$$\kappa^2 > \frac{c_w^{-2} - 1}{1 + D_L(2c_w^{-2} - 1)}\,. \tag{4.36}$$

With $\delta_L \simeq -7.8$ and $c_w^2 \simeq 0.78$, this implies the constraint

$$\kappa \gtrsim 0.66\,. \tag{4.37}$$

Although there will be corrections to this result from terms of order $1/\pi k r_c$, we expect these to be no more than a few percent. To be concrete, we will assume that $\kappa \geq 0.75$ in our analysis.

It is also possible to obtain an approximate upper bound on κ based on perturbativity arguments, as the typical 4-d couplings $g_{4R}^2 \equiv g_{5R}^2/2\pi r_c$ cannot become too strong. A short analysis leads to the constraint that $\kappa \lesssim 4$. To be specific, we will thus limit ourselves to the range $0.75 \leq \kappa \leq 4$ in our study. This agrees with our expectations that on general grounds, the values of g_{5R} and g_{5L} should not be too different, implying that $\kappa \sim 1$.

Next, in order to define the KK couplings to SM fields, we need to discuss the localization of the SM fermions. (Note that we define the strength of the 'weak coupling' via the interaction of the SM $W^\pm$ boson and fermions.) In the original analysis of the WHM [55, 128], the SM fermions were all localized on the Planck brane; for further model-building purposes this need not be so [54]. However, it is well-known that if the fermions are localized close to the Planck brane their gauge couplings can be well approximated by the purely Planck brane values [62, 83]. We have checked that the gauge field wavefunctions are reasonably flat for fermions localized with $\nu \lesssim -0.6$, where the quantity ν is as defined in Ref. [62]. For simplicity, we thus make this assumption below. Under this assumption, the covariant derivative acting on these fields is given by

$$D^\mu = \partial^\mu + i g_{5L} T_L A_L^\mu + i g_{5R} T_R A_R^\mu + i g_{5B} \frac{B-L}{2} B^\mu + i g_{5s} T_s A_C^\mu\,. \tag{4.38}$$

In this case, following Csaki *et al.* [56] and Nomura [128], the couplings of the W_n KK states to the SM fermions are given by

$$g_{W_n}^2 = \Omega^2 \frac{g_{5L}^2 |\chi_n^{L^\pm}(R)|^2}{N_{W_n}}\,, \tag{4.39}$$

with

$$N_{W_n} = \int_R^{R'} dz \, \frac{R}{z} \left\{ |\chi_n^{L^\pm}(z)|^2 [2 + c_L r_c \delta(z - R)] + 2|\chi_n^{R^\pm}(z)|^2 \right\} , \tag{4.40}$$

where the relative factors of 2 arise from the interval extension discussed in the previous section. The coefficient Ω is determined numerically via the self-consistency procedure described above, which demands that for $n = 1$ (*i.e.*. the SM W boson), we recover the usual SM coupling $g^2_{W_1} = g^2_{SM}$. Thus, the W boson coupling automatically retains its known value by construction when we identify $W_1^\pm \equiv W_{SM}^\pm$ as the experimentally observed state (and correspondingly $m_{W_1} = M_W$ through the use of G_F). Using M_W and g^2_{SM} from experiment, we thus can determine the masses and couplings of all the higher KK modes. Here, we assume the LEPEWWG [91] central values of the SM gauge boson masses, $M_W = 80.426\,\text{GeV}$ and $M_Z = 91.1875\,\text{GeV}$ in our analysis.

Figure 4.2 displays the masses of the first few W KK excitations as a function of κ. We see that the masses grow reasonably rapidly as κ increases and can be quite heavy. For example, for $\kappa = 3$, the first $W^\pm$ excitation above the SM-like W boson, $W_2^\pm$, has a mass of $\simeq 2.32$ TeV. The masses of the higher KK states are approximately given by the root relation $x_n^W = x_2^W + (n-2)\pi$. The coupling strength of the gauge KK excitations are small relative to those for the $W^\pm$ and decrease rapidly as the KK mode number increases. *E.g.*, the first $W^\pm$ KK excitation has a fermionic coupling of only $g^2_{W_2} \simeq 0.0431 g^2_{SM}$. As we will see below, this will have important implications in the consideration of unitarity violation in $W_L W_L$ scattering.

We now turn to the neutral KK states and first discuss their mass spectrum. We will refer to these states as Z_n, but they are KK excitations of both the γ and Z and are mixtures thereof. In our analysis, we will force the W and Z bosons to have the correct masses, *i.e.*, those given by experiment, and will also make use of the on-shell definition of the weak mixing angle.

$$\cos^2 \theta_w^{os} \equiv \frac{M_W^2}{M_Z^2} \, . \tag{4.41}$$

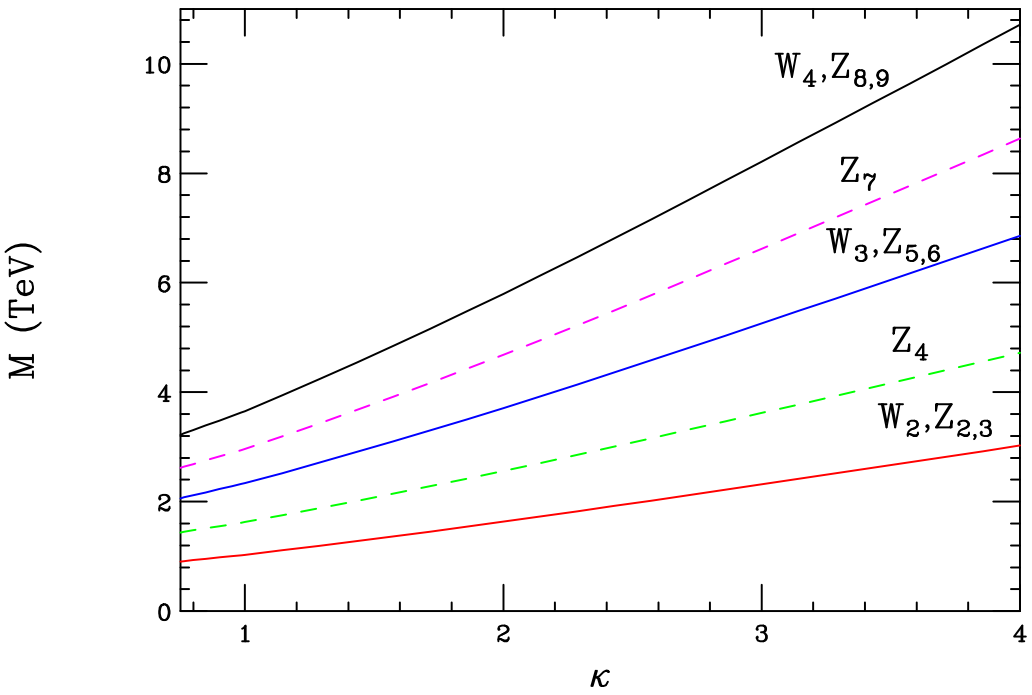

Figure 4.2: Masses of the electroweak gauge KK excitations as a function of κ. The solid curves correspond to the $W^{\pm}$ states, while the Z KK excitations correspond to both the solid and dashed curves as labeled. In the latter case, the solid curves correspond to the almost doubly degenerate states.

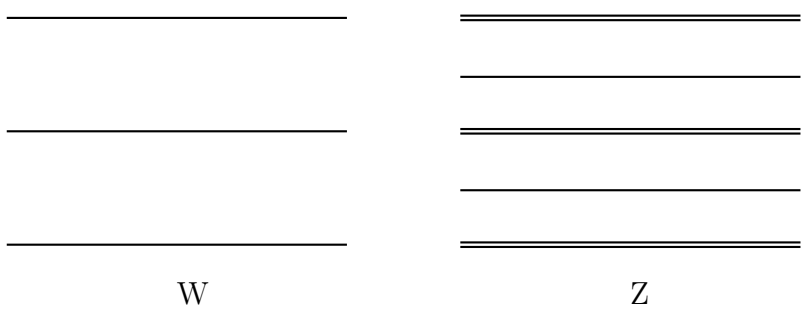

Figure 4.3: Schematic comparison of the $W^{\pm}$ and Z KK mass spectra showing that the $W^{\pm}$ KK states have masses almost identical to those of the degenerate pair of Z KK excitations.

Thus, determining the roots $x_1^W(\kappa)$ from the analysis discussed above, yields

$$x_1^Z(\kappa) = \frac{M_Z}{M_W} x_1^W(\kappa)\,, \tag{4.42}$$

with the ratio M_Z/M_W taken as exactly known. Note that we identify the lightest massive neutral KK state with the Z boson observed at LEP/SLC. In order to solve the Z_n eigenvalue equation (26), we input our chosen value of κ and our determined value of δ_L from which we can obtain δ_Y; λ remains an independent variable, but we pick its value in order to obtain the correct root x_1^Z above. Once this is accomplished, all of the electroweak parameters in the model (except κ) are completely determined, in particular, the Z_n KK tower masses and the wavefunction coefficients $a_{R,B}$ and $b_{L,R,B}$ of Eq. (19).

The masses of the Z_n KK tower states have an unusual behavior; there is a repeating pattern of a pair of almost degenerate states, followed by a single state, *e.g.*, the states Z_2 and Z_3 have a mass splitting of only 1%, Z_4 has no other nearby states, $Z_{5,6}$ are nearly degenerate, and so forth. In addition, the pair of states become more degenerate as the KK mode number increases. This KK mass spectrum is more easily understood by examining Figs. 4.2 and 4.3, where the W and Z KK spectra are displayed. Note that the W KK tower has a conventional mass spectrum, and each W KK mode coincides with the pair of degenerate Z KK states.

The couplings of the SM fermions to the massive Z_n KK tower states can be written in the suggestive form

$$\frac{g_{Z_n}}{c_w}(T_{3L}^f - s_n^2 Q^f)\,, \tag{4.43}$$

with $c_w = \cos\theta_w^{os}$ and $T_{3L}^f(Q^f)$ being the usual fermion third-component of weak isospin (electric charge). Matching with the form of the covariant derivative, the parameter s_n^2 is found to be given by

$$s_n^2 = \frac{-\lambda\chi_n^B(R)}{\chi_n^L(R) - \lambda\chi_n^B(R)}\,, \tag{4.44}$$

with $s_1^2 \equiv \sin^2\theta_{eff}$, *i.e.*, the value of the weak mixing angle obtained on the Z-pole. The values for s_n^2 vary significantly, even in sign, as the KK mode number varies. For example, for $\kappa = 3$, $s_2^2 = 0.743\,, s_3^2 = -0.109\,,$ and $s_4^2 = 0.218$. We note that for the KK levels which are non-degenerate, the value of s_n^2 is not too far from the on-shell value, $\sin^2\theta_w^{os} \simeq 0.22210$, as defined above. This can be understood as being due to the fact that the double states are mixtures of the γ and Z excitations, while the single states are almost pure Z excitations. Turning to g_{Z_n}, we know that in the SM $g_Z = g_W$, *i.e.*, $g_{Z_1} = g_{W_1}$ and it is traditional to define an effective ρ parameter

$$\rho_{eff}^Z = \frac{g_{Z_1}^2}{g_{W_1}^2} = \frac{g_Z^2}{g_W^2}\,, \tag{4.45}$$

which can be directly calculated once the g_{Z_n} are known. Matching with the covariant derivative, we find that these couplings can be written as

$$\frac{g_{Z_n}^2}{c_w^2} = \Omega^2 g_{5L}^2 \frac{|\chi_n^L(R) - \lambda\chi_n^B(R)|^2}{N_{Z_n}}\,, \tag{4.46}$$

where Ω is determined numerically as discussed above. The normalization in the absence of brane kinetic terms is easily obtained,

$$N_{Z_n}^0 = 2\int_R^{R'} dz\,\frac{R}{z}\,\left\{|\chi_n^L(z)|^2 + |\chi_n^R(z)|^2 + |\chi_n^B(z)|^2\right\}\,, \tag{4.47}$$

with the factor of 2 being related to the interval of integration as described above. In order to determine N_{Z_n} in the more general case we must return to the two actions in Eqns. (3) and (4). To simplify the discussion, we first rescale each gauge field by its appropriate 5-d coupling, $A_i \to g_{5i} A_i$, and concentrate solely on the action integrands which we can combine and write symbolically as

$$-\frac{1}{4}F_L^2 - \frac{1}{4}F_R^2 - \frac{1}{4}F_B^2 - \frac{1}{4}F_C^2 - \frac{1}{4}(c_L F_L^2 + c_Y F_Y^2 + c_s F_C^2) r_c \delta(y)\,. \tag{4.48}$$

From this it is clear how to normalize fields [63] which are purely composed of A_L or A_C as in the case of the $W^\pm$ above. The difficulty with the remaining fields is that both the gauge fields and brane terms are a mixture of the two bulk fields as can be seen from the definition of Y in Eq. (16). Rewriting the Y fields in terms of A_R^3 and B, substituting the KK decomposition into the respective field strength tensors for the neutral fields, and neglecting the QCD terms, we see that symbolically

$$\begin{aligned} &-\frac{1}{4}F_L^2 - \frac{1}{4}F_R^2 - \frac{1}{4}F_B^2 - \frac{1}{4}(c_L F_L^2 + c_Y F_Y^2) r_c \delta(y) \to \\ &|\chi_L|^2 + |\chi_R|^2 + |\chi_B|^2 + c_L r_c |\chi_L|^2 \delta(y) + c_Y r_c \left| \frac{g_{5R}\chi_B + g_{5B}\chi_R}{\sqrt{g_{5R}^2 + g_{5B}^2}} \right|^2 \delta(y) \\ &= |\chi_L|^2 (1 + c_L r_c \delta(y)) + |\chi_R|^2 + |\chi_B|^2 + c_Y r_c \left| \frac{\kappa\chi_B + \lambda\chi_R}{\sqrt{\kappa^2 + \lambda^2}} \right|^2 \delta(y)\,. \end{aligned} \tag{4.49}$$

Allowing for the extension of the integration range, this gives

$$\begin{aligned} N_{Z_n} &= \int_R^{R'} dz \, \frac{R}{z} \left\{ |\chi_L^n(z)|^2 (2 + c_L r_c \delta(z - R)) + 2|\chi_R^n(z)|^2 + 2|\chi_B^n(z)|^2 \right. \\ &+ \left. c_Y r_c \frac{|\kappa\chi_B^n(z) + \lambda\chi_R^n(z)|^2}{\kappa^2 + \lambda^2} \delta(z - R) \right\}\,, \end{aligned} \tag{4.50}$$

which reduces to the result above when the c_i are neglected. Note that this expression also tells us how to normalize the photon field, which is a constant (*i.e.*, z-independent) with the substitutions $\chi_L^\gamma = \alpha_L\,, \chi_R^\gamma = \alpha_L/\kappa\,,$ and $\chi_B^\gamma = \alpha_L/\lambda$. We will return to this point below. Given N_{Z_n}, the $g_{Z_n}^2$ are calculable and ρ_{eff}^Z can be directly determined; we find that in all cases $|\rho_{eff}^Z - 1| \lesssim 10^{-4}$. As in the case of

the W KK tower, these couplings are observed to decrease rapidly as the KK mode number increases. For example, if $\kappa = 3$, the first KK excitation above the Z has a coupling strength which is only $\sim 11\%$ of the SM Z boson.

Returning to the case of the photon, we note from the form of the covariant derivative that it couples as

$$\begin{aligned} & g_{5L} T^f_{3L} \chi^\gamma_L + g_{5R} T^f_{3R} \chi^\gamma_R + g_{5B} \frac{B-L}{2} \chi^\gamma_B \\ & = g_{5L} \alpha_L \left(T^f_{3L} + T^f_{3R} + \frac{B-L}{2} \right) \equiv g_{5L} \alpha_L Q^f \,, \end{aligned} \tag{4.51}$$

apart from a normalization factor which can be determined directly from N_{Z_n} above, giving

$$N_\gamma = 2\pi r_c \alpha_L^2 \left(\frac{\kappa^2 + \lambda^2 + \kappa^2\lambda^2}{\kappa^2 \lambda^2} \right) \left\{ 1 + \frac{1}{\pi k r_c} \frac{\kappa^2 \lambda^2 \delta_L + (\kappa^2 + \lambda^2)\delta_Y}{\kappa^2 + \lambda^2 + \kappa^2 \lambda^2} \right\} . \tag{4.52}$$

We thus obtain the α_L independent quantity

$$e^2 \equiv \frac{g_{5L}^2 \alpha_L^2}{N_\gamma} \,, \tag{4.53}$$

from which we can define the mixing angle

$$\sin^2 \theta_{eg} \equiv \frac{e^2}{g_{W_1}^2} \,, \tag{4.54}$$

where $g_{W_1}^2$ has been previously defined.

Note that in the above discussion we have introduced three different definitions of the weak mixing angle: (i) the on-shell value $\sin^2 \theta_w^{os}$, (ii) the effective value on the Z-pole, $\sin^2 \theta_{eff}$, and (iii) $\sin^2 \theta_{eg}$. In the SM, *at tree-level*, the values of these three definitions are, of course, equivalent. In the WHM, they need not be in general; however, if the model is to be consistent with experiment, it is clear that these three quantities must be reasonably close numerically. Fig. 4.4 shows these three definitions of $\sin^2 \theta_w$ as functions of the parameter κ, where $\sin^2 \theta_w^{os}$ is, of course, κ independent. As a rough guide, the figure also shows the current 1σ errors on the value of $\sin^2 \theta_w^{os}$

arising from the measured W and Z mass uncertainties. From this figure, we see that as κ increases the three values of $\sin^2\theta_w$ merge together. This is due to the KK masses becoming heavier as well as the strengthening of the $SU(2)_R$ couplings associated with the custodial symmetry which forces the WHM to become more like the SM. Clearly, for values of $\kappa \simeq 3-4$, the three definitions of the weak mixing angle are quite close numerically. It is interesting to note that this model predicts $\sin^2\theta_{eff}$ to be somewhat smaller than the on-shell value, *e.g.*, for $\kappa = 3$, $\sin^2\theta_w^{os} - \sin^2\theta_{eff} \simeq 0.0006$. This slightly lower value of $\sin^2\theta_{eff}$ is suggestive of the low value obtained from LEP and SLD [91] from measurements of the leptonic couplings of the SM Z.

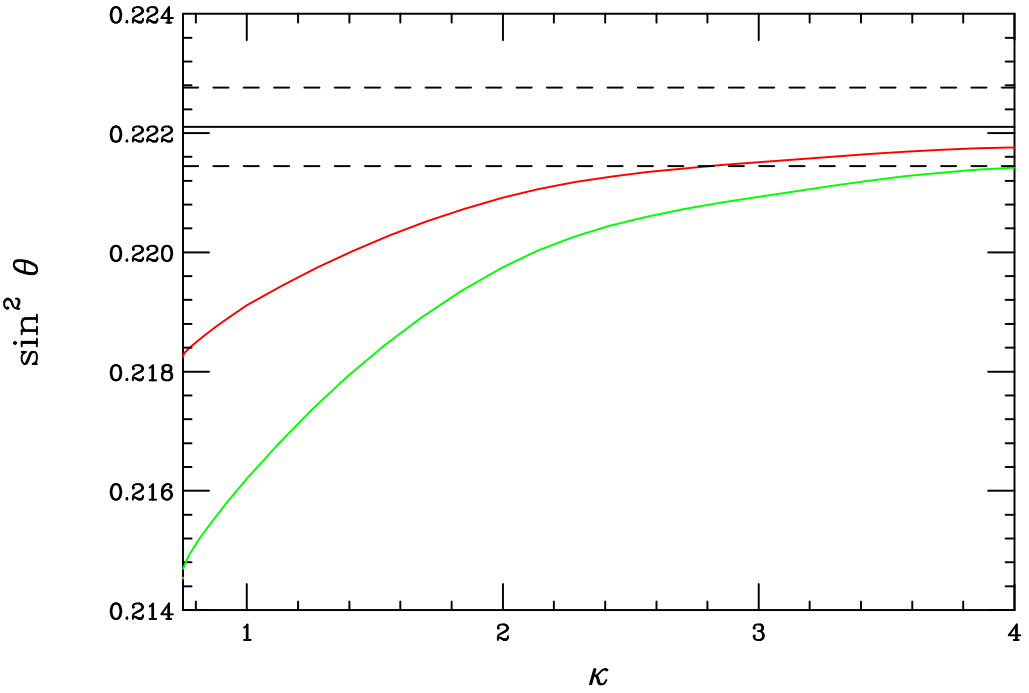

Figure 4.4: $\sin^2\theta$ in each of the three definitions as a function of κ. The black (upper), red (middle), and green (lower) curves correspond to the schemes $\sin^2\theta_w^{os}$, $\sin^2\theta_{eff}$, and $\sin^2\theta_{eg}$ defined in the text. The dotted curves show the present 1σ errors on $sin^2\theta_w^{os}$ from measurements of the Z and W masses.

Before we further discuss the electroweak parameters in the next section, we will conclude this section by examining the KK tower associated with the gluon. In analogy to the case of the photon, the massless gluon zero-mode has a flat, z-independent

wavefunction. This implies that the conventional strong coupling can be defined directly via the zero-mode coupling to fermions following from the boundary conditions and the KK decomposition. We thus can write

$$g_s^2 = \frac{g_{5s}^2}{2\pi r_c Z_0}\,, \tag{4.55}$$

where

$$Z_0 = 1 + \frac{c_s}{2\pi} = 1 + \frac{\delta_s}{\pi k r_c}\,. \tag{4.56}$$

Note that to maintain $Z_0 > 0$, $\delta_s \geq -\pi k r_c$ is required. Solving for g_{5s}^2 we obtain

$$g_{5s}^2 = \frac{2\pi r_c g_s^2}{1 - g_s^2/\tilde{g}_s^2}\,, \tag{4.57}$$

so that

$$\delta_s = \pi k r_c \frac{g_s^2}{\tilde{g}_s^2 - g_s^2}\,. \tag{4.58}$$

Since $1/\tilde{g}_s^2 = 1/\tilde{g}_L^2 \cdot (\beta_s/\beta_L)$ is known, δ_s can be directly calculated. Taking $\alpha_s = 0.118$ we obtain

$$\delta_s \simeq -29.14\,, \tag{4.59}$$

independent of κ.

Knowing the value of δ_s, we can now determine the gluon KK spectrum. Note that this value of δ_s is not far away from the critical region of $\delta = -\pi k r_c \simeq -35.4$ discussed above, where the KK spectrum and couplings become highly perturbed as shown in our earlier work [63]. In fact, for $\delta_s \leq -\pi k r_c$, the system becomes unphysical as ghost states appear. For the value of δ_s computed above, the first gluon KK excitation, g_1, is pushed upwards in mass by $\simeq 10\%$ in comparison to what would be naively expected for smaller values of the brane term, and hence m_{g_1} is roughly 200 GeV heavier than the first gauge KK excitation. The mass splitting for the higher gluon KK states are similar to those of the W KK tower.

The couplings of the gluon KK tower states can be directly calculated as in the

W and Z cases above from the covariant derivative,

$$\frac{g_{s_n}^2}{g_s^2} = 2\pi r_c Z_0 \frac{|\chi_n^C(R)|^2}{N_{s_n}}\,, \tag{4.60}$$

where

$$N_{s_n} = \int_R^{R'} dz\, \frac{R}{z} |\chi_n^C(z)|^2 [2 + c_s r_c \delta(z-R)]\,. \tag{4.61}$$

Here, we note that $g_{s_0}^2 = g_s^2$, the usual QCD coupling. The coupling of the first gluon KK state is displayed as a function of the strong brane term in Fig. 4.5, where we see that the KK states of the gluon are more strongly coupled, scaled to the zero-mode coupling strength, as compared to the other KK towers. For the higher KK levels, the ratio $g_{s_n}^2/g_s^2$ does not decrease as quickly as in, *e.g.*, the case of the corresponding W boson KK tower couplings. For example, $g_{s_2}^2/g_s^2 \simeq 0.233$, while we previously found $g_{W_2}^2/g_W^2 \simeq 0.043$. This is due to the large magnitude of δ_s.

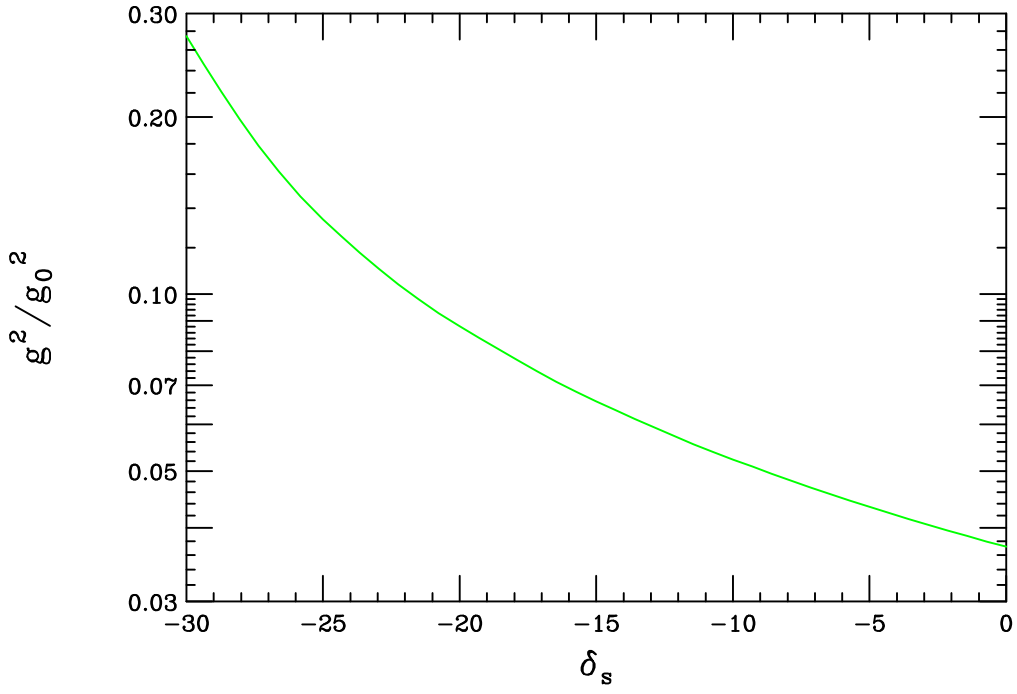

Figure 4.5: Behavior of the coupling of the SM quarks to the first gluon KK excitation as a function of the brane term δ_s, demonstrating the rapid growth in the coupling as $\delta_s \to -\pi k r_c$.

4.4 Electroweak Oblique Parameters

As discussed in the previous section, the WHM leads to a complete determination of the couplings of the $W\,, Z$ and gluon (as well as their KK towers) as a function of κ. We showed that the gauge boson zero-mode couplings to fermions are slightly different from their corresponding tree-level values in the SM, resulting in shifts from the SM expectations for the precision electroweak observables. It has become common practice in the literature to describe the influence of many classes of new physics on electroweak precision data at the one loop level through the use of the oblique parameters $S\,, T\,, U$ [132]. In the present model we have observed substantial deviations from SM expectations, *e.g.*, the three distinct values of $sin^2\theta$, already at the tree level. Similar parameter shifts are known to exist in the case of other sources of new physics, such as in the case of a simple Z' model [139, 14]. Though such corrections are not oblique, it has been shown[139, 14] that the shifts in several electroweak observables can be parameterized in a manner similar to that of $S\,, T\,, U$. In order to not confuse any such parameterization with the usual oblique parameters $S\,, T\,, U$,, we will denote these pseudo-oblique parameters as $\Delta S\,, \Delta T\,,$ and ΔU. We wish to emphasize that these quantities are being introduced solely as a device to demonstrate the deviations of the present scenario from SM expectations and they are not to be interpreted as the ordinary oblique corrections.

We take α, M_Z, and G_F to be input parameters in performing our fit to the electroweak measurements. Usually, when fitting the electroweak data the most important set of quantities to examine is M_W, $sin^2\theta_{eff}$ and the width for either $Z \to l^+l^-$ or $\nu\bar{\nu}$, *i.e.*, the invisible Z width. (Here we will employ the invisible width.) These quantities are either very precisely measured or are most unambiguously sensitive to new physics. We can then *parameterize* any deviations of these quantities away from their SM expectations through the usual definitions, employing the pseudo-oblique

parameters ΔS *etc.* [132, 36, 119]

$$\begin{aligned} \sin^2\theta_{eff} &= \sin^2\theta_0 + \frac{\alpha\Delta S}{4(c_w^2 - s_w^2)} - \frac{c_w^2 s_w^2 \alpha\Delta T}{c_w^2 - s_w^2}\,, \\ M_W^2 &= M_{W_{SM}}^2 \left[1 - \frac{\alpha\Delta S}{2(c_w^2 - s_w^2)} + \frac{c_w^2\alpha\Delta T}{c_w^2 - s_w^2} + \frac{\alpha\Delta U}{4s_w^2}\right]\,, \\ \Gamma_\nu &= \Gamma_{\nu_{SM}}(1 + \alpha\Delta T)\,, \end{aligned} \tag{4.62}$$

where α is the fine-structure constant. Note that here, we are simply exchanging the shifts from the SM predictions for the observables on the left-hand side of this equation for the pseudo-oblique parameters. We write $\Delta S(T, U)$ as shifts in these parameters away from their exact value at tree-level in the SM, *i.e.*, we recover the SM when the pseudo-oblique parameters vanish. Since we are comparing with the SM at tree-level we have $\sin^2\theta_0 = \sin^2\theta_w^{os}$. The ratio $\Gamma_\nu/\Gamma_{\nu_{SM}}$ is equal to ρ_{eff}^Z, using the notation of the previous section. Lastly, we have again imposed the requirement that M_W be in agreement with its SM value as defined by experiment, so that the expression in brackets on the right-hand side of the equation must vanish, thus forcing a relationship between the pseudo-oblique parameters. Since for all values of κ, ρ_{eff}^Z is found to differ from unity only at the order of a few $\times 10^{-5}$, it is clear that ΔT is very small. The expression for M_W then yields

$$\Delta U \simeq \frac{2s_w^2}{c_w^2 - s_w^2}\,\Delta S\,. \tag{4.63}$$

Using the values of ρ_{eff}^Z computed above and $\sin^2\theta_{eff}$ from the previous section, we can determine the pseudo-oblique parameters as a function of κ. This is displayed in Fig. 4.6. Here, we see that ΔT is very small as expected, ΔU tracks ΔS, and ΔS falls rapidly in magnitude as κ increases, as expected. The main point of this figure is to demonstrate that the pseudo-oblique parameters fall rapidly to zero as the value of κ increases; this is as expected since this limit approaches the SM.

The most recent fit to the oblique parameters has been performed by Erler [75] using the data presented at the 2003 summer conferences [91]. The results for this fit are highly correlated; using $m_H = 117$ GeV, Erler obtains the 1σ constraints

$S = -0.13 \pm 0.10$, $T = -0.17 \pm 0.12$ and $U = 0.22 \pm 0.13$. Slightly negative values of S, T are favored while the fit prefers slightly positive values of U. While we cannot directly compare to the data it is clear that the results of Fig 4.6, as well as Fig. 4, strongly suggest that a reasonably large value of $\kappa \gtrsim 3$, approximately reproduces the SM at tree-level.

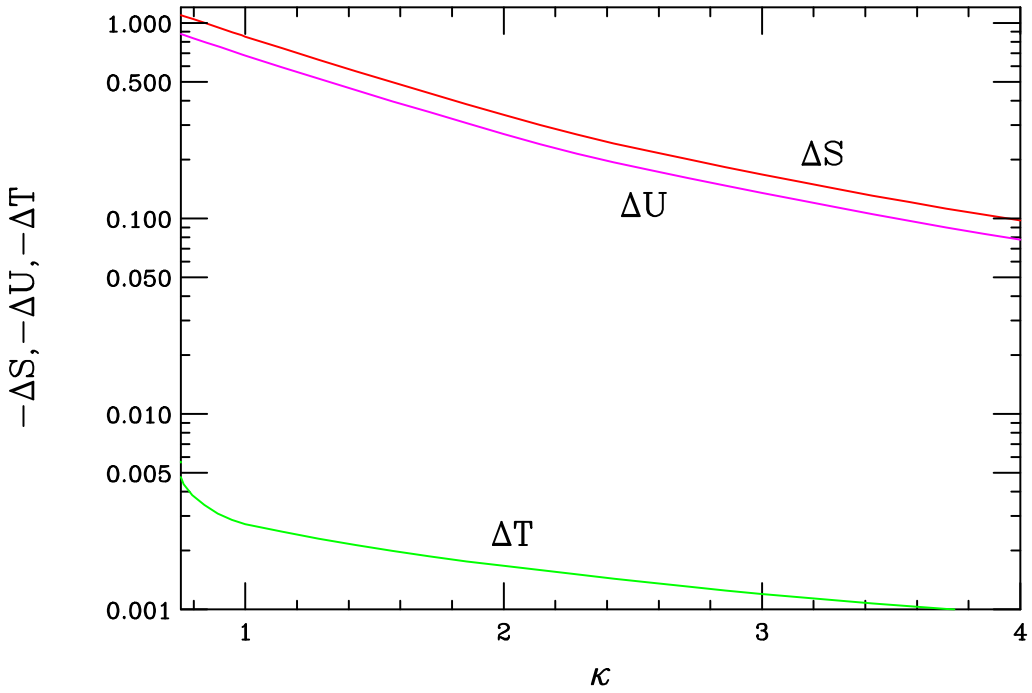

Figure 4.6: Shifts in the values of the pseudo-oblique parameters ΔS, ΔT, and ΔU as a function of κ from the tree-level analysis discussed in the text.

We recall that at loop level, S, T, and U are traditionally determined from the gauge boson self-energies [132]. Note that we are now working with the formal definitions of $S\,, T$ and U from [132]. Loop contributions are of order α, so they may also be important compared to the tree-level values discussed above. To leading order in $1/(\pi k r_c)$ the wavefunctions of the $W_1^{\pm}$ and Z_1 are flat in z, so we can calculate loop contributions in this approximation; the corrections will be of order $\alpha/(k\pi r_c) \simeq 2 \times 10^{-4}$, and can be safely ignored. For the photon, of course, the wavefunction is flat to all orders. The coupling of an approximately flat zero-mode to two

excited modes is then given by, *e.g.*,

$$g_{5L}\Omega \int_R^{R'} dz\, \frac{R}{z}\, \frac{\chi_1^Z \chi_n^W \chi_m^W [2 + c_L r_c \delta(z-R)]}{(N_{Z_1} N_{W_n} N_{W_m})^{1/2}} = g_{5L}\delta_{nm} \tag{4.64}$$

by the orthonormality condition in Ref. [63]. This means that the couplings of the KK W modes (which participate in the loop of the γ/Z self-energy diagram) to the exterior Z or γ are exactly the same as the SM triple gauge couplings in this limit. In particular, the coupling of an excited W to the hypercharge boson is zero. We can write S as [117]

$$S = -16\pi\, \frac{\partial \Pi_{ZY}(q^2)}{\partial q^2}\bigg|_{q^2=0}, \tag{4.65}$$

where $\Pi_{ZY}(q^2)$ is the self-energy mixing between the Z and the hypercharge boson (in this example) through W loops. So we conclude that, at order α, $\Delta S = 0$. We also expect the contribution to T to be small due to the presence of the custodial symmetry and because the mass splittings between the excited W and Z bosons are small. Hence the KK loop contributions to the oblique parameters can be safely ignored.

A more serious problem arises from the fact that the Higgs boson is no longer in the spectrum, and hence cannot run in loops. To estimate the one loop values of S, T, and U correctly, one would need a procedure for systematically removing the effects of the Higgs loops from the precision electroweak observables. It is not clear how this can be accomplished easily, due to the non-gauge invariant nature of the relevant graphs.

It is also possible that there are higher dimension operators localized on the TeV brane that violate S, since there is no symmetry to prevent them (T is protected by the custodial SU(2)). The size of these operators will naively be $M_Z^2/\Lambda_\pi^2 \approx 10^{-4}$, leading to contributions to S of order $\frac{1}{\alpha} M_Z^2/\Lambda_\pi^2 \approx 10^{-2}$.

In Ref. [26], the precision electroweak constraints on the WHM model, within a less general parameter space, were considered. Qualitatively, we agree with their conclusion that in the regime where many KK modes lie below the IR cutoff scale

$\sim \Lambda_\pi$ of the warped space (corresponding to the regime of weakly interacting distinct states), the WHM is excluded by precision electroweak data. In our approach, a similar conflict arises between the electroweak data and unitarity, where the former requires the absolute scale of higher KK modes to lie above ~ 2 TeV, and the latter demands the opposite.

4.5 Perturbative Unitarity in Gauge Boson Scattering

An important function of the Higgs boson in the SM is to insure the perturbative unitarity of the broken gauge theory. In this Higgsless model, we would like to test the claim in Ref. [55, 56] that the KK modes will be able to insure the unitarity in place of the Higgs.

The classic test of perturbative unitarity is the elastic scattering of two longitudinally polarized gauge bosons, $W_L^+W_L^- \to W_L^+W_L^-$ [114]. This amplitude receives tree-level contributions from the four-W vertex, and from the three-boson vertices through exchange of a single neutral gauge boson in the s- and t-channels, as shown in Fig. 4.7. The diagram involving the four-boson vertex contains terms that grow like s^2, s and s^0, as well as innocuous terms involving powers of $1/s$. For the scattering to respect unitarity, the terms that grow with s must cancel against those arising from other graphs in the theory. Csaki *et al.* [55] have investigated the behavior of these terms at large s. Strictly speaking, the expansion they performed is only valid at energies 'above' all the KK masses. In practice, however, it is a good approximation to take values of $\sqrt{s}$ above a sufficiently large number of KK modes. In that region, as shown in Ref. [55], there are two necessary conditions for the terms which grow with energy in the 4-point contribution to be cancelled by those from the one-boson

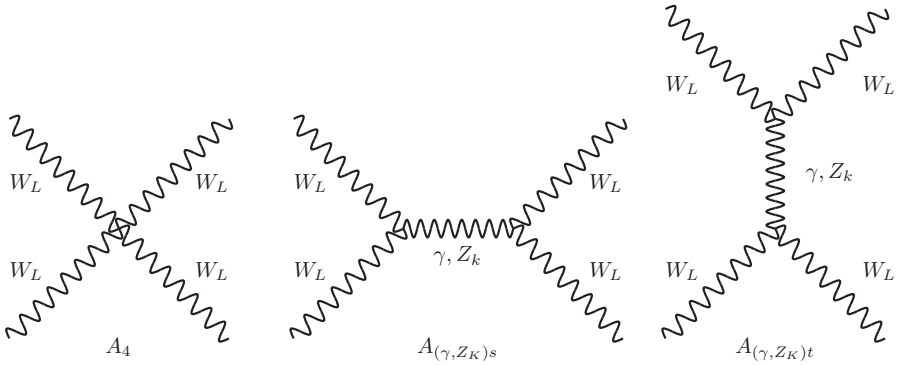

Figure 4.7: Feynman diagrams for the tree-level amplitudes contributing to $W_L^+W_L^-$ scattering.

exchange graphs:

$$g^2_{nnnn} = \sum_k g^2_{nnk}\,,$$
$$4g^2_{nnnn}M_n^2 = 3\sum_k g^2_{nnk}M_k^2\,. \tag{4.66}$$

Here g^2_{nnnn} is the coupling of four gauge bosons with KK-number n, and g_{nnk} is the three boson coupling between two states with KK-number n and one with KK-number k. The first of these conditions insures the cancelling of terms in the amplitude that grow like s^2, and is guaranteed by the original gauge invariance. The second condition is required for the cancellation of the terms that grow like s, and it is not trivial that it will be satisfied in the present model. For the case of ordinary W scattering, $n = 1$.

To test these conditions we have examined numerically the case of $W_L^+W_L^-$ scattering, since this is an important process, and will be measured at future colliders. The relevant couplings are given by

$$g^2_{1111} = g^2_{5L}\Omega^2\int_R^{R'} dz\,\frac{R}{z}\,\frac{1}{N^2_{W_1}}\left(|\chi_1^{L^\pm}|^4[2 + c_L r_c\delta(z-R)] + 2\kappa^2|\chi_1^{R^\pm}|^4\right)\,, \tag{4.67}$$
$$g_{11k} = g_{5L}\Omega\int_R^{R'} dz\,\frac{R}{z}\,\frac{1}{N_{W_1}\sqrt{N_{Z_k}}}\left(|\chi_1^{L^\pm}|^2\chi_k^{L^0}[2 + c_L r_c\delta(z-R)] + 2\kappa|\chi_1^{R^\pm}|^2\chi_k^{R^0}\right)\,,$$

where N_{W_1} and N_{Z_k} are the normalization factors given above. For the first sum rule

we also need the coupling of two $W_1^\pm$ bosons to the photon, which is just e by gauge invariance.

We have numerically evaluated g^2_{1111} and g_{11k} for k extending over the photon, the Z_1, and the first 9 (or more) higher excited states for the entire range of κ. The agreement with the sum rules is quite good, and was observed to rapidly improve as more states were added. If, *e.g.*, $\kappa = 3$, the residuals of these sum rules after including the first 9 excited states are

$$\begin{aligned} 1 - \sum_{k=\gamma,1}^{10} \frac{g^2_{11k}}{g^2_{1111}} &= 7.85 \times 10^{-8}\,, \\ 1 - \frac{3}{4}\sum_{k=1}^{10} \frac{g^2_{11k}}{g^2_{1111}} \frac{M^2_{Z_k}}{M^2_{W_1}} &= 1.96 \times 10^{-3}. \end{aligned} \tag{4.68}$$

This shows that the sum rules are being satisfied, and so in the asymptotic region the cross section will indeed fall like $1/s$. The convergence of these sums as more KK states are added can be seen in Fig. 4.8.

The sum rules, however, are necessary, but not sufficient conditions for perturbative unitarity. In particular, the amplitude for $W_L^+W_L^-$ scattering, which grows like s^2 near a few times M_W^2, could grow too large before sufficiently many KK modes are passed. There is also a term formally independent of s, the coefficient of which could grow as more and more KK modes are included. It is possible that this term will also contribute to unitarity violations. To investigate this issue we examine the full amplitude for $W_L^+W_L^-$ scattering.

The amplitudes due to photon and Z exchange have been previously computed.

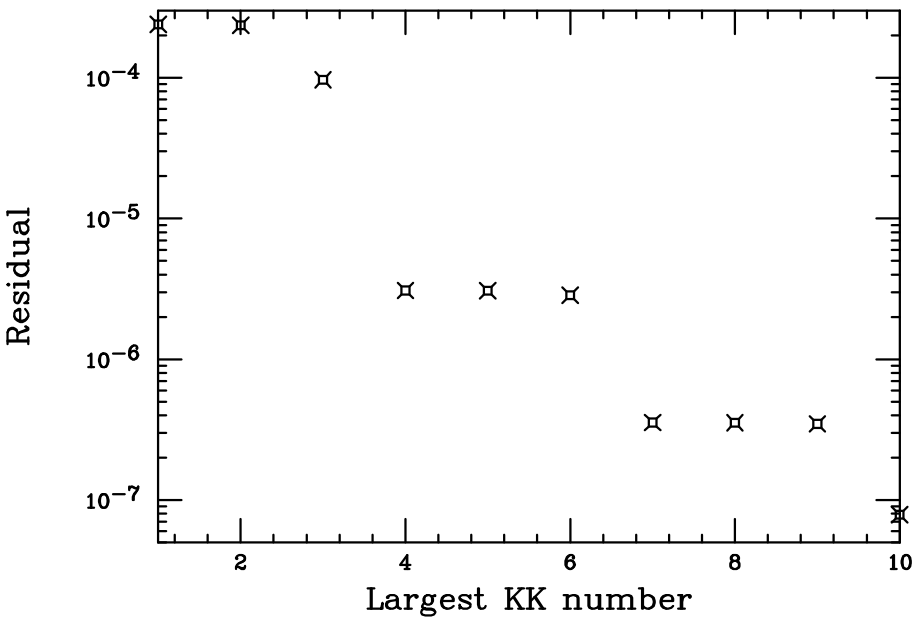

Figure 4.8: The residual of the sum rule $1 = \sum_k g^2_{11k}/g^2_{1111}$ as a function of the highest KK state included in the sum. This shows that the sum rule is converging, and hence the cross section will behave like $1/s$ at asymptotically large $\sqrt{s}$. Here we have assumed that $\kappa = 3$ for purposes of demonstration.

Simple modifications of the formulae in Ref. [72] gives

$$\begin{aligned}
A_{s\gamma} &= -\frac{1}{16} ie^2 s^2 \beta^2 (3-\beta^2)^2 \cos\theta \,, \\
A_{sZ_k} &= -\frac{1}{16} i g_{11k}^2 \frac{s^3}{s-\xi_{Z_k}} \beta^2 (3-\beta^2)^2 \cos\theta \,, \\
A_{t\gamma} &= -\frac{ie^2 s^3}{32t} \left[\beta^2(4-2\beta^2+\beta^4) + \beta^2(4-10\beta^2+\beta^4)\cos\theta \right. \\
&\quad \left. + (2-11\beta^2+10\beta^4)\cos^2\theta + \beta^2 \cos^3\theta \right] \,, \\
A_{tZ_k} &= -\frac{i g_{11k}^2 s^3}{32(t-\xi_{Z_k})} \left[\beta^2(4-2\beta^2+\beta^4) + \beta^2(4-10\beta^2+\beta^4)\cos\theta \right. \\
&\quad \left. + (2-11\beta^2+10\beta^4)\cos^2\theta + \beta^2 \cos^3\theta \right] \,, \\
A_4 &= -\frac{1}{16} i g_{1111}^2 s^2 (1+2\beta^2 - 6\beta^2\cos\theta - \cos^2\theta) \,,
\end{aligned} \tag{4.69}$$

where $\xi_{Z_k} = M_k^2/M_W^2$, $t = -\frac{1}{2}s\beta^2(1-\cos\theta)$, and $\beta = \sqrt{1-4/s}$, and the labels refer to s and t-channel exchanges. Here s and t have been scaled to M_W^2. As is well known, in the SM the sum of these amplitudes grows like s. This growth is cancelled by the Higgs contributions

$$\begin{aligned}
A_{sH} &= -\frac{1}{16} i g^2 s^2 (1+\beta^2)^2 \frac{1}{s-\xi_H} \,, \\
A_{tH} &= -\frac{1}{16} i g^2 s^2 (\beta^2 - \cos\theta)^2 \frac{1}{t-\xi_H} \,,
\end{aligned} \tag{4.70}$$

with $\xi_H = m_H^2/m_W^2$.

As we have seen, in the present model, the terms growing with s are cancelled at large s by the sum over the KK modes. For intermediate regions of s we investigate the full amplitude

$$A = A_4 + A_{s\gamma} + A_{t\gamma} + \sum_{k=1}^{\infty} \left(A_{sZ_k} + A_{tZ_k} \right) \,. \tag{4.71}$$

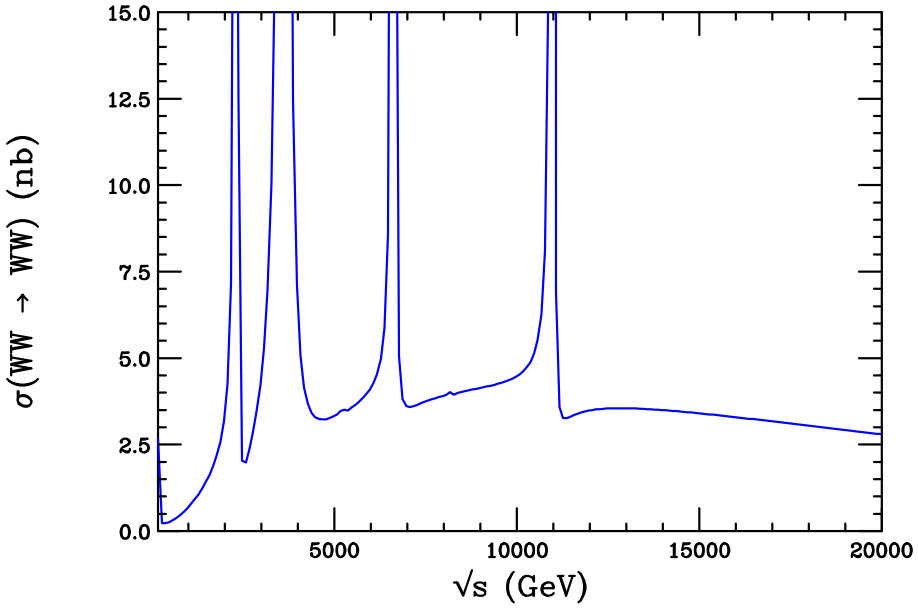

Figure 4.9: The cross section for $W_L^+W_L^- \to W_L^+W_L^-$ scattering with the first 10 KK states included. A heavy fake state has also been included with a mass of 14.7 TeV and coupling $g = 2.8 \times 10^{-4} g_{1111}$ to complete the sum rules and show that the cross section falls like $1/s$ asymptotically. No attempt has been made to smooth the poles at the KK resonances. Here we have assumed that $\kappa = 3$ for purposes of demonstration and have set $z_0 = 0.98$.

For reference, the cross section, with a cut on the scattering angle $|\cos\theta| \leq z_0$, is

$$\sigma = \frac{1}{16\pi s^2 \beta^2} \int_{t_-}^{t_+} dt \, |A|^2 \,, \tag{4.72}$$

with $t_\pm = (2 - \frac{1}{2}s)(1 \mp z_0)$. This cross section, summed over the first 10 KK modes, is shown in Fig. 4.9, taking $z_0 = 0.98$. To demonstrate the asymptotic behavior for the case $\kappa = 3$, we have inserted a heavy fake state with mass $m_{heavy} = 14.7$ TeV and coupling $g = 2.8 \times 10^{-4} g_{111}$ chosen to cancel the residuals in Eq. (68). This heavy fake state is intended to numerically compensate for extending the KK sum out to infinity. When this state is included, the cross section is seen to fall like as expected. However, it is clear that while including 10 KK states is enough to flatten the cross section, as seen in the region below the fake state, it is not enough to make it fall with s.

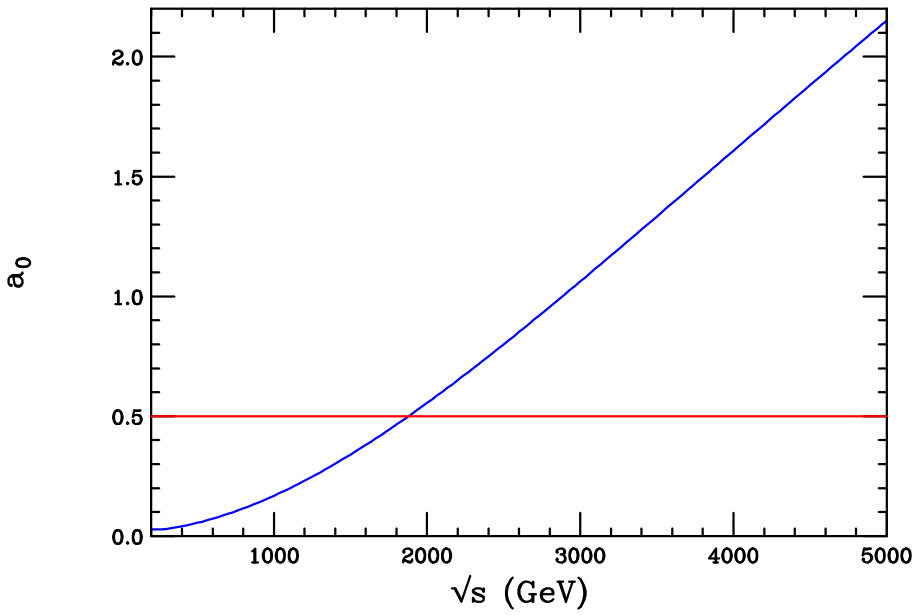

Figure 4.10: The real part of the zeroth partial wave amplitude for $W_L^+W_L^- \to W_L^+W_L^-$ scattering as a function of $\sqrt{s}$. The first 10 KK states have been included. We have taken $\kappa = 3$ and $z_0 = 0.98$. Unitarity is violated if this amplitude exceeds $1/2$, which is seen to occur at $\sqrt{s} \approx 2$ TeV.

A good test of the unitarity of this scattering process is that the first partial wave amplitude should be bounded for all s [114]

$$|\mathcal{R}e\,(a_0)| = \left|\mathcal{R}e\left(\frac{1}{32\pi}\int_{-1}^{1} d\cos\theta(-iA)\right)\right| \leq \frac{1}{2}. \tag{4.73}$$

We have calculated this quantity for the amplitude in Eq. (4.71), again summing over the first 10 (or more) KK modes. Our result is shown in Fig 4.10 for the case $\kappa = 3$. Unitarity is clearly violated at a center of mass energy of $\sqrt{s} \approx 2.0$ TeV, below the mass of the first KK mode. Note that this is only slightly better than the value obtained for the 4-d Standard Model without a Higgs, where unitarity breaks down at $\sqrt{s} \approx 1.7$ TeV. The problem can be traced to the fact that the first higher excited modes are too heavy to have much influence before unitarity is violated. So, while the cross section will behave like $1/s$ at *asymptotically* high energies, unitarity is violated before that regime sets in.

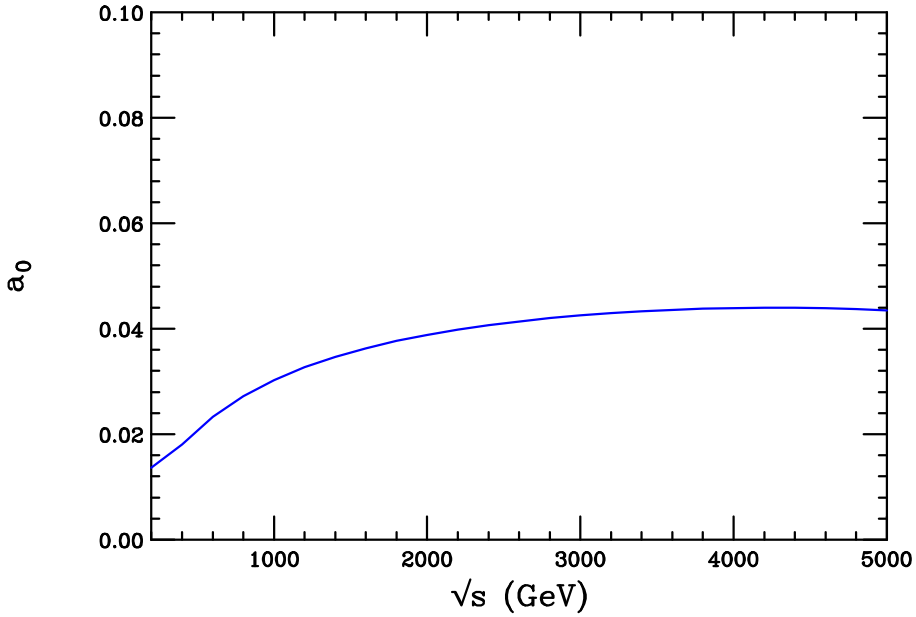

Figure 4.11: The real part of the zeroth partial wave amplitude for $W_L^+W_L^- \to W_L^+W_L^-$ scattering in the flat space equivalent of the WHM. The first 10 KK states have been included and we have taken $\kappa = 3$ and $z_0 = 0.98$. Unitarity is violated if this amplitude exceeds $1/2$, which is seen not to occur. In this case the sum rules are almost saturated well before $\sqrt{s} = 1.7$ TeV, where the SM without a Higgs boson violates unitarity.

For comparison we have performed the same calculation for the equivalent theory in flat space (with $\kappa = 1$), as presented in Section 6 of Ref. [55]. Our results are shown in Fig. 4.11. In that case, the first excited mode sits at 240 GeV, and the spacing between successive modes is 160 GeV. When $\sqrt{s}$ has reached a few TeV many KK modes have been passed and both sum rules are nearly saturated, so the terms growing with s are nearly cancelled. We thus see that the flat space equivalent theory is well-behaved [146, 47].

In order to discern how serious the problem of unitarity violation is in the WHM, we have repeated the above analysis over the entire allowed range of κ, even in the regimes where we do not expect the model to agree with the precision measurements. In particular, one might expect that if unitarity is to be respected it would be in the case when the neutral KK states are as light as possible and where deviations

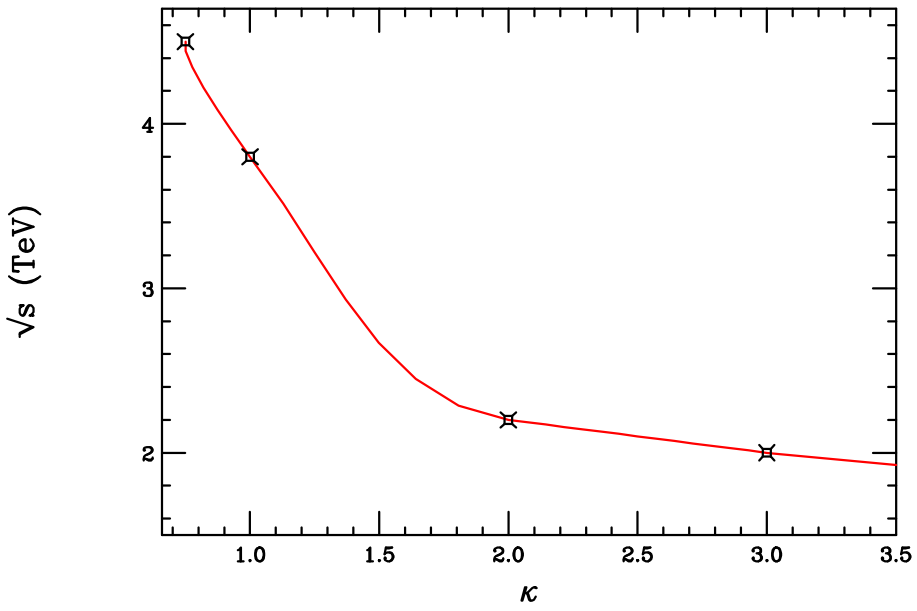

Figure 4.12: The value of $\sqrt{s}$ at which perturbative unitarity breaks down in $W_L^+W_L^- \to W_L^+W_L^-$ scattering as a function of κ, taking $z_0 = 0.98$. The points represent the distinct cases for which we numerically computed the unitarity violation and the curve extrapolates between the points.

from SM couplings are also large, *i.e.*, for small values of κ [26]. However, we find that perturbative unitarity breaks down for *all* values of κ, as shown in Fig. 4.12, although the scale where the violation occurs is somewhat larger when κ is small. We see that for all values of κ, perturbative unitarity is violated below any new scale, such as Λ_π for $k/\overline{M}_{Pl} \leq 0.1$. It is possible that the additional brane terms mentioned in Section 4 could be adjusted to make the theory both unitary and consistent with data. Whether this can be achieved with or without fine-tuning is not clear.

We also note that the $W_L^+W_L^-$ scattering process can proceed by KK graviton exchange, and that this contribution has the opposite sign in the amplitude, so one might hope that unitarity could be restored by destructive interference between the gauge and gravity sectors. However, the ratio of the KK graviton to gauge exchange amplitudes is roughly $M_W^2/(g^2\Lambda_\pi^2) \approx 10^{-4}$, leading to a strong suppression. Numerically we find this effect to be insignificant. A similar situation holds for the contribution of the radion scalar, which is also present in the model. We thus conclude that this

model is not a reliable perturbative framework.

4.6 Collider Signals

Thus far, we have seen that consistency with precision electroweak data demands that the ratio $\kappa = g_{5R}/g_{5L}$ take on larger values, such as $\kappa \sim 3$, which strongly enforces the SM limit. We have also seen that unitarity in gauge boson scattering is problematic in the WHM for such values of κ. Although the sum rules in Ref. [55], which are derived from the amplitude for longitudinal W scattering, are satisfied once enough gauge KK states are included, we demonstrated that the unitarity condition for the zeroth partial wave amplitude is violated. Hence the WHM is not a weakly coupled model. In this section, however, we will take the view that the model may be extended or modified, *e.g.*, with the inclusion of additional non-Higgs states, in such a way as to restore unitarity. We thus examine the general collider signatures of the gauge and graviton KK states, as these are most likely a generic feature in any extended Higgsless model based on a warped geometry.

We first examine the signatures of the neutral gauge KK states, recalling that the mass spectrum of these states and their couplings to the SM fields are derived in Section 3. We will take $\kappa = 3$ throughout this section, in accordance with the constraints from precision electroweak measurements. The resulting spectrum and fermionic couplings for the first few excited neutral gauge KK states above the Z are displayed in Table 4.1, where the couplings are written in the form

$$\frac{g_{Z_n}}{c_w}(T_{3L}^f - s_n^2 Q^f)\,. \tag{4.74}$$

We see a general trend of decreasing coupling strength, g_{Z_n}, with increasing KK mode. These couplings are roughly $7 - 16\%$ (with the exact value depending on the mode number) of the SM weak coupling strength, and hence we can expect smaller production rates for these states. In addition, we note that the pair of nearly degenerate states have different fermionic interactions due to the parameter s_n^2. Measuring these couplings would separate the two degenerate states and uniquely identify this model.

	m_{Z_n} (TeV)	g_{Z_n}/g_{SM}	s_n^2
Z_2	2.30	0.106	0.743
Z_3	2.31	0.163	-0.109
Z_4	3.62	0.065	0.218
Z_5	5.24	0.072	0.748
Z_6	5.26	0.113	-0.104

Table 4.1: Mass spectrum and fermionic couplings for the first five excited neutral gauge KK states above the Z, taking $\kappa = 3$. The KK coupling strength is scaled to the SM weak coupling.

The classic mechanism for producing heavy neutral gauge bosons in hadronic collisions is Drell-Yan production, $pp \to Z_n \to \ell^+\ell^-$, where the Z_n appears as a resonance. The Drell-Yan lineshape is clearly dependent on the total width of the Z_n, which varies in the WHM depending on the placement of the fermions. We have thus allowed for the total width of the nth gauge KK state to float,

$$\Gamma_n = c\,\Gamma_n^0\,, \tag{4.75}$$

where Γ_n^0 corresponds to the case where all the SM fermions reside on the Planck brane. We have taken the range $1 \leq c \leq 100$, which accomodates for the possibility, *e.g.*, that the third generation fermions are in the bulk and are localized far from the Planck brane. The resulting event rate, in the electron channel only, for the nearly degenerate states $Z_{2,3}$ is displayed in Fig. 4.13 for the LHC with an integrated luminosity of 3 ab^{-1}. This high value of integrated luminosity corresponds to that proposed for the LHC upgrades [84]. The apparently isolated single resonance is, of course, a superposition of the Z_2 and Z_3 KK states. The effect of increasing the Z_n width is readily visible; the resonance peak becomes flattened if the total width is too large. However, it is clear that Drell-Yan production provides a clean discovery channel for the first two excited states in the case $\Gamma_n \lesssim 25\Gamma_n^0$. For present design luminosities, ~ 100 fb^{-1}, the event rate is simply scaled by a factor of 30 and the signal remains strong. The next excitation, Z_4, is very weakly coupled, and we have found that the corresponding peak is too small to be observed above the Drell-Yan SM continuum. The corresponding event rate for the higher mass KK states, $Z_{5,6}$,

is also shown in Fig. 4.13, again assuming 3 ab^{-1} of integrated luminosity. Here, we see that the number of events is small, and even when the μ channel is also included these resonances are unlikely to be observed. Hence the LHC is likely to only observe a single resonance peak, corresponding to the superposition of the first two Z excitations. We also expect that only the first W excitation will be observable at the LHC. We note that the visible spectrum of the weak gauge KK states in the WHM at the LHC will appear similar to that from a flat extra dimension with brane terms. The KK states arising from flat space in the absence of brane terms will have a larger production rate [144, 102], due to the larger couplings, and will be differentiable from the WHM.

In principle, neutral gauge KK production may be distinguished from that of more conventional extra gauge bosons arising in, *e.g.*, a GUT model [143]. The presence of the two nearly degenerate KK states (whether they be the $Z_{2,3}$ in the WHM, or the photon and Z KK excitations in flat space) results in a unique resonance shape, which is different from the case of a single new gauge state. In the present case, the Z_2 and Z_3 resonances destructively interfere with the SM background, yielding the dip in the line-shape in the invariant mass bins just below the heavy resonances. This effect is in principle measurable at the LHC [24], given enough statistics, and is a means for identifying the production of gauge KK states. In addition, the indirect exchange of the Z_n (for $\sqrt{s} < m_{Z_n}$) in fermion pair production in e^+e^- annihilation results in a pattern of deviations in the cross sections and corresponding asymmetries which allows for the determination of the fermionic couplings of additional Z bosons [140, 12]. In principle, a TeV class Linear Collider (LC) could thus be able to resolve the Z_2 from the Z_3 and separately measure their couplings. This claim should be verified by an independent study. A multi-TeV LC, such as CLIC, would be able to run on the resonance peaks, measure the individual line-shapes, and perform detailed studies of the couplings for each state.

The KK excitations of the gluon may be produced as resonances in dijet distributions at the LHC. The $2 \to 2$ parton-level subprocesses which contribute to dijet production are $q\bar{q} \to q\bar{q}\,, q\bar{q} \to gg\,, qg \to qg\,, gg \to gg\,,$ and $qq \to qq$. In principle, the gluon KK states can contribute via s-channel exchange in the $q\bar{q}$ and gg initiated

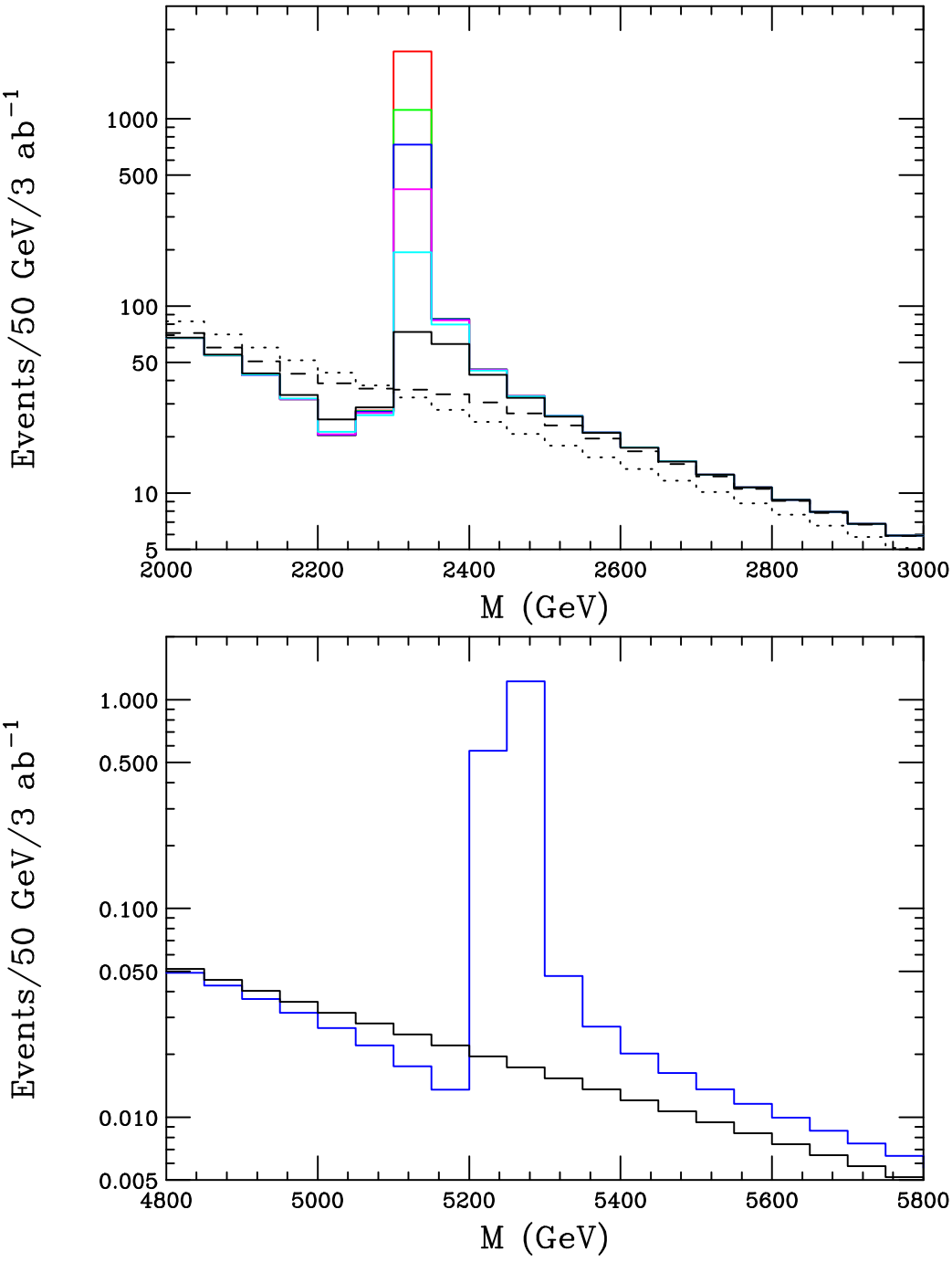

Figure 4.13: Top panel: Event rate for Drell-Yan production of the $Z_{2,3}$ gauge KK states, in the electron channel, as a function of the invariant mass of the lepton pair at the LHC with 3 ab^{-1} of integrated luminosity. The dotted histogram corresponds to the SM background, while the histograms from the top down (represented by red, green, blue, magenta, cyan, solid, and dashed) correspond to letting the width float with a value of $c = 1\,, 2\,, 3\,, 5\,, 10\,, 25\,, 100$. Bottom Panel: Event rate for Drell-Yan production of the $Z_{5,6}$ gauge KK states as a function of the invariant mass of the lepton pair at the LHC with 3 ab^{-1} of integrated luminosity (blue histogram). The bottom solid histogram corresponds to the SM background.

processes, and via t- and u-channel exchange in $qg \to qg$ and $gg \to gg$. Here, we are only concerned with the search for peaks in the dijet invariant mass distribution, and hence neglect the possible gluon KK t- and u-channel contributions. Such contributions would, however, be revealed in dijet angular distributions. We are then left with computing the KK s-channel exchange diagrams, for which we need to first examine the gluon KK couplings to the SM fields. The expression for the $q\bar{q}g_n$ coupling is given in Eq. (60) and its strength is shown in Fig. 4.5 for the first excitation as the brane kinetic term is allowed to vary. For the value of the brane terms present in the WHM, the strength of the square of this coupling is $0.234\,(g_s^{SM})^2$ for the first gluon excitation and $0.143\,(g_s^{SM})^2$ for the second KK mode. These coupling strengths are a larger fraction of the usual SM value as compared to the corresponding couplings of the weak boson KK states due to the large negative value of δ_s. Recalling that the zero-mode gluon wavefunctions are flat in z, it is easy to see that the $g_0 g_0 g_1$ coupling is forbidden by orthonormality. Hence the gg initiated process does not contribute to the resonant production of the KK modes and the $q\bar{q} \to q\bar{q}$ subprocess is the only process we need to consider here. We also recall that the gluon KK mass spectrum tracks that of the W boson KK states with $m_{g_1} = 2.53$ TeV and $m_{g_2} = 5.51$ TeV.

The resulting event rate for the dijet invariant mass distribution is displayed in Fig. 4.14 for the first and second KK excitations, taking 100 fb^{-1} and 3 ab^{-1} of integrated luminosity, respectively. Here, we have employed the cuts $|\eta| < 1$ and $|p_T^{jet_1}| > 800(1500)$ GeV for the first (second) excitation. We see that the event rates are enormous and that both excitations will be observable at the LHC. Varying the width, as done above in the case of Drell-Yan production, will flatten the peak, but should not affect the visibility of the signal unless the width grows very large. Observation of the first dijet resonance, in addition to the peak present in the Drell-Yan distribution, will signal that the full SM gauge sector resides in the bulk. The slightly different value of the mass for g_1, as compared to that for $Z_{2,3}$, with the g_1 being roughly 200 GeV heavier than the Z KK states, will signal that brane kinetic terms are present in the model. Given the large event rate for the production of these KK states, this mass difference should be measurable. Observation of the second gluon KK dijet peak will reveal the mass gap between the states in the KK tower, and will

signal the presence of a warped, rather than flat, geometry. Hence, observation of the KK dijet resonances is critical to the identification of this model.

We now turn to the production of the graviton KK states and first consider the case of resonant graviton production. This is well-known to be the main signature of the original RS model [61, 60]. In principle, resonant graviton production can proceed via $q\bar{q}$ and gg initiated subprocesses. However, in the WHM scenario where the fermions are localized on the Planck brane, the graviton KK tower couples to fermions with $\overline{M}_{Pl}^{-1}$ strength or smaller since no warp factor is generated in the coupling. Hence the graviton KK tower decouples from the fermion sector. Examining the couplings of the graviton excitations to the zero-mode vector bosons, we see that in the absence of brane terms these are given simply by [62]

$$g^0_{V_0V_0G_n} = \frac{2}{\Lambda_\pi \pi k r_c}\left(\frac{1-J_0(x_n^G)}{(x_n^G)^2|J_2(x_n^G)|}\right), \tag{4.76}$$

where x_n^G denotes the roots which determine the graviton KK mass spectrum and, for example, $V_0 = g$. In the presence of brane kinetic terms, both the V_0 wavefunction and the $V_0V_0G_n$ interaction are modified; in the case $V_0 = g$,

$$g_{V_0V_0G_n} = \frac{N_{V_0}(\delta_i = 0)}{N_{V_0}}\left\{g^0_{V_0V_0G_n} + \cdots\right\}, \tag{4.77}$$

where δ_i denotes the appropriate brane term. The omitted terms in the bracket are proportional to $(x_n^G)^2 e^{-2\pi k r_c}$ for $n > 0$ and thus are negligible. Note that these terms are essential, however, to retain the $\overline{M}_{Pl}^{-1}$ behavior of the zero-mode graviton coupling. For the case of the graviton KK tower, the only influence of the brane terms on the $V_0V_0G_n$ coupling arises from modifications of the vector boson wavefunction.

Resonant graviton KK production thus proceeds through $gg \to G_n \to \gamma\gamma\,, gg\,, ZZ\,, WW$. Since the G_n coupling is significantly weaker than that for the gluon excitations, we expect that the gg channel and ZZ, WW decay to hadronic final states will be overwhelmed by the SM background. Likewise, we expect the rate for the leptonic final states to be small due to the low ZZ, WW leptonic branching fractions. Thus, we only consider the $\gamma\gamma$ final state. The SM diphoton background arises from $q\bar{q} \to \gamma\gamma$

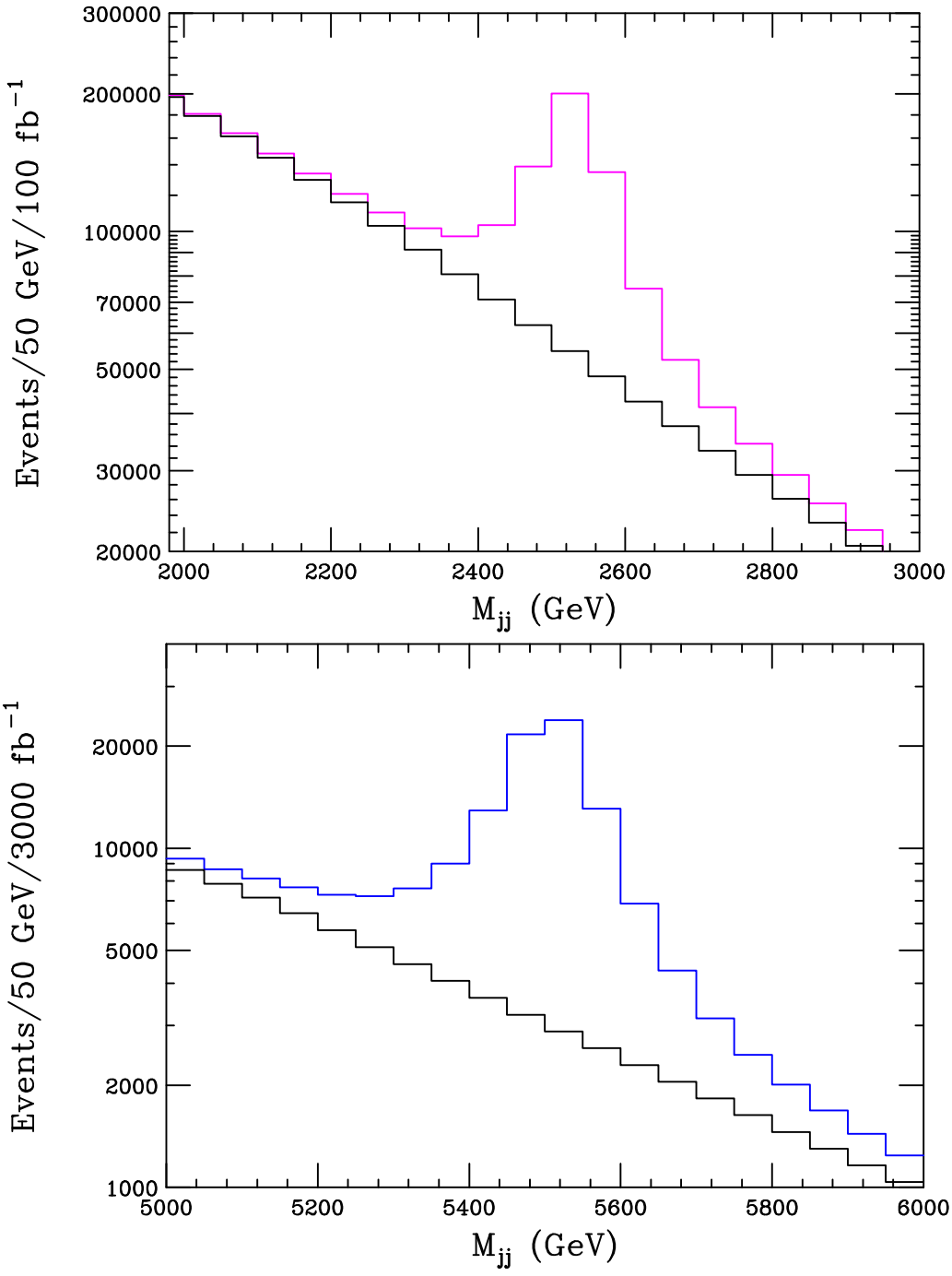

Figure 4.14: Production of the first (top panel) and second (bottom panel) gluon KK excitation in the dijet channel as a function of the dijet invariant mass. The SM background is given by the black histogram.

and $gg \to \gamma\gamma$, where the latter process proceeds through a box diagram. We include both of these SM processes in our background calculation. The event rate at the LHC, with 3 ab^{-1} of integrated luminosity, is displayed in Fig. 4.15 for the first graviton excitation and the SM background as a function of the diphoton invariant mass. In our numerical calculations, we assume $k/\overline{M}_{Pl} = 0.1$. We see that the G_1 production has a very small event rate and is indistinguishable from the background. Hence, the WHM differs from the usual RS scenario in that graviton resonances will not be observed.

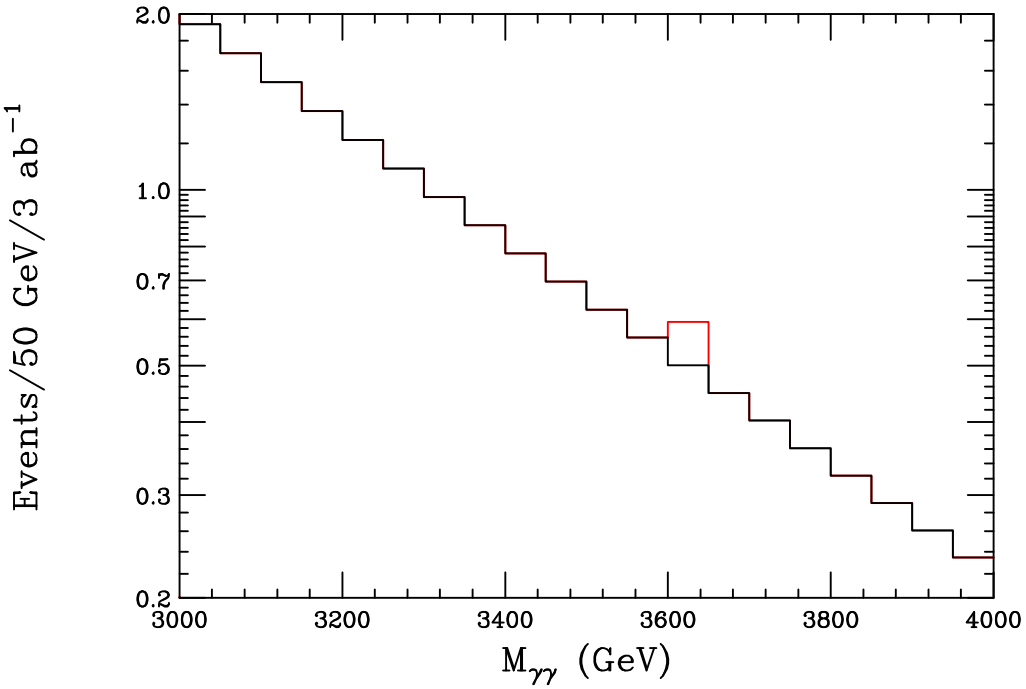

Figure 4.15: Production rate for the first graviton excitation at the LHC via the process $gg \to G_1 \to \gamma\gamma$ as a function of the diphoton invariant mass. The SM diphoton background is also shown. The two histograms are indistinguishable except for the small blip at $M_{\gamma\gamma} = m_{G_1}$

For completeness, we also considered the associated production of KK gravitons via $gg \to G_n + g$. Appropriately modifying the expressions in Ref. [87, 124] for the WHM we computed the event rate at the LHC for G_1 production as a function of jet energy using an integrated luminosity of 3 ab^{-1}. We found that for typical jet

energies of $E_j = 200$ GeV the cross section was of order 0.016 ab, and hence is also too small to be observed, even with the proposed LHC luminosity upgrades. We thus conclude that in this model, the graviton KK tower can not be observed at high energy colliders.

Lastly, we note that there exists a radion scalar in this model and that it may have distinctive collider signatures.

4.7 Conclusions

Various phenomenological aspects of a Higgsless 5-d model [56], based on the RS hierarchy proposal [136], were studied in this paper. We considered independent left and right bulk gauge couplings and included the effects of UV brane localized kinetic terms for the gauge fields [128]. These terms were assumed to be radiatively generated, which is a generic expectation in orbifold models [80]. Our analysis was not limited to leading order bulk-curvature effects unlike in Refs. [56, 128], and also allowed for a more general set of parameters than that discussed in Ref. [26].

We computed the mass spectrum and the relevant couplings of the $W^{\pm}$ and γ/Z KK towers, and studied experimental constraints on the model parameters. Our main conclusion is that in the region of parameter space allowed by precision EW data, this model is not perturbatively unitary at tree level above $\sqrt{s} \approx 2$ TeV, which is below the scale of the new KK states. Futhermore, we find that tree-level unitarity is violated over the entire parameter space, even in those regions where comparisons with the precision measurements are anticipated to be quite poor. Thus, to make reliable calculations based on the WHM, one must extend this model in order to unitarize the amplitudes. Setting the issue of perturbative unitarity aside, it was also observed that quantum contributions to the S, T, U oblique parameters [132, 36, 119] are expected to be small. However, in the absence of the Higgs, regularization of the relevant loop diagrams may require non-renormalizable TeV brane counter terms whose coefficients are unknown. This imposes a degree of uncertainty on loop corrections. Further work regarding loop corrections is needed before more precise statements could be made in this regard.

Finally, we considered the collider signatures of the model, assuming that unitarity could somehow be restored without significantly modifying our numerical results. These signatures depend on the 5-d configuration of bulk fermions. We assumed a simple setup, where all fermions, except perhaps for the third generation, are localized near the Planck brane. The effect of different localizations of quarks was then taken into account by varying the widths of the KK resonances. Generically, we found that the low-lying gauge boson KK modes, including the gluons, would be observable, whereas the most distinct RS signature, the spin-2 graviton KK resonances, would most likely evade detection at the LHC.

The AdS/CFT correspondence [120] provides a 4-d interpretation of this model in terms of strong dynamics. Thus, the tools and insights of both five and four dimensional model building can be employed in making this scenario more realistic such that it agrees with the SM at low energies. This setup provides an entirely higher dimensional explanation of the observed weak interaction mass scales, directly linking them to the IR scale in the RS model. Thus, it is worth the effort to find solutions for the problems that plague the present form of the WHM.

Chapter 5

Higgsless models with IR brane kinetic terms

5.1 Introduction

As we enter the era of the LHC experiments, it is appropriate to examine the features of various approaches to Electroweak Symmetry Breaking (EWSB). One of the latest attempts for describing EWSB is the proposal of Refs. [55, 56]. In this approach, a judiciously chosen set of boundary conditions in a 5–d Higgsless $SU(2)_L \times SU(2)_R \times U(1)_{B-L}$ model gives rise to a pattern of gauge boson masses and couplings that are similar to those obtained in the Standard Model (SM) via a Higgs doublet condensate. The geometry of this model is based on the Randall–Sundrum (RS) hierarchy solution [136], where two branes reside at the boundaries of a 5–d Anti-de Sitter space[1]. In this scenario, the boundary conditions give rise to the breaking chain $SU(2)_R \times U(1)_{B-L} \to U(1)_Y$ at the Planck scale with the subsequent breaking $SU(2)_L \times U(1)_Y \to U(1)_{QED}$ at the TeV scale. After the Planck scale symmetry breaking occurs, a global $SU(2)_L \times SU(2)_R$ symmetry remains in the brane picture; this breaks on the TeV–brane to a diagonal group $SU(2)_D$ corresponding to the custodial $SU(2)$ symmetry present in the SM [9].

[1] In the RS background, holographic arguments based on the AdS/CFT correspondence [120] have been useful in elucidating the features of the Higgsless theory[56, 128, 26, 35].

It has been shown [56, 128, 9] that due to the presence of the $SU(2)_D$ custodial symmetry, this Warped Higgsless Model (WHM) enjoys good agreement with precision EW data at the level of a few percent. However, it has been argued [26, 35] and demonstrated [58] that the region of parameter space in the WHM that results in good agreement with the EW data leads to perturbative unitarity violation (PUV) in $W_L^+W_L^-$ scattering at energies of order $\sim 2-3$ TeV. Furthermore, a scan of the parameter space of the WHM shows that the scale of perturbative unitarity violation is never significantly raised, even in those regions where comparisons with the precision measurements are anticipated to be quite poor [58]. To restore unitarity in gauge boson scattering, additional new physics is required at or below the RS cutoff of the effective theory on the TeV–brane. Even though this does not by itself rule out the model, it suggests that interactions in the gauge sector are problematic above the TeV scale.

To address some of these issues, the authors of Ref. [38] have examined the effects of including IR(TeV)–brane terms for the $U(1)_{B-L}$ and the custodial $SU(2)_D$ gauge symmetries. It is well-known that the introduction of brane terms can alter the couplings and masses of the corresponding Kaluza-Klein (KK) tower states [42, 64, 63, 41] and this would hence affect their contributions to the precision EW observables and to $W_L^+W_L^-$ scattering. These authors concluded that the addition of the $U(1)_{B-L}$ brane term could lead to improved agreement with the EW data, and, in addition, lowers the mass of the lightest KK state to ~ 300 GeV. Light KK states are generically expected to help restore perturbative unitarity in high energy gauge boson scattering, however the analysis of Ref. [38] did not quantify this point.

In this paper, we also study the effects of the IR–brane kinetic terms associated with both the $U(1)_{B-L}$ and $SU(2)_D$ symmetries; here, we pay particular attention to low energy perturbative unitarity violation. For the $U(1)_{B-L}$ boundary term, we find that the scale of PUV in the model is *independent* of the size of the brane term. We also demonstrate that increasing the ratio of the 5–d couplings, $\kappa \equiv g_{5R}/g_{5L}$, improves the agreement with the tree-level SM relations in the electroweak sector, but lowers the scale at which perturbative unitarity is violated, similar to our previous results [58]. In the case of the $SU(2)_D$ kinetic term, we find that perturbative unitarity

violation in $W_L^+ W_L^-$ scattering could be delayed to center of mass energies of order $\sim 6-7$ TeV. However, agreement with the tree-level SM relations is rather poor, with the disparity worsening as the size of the $SU(2)_D$ brane term increases. In addition, we compare the predictions for the lowest lying gauge KK state to the searches for new gauge bosons at the Tevatron Run I and II and for contact interactions at LEP II and find that the collider bounds restrict the potential size of the IR–brane kinetic terms. However, these collider bounds allow for the PUV scale to approach $6-7$ TeV.

We describe our setup in the next section. The EW and collider constraints are discussed in section 3. Perturbative unitarity in this model is the subject of section 4 and our concluding remarks are given in section 5.

5.2 The Model

Here, we briefly discuss the modifications induced in our earlier analysis [58] due to the presence of the $U(1)_{B-L}$ and $SU(2)_D$ brane terms; these changes are quite straightforward. We employ the notation introduced in our previous work. In what follows, when we consider the effects of the $U(1)_{B-L}$ kinetic term we also include the UV–brane terms associated with the $SU(2)_L$ and $U(1)_Y$ symmetries in our analysis; these UV kinetic terms were included in our earlier results. However, for simplicity, we omit the UV terms in our study of the $SU(2)_D$ kinetic term.

The introduction of new kinetic terms on the TeV brane leads to a shift in the original action (given in Eq.(4) of Ref.[58]) by an amount

$$\delta S_{brane} = \int d^4x dy \sqrt{-g}\, \delta(y-\pi r_c) \Big[-\frac{1}{4} r_c c_B F_{B-L}^2 - \frac{1}{4(g_{5L}^2+g_{5R}^2)} r_c c_D (g_{5R} F_L + g_{5L} F_R)^2 \Big], \tag{5.1}$$

with $g_{5L(R)}$ being the 5–d $SU(2)_{L(R)}$ gauge coupling, πr_c is the brane separation in the RS model, and $c_{B,D}$ are dimensionless parameters which quantify the size of the IR–brane kinetic terms. Here F_{B-L} is the field strength tensor for the $U(1)_{B-L}$ gauge field, and similarly $F_{L,R}$ corresponds to $SU(2)_{L,R}$. For later purposes it is convenient to introduce the quantities $\delta_{B,D} \equiv k r_c c_{B,D}/2$ as in our earlier analysis

where k is the RS curvature parameter. We next observe that a non-zero value for δ_B will alter the $\partial_z B = 0$ boundary condition [56] on the TeV brane; instead, we now find $\partial_z B - \delta_B x_n^2 k\epsilon B = 0$, where x_n represents the roots defining the KK spectra, $\epsilon \equiv e^{-\pi k r_c}$, and B represents the $U(1)_{B-L}$ gauge field. A similar shift is observed in the case of the combination of fields associated with the $SU(2)_D$ brane term, *i.e.*, $\partial_z(g_{5R}A_L + g_{5L}A_R) - \delta_D x_n^2 k\epsilon(g_{5R}A_L + g_{5L}A_R) = 0$. Solving these new boundary conditions leads to alterations of the wavefunction coefficients as well as the eigenvalue equations for the KK tower masses. It is important to note, however, that the $W^\pm$ KK tower masses and couplings are left unaltered by a non-zero value of δ_B, but are modified by δ_D.

In calculating the couplings to both fermions and $W^\pm$ pairs for the photon, the Z, as well as the rest of the KK tower states, one of the dominant effects due to the new brane terms is the shift in the normalizations of the $W_n^\pm$ and Z_n wavefunctions. These normalizations now pick up additional terms; for the case of the Z_n, in comparison to our earlier result (Eq.(50) of Ref.[58]); we now obtain:

$$\begin{aligned} N_{Z_n} &= \int_R^{R'} dz\, \frac{R}{z}\, \Big\{ |\chi_L^n(z)|^2(2 + c_L r_c \delta(z-R)) + 2|\chi_R^n(z)|^2 + 2|\chi_B^n(z)|^2 \\ &+ c_Y r_c \frac{|\kappa\chi_B^n(z) + \lambda\chi_R^n(z)|^2}{\kappa^2+\lambda^2}\delta(z-R) + c_B r_c |\chi_B^n(z)|^2 \delta(z-R')/\epsilon \\ &+ c_D r_c \frac{|\kappa\chi_L^n(z) + \chi_R^n(z)|^2}{1+\kappa^2}\delta(z-R')/\epsilon \Big\}\,, \end{aligned} \tag{5.2}$$

where χ_i^n are the wavefunctions for the relevant gauge KK state, and λ is defined as the ratio $\lambda \equiv g_{5B}/g_{5L}$. A similar shift in the $W_n^\pm$ normalization also occurs,

$$\begin{aligned} N_{W_n} &= \int_R^{R'} dz\, \frac{R}{z}\, \Big\{ |\chi_L^n(z)|^2(2 + c_L r_c \delta(z-R)) + 2|\chi_R^n(z)|^2 \\ &+ c_D r_c \frac{|\kappa\chi_L^n(z) + \chi_R^n(z)|^2}{1+\kappa^2}\delta(z-R')/\epsilon \Big\}\,. \end{aligned} \tag{5.3}$$

These new TeV brane terms also lead to additional contributions to the normalization

of the photon wave function,

$$N_\gamma = 2\pi r_c \alpha_L^2 \left(\frac{\kappa^2 + \lambda^2 + \kappa^2\lambda^2}{\kappa^2\lambda^2} \right) \left\{ 1 + \frac{1}{\pi k r_c} \frac{\kappa^2\lambda^2\delta_L + \kappa^2\delta_B + (1+\kappa^2)\lambda^2\delta_D + (\kappa^2+\lambda^2)\delta_Y}{\kappa^2 + \lambda^2 + \kappa^2\lambda^2} \right\}, \tag{5.4}$$

where α_L is a numerical constant which is determined from the boundary conditions and appears in the KK decomposition of the A_L^3 gauge field. Due to the abelian nature of the $U(1)_{B-L}$ group, new brane term contributions to the W 4-point or gauge 3-point functions do not occur. However, such contributions are induced in the case of the $SU(2)_D$ brane term.

5.3 Precision Measurements and Collider Bounds

Our analysis now proceeds by analogy with our earlier work [58]: we hold $M_{W,Z}$ as well as the UV–brane kinetic terms $\delta_{L,Y}$ fixed and explore the parameter space spanned by the parameters κ and $\delta_{B,D}$.

We previously introduced the three different quantities related to the weak mixing angle: $\sin^2\theta_{os} = 1 - M_W^2/M_Z^2$, $\sin^2\theta_{eg} = e^2/g_{W_1}^2$ (where g_{W_1} is the coupling of the particle we identify as the W to the SM fermions), and $\sin^2\theta_{eff}$, which is defined at the Z-pole. All three must take on the same value at the tree-level in the SM. They can differ significantly in the present scenario; however, there are preferred parameter space regions, *i.e.*, when κ is large [58], that yield consistent values. The first question to address here is the variation of $\sin^2\theta_{eg,eff}$ with respect to the fixed on-shell value, $\sin^2\theta_{os}$, as $\delta_{B,D}$ are allowed to change for fixed κ. The results of this analysis are shown in Fig. 5.1. In the top panel we observe that $\sin^2\theta_{eff}$ is δ_B-independent, which we have verified analytically, while $\sin^2\theta_{eg}$ increases as δ_B increases. In fact we see that for $\kappa = 1(3)$ excellent agreement between the on-shell and effective values is obtained when $\delta_B \simeq 8(10)$. Overall, however, the case $\kappa = 3$ yields more consistent values, as in our earlier work, due to the large separation between the quantities $\sin^2\theta_{os}$ and $\sin^2\theta_{eff}$ when $\kappa = 1$. Clearly, a non-vanishing value of δ_B does help to bring the values of the various definitions of $\sin^2\theta$ into agreement. In contrast, in the bottom panel we see that as δ_D increases both of the different $\sin^2\theta$ values shrink in

size and move away from the on-shell value thus getting further from the SM limit. Of course the $\kappa = 3$ values remain closer to the SM than do those for $\kappa = 1$, but in all cases the agreement is poor.

Since $\delta_{B,D}$ shift the the $\sin^2\theta_{eg}$ curves in opposite directions, it is interesting to see what happens when these brane terms are simultaneously nonzero. This can be seen in Fig. 5.2 for $\kappa = 1$. For the range of δ_D of interest we see that we can always find a value of δ_B for which $\sin^2\theta_{os} \simeq \sin^2\theta_{eg}$. Unfortunately, since $\sin^2\theta_{eff}$ is δ_B independent, including this brane term does not bring this quantity into accord with the others for $\kappa = 1$; larger values of κ may help in this regard.

Another quantity of interest is the value of the overall strength of the Z boson coupling, denoted as ρ^Z_{eff}, and in particular, its deviation from unity, *i.e.*, $\delta\rho^Z_{eff} \equiv \rho^Z_{eff} - 1$. This deviation is related to the pseudo-oblique parameter T^* as $T^*/\alpha \equiv \delta\rho^Z_{eff}$. The pseudo-oblique parameters are defined in such a way so that they all take on the value zero in the tree level SM. They are introduced to guide our thinking about the direction in parameter space which approaches the SM. We note that it is important *not* to confuse these pseudo-oblique parameters with the conventionally defined purely oblique S, T, U. The dependency of $\delta\rho^Z_{eff}$ on $\delta_{B,D}$ for two different values of κ is shown in Fig. 5.3. Note that this parameter remains relatively small in magnitude for both values of κ as long as either $\delta_{B,D}$ does not become too large.

The other pseudo-oblique parameters S^*, U^*, as defined in Ref. [58], are also functions of $\delta_{B,D}$ as shown in Fig. 5.4. For U^*, some values of δ_B improve the agreement with the SM limit, while S^* tends away from its SM value. We see that, overall, smaller values of δ_B are again preferred. In the case of δ_D we see that both S^* and U^* move away from the SM limit with the shifts being much more significant in the case of $\kappa = 1$.

Our approach to calculating the pseudo-oblique observables, $S^*T^*U^*$, differs from that of STU as calculated by Csaki *et al.*[38]. In our approach, we numerically fix the masses of the first charged and neutral gauge KK excitations to be those of the physical W and Z bosons observed at colliders. We use these as input to our analysis, together with the strength of the charged current coupling determined by G_F. From these the couplings and masses of all the gauge KK states can be obtained.

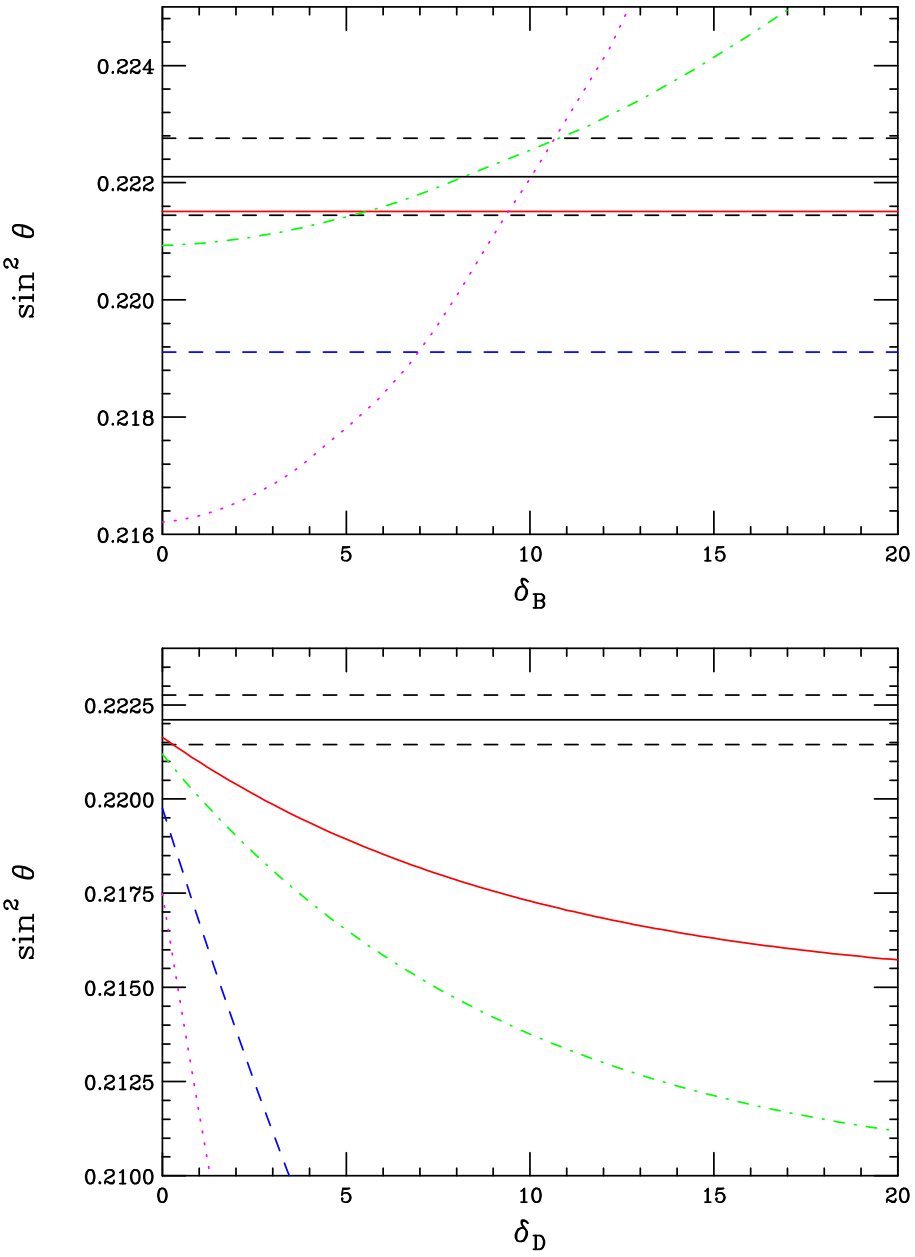

Figure 5.1: $\sin^2\theta$ in each of the three definitions as a function of $\delta_{B,D}$. The black horizontal solid and dashed curves correspond to the on-shell value $\pm 1\sigma$, the solid red (dashed blue) curve represents $\sin^2\theta_{eff}$ for $\kappa = 3(1)$ while the dash-dotted green (dotted magenta) curve is for $\sin^2\theta_{eg}$. The top (bottom) panel illustrates the effects of including the $U(1)_{B-L}$ ($SU(2)_D$) kinetic term. We take only one IR kinetic term to be non-vanishing at a time.

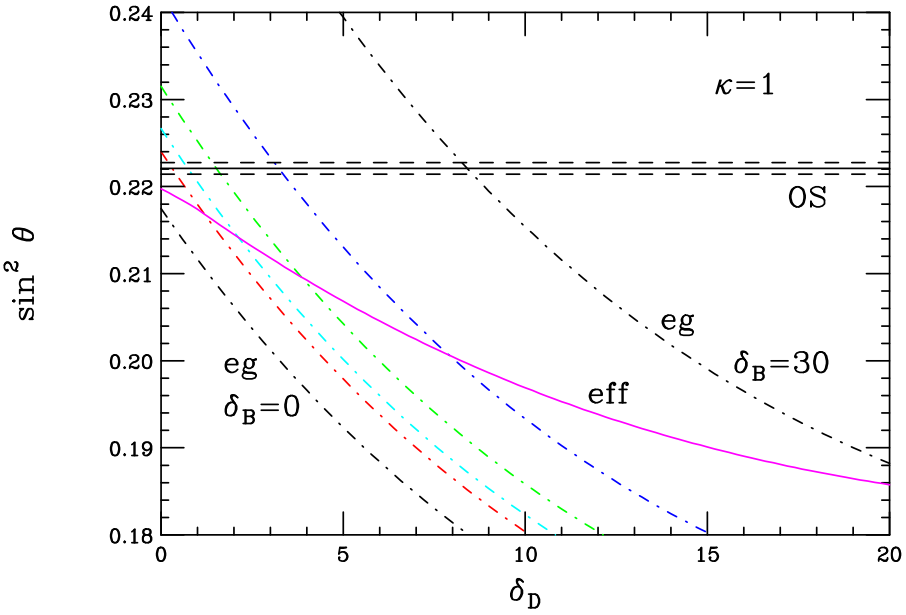

Figure 5.2: Same as in the previous figure but now with both $\delta_{B,D}$ nonzero for the case $\kappa = 1$. The solid magenta curve is the value of $\sin^2\theta_{eff}$ while the dash-dotted curves are all for $\sin^2\theta_{eg}$ for, from left to right, $\delta_B = 0, 10, 12, 15, 20$ and 30, respectively.

The pseudo-oblique parameters are then defined in terms of observables via the W mass, the invisible width of the Z and the fermionic couplings determined at the Z-pole. $S^*T^*U^*$ are chosen to vanish at the tree-level in the SM. Csaki *et al.* choose a different scheme wherein the SM gauge couplings g and g' are used as input parameters together with the usual relationship $1/e^2 = 1/g^2 + 1/g'^2$. This fixes $\sin^2\theta$ and hence the couplings of the W and Z. From this the W and Z and other KK masses, as well as their couplings, can be determined. The STU parameters in Ref. [38] can then be calculated as shifts in the masses as well as the wavefunctions and normalizations for the W and Z. It is clear that these two sets of electroweak parameters probe different relationships between the masses and couplings of the W and Z described by distinct choices of input parameters. In either case they allow for a measure of how far the model predictions are from the tree level SM. However, without employing the full loop corrections and overcoming the problem of 'subtracting out' the Higgs loop effects (described in [58]) neither set of parameters can be directly compared with

data.

To go further in the analysis of this model, we need to consider how non-zero values of $\delta_{B,D}$ lead to modifications of the KK spectra. Clearly, the $U(1)_{B-L}$ brane term does not influence the W KK tower so we turn our attention to the neutral KK states. The major effect of a non-zero δ_B on neutral KK states can be clearly seen in the upper panel of Fig. 5.5 for the case of $\kappa = 1$; the same qualitative behavior occurs for other values of κ. Here we immediately observe that the single, non-degenerate states are unaffected while one member of the nearly degenerate paired states, the one which couples mainly to $B - L$, gets its mass reduced as δ_B is increased. The remaining member of the pair stays unaffected. In particular, we see that the state Z_2 becomes light (note that here, Z_1 is the lightest state and corresponds to the SM Z). Further increasing δ_B leads to the appearance of new sets of almost degenerate pairs of states. Including δ_D has the opposite effect in that the member of the pair which couples mainly to T_{3L} gets its mass lowered. The other states are only slightly affected. In the case of $SU(2)_D$, the charged KK states have all of their masses lowered in analogy with the falling curves in the lower panel[2]. This figure demonstrates that the $U(1)_{B-L}$ and $SU(2)_D$ brane terms are at least partly doing what we had expected, *i.e.*, lowering the KK masses so that the now lighter states can have a potentially greater influence on unitarity in $W_L^+ W_L^-$ scattering. They do, however, lower the masses of *different* sets of KK states and this is critical for unitarity considerations as we will see below.

One may wonder, since some of the KK states are becoming so light, if there are conflicts with direct searches for new vector bosons at the Tevatron as well as with indirect searches such as those for contact interactions at, *e.g.*, LEP II. We recall that while the Tevatron experiments search for new resonances decaying into leptons via Drell-Yan production, the LEP bounds result from searches for deviations in cross sections and angular distributions from SM expectations below production threshold. In the case of the charged KK states, whose masses are lowered by the $SU(2)_D$

[2]Note that the root corresponding to the observed W is also lowered. Since the mass scale of the heavier KK states is obtained by matching this root to M_W, the mass of the neutral states rises.

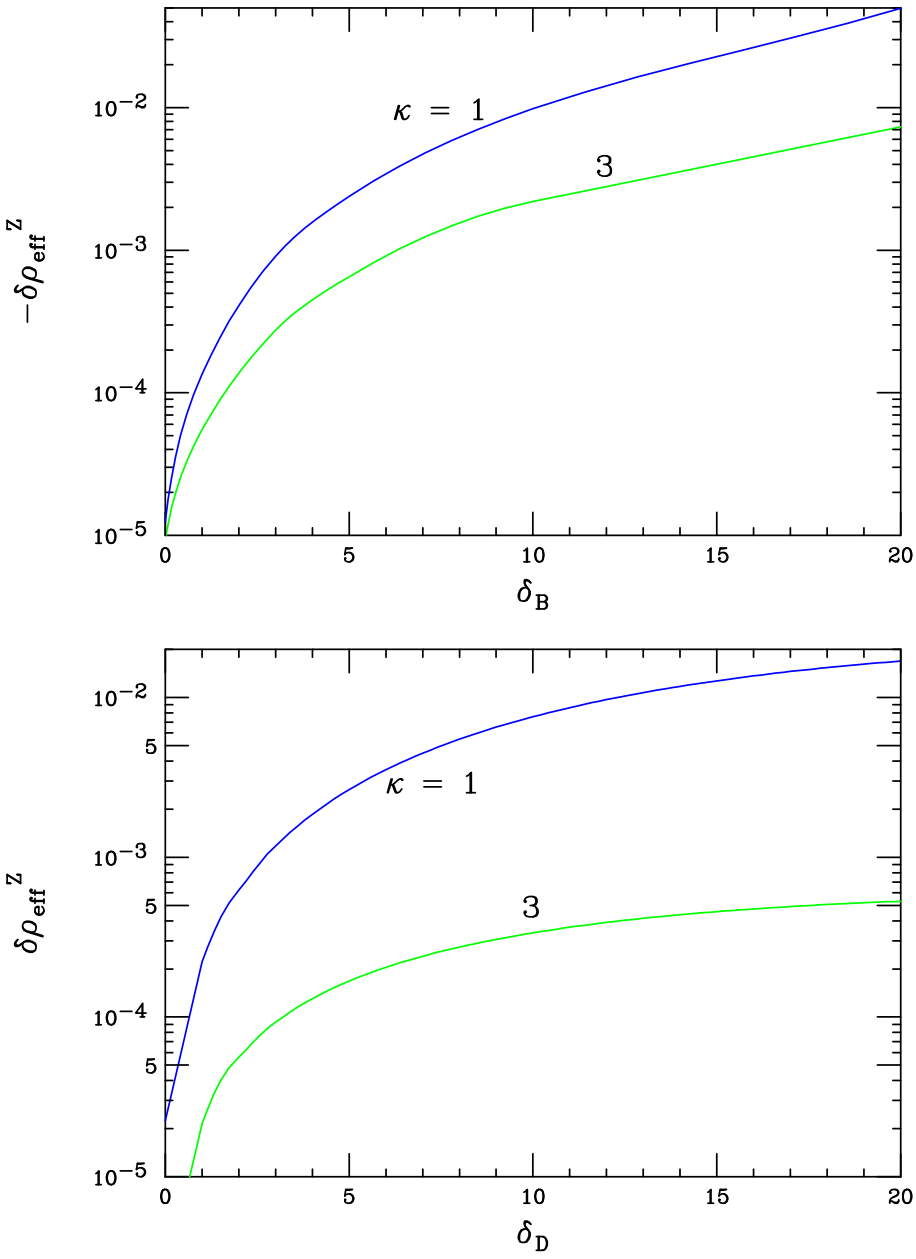

Figure 5.3: $\delta\rho^Z_{eff}$ as a function of $\delta_{B,D}$ for $\kappa = 1$ and 3. We take only one IR kinetic term to be non-vanishing at a time.

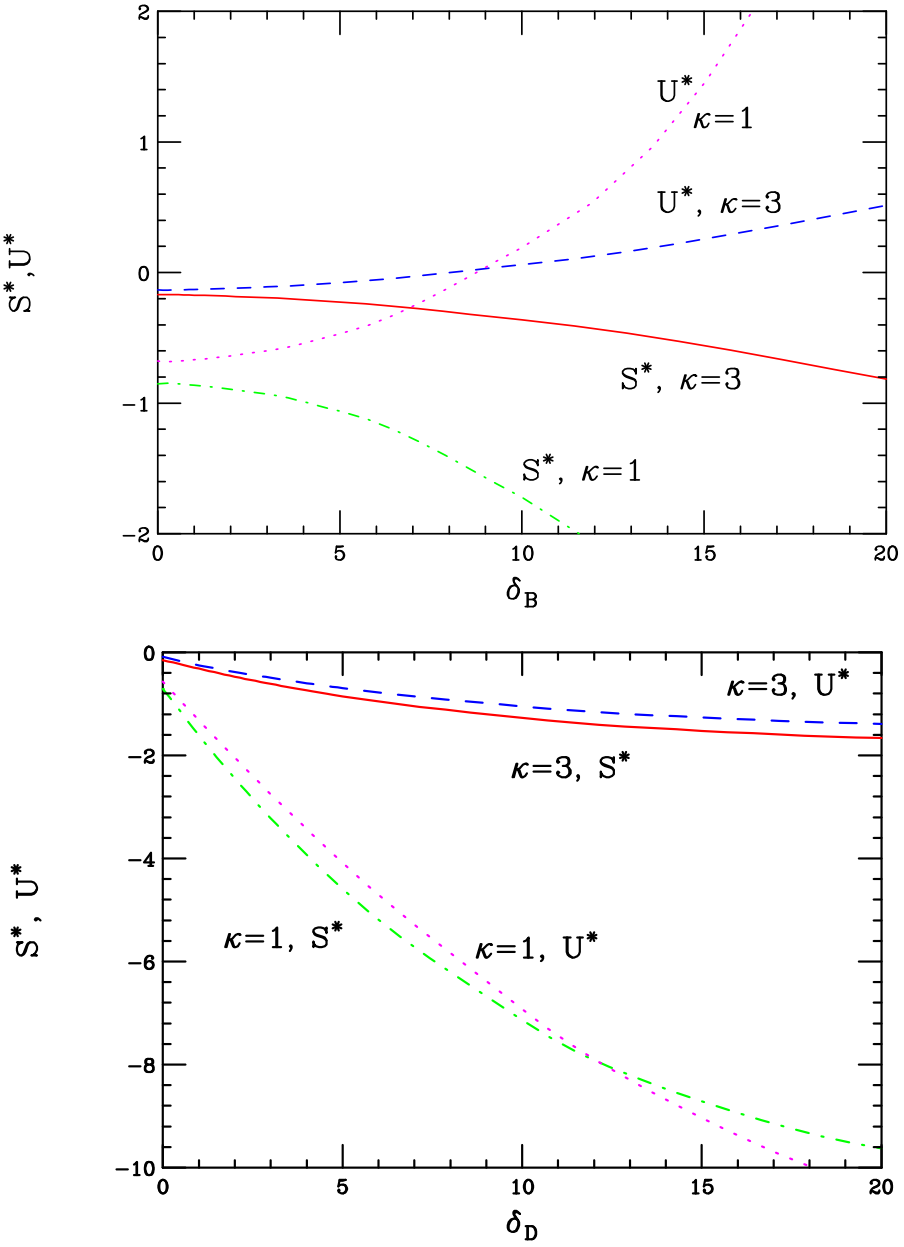

Figure 5.4: Values of the pseudo-oblique parameters S^* (solid red, dash dotted green) and U^* (blue dashed, dotted magenta) for of $\kappa = (3, 1)$ as labeled as functions of δ_{B_D}. We take only one IR kinetic term to be non-vanishing at a time.

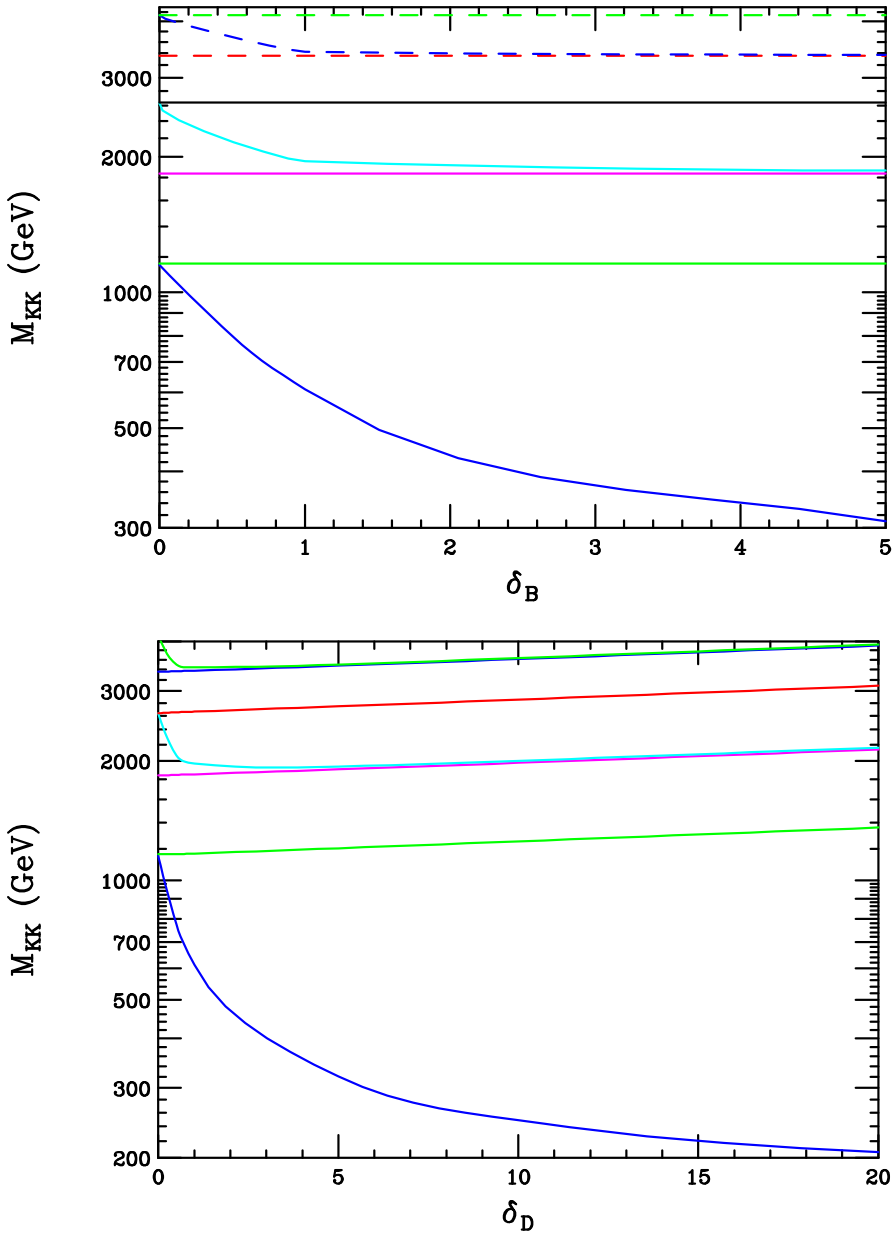

Figure 5.5: Behavior of the neutral KK mass spectrum as a function of $\delta_{B,D}$. From bottom to top on the left the curves correspond to the states $Z_{2,3,..}$. $\kappa = 1$ has been assumed. We take only one IR kinetic term to be non-vanishing at a time.

brane terms, the best limit comes from the Run I search at the Tevatron [5]. The strongest bounds on the direct production of Z'-like states come from Run II data using 200 pb^{-1} of integrated luminosity, while indirect bounds on such states have been supplied by the LEPEWWG [91]. All of these sets of data have been employed in obtaining the results which follow. Figures 5.6 and 5.7 show the $\delta_{B,D}$ dependence of the lightest KK excitation mass for $\kappa = 1, 3$ as well as the corresponding bounds on this state from LEP II and the Tevatron. The non-trivial nature of these bounds arises from the modification in the W_2 and Z_2 couplings as $\delta_{B,D}$ are varied. Note that in the case of an $SU(2)_D$ [$U(1)_{B-L}$] brane term, the best limit from the Tevatron arises from constraints on W' [Z'] production. The reason for this is that, in the case of $SU(2)_D$, both W and Z KK excitations may be light and the Tevatron constraints on W' production are generally stronger than those for Z' production since the cross section times leptonic branching fraction is larger in the W' case. For both values of κ we again see that smaller values of $\delta_{B,D}$ are in better agreement with the data. Note that while the Tevatron bounds are somewhat sensitive to the assumption that all the SM fermions are localized close to the Planck brane due to possible variations in the width of the W_2 and Z_2, this is *not* true for those from LEP. For example, one can imagine that for model building purposes, the right-handed top-quark might be moved away from the Planck brane; this could significantly alter the bounds from the Tevatron but those from LEP II would remain intact.

As we will see below, the masses of the first W and Z KK excitations must be relatively light, ≤ 1 TeV, for there to be any impact on PUV. Though their couplings to the SM fermions are somewhat reduced, such states will not escape detection at the LHC and may even be observed in the near future at the Tevatron. The first neutral KK state may be sufficiently light to be produced on resonance at a TeV-scale linear collider.

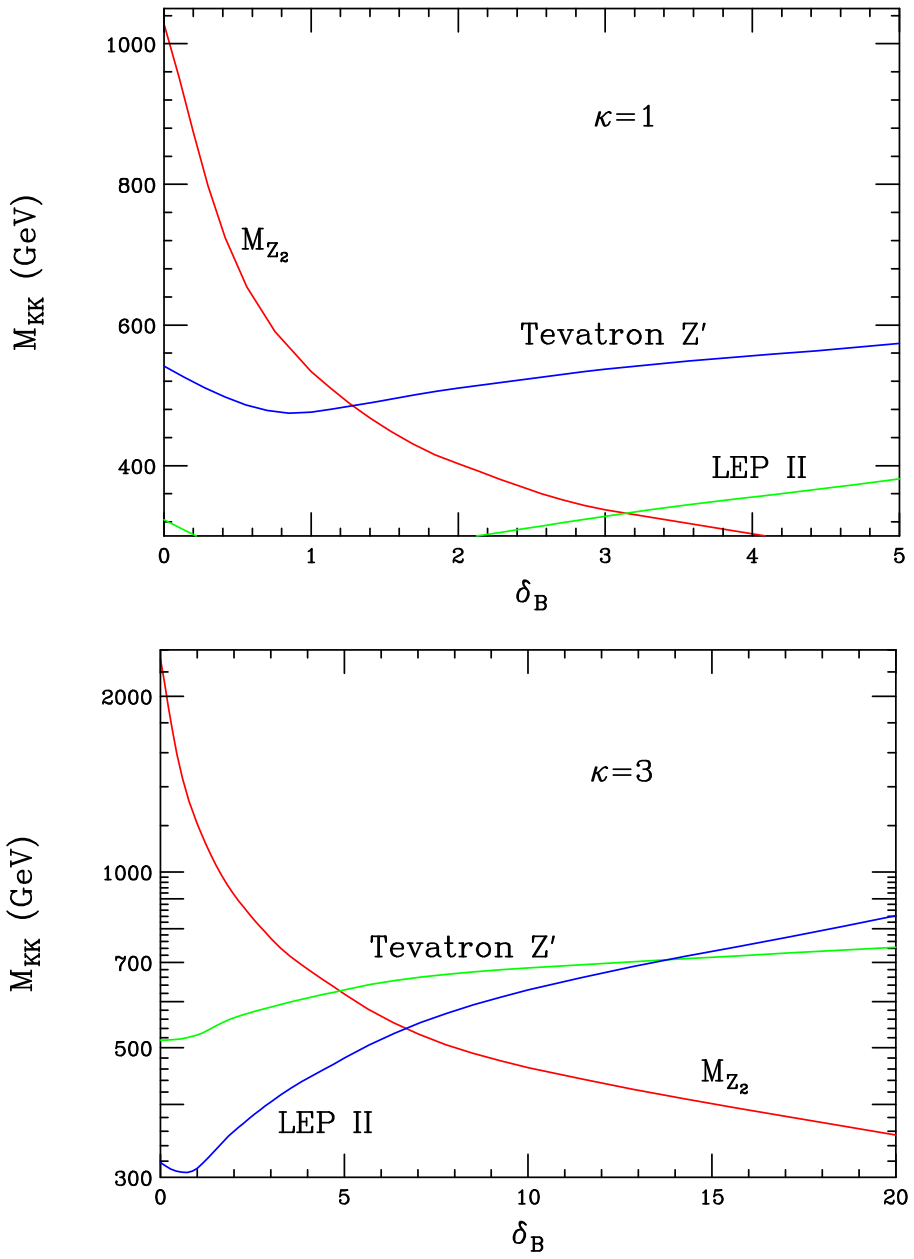

Figure 5.6: The predicted mass of the lightest KK excitation, the lower bound on the mass from the Run II Tevatron Z' searches as well as the lower bound from LEPII as a function of δ_B, assuming $\delta_D = 0$. The collider limits are discussed in detail in the text.

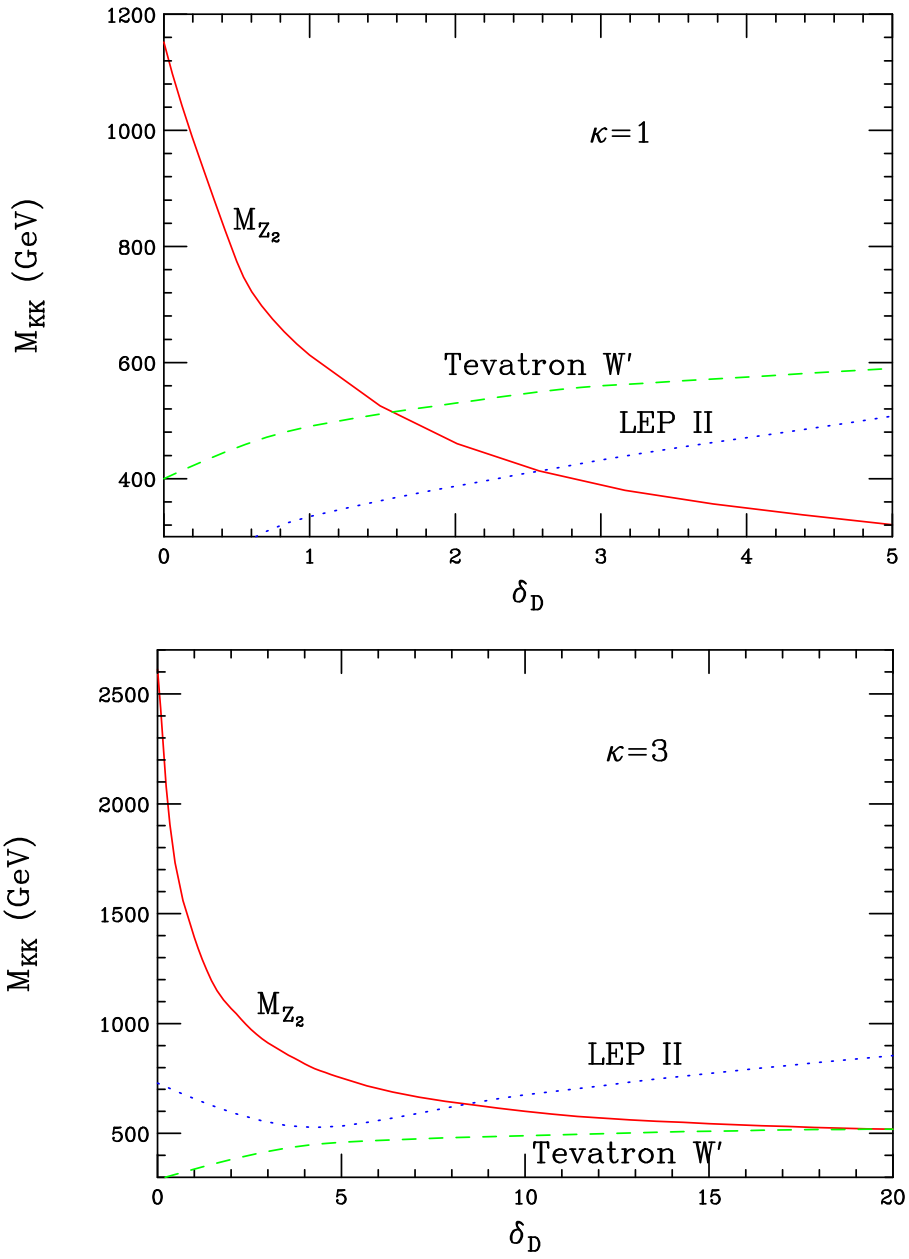

Figure 5.7: The predicted mass of the lightest KK excitation, the lower bound on the mass from the Run I Tevatron W' searches as well as the lower bound from LEPII as a function of δ_D, assuming $\delta_B = 0$. The collider limits are discussed in detail in the text.

5.4 Unitarity in $W_L^+W_L^-$ Scattering

We will now investigate the question of whether perturbative unitarity is preserved in this model. As before, we examine the amplitude for the $W_L^+W_L^- \to W_L^+W_L^-$ elastic scattering process. In Ref. [55], two sum rules were derived that insure the cancellation of terms growing with energy at high energy. Here, we find that, as in our previous analysis, these sum rules are satisfied to good precision once sufficient KK states are included. However, these sum rules are technically only valid at infinite center of mass energy. If the scattering occurs at a finite value of $\sqrt{s}$, then the amplitude cannot receive contributions from states much heavier than $\sqrt{s}$. Therefore, we investigate the full amplitude in detail in the intermediate energy region, between m_Z and the high-energy regime where the sum rules are valid. If unitarity is violated it will be in this region. Since the relevant expansion parameters, M_{KK}^2/s, are not small, we use the full tree-level amplitude from Ref. [72]. We numerically calculate the couplings using the $\delta_{B,D}$ generalized versions of Eq. (67) from Ref. [58]. We then numerically evaluate the amplitude and apply the partial wave unitarity condition $|\mathcal{R}e\, a_0| \leq 1/2$, where a_0 is the zeroth partial wave amplitude. The couplings were obtained independently on two different computing platforms, Maple and Mathematica. The partial wave amplitude was computed independently by three calculations, using Mathematica and Fortran. We have included all KK states with masses up to 10 TeV and checked that the results are stable against including more states. For $\delta_B \neq 0\,, \delta_D = 0$ we find that perturbative unitarity is violated and, furthermore, the scale of PUV is *independent* of δ_B. For $\kappa = 1$ the violation occurs at 3.8 TeV; for $\kappa = 3$ it occurs at 1.9 TeV, close to the SM value. We have also checked the case $\delta_L = 0, \delta_B = 4, \kappa = 1$ which roughly corresponds to the case studied in [38]; we found PUV at 3.15 TeV. For non-zero δ_D, with all other δ_i set to zero, we find that the scale of PUV is increased over some of the parameter space, reaching energies $\sim$ 7 TeV, as displayed in Fig. 5.8.

These results can be understood heuristically. Naively, one expects that the unitarity violations will be softened as the masses of the KK states contributing to unitarity restoration are lowered. Hence, one expects that a high value of δ_B will at least

raise the scale of unitarity violation. However, note that gauge boson scattering is a fundamentally non-Abelian process. In the present model, it is therefore an $SU(2)_L$ process, and should not depend on the $U(1)_{B-L}$ dynamics. When δ_B is turned on, the mass of one state in a pair responds dramatically, while the other is unaffected. It is clear that the state that responds should be predominantly a hypercharge boson, with very little mixture of W^3 in its wavefunction. Indeed, we can write [58] the couplings of the neutral KK states to SM fermions as $(g_{Z_n}/c_w)(T^f_{3L} - s^2_n Q^f)$. Calculation of the s^2_n parameters confirms that the light state couples as a hypercharge boson. Numerically, we can look at the coupling of the light state to two W_L bosons. At $\delta_B = 0$ this coupling is a factor of 6 smaller than that for the next neutral KK state, which is predominantly W^3. As δ_B is increased to 20 the couplings of the two states become comparable. However, the light state still makes a negligible contribution to the part of the amplutude responsible for PUV. To see this, note that the PUV can be traced to incomplete cancellations in the term that grows linearly with s at high energies. The contribution of the kth state to this sum rule is proportional to $m^2_k g^2_{11k}$, so the light state has little effect. In the case where δ_D is non-vanishing, it is the other member of the degenerate KK pair whose mass is lowered. In this case, the light state then couples mostly to isospin, and is capable of significantly modifying the $W^+_L W^-_L$ scattering amplitude.

A note about numerical instabilities is in order. We find that the sum rule governing the coefficient of the s^2 term is satisfied at the level of 10^{-6} after the first KK state is included, while the sum rule for the s term is satisfied to the level of 10^{-2}. After a few more states are included, the first sum rule is satisfied to $\mathcal{O}(10^{-9})$, and the second to $\mathcal{O}(10^{-3})$. This demonstrates that the PUV is due to incomplete cancellations in the term growing like s, as well as the presence of the constant term. However, consider the case where there is a numerical instability in the calculation of the couplings at the 10^{-8} level. Then we can estimate the energy scale at which this becomes important by noting that the amplitude goes like $10^{-8}(s^2/M^4_W)$. This becomes of order unity when $\sqrt{s} \sim 8\,\mathrm{TeV}$, implying that a calculation good to only 8 digits will give incorrect results when the scale of PUV is in the few TeV range. Since

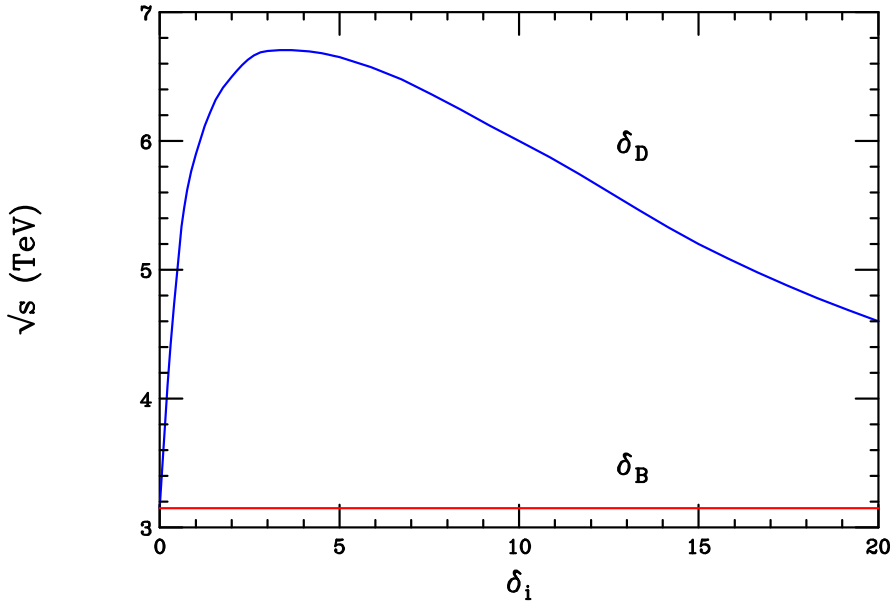

Figure 5.8: The scattering energy at which perturbative unitarity is violated in $W_L^+W_L^-$ scattering as a function of the kinetic terms. We take $\kappa = 1$.

unitarity depends on delicate cancellations, it could be expected that any error will decrease the scale of PUV. However, we have, somewhat surprisingly, found that this is *not* necessarily true. The reason is that the terms growing like s and s^2 have the opposite sign. A numerical error can thus cause the s^2 term to turn on prematurely and cancel the contribution from the s term, leading to an apparent scale of PUV *higher* than it actually is. For example, we studied one case where a numerical error at the level of 10^{-8} caused the apparent scale of PUV to be 12 TeV, while the correct scale was actually 6 TeV. For this reason, all our results were computed independently on two platforms, with agreement to greater than 12 digits.

5.5 Conclusions

The Warped Higgsless Model, which breaks the electroweak symmetry via boundary conditions associated with an extra dimension, offers a promising alternative to the Higgs mechanism. A custodial $SU(2)_D$ symmetry is present in the model, so that

reasonable agreement with precision electroweak data is conceivable. However, the degree of such agreement varies as the parameter space of the model is explored, and some regions can be excluded. Here, we examined the effects of including IR(TeV)–brane kinetic brane terms associated with the $U(1)_{B-L}$ and $SU(2)_D$ gauge symmetries of the model. We found that the addition of the $U(1)_{B-L}$ kinetic term enhances the agreement with the tree-level SM electroweak relations, particularly for larger values of the ratio of the 5–d couplings g_{5R}/g_{5L}, with reasonable values of the brane term parameter δ_B. However, including the $SU(2)_D$ brane term alone results in a stark disagreement with the SM tree level relations in the electroweak sector. We performed a limited exploration of the full parameter space and found it is possible that a combination of the two IR–brane terms may result in a reasonable consistency with the tree-level SM relations.

In its original form, the WHM has some difficulties in the gauge sector in that perturbative unitarity is violated at the TeV-scale in $W_L^+W_L^-$ scattering. This does not exclude the model from being viable, but does suggest that interactions in the gauge sector are problematic. To restore unitarity in the gauge sector, additional new physics must be introduced. Here, we again examined the effects of including the IR(TeV)–brane kinetic brane terms. It is well-known that the addition of brane terms can alter the couplings and masses of gauge KK states, and this would thus affect the KK contributions to $W_L^+W_L^-$ scattering. While we found that the $U(1)_{B-L}$ brane term does modify the gauge KK spectrum, we also discovered that PUV in $W_L^+W_L^-$ scattering is independent of such a brane term and hence remains unaffected by its presence. This is because this scattering process is inherently non-Abelian and should not depend on the $U(1)_{B-L}$ dynamics. In contrast, the inclusion of the $SU(2)_D$ kinetic term does affect $W_L^+W_L^-$ scattering; for moderate values of the brane term, violation of perturbative unitarity is delayed until $\sqrt{s} \approx 7$ TeV. In addition, we also investigated the collider bounds on the production of the lightest gauge KK excitation as a function of the brane terms. Searches for new gauge bosons at the Tevatron and LEP II exclude large values of the kinetic term parameters $\delta_{B,D}$.

Our analysis shows how various directions in the parameter space of the WHM affect its phenomenology. Requiring a model that is perturbatively sensible up to

$\mathcal{O}(10)$ TeV favors $\kappa = 1$ and $1 \lesssim \delta_D \lesssim 10$, regardless of the size of δ_B. Collider constraints on the KK modes of the gauge bosons can accommodate this range of parameters, as long as $\delta_{B,D} \lesssim 2 - 3$, with the Tevatron bounds depending on the fermion localization. We observe that the requirements of multi-TeV perturbative unitarity and those imposed by tree level SM relations, as represented by the pseudo-oblique parameters and various values of $\sin^2\theta$, do not coexist without tension in this model. However, a direct comparison of these latter quantities with the electroweak data requires a computation of the radiative corrections in the WHM, which lies outside the scope of this work. Thus, it remains an open possibility that this model could provide a viable alternative for electroweak symmetry breaking, valid far above the weak scale.

Acknowledgements

We would like to thank Csabi Csaki, Graham Kribs, Hitoshi Murayama, and John Terning for discussions related to this work. The work of H.D. was supported by the Department of Energy under grant DE-FG02-90ER40542.

Chapter 6

Monte Carlo exploration of warped Higgsless models

6.1 Introduction

As the time of the LHC turn-on draws nearer, the search for alternative theories to the standard single Higgs boson picture of electroweak symmetry breaking is intensifying. One such scenario [56] is particularly appealing in that it employs a minimal particle content in a 5-dimensional spacetime and exploits the geometry of the additional dimension to break the electroweak symmetry. The model is based on the Randall-Sundrum framework [136] with an $SU(2)_L \times SU(2)_R \times U(1)_{B-L}$ gauge group in 5-d Anti-de Sitter space. The AdS_5 slice is bounded by two branes, with the scale of physics on the IR(TeV)-brane being given by $\Lambda_\pi \equiv \overline{M}_{Pl} e^{k\pi r_c}$, with k corresponding to the RS curvature parameter and r_c being the radius of the compactified dimension. The set of boundary conditions, which differ for the two branes, generate the breaking chain $SU(2)_R \times U(1)_{B-L} \rightarrow U(1)_Y$ at the Planck scale with the subsequent breaking $SU(2)_L \times U(1)_Y \rightarrow U(1)_{QED}$ at the TeV scale. The electroweak symmetry is thus broken without the introduction of a Higgs field. After the Planck scale symmetry breaking occurs, a global $SU(2)_L \times SU(2)_R$ symmetry is present in the brane description. This breaks on the TeV-brane to a diagonal group $SU(2)_D$ which corresponds [9] to the custodial $SU(2)$ symmetry of the Standard Model (SM) and helps preserve

the SM tree-level relation $\rho = 1$. We denote this scenario as the Warped Higgsless Model (WHM).

In this scenario, the role of the Goldstone boson in generating masses for the W and Z bosons is played by the would be zero-mode of the KK tower corresponding to the 5^{th} component of the bulk gauge fields (*i.e.*, A_0^5). The Z boson observed at LEP/SLC/Tevatron is the first excitation of a neutral gauge boson KK tower, while the photon corresponds to the massless zero-mode of this tower. The W boson observed in experiments is then the first state of a KK tower of charged gauge bosons, and there is no charged massless zero-mode. The experimentally observed values of the W and Z masses and couplings are essentially reproduced in this model. However, the presence of the gauge KK states affect a number of processes. In particular, much work has been performed analyzing the contributions to the set of precision electroweak measurements in Higgsless scenarios [128, 27, 58, 35, 38, 27, 49, 76, 43]. In the flat space analog of the WHM [55], *i.e.*, a Higgsless model based on a flat higher dimensional spacetime, unacceptably large deviations from precision electroweak data are generated. However, good agreement with the data can be obtained at tree-level in the warped Higgsless scenarios, provided that the masses of the KK excitations are sufficiently heavy. In addition, the KK excitations must satisfy the constraints from direct production of new gauge bosons at the Tevatron and from their contribution to contact interactions in four fermion processes at LEPII.

Note that precision observables are sensitive to one-loop electroweak effects. In general, the loop corrections in this model will be qualitatively similar to those in the SM (up to small shifts in the couplings). However, there are three types of loop corrections that may cause large deviations: the gauge KK excitations, the absence of loops with a physical higgs, and the top quark. Since the gauge KKs are playing the role of the physical Higgs in WW scattering, it is expected that they will do the same here, so the first two effects should largely cancel. In our model all fermions are localized to the Planck brane, and the parameters of the model are adjusted so the couplings are as close to the SM couplings as possible. Hence, the top corrections should again approximate the Standard Model values. (In a model where the top mass is generated on the TeV brane [54] a more careful treatment would be needed.)

Since we expect all loop corrections to qualitatively approximate the SM corrections, we will require that the tree level WHM approximate the tree level SM as closely as possible in the analysis below.

In the absence of a Higgs boson, or any other new physics, perturbative unitarity (PU) in elastic $W_L^+W_L^-$ scattering is violated at an energy scale of $\simeq 1.7$ TeV. However, in these Higgsless scenarios, it is in principle possible that the exchange of the neutral gauge KK tower in $W_L^+W_L^- \to W_L^+W_L^-$ can restore PU, provided that a set of conditions on the KK masses and couplings are satisfied [55]. This works well in the flat space analog of the WHM, but is problematic within the warped scenario. In particular, the region of parameter space which enjoys good agreement with the precision electroweak and collider data leads to low-scale ($\sim$ 2 TeV) perturbative unitarity violation (PUV) in gauge boson scattering [58]. One would at least expect the theory to remain perturbative up to the cutoff scale of the effective theory on the TeV-brane, Λ_π, where Λ_π is roughly on the order of 10 TeV. This leads to a tension in the model parameter space in terms of finding a region which simultaneously satisfies all of the model building requirements as well as the experimental constraints.

In [38, 59] the effects of including the IR-brane terms associated with the $U(1)_{B-L}$ and $SU(2)_D$ gauge symmetries were examined; the presence of such terms is known to alter the corresponding KK spectrum and couplings [42, 64, 63, 41]. In these analyses it was found that the addition of the $U(1)_{B-L}$ IR-brane term could lead to improved agreement with the electroweak data [38] and the inclusion of the $SU(2)_D$ brane term could delay PUV in $W_L^+W_L^- \to W_L^+W_L^-$ to scattering energies of order $\sim 6-7$ TeV [59]. However, a scan of the full parameter space was not performed in order to determine whether there exists a region where all the constraints discussed above are simultaneously satisfied.

In this paper, we perform a detailed exploration of the WHM parameter space via Monte Carlo techniques. There are a number of parameters present in this scenario: (i) the set of coupling strengths for each gauge symmetry: g_{5L} which is fixed by G_F, the ratio $\lambda \equiv g_{5B}/g_{5L}$ which is fixed by the value of M_Z, and the ratio $\kappa \equiv g_{5R}/g_{5L}$ which lies in the restricted range $0.75 \lesssim \kappa \lesssim 4.0$, but is otherwise free. (ii) The brane kinetic terms associated with the IR-brane, $\delta_{B,D}$, and the UV-brane, $\delta_{L,Y}$. Here the brane

terms will be treated as free phenomenological parameters but should in principle be calculable from the full theory once the UV-completion is known. The parameter space is sufficiently large such that it is best scanned by Monte Carlo sampling. For each set of parameters, we subject the model to a succession of tests: (i) model requirements, such as the absence of ghosts and tachyon states, (ii) consistency with the precision electroweak data, (iii) consistency with the direct and indirect collider bounds on new gauge boson production, and (iv) PU in elastic $W_L^+W_L^-$ scattering. In particular, we require that this scattering process be unitary up to $\Lambda_\pi \simeq 10$ TeV. We find that the conditions (i-iii) are relatively easy to simultaneously satisfy, but that none of the models satisfied perturbative unitarity beyond the scale of $\simeq 2$ TeV. We conclude that if a successful model of this type exists, it must be highly fine-tuned, or must contain other sources of new physics.

We present our analysis in the next two sections. The formalism of the WHM is presented in detail in our earlier work [58, 59] and will not be reproduced here.

6.2 Analysis: Electroweak and Collider Constraints

As discussed above, the model in its present form contains five free parameters: $\kappa = g_R/g_L$, the ratio of the two $SU(2)_{L,R}$ gauge couplings which is expected to be of order unity, and the four brane kinetic term parameters, $\delta_{B,D,L,Y}$, corresponding to the various unbroken gauge groups on the TeV and Planck branes: $U(1)_{B-L}, SU(2)_D, SU(2)_L$ and $U(1)_Y$, respectively. Our approach is to choose a value for κ and then explore the parameter space spanned by $\delta_{B,D,L,Y}$ via Monte Carlo methods. To be definitive we will assume that all the δ_i are constrained to lie in the range $-\pi kr_c \leq \delta_i \leq \pi kr_c$ as suggested in [42, 64, 63, 41], and we fix $kr_c = 11.27$ in our numerical study. For each set of values of the δ_i we define a successful model as one which passes through a number of cuts and filters that we now describe in some detail. Our results are compiled in Tables 1 and 2, which displays the amount of statistics generated for each value of κ and the number of models which survive each successive constraint. Our statistics are concentrated near $\kappa = 1$ as in this case the KK spectrum is relatively light and we are more hopeful that PU constraints will be satisfied.

Upon generating a set of δ_i we first calculate a group of model parameters which are associated with the lightest massive charged and neutral gauge bosons, and ensure that they are identified with the observed SM fields, $W_1 = W$ and $Z_1 = Z$. We take the experimental values of their masses $M_Z = 91.1875$ GeV and $M_W = 80.426$ GeV [91] as input to our analysis. This numerically fixes the low energy scale $ke^{-\pi kr_c}$ that gives the masses of the KK excitations in the RS model, as well as the value of the on-shell weak mixing angle, $\sin^2\theta_{OS} = 1 - M_W^2/M_Z^2$. Next, the requirement of the absence of ghosts in the unitary gauge of any physical theory implies that these two states, W_1 and Z_1, must have positive norms. Similarly, the field that represents the photon must also have a positive norm. In addition to these constraints, we demand that the ratio of the squares of the gauge couplings, $\lambda^2 = g_{B-L}^2/g_L^2$, be positive definite. As can be seen from Table 1, these few simple cuts can remove as much as $\sim 40\%$ of the parameter space volume.

Assuming that the SM fermions (at least the first two generations) are localized near the Planck brane we can now calculate a number of electroweak quantities. Recall that our philosophy is that we want the tree level Higgsless model to match the tree level SM as closely as possible, outside of the Higgs sector, since in many cases we expect approximately similar one-loop radiative corrections. As we found in our earlier works [58, 59], a description of the γ, W and Z couplings to the SM matter fields can be parameterized in terms of two other definitions of the weak mixing angle in addition to $\sin^2\theta_{OS}$. These two additional angles are defined via: $\sin^2\theta_{eg} = e^2/g_W^2$, with $g_W = g_{ffW_1}$ being the coupling of the W to SM fermions on the Planck brane, and $\sin^2\theta_{eff}$ being given by the couplings of the Z to the same fermions at the Z-pole as discussed below. The electromagnetic coupling is, as usual, defined through the interaction of the massless neutral mode, Z_0, which we identify as the photon, to the SM fields. All three definitions of the weak mixing angle are identical at the tree level in the SM but are, in general, quite different numerically in the WHM.

Writing the Z-pole couplings to SM fermions as

$$\frac{g_Z}{c_{OS}}(T_3 - \sin^2\theta_{eff}\ Q)\,, \tag{6.1}$$

Cuts κ	0.75	0.9	1.0	1.25	1.5	2.0	3.0	4.0
Initial Sample	308,710	141,950	1,307,463	251,970	271,570	145,570	181,274	136,920
$\lambda^2 > 0$	130,286	62,202	585,011	115,455	125,035	67,662	82,583	16,204
No γ, Z ghosts	130,286	62,202	585,011	115,455	125,035	67,662	82,583	16,204
$\lvert\delta\rho\rvert < 0.005$	16,181	7,887	76,994	16,728	20,183	13,799	24,223	2,958
$\lvert s^2_{\rm eff} - s^2_{\rm os}\rvert < 0.005 s^2_{\rm os}$	676	387	3,665	875	1,356	1,328	3,838	2,899
$\lvert s^2_{\rm eg} - s^2_{\rm os}\rvert < 0.005 s^2_{\rm os}$	242	159	1,539	332	545	576	1,805	2,013
No Z' ghost	242	159	1,539	322	545	576	1,805	2,013
Z' Tevatron	150	102	1134	217	393	439	1,556	1,830
$m_{Z'} < 1.5$ TeV	74	50	644	90	180	202	828	1,581
LEPII indirect	70	45	550	72	80	175	796	1,178
Isospin coupling	24	13	112	12	8	12	65	0
No Tachyons	0	0	0	0	0	0	7	0
PUV	0	0	0	0	0	0	0	0

Table 6.1: Data samples and their responses to the various constraints as described in the text. The values represent the number of cases surviving each of the cuts.

in obvious notation, we also can define an auxiliary quantity, $\rho^Z_{eff} = g^2_Z/g^2_W$, which relates the strengths of the W and Z gauge boson interactions. We identify $g_Z/c_{OS} = g_{ffZ_1}$. In the SM at tree-level $\rho^Z_{eff} = 1$, of course. We note that all of the electroweak observables at the W, Z mass scale can now be described in terms of the three weak mixing angles, M_Z, and ρ^Z_{eff} and we have no need to introduce any other parameterizations.[1] It is clear that if we wish to reproduce the tree-level SM we must have all three values of $\sin^2\theta$ be almost equal as well as require that ρ^Z_{eff} be very close to unity. In our numerical study we will demand that the three definitions of $\sin^2\theta$ all be equal within 0.5% and additionally require $|\delta\rho^Z_{eff}| = |\rho^Z_{eff} - 1|$ to be less than 0.005. The magnitude of these constraints should be comparable to the size of the one-loop generated electroweak corrections. This set of constraints is extremely powerful for the full WHM parameter space, but is especially strong for low values of κ as can be seen from Table 1; only a few percent of the original model parameter space remains after applying these cuts. Note that models with larger values of κ are generally favored by these electroweak constraints. This is not unexpected; we saw in our earlier work that the SM limit is approached rapidly as the value of κ is increased. The price one pays for this is a rapid increase in the masses of the KK states leading to an obvious failure in PU as discussed below.

We now turn our attention to the mass and couplings of the next lightest neutral KK state, Z_2; these parameters are highly constrained by both experimental data as well as our requirement of PU as we will see below. We first impose the obvious

[1] It can be easily shown that there is a unique mapping of the above parameters, together with G_F which now involves a KK sum, over to the ϵ_i of Altarelli and Barbieri[13].

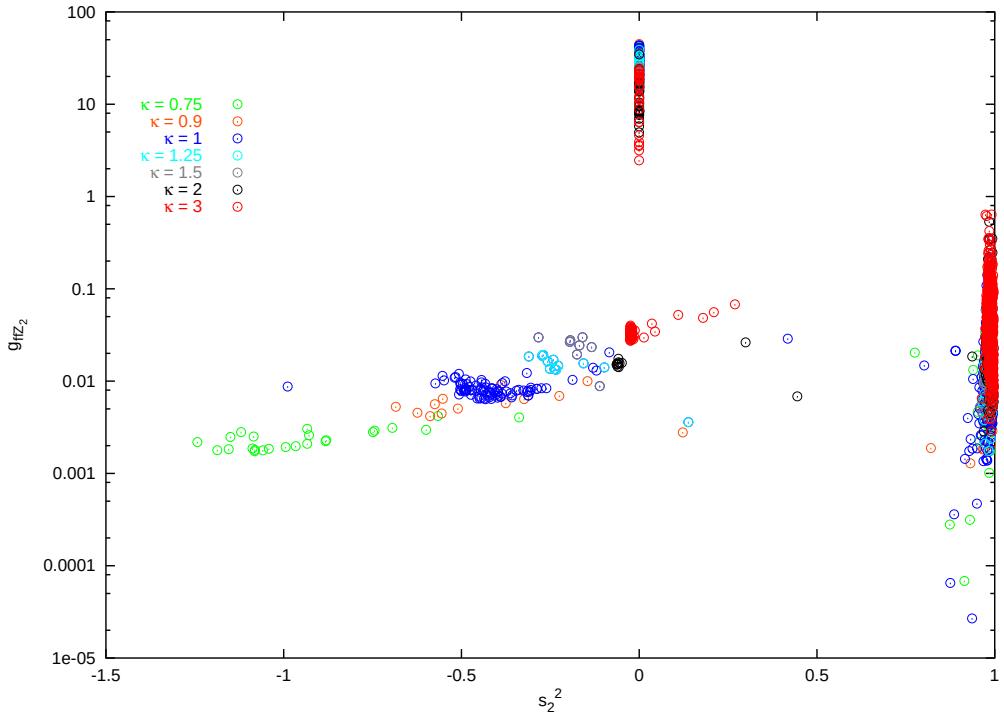

Figure 6.1: The coupling strength of the first neutral KK excitation beyond the Z in units of g_W as a function of its effective $\sin^2\theta$. The color coding labels models with different values of κ. All electroweak constraints have been applied to the cases shown as well as the bounds from the TeVII direct searches. A cut of $M_{Z_2} < 1.5$ TeV has also been applied. Indirect LEPII constraints have not yet been imposed.

constraints that this state not be a ghost and that it has not (yet) been observed in *direct* Z'-like production searches at LEPII or the Tevatron[2]. This places a correlated cut on the mass of this state as a function of its couplings to the SM fermions on the Planck brane. Futhermore, we note that the *indirect* search constraints for Z'-like states must also be satisfied. To be specific we will demand that the masses of the Z_2's as well as their couplings to SM fermions are such as to have avoided the LEPII contact interaction constraints. This constraint is actually quite powerful and removes an entire region in the Z_2 mass vs. coupling plane which survives the electroweak and Tevatron bounds. After imposing all these requirements we see from Table 1 that there are a respectable number of surviving cases.

The particular properties of the surviving cases will be examined in detail below. Figures. 1 and 2 show the values of the Z_2 mass and coupling for those models passing all of our above cuts except the constraints imposed by LEPII; in these figures an additional requirement for PU that $M_{Z_2} \leq 1.5$ TeV, to be discussed further below, has been imposed. The Tevatron direct search constraint is responsible for the sharp diagonal boundary in the bottom panel of Fig. 2. Note that the couplings of the Z_2 can always be written in a form similar to the Z above except we denote the overall coupling strength as g_{ffZ_2} and the value of the corresponding weak mixing angle as $s_2^2 = \sin^2\theta_{eff}(Z_2)$, *i.e.*, $(g_{ffZ_2}/c_w)(T_{3L}^f - s_2^2 Q^f)$. Note the large set of models near $s_2^2 = 0$ and 1, the former with large couplings and masses between ~ 1 and 1.5 TeV. These strongly coupled cases are entirely removed by the LEPII contact interaction bound and will not concern us further. It is important to note that at this point there *are* a reasonable of surviving models subsequent to applying this rather strict set of electroweak and collider constraints on the model parameter space. This situation is in contrast with results previously obtained by Barbieri *et al.*[27] in the case of the flat space analog where no warping is present. These authors showed that there was no significant region of parameter space which simultaneously satisfied the collider and precision electroweak constraints. We have performed a Monte Carlo study of

[2]The strongest bounds at present are given by the D0 Collaboration in D0note 4375-Conf, v2.1 based on $\sim 200\ pb^{-1}$ of Run II data. The analysis of LEPII data leading to bounds on new gauge boson-like signatures can be found in C. Geweniger *et al.*, LEP Electroweak Working Group note LEP2FF/02-03(2002)

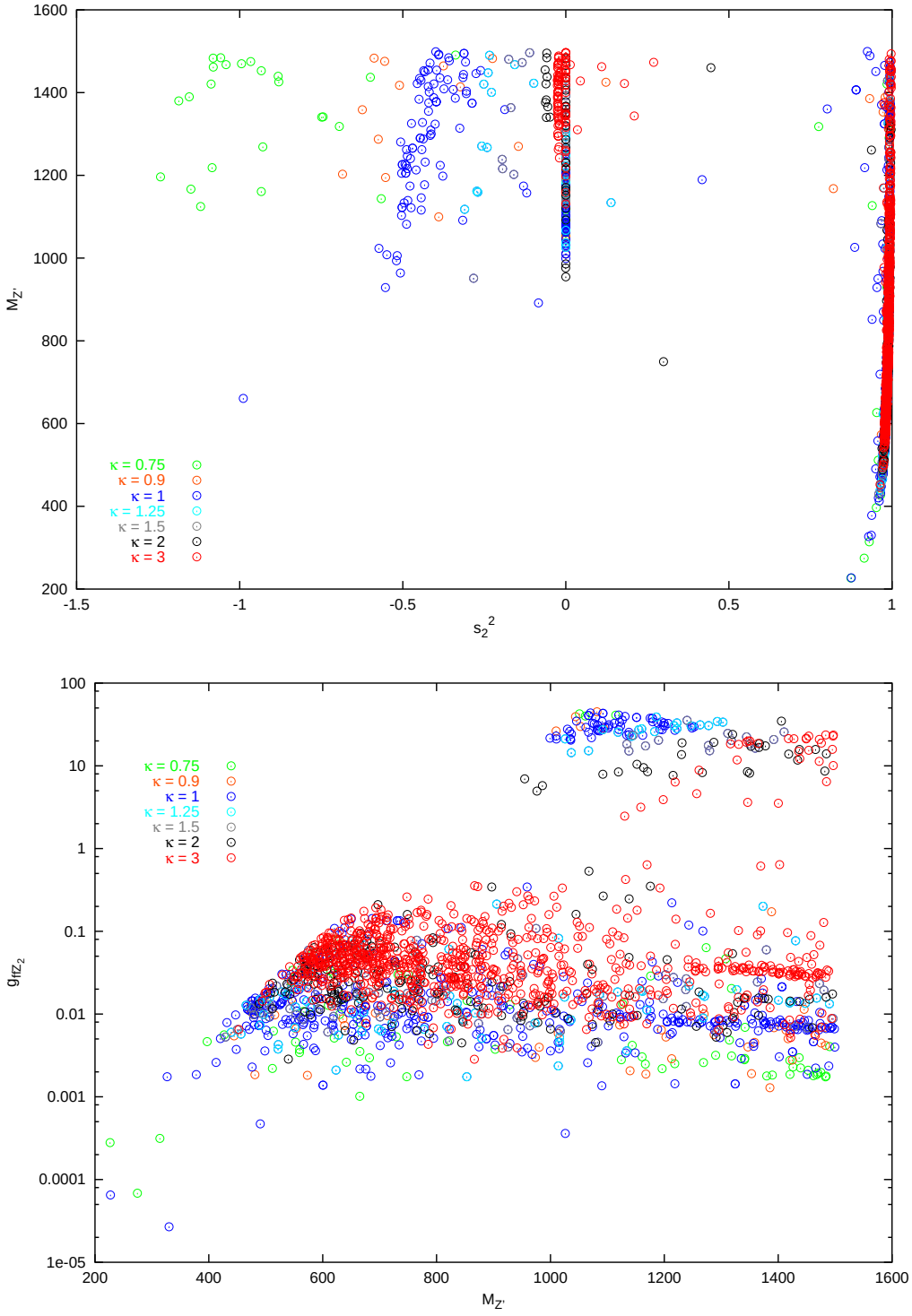

Figure 6.2: Same as in the previous figure but now showing the mass-coupling strength and s_2^2 correlations.

the flat space analog model, imposing the constraints presented above, and effectively confirm their results. We note for completeness that if we strengthen our electroweak cuts such that $0.5\% \to 0.1\%$ in the analysis above, the number of surviving cases is reduced by a factor $\simeq 10$.

6.3 Analysis: Perturbative Unitarity and Tachyons

Unitarity is an important property of any gauge theory[145, 105, 129]. Before examining PU directly, two further filters can be applied that will help us to focus on models which may satisfy our basic requirements. If the Z_2 in any of the models that survive both the electroweak and collider constraints is to contribute significantly to the $W_L^+W_L^-$ amplitude it must predominantly couple to isospin and not to $B-L$ or hypercharge Y. Note that when s_2^2 is near unity(zero), the Z_2 couples almost purely to Y(isospin). To ensure that the Z_2 has significant isospin-like coupling, we will demand that $s_2^2 < 0.7$. We make exception for the special set of cases where the Z_2 mass is less than $\simeq 400$ GeV. The reason for keeping these $B-L$-like coupled states is that their light masses may help induce a potentially large contribution to the $W_L^+W_L^-$ elastic scattering amplitude. Furthermore, there may exist somewhat heavier excitations not too far away in mass which *are* coupled to isospin. This cut on s_2^2 appears to be rather loose, but many of the surviving models have great difficulty satisfying it. It is interesting to note that at this point in the parallel analysis of the flat space analog model [55] none of the cases satisfy this constraint; all of the possible cases in the flat space model surviving both collider and electroweak constraints are found to essentially couple to $B-L$ or Y.

In addition to the above, the Z_2 satisfying the collider constraints must still be sufficiently light as to make a significant contribution to $W_L^+W_L^-$ elastic scattering. Recall that in the SM without a Higgs boson, PUV occurs near $\sqrt{s} \simeq 1.7$ TeV. This implies that there must be at least one, and more likely several, neutral KK states below this scale if they are to 'substitute' for the SM Higgs in restoring unitarity. We thus impose the rather weak requirement that the lightest new neutral KK state, Z_2, must exist with a mass below 1.5 TeV; we make no further requirements on the

spectrum for now.

This pair of constraints on the mass and nature of the Z_2 couplings are rather difficult to satisfy simultaneously for the models that have passed the electroweak and collider cuts; relatively few cases survive at this point as can be seen from Table 1. Most of the models passing the electroweak and collider bounds tend to be either too massive or predominantly coupled to hypercharge. We can also see this from Figs. 1 and 2 where the densely populated region near $s_2^2 = 1$ with a mass greater than 400 GeV is now removed by these cuts. At this point, the remaining models are presented in Figs. 3 and 4; their distribution in δ_i space is shown in Fig. 5.

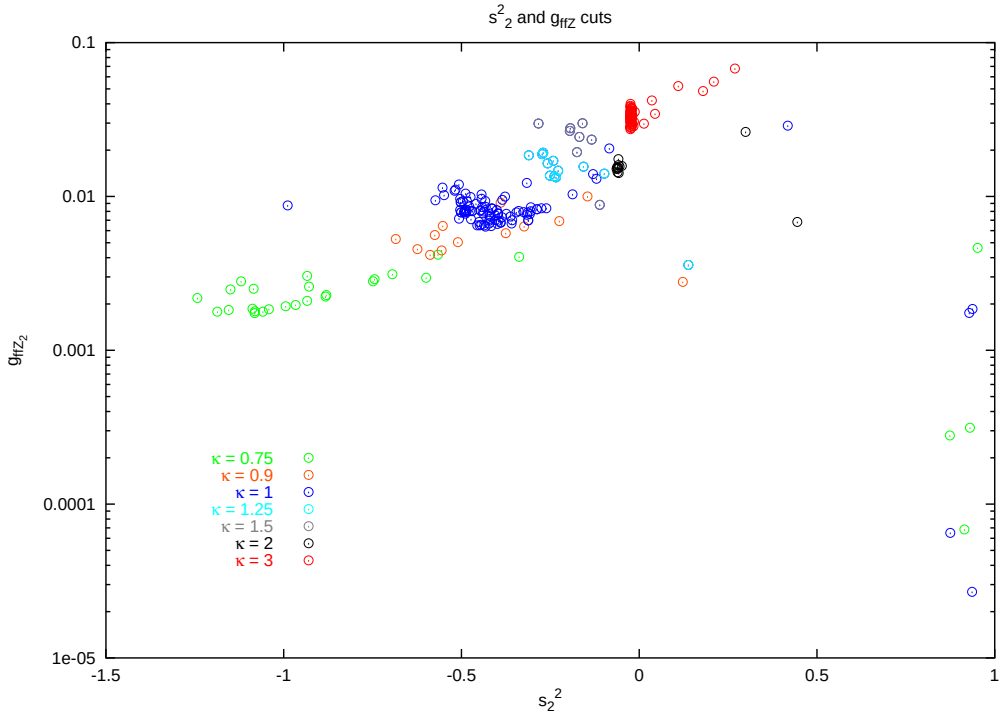

Figure 6.3: Same as Fig.1, but now applying the constraints from LEPII and the correlated mass-s_2^2 cuts to remove the KK states coupling to $B - L$ and hypercharge as described in the text.

At this point we are ready to examine the PU characteristics of the remaining cases shown in Figs. 3-5 in detail. First we note that these models fall into two broad classes: those few with all positive δ_i and those with at least one of the δ_i being negative. An analysis of PU in $W_L^+ W_L^-$ elastic scattering for the cases with all

Cuts κ	1.0	1.5	2.0	2.5	2.75	3.0	4.0
Initial Sample	611,150	304,680	178,320	122,801	266,801	169,862	70,661
$\lambda^2 > 0$	611,150	304,680	178,320	122,801	266,801	169,862	70,661
No γ, Z ghosts	611,150	304,680	178,320	122,801	266,801	169,862	70,661
$\lvert\delta\rho\rvert < 0.005$	168,732	159,537	107,709	89,124	211,944	146,087	69,867
$\lvert s^2_{\rm eff} - s^2_{\rm os}\rvert < 0.005 s^2_{\rm os}$	0	502	1,506	2,734	8,600	7,456	8,724
$\lvert s^2_{\rm eg} - s^2_{\rm os}\rvert < 0.005 s^2_{\rm os}$	0	244	760	1,505	4,887	4,308	5,317
No Z' ghost	0	244	760	1,505	4,887	4,308	5,317
Z' Tevatron	0	6	145	530	2,204	2,233	4,174
$m_{Z'} < 1.5$ TeV	0	6	143	530	2,086	2,112	3,919
LEPII indirect	0	6	143	509	2,086	2,112	3,919
Isospin coupling	0	0	0	0	0	0	0
No Tachyons	0	0	0	0	0	0	0
PUV	0	0	0	0	0	0	0

Table 6.2: Same as the previous table but now for a special set of runs assuming all the $\delta_i \geq 0$. Note that many cases survive until the $B - L$ or Y cut is employed.

positive δ_i follows the standard procedure described in our earlier work [58, 59] which makes use of the scattering amplitude as given by [72] augmented to include additional neutral KK exchanges. Our proceedure is to calculate the complete amplitude using the expressions of Duncan *et al.*[72] which we modify to include an an arbitrary number of neutral KK exchanges in the $s-$ and $t-$ channels as well as an arbitrary W 4-point coupling. We then integrate this amplitude to extract out the $J = 0$ patial wave, a_0, subject to angular integration cuts imposed to avoid the photon $t-$channel pole. For our test of PU we demand that $|Re\ a_0| < 1/2$, as is widely done in the literature. This analysis reveals that *none* of these models are much improved in comparison to the SM without a Higgs boson, *i.e.*, PUV occurs at $\simeq 2$ TeV. The main reason for this is that these cases tend to have a light Z_2 which is predominantly coupled to Y as discussed above. To restate, if the δ_i are all chosen positive, the models surviving the electroweak and collider constraints *do not* lead to theories which have PU beyond the $\simeq 2$ TeV scale.

In order to verify this result we generated a larger statistical sample, an additional $\sim 1.7 \cdot 10^6$ models, distributed over various values of κ, assuming all of the $\delta_i \geq 0$. The results from performing these runs are shown in Table 2 using the same cuts as above. Here we see that although many models pass the combined collider and

electroweak constraints none of them survive the non-$B-L/Y$ coupling requirement. Thus all of these models fail, confirming our previous results. We checked that this also occurs in the analog flat space model.

We now return to the models with at least one negative δ_i. Ordinarily, such models would not be considered since having negative δ_i at the tree-level implies the existence of tachyons with all their related difficulties [110]. Indeed, we have verified numerically that such tachyonic states do indeed exist in the spectrum for all the models in this class, and found that the tachyon masses are quite sensitive to the magnitudes of the δ_i. Nomura [128], however, has argued that potentially large and negative boundary terms associated with the Planck brane may be benignly generated at loop level without the significant influence of tachyons. These negative brane terms can be of sufficient importance numerically as to require their inclusion in a detailed tree-level analysis such as we are performing here. In such a case one could view the existence of tachyons as an artifact of including only partial one-loop effects. Since we are ignorant of the possible origin of negative δ_i in the full UV-completed theory, we must in principle consider these cases further.

When analyzing the models with negative δ_i, one has to take care that the existence of tachyons at the tree level does not have important phenomenological effects, *e.g.*, tachyons that have significant couplings to SM fermions or which contribute substantially to SM processes such as $W_L^+W_L^-$ scattering. At the very least, if we are to consider models with such states, the tachyons must be *truly* benign. Certainly models where these tachyons can lead to important physical effects must not be allowed. However, if the tachyons are significantly decoupled from the SM fields we will consider such theories as benign and examine their PU properties. Based on the analysis of Nomura [128], as well as our previous work [58, 59], one might suspect that the tachyons induced by Planck brane kinetic terms, $\delta_{L,Y}$, are benign while those arising from kinetic terms on the TeV-brane, $\delta_{B,D}$, may not be.

As an initial filter, we analyze the couplings of tachyons to the SM fermions localized near the Planck brane; clearly, these couplings can depend sensitively on the magnitude of the δ_i. First, we must determine the number of tachyon states that are in the spectrum. In the flat space analog [55] of WHM it is easy to see that

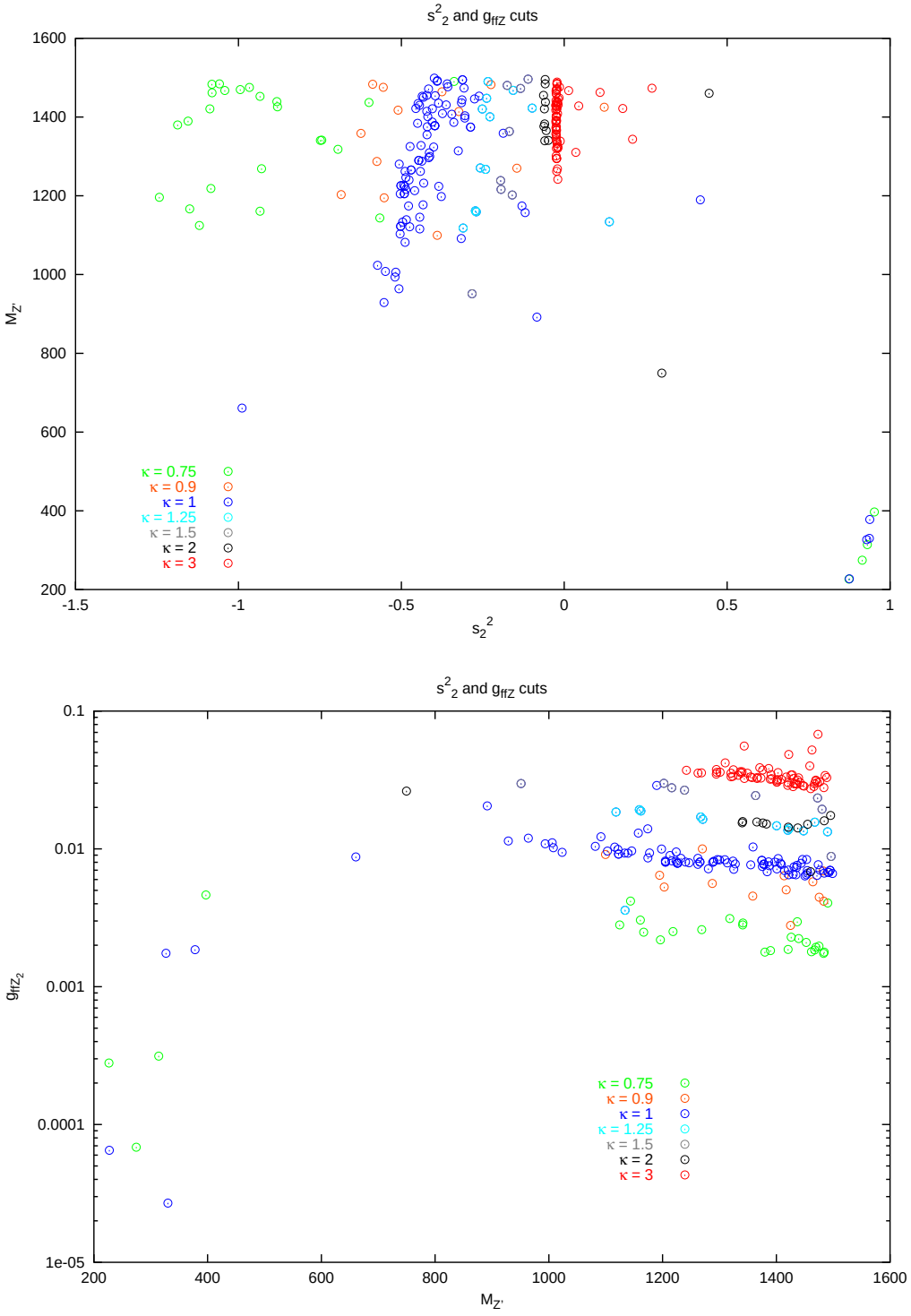

Figure 6.4: Same as in the previous figure but now showing the alternate projections in the mass-coupling strength-s_2^2 parameter space.

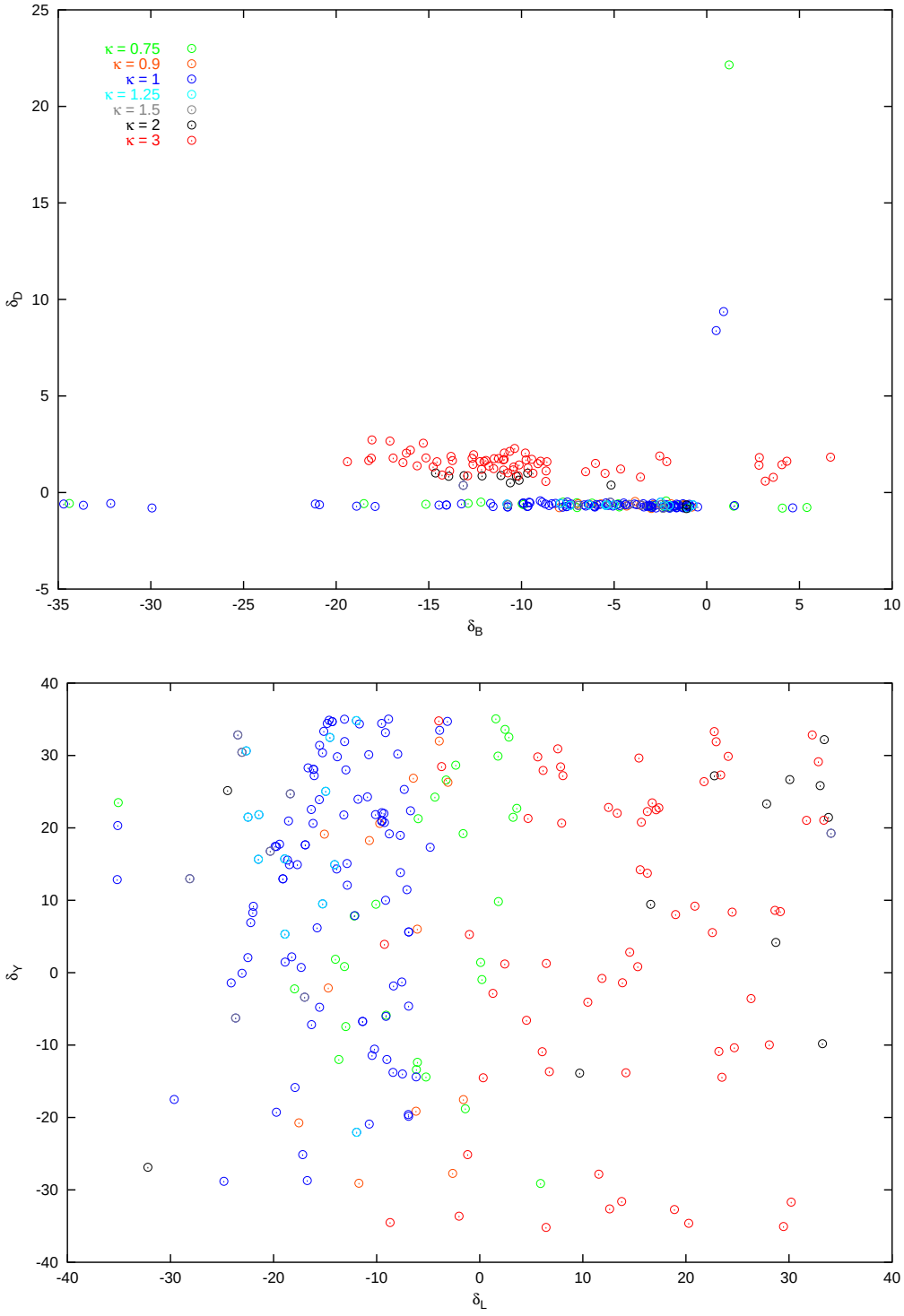

Figure 6.5: Same as in the previous figure but now showing the values of the δ_i for the surviving models..

there can be only a single complex conjugate pair of tachyons in each of the neutral and charged KK towers; we expect this result to be equally valid in the warped case. A numerical study verifies these expectations and so we need to concern ourselves with only two tachyonic states, T^0 and $T^\pm$. We find that in all the sample cases examined the relevant couplings of these states to the SM fermions are suppressed by powers of $\epsilon = e^{-\pi k r_c}$ and are thus exponentially small. Such a result might have been anticipated since the Bessel functions of an imaginary argument, I_n and K_n, which are needed to describe the tachyonic wavefunctions, are asymptotic to exponentials instead of sines and cosines as is case for the usual J_n and Y_n. This suppression of couplings is similarly observed to take place in the flat space analog of the current model, though in a more modest fashion due to the absence of warping, where sinh's and cosh's replace the usual sines and cosines in the expression for the tachyonic wavefunctions. Thus consideration of the fermion-fermion-tachyon coupling places no additional constraints on any of the models under consideration. One should note, however, that such constraints may be of some importance in a wider class of models.

As a second test we turn to $W_L^+ W_L^-$ elastic scattering. Here we expect a different result as the gauge fields are in the bulk and their wave functions sample the entire region between, as well as on, the two branes. A quick way to analyze this case is to consider the contribution of the neutral tachyon to the first sum rule of Csaki *et al.* [55], which is one of the conditions for PU. Their derivation of this sum rule relies heavily on the completeness of the set of eigenstates of Hermitian operators; thus the neutral KK spectrum in the case of $\delta_i < 0$ is not complete unless the tachyon state is included. Clearly as the magnitude of the negative brane terms increase the couplings of the tachyon to SM gauge fields will also increase and the tachyon will become lighter. The important issue for us is whether or not the tachyon state makes a numerically *significant* contribution to the sum rule.

Our results show that there are essentially three possibilities: (*i*) When $\delta_D < 0$, we find that the tachyon makes a substantial contribution to the sum rule, which is on the order of 10% or more of that of the photon, even when the magnitude of δ_D is small. In addition, this contribution is *negative*, *i.e.*, the tachyon is also a ghost state! Certainly all such cases must be excluded. This is a powerful constraint as many

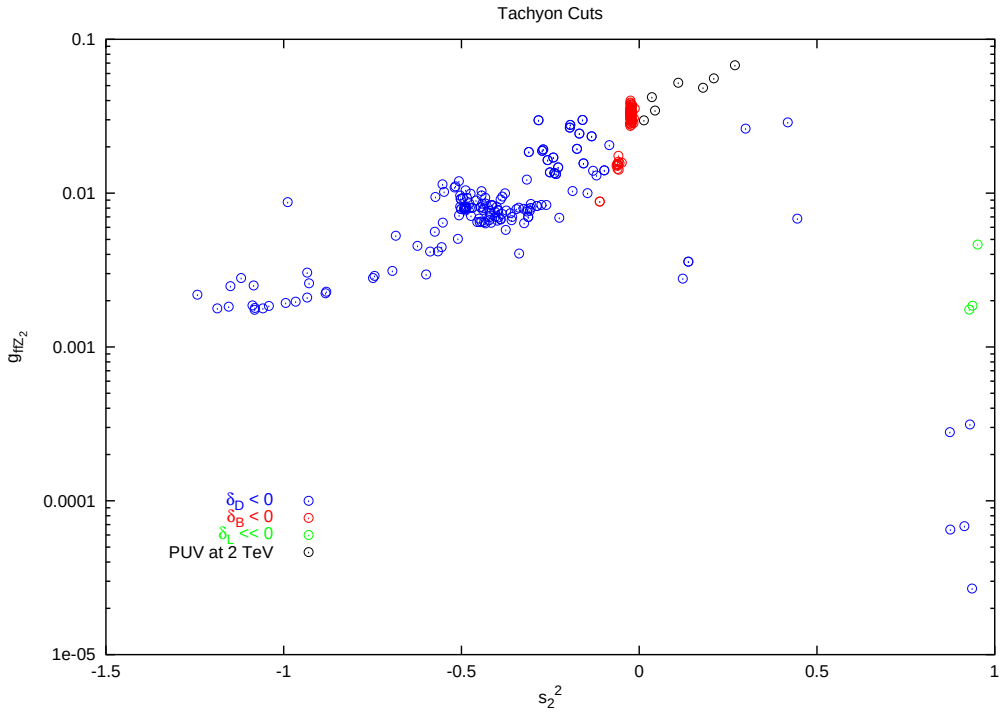

Figure 6.6: Same as Fig.3 but now showing the effects of removing the models with potentially dangerous tachyons. The models surviving the tachyon cuts are also shown.

of the surviving models shown in Figs. 3-5 have negative values of δ_D in the region near ~ -0.7. (*ii*) When $\delta_{L,Y} < 0$, the tachyon is generally sufficiently decoupled as to make almost no significant contribution to the sum rule. Not only are the couplings weak but the masses tend to lie in the multi-TeV range. For example, when $\delta_L \simeq -35$, a very extreme value, the tachyon coupling to WW is found to be $g_T^2 \sim 10^{-6}$ which is only dangerous if the tachyon is light. For δ_L values of lesser magnitude the couplings are significantly smaller. This is as expected since we showed in our earlier work[58] that in, *e.g.*, a model with $\delta_L \sim -7.5$, the sum rules were very well satisfied without including any tachyonic contributions. Thus we will retain all such models for further study. (*iii*) The remaining case where $\delta_B < 0$ is a bit more problematic. As we saw in earlier [59], $\delta_B \neq 0$ has little influence on $W_L^+ W_L^-$ elastic scattering since it only modifies the spectrum and couplings of the neutral KK's which couple predominantly to $B - L/Y$. The tachyon $W_L^+ W_L^-$ coupling is found to be generally intermediate in strength between that of the $\delta_D < 0$ case and those for $\delta_{L,Y} < 0$, unless the magnitude of δ_B is reasonably large $\simeq 10$. Our analysis of the surviving sample of models, however, indicates that the values of δ_B are indeed of this magnitude or larger. Correspondingly the masses of these states are also dangerously light implying that they can significantly contribute to SM processes. We thus drop these cases from further consideration below.

Summarizing, our numerical study confirms our expectations that the tachyons induced by negative TeV-brane kinetic terms are dangerous while those induced by the corresponding Planck brane terms are benign unless δ_L is very near its lower bound. Figures 6 and 7 show what little remains of our surviving models after we employ the requirement that $\delta_{B,D} \geq 0$. These 10 cases are mostly clustered (those with large negative δ_Y) at high Z_2 masses in excess of 1.3 TeV and have pure isospin-like couplings. Those with negative δ_L tend to have much lighter Z_2 masses, of order less than 400 GeV. Their rather small couplings to fermions place them outside the range accessible to the Tevatron. These are the cases with small masses and large $B - L/Y$-like couplings that have survived the $B - L/Y$ cut imposed above. Unfortunately, these models all have values of $\delta_L \simeq -\pi k r_c$ and thus have light tachyons with potentially significant couplings $\sim 10^{-6}$ and are thus dropped from further consideration. This

leaves only the 7 cases with negative δ_Y for further examination.

We now turn to the PU characteristics of these few surviving models; naively we expect all these cases to be problematic since the first KK excitation is always in excess of 1.3 TeV even though they are isospin-like coupled. Indeed all of these cases lead to PUV in the 1.9-2.2 TeV range which is not a significant improvement over the case of the SM without a Higgs boson. We thus conclude that none of the surviving models pass our PU requirements leaving us with no remaining models. Note that in obtaining these results we have not required PU to be valid up to the cutoff but only that the successful model to reasonably better than the SM without a Higgs.

Since we found that PUV occured at $\sqrt{s} \simeq 2$ TeV in the surviving models it is interesting to compare this value to that of the cutoff scale, Λ, as determined by Naive Dimensional Analysis[130], *i.e.*,

$$\Lambda = \epsilon \frac{24\pi^3}{g_{5L}^2}\,, \tag{6.2}$$

Following the notation of our earlier work, $g_W^2 = N_\delta g_{5L}^2/2\pi r_c$, where N_δ is a number near unity which depends in detail on the values of the δ_i. With g_W fixed via G_F this now yields

$$\Lambda = \frac{12\pi^2}{g_W^2}\frac{N_\delta}{kr_c} k\epsilon\,, \tag{6.3}$$

where $kr_c = 11.27$ in our analysis. Taking typical model values we find that $\Lambda \simeq \Lambda_\pi \simeq 10$ TeV, which is much larger that the $\sqrt{s}$ values obtained above for PUV. Thus PUV is apparently lost long before the cutoff is reached.

6.4 Conclusions

In this paper we have performed a detailed tree-level Monte Carlo exploration of the parameter space of the 5-d warped Higgsless model which is based on the $SU(2)_L \times SU(2)_R \times U(1)_{B-L}$ gauge group in the Randall-Sundrum bulk. We have generated several millions of test models allowing for arbitrary gauge kinetic terms on both the Planck and TeV branes which are parameterized through the δ_i coefficients. As we have seen from our earlier work this scenario suffers from a serious tension between

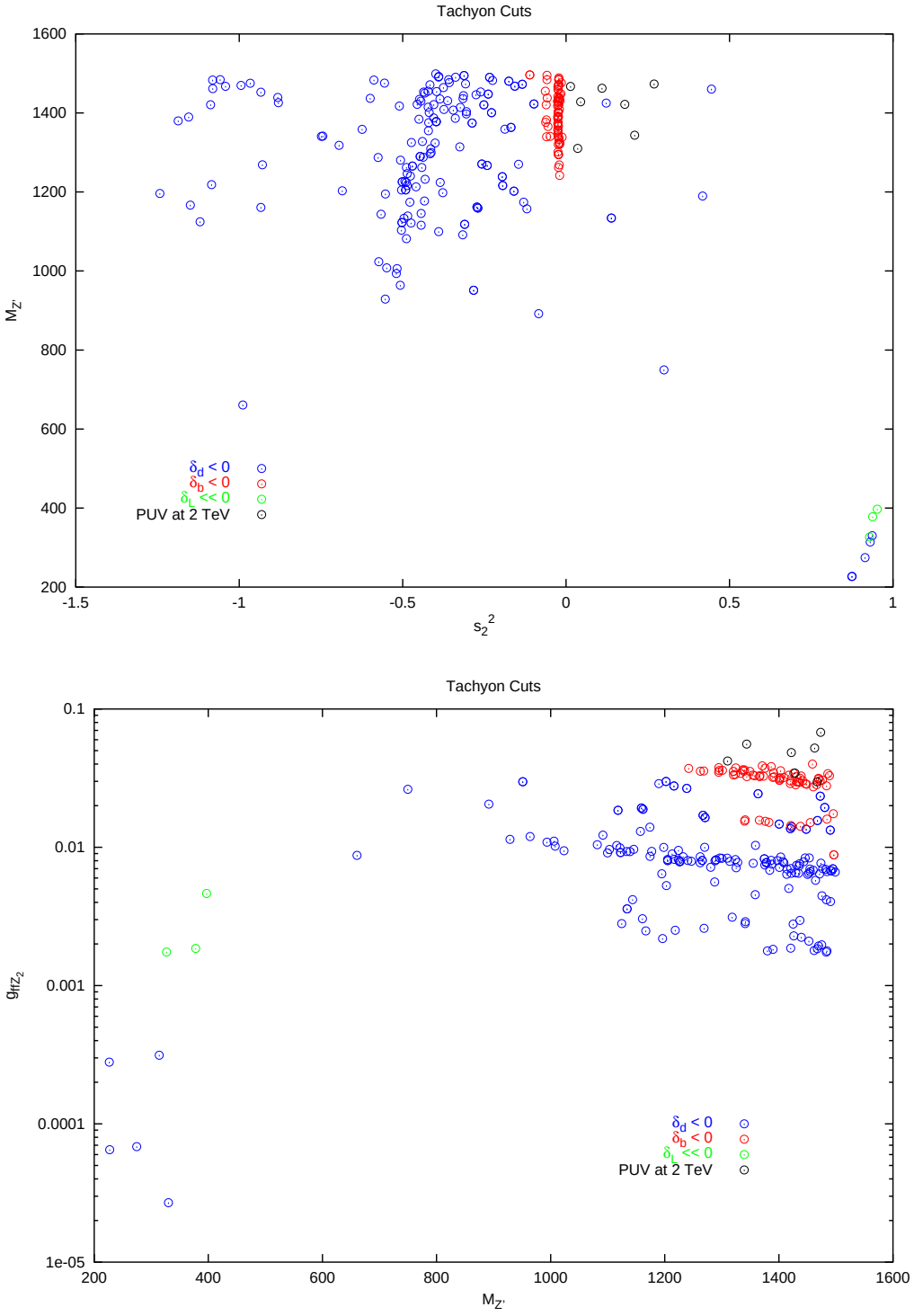

Figure 6.7: Same as in the previous figure but now showing the alternate projections in the mass-coupling strength-s_2^2 parameter space.

constraints arising from precision electroweak measurements and collider data as well as the requirements of perturbative unitarity in $W_L^+W_L^-$ elastic scattering up to the $\Lambda_\pi \sim 10$ TeV scale. We have shown that it is relatively easy to find a class of models which satisfy all of the current direct and indirect collider bounds and yet has electroweak properties which are extremely close to those of the tree-level SM. As before, the size of the parameter space that satisfies the precision EW constraints increases dramatically as κ increases. The real difficulty arises when we require the same theories to also satisfy perturbative unitarity while being free of dangerous tachyons. Though we have generated a fairly large data sample, none of the models we have examined have been able to satisfy all of our requirements simultaneously. We do note that if a generic solution of the PUV problem is found, there appears to be enough room in the parameter space to accomodate precision EW constraints. Absent such a solution, we can thus conclude that either successful models of this type are highly fine-tuned or must include additional sources of new physics [79] which unitarizes the $W_L^+W_L^-$ scattering amplitude.

Chapter 7

Collider phenomenology of Higgs bosons in Left-Right symmetric Randall-Sundrum models

7.1 Introduction

While the Standard Model (SM) is a spectacularly successful description of high energy particle phenomena, it leaves unexplained why the Electroweak scale is much smaller than the GUT or Planck scales. Recently, it has been proposed that this hierarchy might be explained by the presence of additional compactified dimensions. These could be TeV scale and flat [20, 16], or Planck scale with a warped geometry [136]. In this second scenario, the Randall-Sundrum (RS) model, there is a single extra dimension and the spacetime has the geometry of five-dimensional Anti-de Sitter space, AdS_5, compactified on an orbifolded circle, S^1/Z_2. One 3-brane is localized on each end of the orbifold, and the warping between them generates the Electroweak scale.

In the original RS model, all SM fields are localized on the TeV (or IR) brane. The observable phenomenology in this case comes from the new spin-2 graviton resonances [61]. However, there is no reason for the fermions and gauge fields not to propagate in the bulk [60, 89, 62, 134]. Indeed, bulk fermions have a zero mode which is

exponentially localized near one of the branes. Choosing $\mathcal{O}(1)$ Lagrangian parameters for different fermions can select exponentially different overlaps on the IR brane, and hence different masses, providing a possible explanation of the fermion mass hierarchy [62, 82, 101]. There have been many investigations into the phenomenology of this model [53, 42, 41, 64, 108]. One important conclusion is that simply putting the SM gauge group in the bulk produces a large Peskin-Takeuchi T-parameter [132]. The can be fixed by expanding the gauge group to be left-right symmetric, $SU(2)_L \times SU(2)_R \times U(1)_{B-L}$ [9] or by introducing brane localized kinetic terms for the fermions [40]. It is also possible to extend this to a Grand Unified group which then contains a dark matter candidate [11, 10].

More recently, there has been a proposal that no Higgs is needed in this model, as the geometry can set the gauge boson masses [55, 56, 128], as well as the fermion masses [54]. The most straightforward application of this model produces large electroweak corrections, and does not preserve tree-level unitarity in longitudinal gauge boson scattering at finite center-of-mass scattering energies [26, 63, 129, 58, 59, 100, 145, 38, 105]. They do, however, contain a rich collider phenomenology which is largely independent of those considerations [29]. There have been several variations on the model, including deconstructing the extra dimension [50, 49, 51, 48, 147, 43, 76], adding additional dimensions [79], and adding additional branes [37].

The Higgsless models can be obtained as the limit of a model with a Higgs where the vev, v, is taken to be large compared to the AdS curvature k; that is $v/k \gg 1$. The fact that Higgsless scenarios have difficulty accommodating the precision electroweak observables leads to the speculation that the agreement may be improved by including the effects of a finite Higgs vev.

Additionally, analyses of the Higgs scenario, $v/k \ll 1$ show that this model is allowed by precision electroweak data. However, in this case, with Kaluza-Klein (KK) masses, $m_{KK} \approx 2 - 3\,\text{TeV}$, we have $v/k \approx 1/4$, which is not particularly small. In fact, this is expected from RS effective field theory arguments which tell us that all Lagrangian level mass parameters should be of the same order, M_{Pl}. Hence, it makes sense to study the corrections to collider observables induced by a finite, but not large, Higgs vev.

In this paper we will examine the numerical behavior of explicit solutions for the gauge and fermion wavefunctions in RS with a finite and arbitrary value for v/k. From this we can extract both the small vev limit and the Higgsless limit.

Note that the RS models can be thought of as large N 4D conformal gauge theories through the AdS/CFT correspondence [120]. Analyses have also been performed on the CFT side of the Higgsless model [35], and the Higgs model [7, 8].

In Section 7.2 we develop the formalism that will be employed in this paper. Section 7.3 shows the behavior of the Kaluza-Klein spectra as the Higgs vev is varied. We investigate the gauge couplings and precision electroweak constraints in Section 7.4, and the corrections to Higgs properties in Section 7.5. Section 7.6 concludes.

7.2 Formalism

We work in a slice of AdS_5, with metric (in conformal coordinates)

$$ds^2 = \left(\frac{R}{z}\right)^2 (dx^2 - dz^2) \tag{7.1}$$

where $R = 1/k$ is the inverse of the curvature scale. There is one brane located at $z = R$ (the Planck or UV brane), and a second brane at $R' = (M_{\rm Pl}/TeV)R$ (the TeV or IR brane). This gives $\log(R'/R) \sim 35$. We define $\epsilon = R/R' \sim 10^{-15}$ for later convenience.

We are interested in models with a bulk $SU(2)_L \times SU(2)_R \times U(1)_{B-L}$ gauge symmetry. The additional $SU(2)_R$ factor over the SM provides a bulk custodial $SU(2)_{\rm c}$, which can successfully protect the T parameter [9]. The bulk gauge action is then

$$S_{bulk} = \int d^5x\sqrt{g}\left(\frac{-1}{4g_{5L}^2}F^L_{MN}F_L^{MN} + \frac{-1}{4g_{5R}^2}F^R_{MN}F_R^{MN} + \frac{-1}{4g_{5B}^2}F^B_{MN}F_B^{MN}\right) \tag{7.2}$$

We will make use of the ratios of gauge couplings

$$\kappa = g_{5R}/g_{5L}, \qquad \lambda = g_{5B}/g_{5L}. \tag{7.3}$$

Clearly, this group needs to be broken to $U(1)_{\rm EM}$. We accomplish this by separating the breaking into two sectors. On the Planck brane we break $SU(2)_R \times U(1)_{B-L} \to U(1)_Y$. Since the UV brane is the only place where the $SU(2)_{\rm c}$ is broken, we can see why the effects on the T parameter will be small. On the TeV brane we break $SU(2)_L \times SU(2)_R \to SU(2)_D$, where $SU(2)_D$ is the diagonal subgroup of $SU(2)_L$ and $SU(2)_R$.

We will work in the $A^5 = 0$ (unitary) gauge. The gauge condition can potentially be complicated by the fact that the brane localized Goldstone modes, the G^i can mix with the A^5 modes. This means that the physical longitudinal polarization for each vector is a combination of bulk and brane modes. However, for the breaking pattern used here there is no zero mode for any of the A^5 fields, and hence no extra physical zero-mode scalar. We can therefore safely work in the gauge where $A^5 = G^i = 0$.

We now ask what drives the breaking on each brane. On the planck brane all degrees of freedom will have Planck scale masses, so we can ignore them. We can then implement the breaking with boundary conditions to good approximation. This leads to the boundary conditions at $z = R$

$$\begin{aligned} \partial_z \left(\frac{\kappa}{\lambda} A_R - A_B\right) = 0, \qquad & \partial_z A_L = 0, \\ A_B - \frac{\kappa}{\lambda} A_R^3 = 0, \qquad & A_R^{\pm} = 0. \end{aligned} \tag{7.4}$$

On the TeV brane, the masses will be TeV scale, so we should look at the Higgs sector in detail. The simplest structure that will create the breaking pattern is a real Higgs that is a bidoublet under $SU(2)_L \times SU(2)_R$. This leads to the boundary conditions at $z = R'$

$$\begin{aligned} \partial_z (A_L + \kappa A_R) = 0, \qquad & \partial_z A_B = 0, \\ \partial_z (\kappa A_L - A_R) = -\frac{g_{5L}^2 v^2}{4} (\kappa A_L - A_R). \qquad & \end{aligned} \tag{7.5}$$

Note that in the $v/k \to \infty$ limit we obtain the usual Higgsless boundary conditions. Instead of the real bidoublet, we could also use the complex bidoublet familiar from Left-Right symmetric models with minimal changes. See Appendix A for details.

To write down the effective 4D theory we expand the 5D fields into Kaluza Klein (KK) fields.

$$A(x,z) = \sum_n \zeta_A^{(n)}(z) A^{(n)}(x) \tag{7.6}$$

We can now obtain the gauge boson wavefunctions by solving the equation of motion subject to the boundary conditions (7.4) and (7.5). The generic solution for the wavefunctions is

$$\zeta_A^{(n)}(z) = z(A_A^{(n)} J_1(m_n z) + B_A^{(n)} Y_1(m_n z)). \tag{7.7}$$

Here the label A refers to the particular gauge field being expanded. One of the coefficients, $A^{(n)}$ and $B^{(n)}$, and the mass are determined by inserting eq. (7.7) into eqs. (7.4) and (7.5). The other coefficient is fixed by the normalization condition. We will use 4D canonical normalization for all fields, giving

$$N_W^{(n)2} = \int_R^{R'} \frac{dz}{z} R \left(|\zeta_{A_L^\pm}^{(n)}(z)|^2 + |\zeta_{A_R^\pm}^{(n)}(z)|^2 \right), \tag{7.8}$$

for the charged gauge bosons, and

$$N_Z^{(n)2} = \int_R^{R'} \frac{dz}{z} R \left(|\zeta_{A_L^0}^{(n)}(z)|^2 + |\zeta_{A_R^0}^{(n)}(z)|^2 + |\zeta_{B_R}^{(n)}(z)|^2 \right), \tag{7.9}$$

for the neutral tower.

The fermion sector of the theory is more intricate. First, we will need to arrange the SM fermions into representations of $SU(2)_R$. There are two ways to do this in the RS model. The most straightforward is to pair corresponding $SU(2)_L$ singlets into a single $SU(2)_R$ doublet. So, *e.g.*u_R and d_R become $\begin{pmatrix} u_R & d_R \end{pmatrix}^\top$. The other option is to make each right-handed field part of a different $SU(2)_R$ doublet. So $u_R \to \begin{pmatrix} u_R & d'_R \end{pmatrix}^\top$, etc.. Orbifold projections are then required to insure that there is no light mode for the new fermion states. The first option follows more naturally from Grand Unified theories, and allows the possibility of an explicit Z_2 symmetry

that exchanges the Left and Right gauge groups. The second makes it easier to obtain top-bottom splitting and to suppress corrections to the $Zb\bar{b}$ vertex, and is compatible with the GUT scenario in [10]. Here we will study the case where there is an explicit Z_2, and hence choose to combine right-handed fields into a single $SU(2)_R$ multiplet.

We write the 5D fermion as two 4D Majorana fermions, $\Psi_i = (\psi_i \ \chi_i)^\top$. The orbifold conditions tell us that one component must be even and the other odd [89]. We will pick the ψ_i to be even for fields corresponding to the left-hand SM fermions, and the χ_i even for the right-handed ones. The Yukawa couplings to ϕ, the Higgs on the IR brane, will connect the left and right-handed zero modes and lift them. These couplings are

$$S_{IR} = \sum_f \int d^4x \left(\frac{R}{z}\right)^4 \lambda_f \phi \left(\psi^f_{Ri}\chi^f_{Li} + \bar{\chi}^f_{Li}\bar{\psi}^f_{Ri} + \psi^f_{Li}\chi^f_{Ri} + \bar{\chi}^f_{Ri}\bar{\psi}^f_{Li}\right). \tag{7.10}$$

Here f labels the fermion flavor. Eq. (7.10) induces the boundary conditions at $z = R'$

$$\psi^f_L = -\lambda_f v \psi^f_R \qquad \chi^f_R = \lambda_f v \chi^f_L. \tag{7.11}$$

This is equivalent to introducing a Dirac mass $\lambda_f v$ on the IR brane. Note that this is $SU(2)_D$ symmetric, and hence can not generate different masses for the up and down-type quarks. That splitting must be generated on the UV brane, which is the only place where the custodial symmetry is broken. It was demonstrated in [54] that the simplest way to do this with a complex fermion is to introduce brane-localized fermions that can mix with the bulk states. So we include a contribution to the brane action for each SM right-handed fermion

$$S_{\rm UV} = \int d^4x \sum_f \left(-i\bar{\xi}^f\bar{\sigma}^\mu\partial_\mu\xi^f - i\eta^f\bar{\sigma}^\mu\partial_\mu\bar{\eta}^f + F(\eta^f\xi^f + \bar{\eta}^f\bar{\xi}^f) + M_f R^{1/2}(\psi^f_R\xi + \bar{\xi}\bar{\psi}^f_R)_{z=R}\right) \tag{7.12}$$

where ξ_i and η_i are the brane localized states, ψ_{Ri} is the component of the bulk state that has a zero mode, and the index f runs over all SM right-handed fermions. This

leads to the boundary condition

$$\psi_L^f = 0 \qquad \chi_R^f = m_n M_m^{f2}/F^2 \psi_R^f. \tag{7.13}$$

The fermion KK expansion will take the form[1]

$$\chi = \sum_n g^{(n)}(z) z^{3/2} \chi^{(n)}(x), \qquad \bar{\psi} = \sum_n f^{(n)}(z) z^{3/2} \bar{\psi}^{(n)}(x). \tag{7.14}$$

Again, we will normalize these canonically, giving

$$\int \frac{dz}{z} \chi^{(n)*}(z) \chi^{(m)}(z) = \delta_{nm}, \tag{7.15}$$

and similarly for the $\psi^{(n)}$. Note that 5D fermions are achiral, so we can always write down a mass term in the bulk

$$m_5^f \bar{\Psi}\Psi = \frac{c^f}{k} \bar{\Psi}_f \Psi_f. \tag{7.16}$$

Even in the presence of this mass term there is still a 4D zero mode for the orbifold even components of Ψ when $v = 0$. The c^f determine the shape of the wavefunction in the extra dimension. This would-be zero mode wavefunction is

$$f_f^{(0)}(z) = A_f^{(0)} \left(\frac{z}{R}\right)^{c^f - 1/2} \tag{7.17}$$

We can see that for $c > 1/2$ the zero mode is localized to the Planck brane, and for $c < 1/2$ it is localized to the TeV brane.

7.3 Kaluza-Klein spectra

We can solve Eq. (7.7) subject to (7.4) and (7.5) to obtain $x_W^{(n)} \equiv m_W^{(n)}/k\epsilon$. Figure 7.3 shows the behavior of $x_W^{(1)}$ as a function of v/k. Demanding that $m_W^{(1)} = m_W$ sets the

[1]The choice of what powers of z to include in the wavefunctions is, of course, arbitrary. This choice makes transparent on which brane the fermion zero mode is localized.

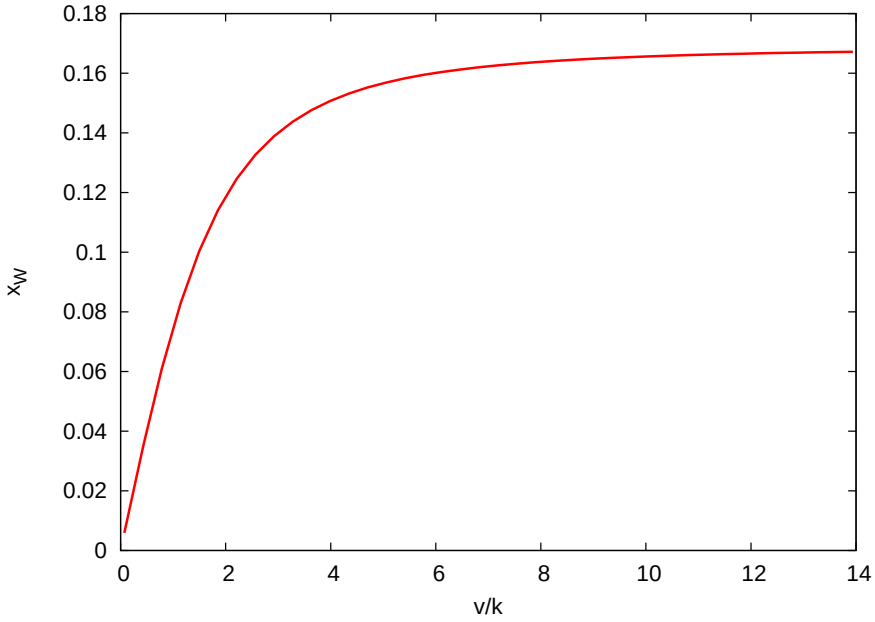

Figure 7.1: Behavior of the first charged boson mass (corresponding to the observed W) as a function of v/k at fixed k. The linear behavior at small v/k corresponds to the ordinary Higgsed model limit, and the flat behavior as $v/k \to \infty$ to the Higgsless limit.

mass scale $k\epsilon$. In the region with v/k small we have $x_W^{(1)} \approx \frac{g}{2}\frac{v}{k}$ giving the standard result $k\epsilon \approx \frac{2}{g} m_W \frac{k}{v}$. This reflects the fact that as v/k gets small, the KK scale gets large. When v/k is large, $x_W^{(1)}$ asymptotes to the Higgsless value $x_W^{(1)2} = 1/\log(R'/R)$ [56].

Once this scale has been set, we can solve for the rest of the KK gauge boson masses. For the neutral sector this depends on the additional parameter, λ. We can solve Eq (7.7) for the neutral gauge sector for λ in terms of $x_Z^{(1)}$, the mass of the observed Z boson. We will use this to choose λ, and hence with our choice of input parameters the on-shell definition of the weak mixing angle, $\sin^2\theta_{\rm os} \equiv 1 - m_W^2/m_Z^2$, is automatically set to the experimental value $\sin^2\theta_{\rm os} = 0.222$ [92]. These inputs completely determine the gauge KK mass spectrum. Figure 7.3 shows this spectrum for neutral bosons. Note that each KK level in the v/k small region starts as a degenerate triplet and splits into the doublet-singlet structure seen in Higgsless theories as v/k gets large. These masses are large enough that these states are not

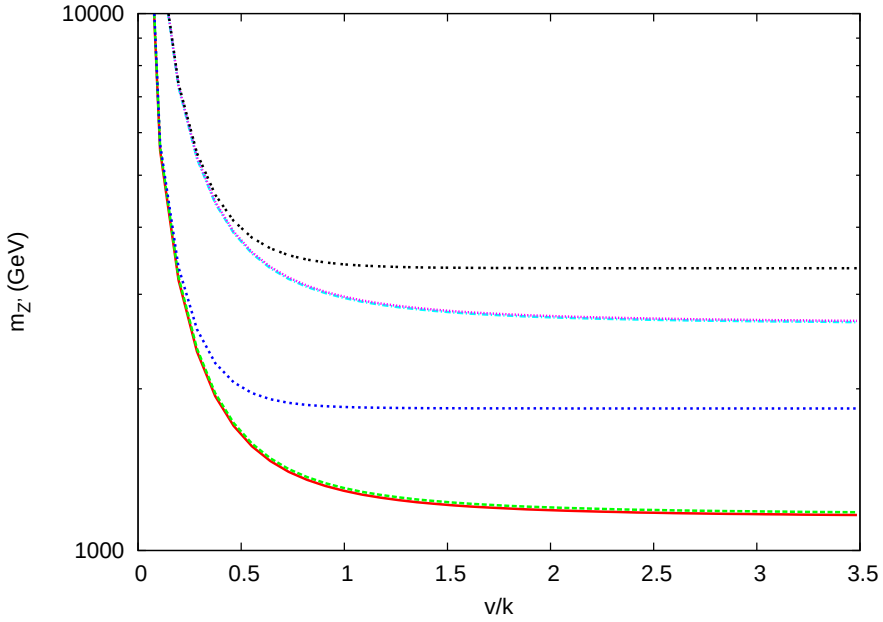

Figure 7.2: Masses of the first six neutral boson KK excitations lying above the SM Z as a function of v/k with the W and Z masses held fixed at their physical values.

bounded by direct detection constraints at the Tevatron[1]. Also, the couplings to light fermions are small enough that they also avoid the LEP II contact interaction constraints [59].

The fermion masses depend on both the brane localized Yukawa couplings to the Higgs and the bulk masses. Eq. (7.11) shows that the Yukawa couplings provide an effective Dirac mass on the IR brane, and it is this mass that controls the lowest fermion mass (*i.e.* the mass of the observed SM particle). Hence, the relevant dimensionless parameter is $\lambda_i v/k$ (where λ_i is the relevant Yukawa coupling), rather than v/k. In this paper we consider the case where the fermion mass hierarchy generated by the different bulk masses, and not the Yukawas. To correctly produce the top mass, the top/bottom Yukawa must be order 1. We will assume that the other generations have universal Yukawa couplings λ_{light}. Since we are assuming an explicit Z_2 symmetry that exchanges the $SU(2)_L$ and $SU(2)_R$ we have $c_L^f = -c_R^f \equiv c^f$ (the minus sign arises from the choice of orbifold parities). We will pick the parameters c^f to produce the correct fermion masses for a given Yukawa coupling and Higgs vev.

In the quark sector we pick the c^f to match the up-type masses. We then introduce mixing with UV brane fermions as in Eq. (7.12) to generate the up-down splitting. In the lepton sector we simply match the charged lepton masses by picking the c^f, and leave the neutrinos massless. We can then solve for the KK masses, shown in Fig. 7.3. Note that a large Dirac mass on the IR brane makes the first KK excitation light. This behavior corresponds to that seen in [10]. To avoid light KK leptons we will need $y_{\text{light}} \lesssim 1/2$.

7.4 Gauge-fermion couplings

Here we will examine how the shifts in couplings of the W and Z to fermions depend on the Higgs vev. The 5D covariant derivative acting on a fermion ψ is (suppressing Lorentz indices)

$$D\psi = \left(\partial_\mu + \int_R^{R'} \frac{dz}{z} g_{5L} \left(A_{L\mu} T_L + \kappa A_{R\mu} T_R + \lambda Q_{B-L} A_{B\mu}\right)\right) \psi \tag{7.18}$$

with $Q_{B-L} = (B-L)/2$. The electromagnetic charge is $Q = T_L^3 + T_R^3 + Q_{B-L}$. We can rewrite the pieces of D corresponding to the neutral gauge boson couplings as

$$g_{5L}(I_{3L}^f - \lambda I_B^f)\left(T_L^3 + \frac{\kappa I_{3R}^f - \lambda I_B^f}{I_{3L}^f - \lambda I_B^f} T_R^3 + \frac{\lambda I_B^f}{I_{3L}^f - \lambda I_B^f} Q\right). \tag{7.19}$$

Where the $I_i^f = \int_R^{R'} dz/z\, \zeta_i \bar{\psi}_f \psi_f$ encode the extra dimensional physics. This can be matched onto the covariant derivative from the effective 4D theory

$$g_{Z_1 f \bar{f}}(T_L^3 + \sin^2\theta_{R,f} T_R^3 - \sin^2\theta_{\text{eff,f}} Q). \tag{7.20}$$

This identifies the strength of the Z coupling to fermion f as $g_{Z_1 f \bar{f}} = g_{5L}(I_L^3 - \lambda I_B)$, the effective weak mixing angle for that coupling $\sin^2\theta_{\text{eff,f}} = -\lambda I_B/(I_L^3 - \lambda I_B)$, and a new quantity that measures the strength of the right-handed couplings: $\sin^2\theta_{R,f} = (\kappa I_R^3 - \lambda I_B)/(T_L^3 - \lambda I_B)$. We can also write an expression similar to Eq. (7.19) for

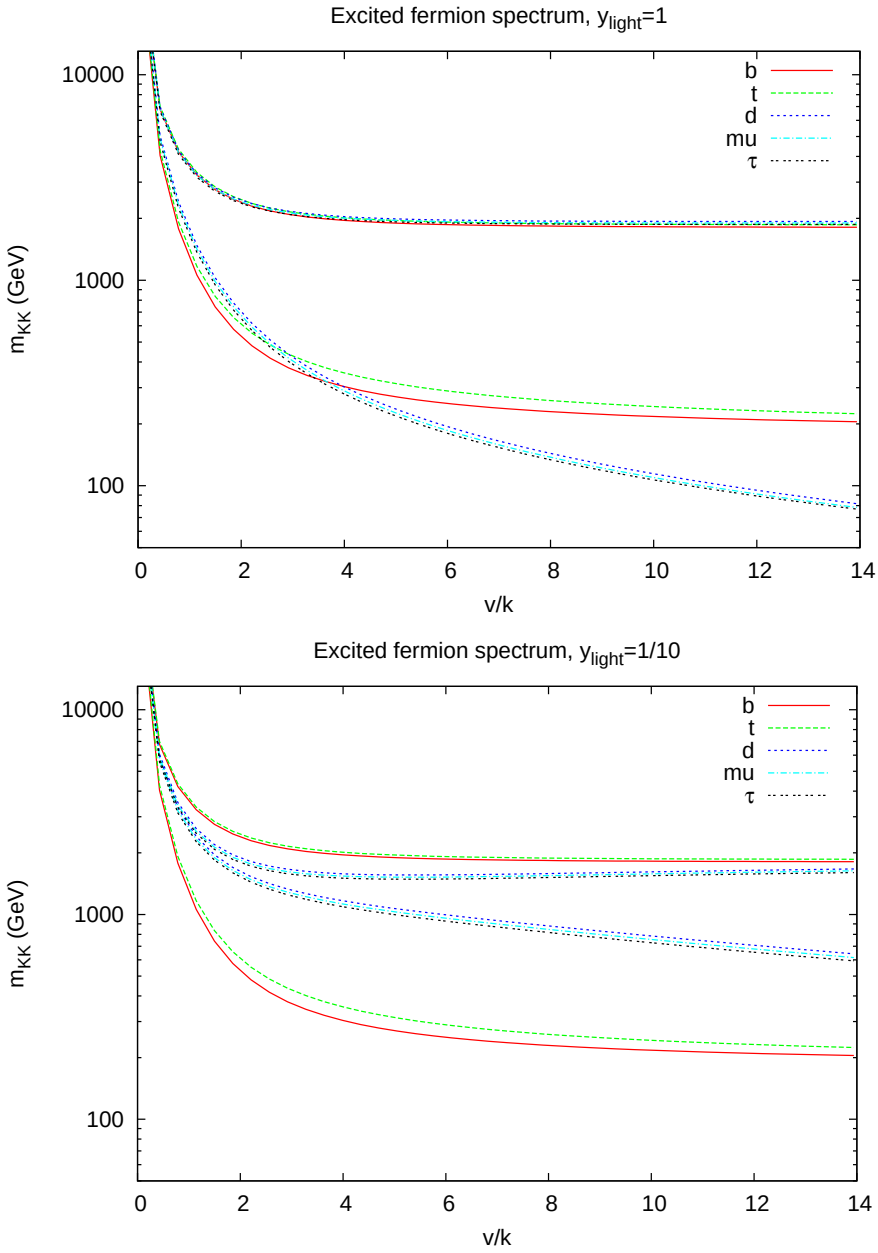

Figure 7.3: Masses of the first two excited KK fermions as a function of v/k for several species. Note that the mass of the first excitation depends strongly on the IR-brane mass term, but the second excitation does not.

the charged sector

$$g_{5L} I^f_{\pm L} \left(T^\pm_L + \frac{\kappa I^f_{\pm R}}{I^f_{\pm L}} T^\pm_R \right), \tag{7.21}$$

giving the strength of the left and right handed couplings.

Note that the wavefunctions for all electroweak particles, with the single exception of the zero mode photon, have non-trivial dependence on the extra dimension. In particular the different flavors of fermions will have different wavefunctions that can be probed by the W and Z. Hence, all quantities defined above will depend on the fermion species, as indicated by the label f.

Since the photon wavefunction is flat in the extra dimension, the electromagnetic coupling is simply given by (using the normalization from Eq. (7.9))

$$e^2 = \frac{g^2_{5L}}{R \log(R'/R)} \frac{\kappa^2 \lambda^2}{\kappa^2 + \lambda^2 + \kappa^2 \lambda^2}. \tag{7.22}$$

We can use this to define the 5D coupling in terms of the fine structure constant α by

$$\frac{g^2_{5L}}{R} = 4\pi\alpha \log(R'/R) \left(1 + \frac{1}{\lambda^2} + \frac{1}{\kappa^2} \right). \tag{7.23}$$

The advantage of this definition is that it is the only coupling that is independent of the fermion species, and allows us to relate g_{5L} to the measured quantity α without ambiguity.

With these definitions we can find the shifts in the couplings. Fig 7.4 shows the shift in $g_{Zf\bar{f}}$ as a function of v/k. Note that the shifts are only large for the third generation quarks. This is expected since they are the only fermions with substantial overlap on the IR brane where the W and Z wavefunctions are distorted. Imposing the LEP and SLD bound on the shift in the $Zb\bar{b}$ vertex of $\sim 1\%$ [92], we find that $v/k < 1/2$. This gives $k\epsilon > 800\,\text{GeV}$, and $v\epsilon < 400\,\text{GeV}$. In Fig. 7.4 we see the shifts in the effective weak mixing angle in Z-pole observables relative to the on-shell value. The experimental error on this measurement is ± 0.00036 [92], so for $v/k \leq 1/4$ the

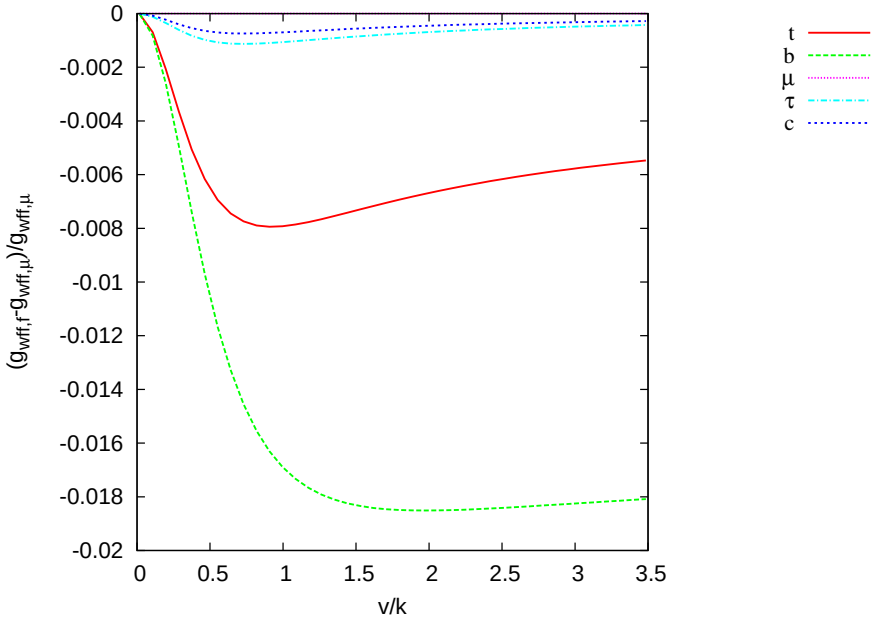

Figure 7.4: Shifts in the coupling of fermions to the Z induced by the Z wavefunction distortions. The large shift to the $Zb\bar{b}$ coupling is the dominant constraint on v/k.

model shifts correspond to a 2σ deviation. Fig. 7.4 shows $\sin^2\theta_R$, the magnitude of the right handed couplings to SM fermions relative to the left handed coupling. Note that the boundary conditions in Eq. 7.4 cause this to vanish for Planck brane localized fermions. Indeed we see that the closer the fermion to the UV brane, the smaller the effect. In all cases, however, the effect is unobservable in the allowed region $v/k \leq 1/4$.

7.5 Higgs couplings

We now investigate the shifts in couplings of particles to the physical Higgs boson. As shown above, the main effects come from distortions of the gauge wavefunctions near the IR brane. Schematically, the coupling of a Higgs to two bulk modes will simply be the product of the bulk wavefunctions evaluated at the IR brane, times a Lagrangian parameter. So for the coupling to gauge bosons we have

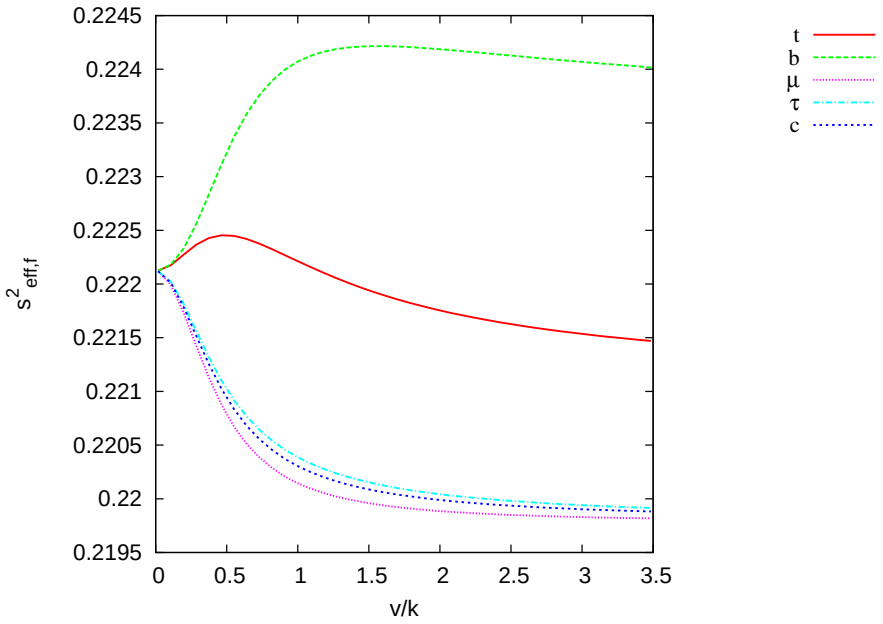

Figure 7.5: Corrections to the effective weak mixing angle for couplings of fermions to the Z on the Z-pole.

$$g_{hWW} = \frac{g_{5L}v}{2m_W}\frac{1}{1+\kappa^2}\left(\zeta^{(1)}_{A^{\pm}_L}(R') - \kappa\zeta^{(1)}_{A^{\pm}_R}(R')\right)^2, \tag{7.24}$$

and

$$g_{hZZ} = \frac{g_{5L}v}{2m_Z}\frac{1}{1+\kappa^2}\left(\zeta^{(1)}_{A^{3}_L}(R') - \kappa\zeta^{(1)}_{A^{3}_R}(R')\right)^2. \tag{7.25}$$

The wavefunction suppression near the TeV brane will decrease these couplings, with $g_{h(WW,ZZ)} \to 0$ as $v/k \to \infty$. This coupling is shown in Fig. 7.5.[2] This reduction will weaken the LEP bound on the Higgs mass [25]. For $v/k \leq 1/4$ the constraint is relaxed only a few GeV. However, the bound is moves rapidly after that point, so for $v/k = 1/2$ the bound is 80 GeV.

Using the above relations we can find the width for the decay into vector pairs,

[2]Note that the constraint $v/k \leq 1/4$, coming from precision electroweak observables, is highly sensitive to variations on the model. Many of the features discussed in this section, however, are generic. Consequently, we will continue to examine the full range of v/k, keeping in mind the electroweak constraints.

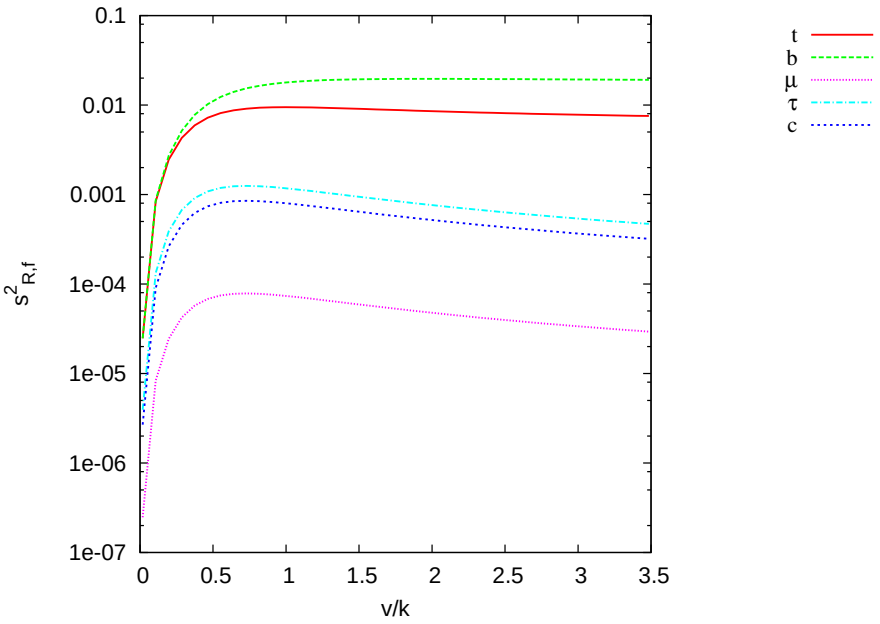

Figure 7.6: The effective size of the right-handed currents induced by the $SU(2)_R$ gauge bosons.

which is simply

$$\Gamma(h \to (WW, ZZ)) = \left(\frac{1}{2}\right) \frac{g^2_{h(WW,ZZ)} m^3_{(W,Z)}}{64\pi m_h^2} (\xi - 4)^{1/2} (12 - 4\xi + \xi^2), \tag{7.26}$$

with $\xi = m_h^2/m_{W,Z}^2$, and the first factor of $1/2$ is a symmetry factor relevant only for the ZZ final state.

The decay modes where one vector is off-shell can also be important [138]. These decay widths are

$$\Gamma(h \to WW^*) = \frac{3 g^2_{hWW} g^2 m_H}{512\pi^3} H_W(m_W/m_H), \tag{7.27}$$

$$\Gamma(h \to ZZ^*) = \frac{g^2_{hZZ} g^2 m_H}{2048\pi^3 \cos^4\theta} \left(7 - \frac{40}{3}\sin^2\theta_W + \frac{160}{9}\sin^4\theta_W\right) H_Z(m_Z/m_H), \tag{7.28}$$

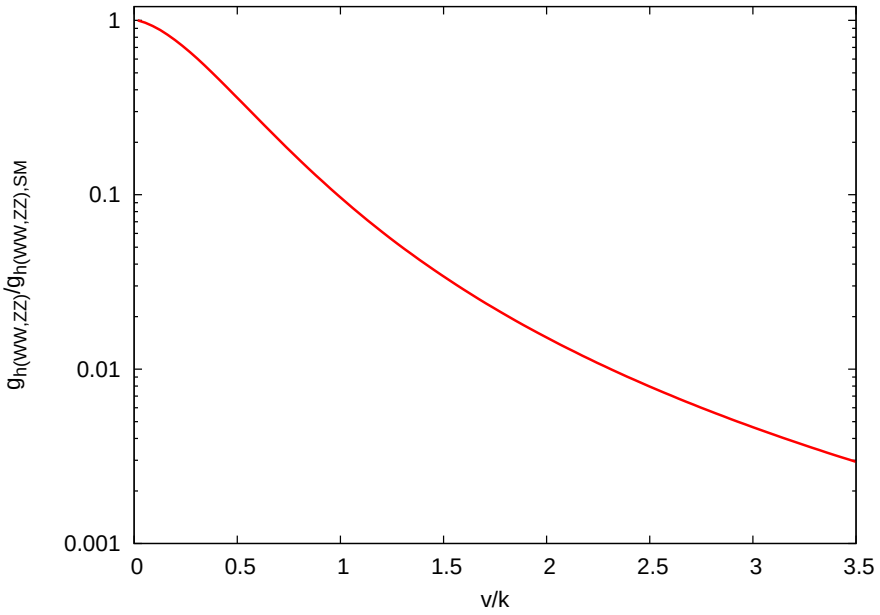

Figure 7.7: Coupling of the Higgs to vector boson pairs compared to the SM value as a function of v/k. Again, the W and Z coupling strengths are nearly identical due to the custodial symmetry.

where

$$H_{W,Z}(x) = \int_{2x}^{1+x^2} dy \frac{(y^2-4x^2)^{1/2}}{(1-y^2)^2 + x^4\Gamma_{W,Z}^2/M_{W,Z}^2}(y^2 - 12x^2y + 8x^2 + 12x^4), \quad (7.29)$$

and we have ignored the corrections to the $Wf\bar{b}$ and $Zf\bar{f}$ couplings which are small for $v/k \leq 1/4$. It is necessary to include the effects of the finite widths, $\Gamma_{W,Z}$, to match onto Eq. (7.26).

The fermion couplings to the Higgs are similar; they take the form of the fermion wavefunctions evaluated on the TeV brane times a Yukawa coupling. Specifically,

$$\lambda_{f,n} = \lambda_f \left(\chi_L^{f(n)}(R')\psi_R^{f(n)}(R') - \psi_L^{f(n)}(R')\chi_R^{f(n)}(R') \right). \quad (7.30)$$

Note that, since the Kaluza-Klein excitations are localized near the TeV brane, this coupling will be enhanced by the factor $\sqrt{\log(R'/R)}$. In the case of the 3rd generation quarks, which have $\mathcal{O}(1)$ Lagrangian level Yukawa couplings, these enhancements

make the couplings quite large, though in all cases they are perturbative. Again, the width into fermion pairs is simply

$$\Gamma(h \to f\bar{f}) = \frac{N_c \lambda_{f,1}^2 m_h}{32\pi} \left(1 - \frac{4m_f^2}{m_h^2}\right)^{3/2}, \tag{7.31}$$

where N_c counts the fermion's color degrees of freedom.

Finally, two of the most important couplings for the discovery of the Higgs boson at the LHC are the Higgs-glue-glue, and Higgs-gamma-gamma vertices. These couplings are absent at tree-level, but are generated radiatively by loops containing fermions and W-bosons. In the present model, these vertices receive corrections from two sources. First, the KK excitations of all fermion species can run in the loop (along with the W KK excitations in the case of the $\gamma\gamma$ couplings); since these have substantial couplings to the Higgs these corrections can be large. Second, the suppression in g_{HWW} from the distortion of the W wavefunction can suppress the coupling of the Higgs to two photons. To calculate these contributions, we can adapt the formulae from [94] and [133]. The parton level cross section for producing a Higgs from gluon fusion is

$$\sigma_{gg\to h} = \frac{G_F[\alpha_s(m_H)]^2}{32\sqrt{2}\pi m_H^4} \left|\sum_i F^i\right|^2. \tag{7.32}$$

Here the sum runs over all KK states (including the zero modes) of all colored fermions, with i labeling the flavor. The kinematic function F^i is

$$F^i = 2m_i \sum_n m_{i,n}\lambda_{i,n}\{-2 + (m_H^2 - 4m_{i,n}^2)C_0(m_{i,n})\}, \tag{7.33}$$

where $C_0(x)$ is an abbreviation for the three-point scalar Passarino-Veltman function [131]

$$C_0(x) = C_0(m_H^2, 0, 0; x, x, x). \tag{7.34}$$

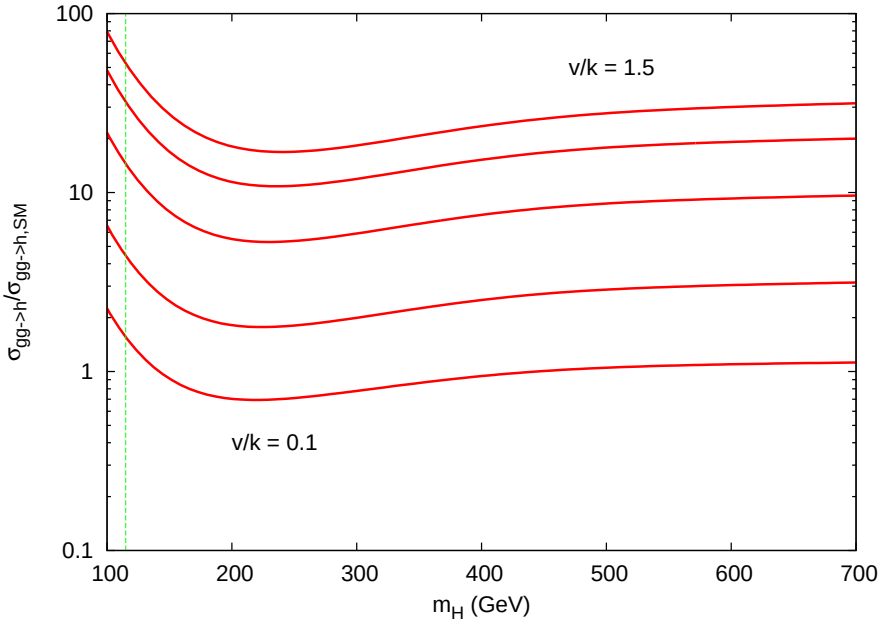

Figure 7.8: Ratio (at lowest order) of the production cross section for $gg \to h$ compared with the value in the SM. The different curves correspond to the values of v/k from top to bottom of (1.5, 1.1, 0.8, 0.4, 0.1). Here we have taken $y_{\text{light}} = 1/10$.

This can be expressed simply as [133]

$$C_0(m^2) = \begin{cases} -\frac{2}{m_H^2}\left[\arcsin\left(\frac{1}{\sqrt{\tau}}\right)\right]^2 & : \quad \tau \geq 1 \\ \frac{1}{2m_H^2}\left[\ln\left(\frac{1+\sqrt{1-\tau}}{1-\sqrt{1-\tau}}\right)\right]^2 & : \quad \tau < 1 \end{cases}, \tag{7.35}$$

with $\tau = 4m^2/m_H^2$. Figure 7.5 shows the ratio of the $gg \to h$ cross-section to that of the Standard Model as a function of the Higgs mass for $y_{\text{light}} = 1/10$. As expected, there can be large corrections, even in the small v/k region.

For the decay $h \to \gamma\gamma$ we have

$$\Gamma_{h\to\gamma\gamma} = \frac{\alpha^2}{\pi^3 m_H m_W^2}\left|\sum_i F^i\right|^2 \tag{7.36}$$

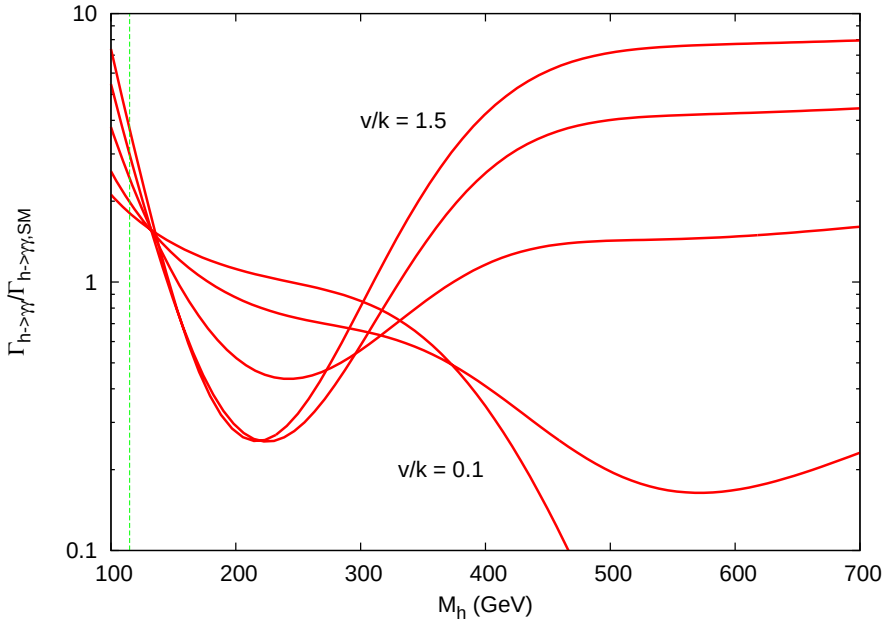

Figure 7.9: Ratio of the decay of a Higgs to $\gamma\gamma$ compared with the value in the SM. The different curves correspond to the values of v/k from top to bottom on the right edge of the graph of (1.5, 1.1, 0.8, 0.4, 0.1). Again, we have taken $y_{\rm light} = 1/10$.

where the F^i are as in Eq. (7.33) for fermions and

$$F^W = \sum_n \left(\frac{m_H^2}{2} + 4m_W^2 - [4m_W^2(m_H^2 - 2m_{W^{(n)}}^2) - m_{W^{(n)}}^2]C_0(m_W^2) \right) \tag{7.37}$$

This is shown in Fig. 7.5. The m_H dependence looks complicated, but the qualitative features are easy to understand. The initial enhancement is from the KK fermion contribution. As the Higgs mass approaches the gauge boson threshold the suppression to the hWW vertex becomes more important, and this suppression increases with v/k as expected. For large Higgs masses the top and other fermion KK contributions dominate and result in an enhancement.

Putting all of this together we can compute the branching ratios, shown in Fig 7.5 for $v/k = 1/10$, $y_{\rm light} = 1/10$. Several features are visible. First, the WW and ZZ coupling suppression results in a delayed dominance of these modes, although they do dominate eventually for all allowed values of v/k. Second, the Z_2 left-right symmetry

requires the b and t couplings to be equal, and hence the width to $b\bar{b}$ is always larger than the width to $t\bar{t}$ (they would, of course, be equal if $m_t = m_b$). Finally, this enhancement in the b coupling suppresses all other modes. In particular, the $h \to \gamma\gamma$ mode is unobservable. Note that even if the b coupling were not enhanced, the $\gamma\gamma$ mode would be reduced over a large region of parameter space by the hWW coupling suppression. This means searches for Higgs bosons at the LHC which depend on the $h \to \gamma\gamma$ decay mode will have dramatically reduced signal, and will likely not be viable if this model is correct.

It has been observed that Higgsless models with KK masses $\gtrsim 1\,\text{TeV}$ show a breakdown of perturbative unitarity in longitudinal gauge boson scattering [58]. Of course, in a purely Higgsed 4D model, unitarity is maintained to arbitrarily high scales. It is therefore interesting to see the behavior of the amplitude for $W_L W_L \to W_L W_L$ [72] as a function of v/k. This is shown in Fig. 7.5 for a fixed Higgs mass of 150 GeV. Note both the rapid falloff and the fact that, in the region $v/k \leq 1/4$, unitarity is maintained to scales above 6 TeV.

7.6 Conclusion

In this paper we have investigated the effects of a finite Higgs vev in the Left-Right symmetric Randall-Sundrum model with fermions and gauge bosons in the bulk. The main effects come from distortions of the W and Z wavefunctions near the IR brane. We found that the model is free of existing constraints as long as $v/k \lesssim 1/4$. In this region the Higgs coupling to the gauge bosons can be suppressed by a factor of up to $1/3$, and the Higgs couplings to gg and $\gamma\gamma$ can be substantially shifted. This results in a new pattern of branching ratios as a function of m_H.

It has been shown previously that the precision electroweak observables can be shifted by inclusion of brane localized kinetic terms for the gauge bosons and fermions [64, 42, 40]. This will shift the allowed region of v/k, but will not qualitatively alter the properties of the Higgs couplings.

In this model it will be difficult to discover the Higgs, since the $\gamma\gamma$ mode is invisible over much of the parameter space and the massive gauge boson couplings to

the Higgs are reduced. However, when it is found the properties of the Higgs will be an important tool in mapping out the parameters of the full model.

Appendix A - Bidoublet Higgs

Instead of the real bidoublet used in Section 7.2, we could use a complex bidoublet Higgs field, producing a version of the Two Higgs Doublet Model. We can parameterize this field as

$$\varphi = \begin{pmatrix} \varphi_1^0 & \varphi_1^+ \\ \varphi_2^- & \varphi_2^0 \end{pmatrix} \tag{7.38}$$

The most general form of the potential for complex bidoublet field is [93]

$$\begin{aligned} V(\varphi) = &-\mu^2 \mathrm{Tr}\varphi^\dagger\varphi + \lambda_1(\mathrm{Tr}\varphi^\dagger\varphi)^2 + \lambda_2 \mathrm{Tr}\varphi^\dagger\varphi\varphi^\dagger\varphi + \frac{1}{2}\lambda_3(\mathrm{Tr}\varphi^\dagger\tilde{\varphi} + \mathrm{Tr}\tilde{\varphi}^\dagger\varphi)^2 \\ &+ \frac{1}{2}\lambda_4(\mathrm{Tr}\varphi^\dagger - \mathrm{Tr}\tilde{\varphi}^\dagger\varphi)^2 + \lambda_5 \mathrm{Tr}\varphi^\dagger\varphi\tilde{\varphi}^\dagger\tilde{\varphi} + \frac{1}{2}\lambda_6(\mathrm{Tr}\varphi^\dagger\tilde{\varphi}\varphi^\dagger\tilde{\varphi} + \mathrm{Tr}\tilde{\varphi}^\dagger\varphi\tilde{\varphi}^\dagger\varphi), \end{aligned} \tag{7.39}$$

where $\tilde{\varphi} = \sigma_2\varphi^*\sigma_2$, and σ_2 is the ordinary Pauli matrix. We expect that there will be solutions where the neutral fields acquire vevs, so we try $\langle\varphi_1^0\rangle = v_1$, $\langle\varphi_2^0\rangle = v_2$. Stability of this solution requires the two conditions $\partial V/\partial v_{1,2} = 0$, where all fields are evaluated at their vevs. These then imply

$$\left({v_1}^2 - {v_2}^2\right)\left(-4\,\lambda_3 - \lambda_5 + \lambda_2 - \lambda_6\right). \tag{7.40}$$

There is no symmetry that can require the second factor to vanish, so we can see that aside from a vanishingly small and unnatural region of parameter space we have $v_1^2 = v_2^2 \equiv v^2/2$. The second stability condition then gives

$$v^2 = \frac{1}{2}\,\frac{\mu^2}{4\,\lambda_3 + 2\,\lambda_1 + \lambda_2 + \lambda_5 + \lambda_6}. \tag{7.41}$$

Inserting this solution into Eq. (7.39) we can read off that the mass eigenstates are

$$\begin{aligned} h &\equiv \mathcal{R}e\,(\varphi_1^0 + \varphi_2^0) & H &\equiv \mathcal{R}e\,(\varphi_1^0 - \varphi_2^0) \\ A &\equiv \mathcal{I}m\,(\varphi_1^0 + \varphi_2^0) & G^0 &\equiv \mathcal{I}m\,(\varphi_1^0 - \varphi_2^0) \\ h^+ &\equiv \varphi_1^+ + \varphi_2^+ & G^+ &\equiv \varphi_1^+ - \varphi_2^+. \end{aligned} \tag{7.42}$$

The G^i are the would-be Goldstone fields, and hence have no mass terms in the potential. Furthermore, the structure of the potential requires $m_H = m_{h^+}$. However, there are enough parameters that the masses are otherwise arbitrary. To parameterize this, we can write

$$m_h^2 = \lambda_h v^2, \qquad m_H^2 = m_{h^+}^2 = \lambda_H v^2, \qquad m_A^2 = \lambda_A v^2. \tag{7.43}$$

CP symmetry tells us that there is no three-point vertex coupling two gauge bosons to the CP-odd scalar. Hence, restricting ourselves to the neutral sector, we find the analysis from the main part of the paper goes through with minimal changes.

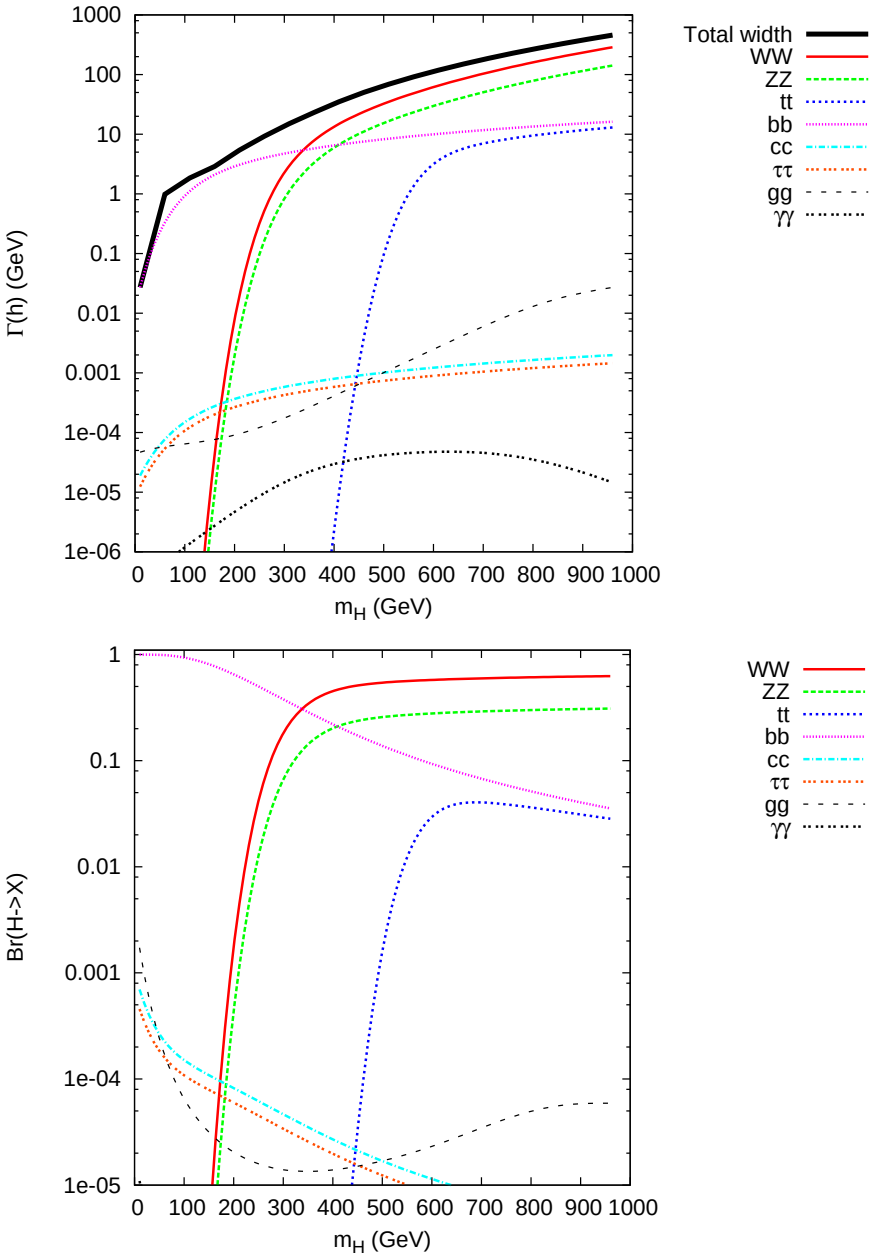

Figure 7.10: Partial widths (top) and branching ratios (bottom) for Higgs decay into various channels as a function of the Higgs mass at fixed $v/k = 1/10$ and $y_{\text{light}=1/10}$.

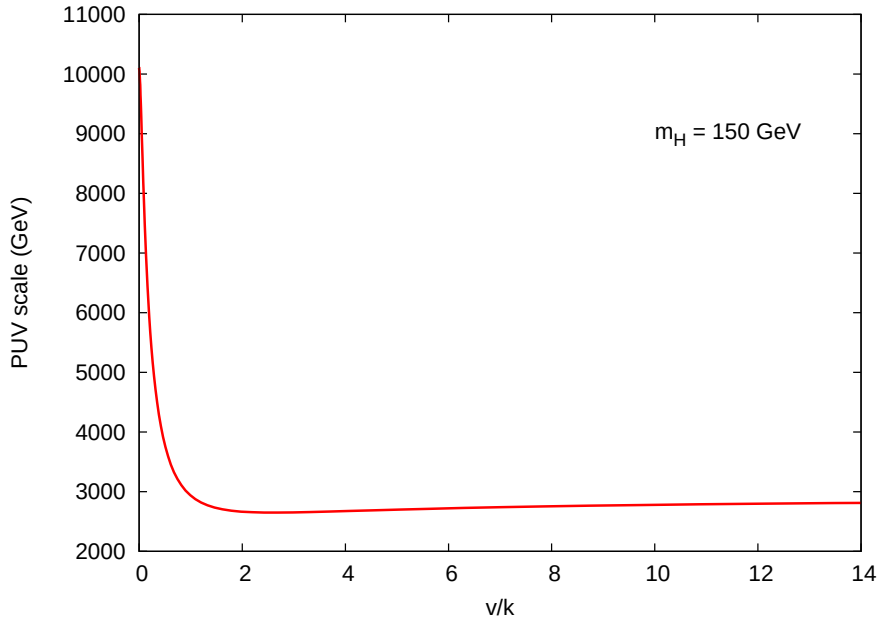

Figure 7.11: The center-of-mass energy at which tree-level perturbative unitarity is violated in $W_L^+W_L^- \to W_L^+W_L^-$ scattering.

Chapter 8

Black holes in many dimensions at the LHC: testing critical string theory

One of the most difficult questions facing theoretical high-energy physics for many years has been how to consistently combine General Relativity with Quantum Mechanics, as naive quantization produces unrenormalizable divergences. This issue is exacerbated by the hierarchy problem, which asks why the electroweak scale, $M_{wk} \sim$ TeV, is so small compared with the (reduced) Planck scale, $\overline{M}_{Pl} \sim$ a few 10^{18} GeV, which is associated with the energy at which non-renormalizable Einstein gravity becomes strong. It appears that resolution of these puzzles may require a complete theory of quantum gravity.

As of now, the best candidate for such a possibility is (critical) string theory (CST), which reduces to Einstein gravity at low energies and allows for the computation of finite $S-$matrix amplitudes. For CST to be a consistent theory there are three essential ingredients: (i) the fundamental objects of the theory are no longer point-like and must have a finite size of order M_s, the string scale; (ii) supersymmetry must be a good symmetry, at least at scales $\gtrsim M_s$; (iii) space-time must be ten or eleven dimensional, (*i.e.*, $D = 4 + n = 10$, if the string coupling is perturbative, $D = 11$ if it is non-perturbative), with the additional dimensions being compactified at a

radius $R_c \gtrsim 1/M_s$. Most research in string theory so far has focused on critical string theories, where the world-sheet anomalies are automatically canceled. It is precisely this anomaly cancelation that requires $D = 10$. However, there are consistent non-critical backgrounds of string theory in arbitrary numbers of dimensions. Here, the anomalies are canceled by solving the equations of motion taking into account the tree level moduli potential as well as contributions to the equations of motion from other sources such as fluxes, orientifolds, and branes [127, 121]. In either case, the common expectation is that M_s is slightly below or equal to $\overline{M}_{Pl}$ which would imply that the predictions of CST are difficult to test directly. Currently there is no evidence for any of these basic assumptions. If indeed $M_s \sim \overline{M}_{Pl}$ it may be that CST can never be directly tested in laboratory experiments. Furthermore, even if supersymmetry and/or extra dimensions were discovered in future experiments, this would be no guarantee that CST represents the correct theory of nature.

In recent years it has been proposed that the fundamental scale of gravity might not be $\overline{M}_{Pl}$, but rather $M_* \sim$ TeV [16, 118, 155, 20]. There is then no large hierarchy between the gravitational and electroweak scales. In this scenario, the observed weakness of gravity results from the presence of extra dimensions with large radii. In the simplest picture, gravity is able to propagate in all D dimensions, but the SM fields are restricted to a $3+1$ dimensional "brane". The strength of gravity at long distances is then diluted by the volume of the extra dimensions. If string theory is correct, the string scale must then be near a TeV in this scenario. Signals of string theory, such as string resonances would then be visible at future colliders, such as the Large Hadron Collider (LHC) at CERN [71, 57]. However, the interpretation of these signals is likely to be ambiguous, especially if the string coupling is non-perturbative. In the large extra dimensions picture of Arkani-Hamed, Dimopoulos and Dvali (ADD) [20], M_* and $\overline{M}_{Pl}$ are related by $\overline{M}_{Pl}^2 = V_n M_*^{n+2}$, where V_n is the volume of the n compactified large dimensions. If CST is correct $D = 10(11)$, thus we must have $n \leq 6(7)$ (note that all of the extra dimensions need not be large). It is *impossible* to have $n > 6(7)$ in the CST realization of ADD; an experimental determination that $n > 6(7)$ would thus *exclude* CST.

In this paper we propose a 'null' test of CST; this test can *only* reveal whether

CST is excluded and cannot tell us if it is the correct theory of nature. We will do this by examining the properties of black hole (BH) production and decay at the LHC with different numbers of extra dimensions. From this, we will show that the number of compactified large dimensions can be determined; if $n > 6(7)$ is measured with high confidence then CST is excluded, however if $n \leq 6(7)$ is measured then very little information about CST is obtained. We will show that if n is sufficiently large, then the region $n \leq 6(7)$ as required by CST will be highly disfavored by many standard deviations. There are, of course, more general reasons for determining the number of extra dimensions from BH production: (*i*) It allows one to differentiate a BH in the ADD 'flat' extra-dimensions scenario from one in a Randall-Sundrum-like model [136] with warped geometry and very weakly coupled graviton resonances [58]. (*ii*) If string resonances are observed at colliders this test is the only way to determine whether or not they arise from CST. (*iii*) Whatever the theory of quantum gravity, the energy region near M_* is likely to be fairly complex; measuring BH properties may be one of the few handles on this physics. As a proof of principle for our proposal, we will show that there exists a region in the (n, M_*) parameter space of the ADD model where we can experimentally exclude the case $n \leq 6(7)$ at 5σ significance.

For simplicity in what follows, we will assume that this $n-$dimensional space is compactified on a torus of equal radii so that $V_n = (2\pi R_c)^n$, where R_c is the compactification radius. Given $\overline{M}_{Pl}$ and $M_* \sim$ a few TeV, R_c becomes completely fixed by the relation above. Note that the case $n = 1$ is excluded while $n = 2$ with low M_* is disfavored by current data [102]. For the case of a torus, the graviton has Kaluza-Klein(KK) excitations $h^{(n)}_{\mu\nu}$, with masses given by $M_n^2 = \mathbf{n}^2/R_c^2$, where $\mathbf{n}$ labels a set of occupation numbers. The KK graviton couplings to the Standard Model (SM) fields are described by the stress-energy tensor $T^{\mu\nu}$, given in D dimensions by $\mathcal{L} = -\sum_n h^{(n)}_{\mu\nu} T^{\mu\nu}/M_*^{1+n/2}$. The ADD scenario has three distinct experimental signatures which have been studied in some detail in the literature: (*i*) missing energy events associated with KK graviton emission in the collisions of SM fields; (*ii*) new contact interactions associated with spin-2 KK exchanges between SM fields [97, 103, 87, 124, 141]; (*iii*) black hole production in particle collisions [19, 69, 86].

Is there any guide as to what values of $n > 6(7)$ we should consider? For ADD

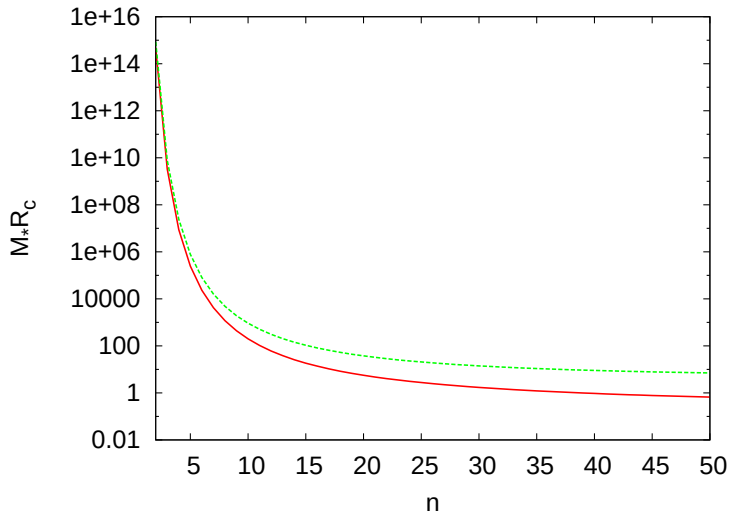

Figure 8.1: M_*R_c as a function of n for $M_* = 1$ TeV for a torus (solid) and sphere (dashed) compactifications.

with $n \leq 6$ it is well known that the hierarchy problem is *not* truly solved. Although we have reduced M_* to a few TeV, $M_*R_c \gg 1$, as seen in Fig 8.1. By contrast, with n large we could have $M_*R_c \lesssim 10$. Note that, if $M_*R_c < 1$ the theory would lose its predictive power since the compactification scale is above the cutoff. To obtain the interesting range of compactification radii, $1 \lesssim M_*R_c \lesssim 10$, requires $17 \lesssim n \lesssim 39$, hence we will focus on this set of values in what follows. If the compactification topology is a sphere, rather than a torus, this changes to $n \geq 30$, as seen in Fig 8.1. It is important to notice that this model does solve the hierarchy problem for large n, but that would lie outside the realm of CST. Note that some other modifications of the compactification geometry can obtain $RM_* \lesssim 10$ [111]. For such large values of n the Kaluza-Klein masses are at the TeV scale. Since each KK state is coupled with 4 dimensional Planck strength, $\overline{M}_{Pl}$, to the SM fields, it is clear that this sufficiently weakens the KK contributions to the processes (i) and (ii) above, such that no meaningful constraints are obtainable. For example, with $n = 2$, precision measurements at the International Linear Collider at $\sqrt{s} = 1\,\text{TeV}$ will be sensitive to $M_* \lesssim 10\,\text{TeV}$, while with $n = 21$, this drops to $M_* \lesssim 1\,\text{TeV}$. Thus for reasonable values of M_* the *only* signal for large n in ADD is black hole production.

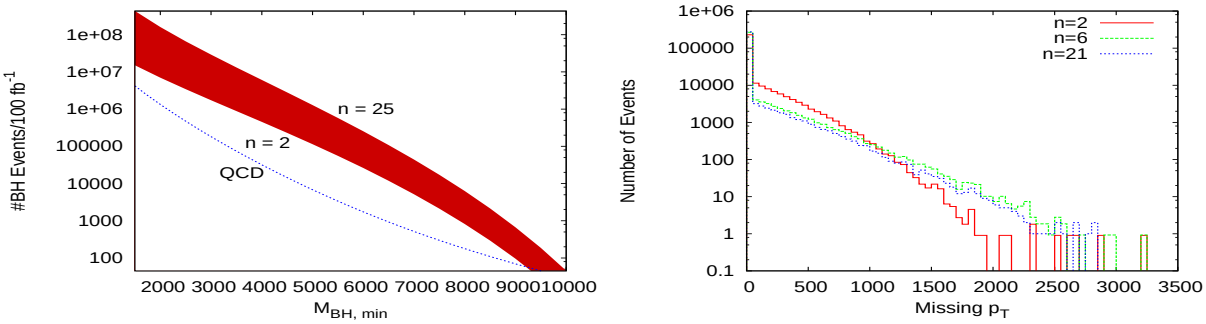

Figure 8.2: Top panel: Cross-section for production of black holes with mass $M > M_{BH,min}$ with $M_* = 1.5\,\mathrm{TeV}$, for $n = 2$(bottom) to 25(top) of the band. Also shown is the QCD dijet cross-section for dijet invariant mass $M \geq M_{BH,min}$, and $|\eta| < 1$. Bottom panel: $\not{p}_T$ distribution of BH events passing cuts described in the text for $M_* = 1\,\mathrm{TeV}$ and $n = 2, 6, 21$.

We now investigate BH production at the LHC in detail; for previous studies see [98, 152]. When $\sqrt{s} \gtrsim M_*$ BHs are produced with a geometric (subprocess) cross section, $\hat{\sigma} \simeq \pi R_s^2$. Here R_s is the Schwarzschild radius corresponding to a BH of mass $M_{BH} \simeq \sqrt{\hat{s}}$. R_s is given by [112]

$$M_* R_s = \left[\frac{\Gamma(\frac{n+3}{2})}{(n+2)\pi^{(n+3)/2}} \frac{M_{BH}}{M_*} \right]^{1/(n+1)} . \tag{8.1}$$

Note that $\hat{\sigma} \sim n$ for large n. Numerical simulations and detailed arguments have shown that the geometric cross section estimate is good to within factors of a few [85, 156]. The total number of BH events at the LHC with invariant mass above an arbitrary value $M_{\mathrm{BH,min}}$ is shown in Fig. 8.2. The scale of the total inclusive BH cross-section, ~ 100 pb, is huge compared to that which is typical of new physics processes, $\lesssim 1$ pb. Thus, over much of the parameter space the LHC will be producing over a million BH events per year. This high rate means that there will be tremendous statistical power, and essentially all measurements will be systematics limited.

The semiclassical treatment, used here and in all previous studies [112], may recieve potentially large corrections from two sources: (*i*) distortions from the finite compactification scale as R_s approaches R_c, and (*ii*) quantum gravity. Case (*i*) is easily controllable. We know that in 5 dimensions the critical point for instabilities

due to finite compactification is $(R_s/R_c)^2 \approx 0.1$ [88]. For LHC energies we always have $(R_s/R_c)^2 \ll 0.1$, so these corrections are negligible. In more dimensions the ratio of the volume of a BH with fixed R_s to the volume of the torus with fixed R_c drops rapidly with n, so we expect the corrections to be even smaller. Case (*ii*) is more problematic; we estimate the quantum gravity effects by looking at the corrections from higher curvature terms in the action, *e.g.*

$$S = \frac{M_*^{D-2}}{2} \int d^D x \, \left(R + \frac{\alpha_1}{M_*^2} \mathcal{L}_2 + \frac{\alpha_2}{M_*^4} \mathcal{L}_3 + \ldots \right). \tag{8.2}$$

Here R is the Ricci scalar, and $\mathcal{L}_i$ is the ith order Lovelock invariant, with $\mathcal{L}_2$ being the Gauss-Bonnet term [116]. This equation also defines our convention for the fundamental scale M_*.[1] Schwartzchild solutions are known for arbitrary values of the α_i [153]. If we assume that the higher curvature terms are radiatively generated, and hence each α_i is the ith power of an expansion parameter α (as occurs in string models [158, 30, 157]), we find that $\alpha n^2 \leq 1$. For α of this size we find that the corrections are always less severe as n increases, with a $\sim 20\%$ correction to R_s for $n = 20$. This does not qualitatively affect our conclusions here; for a more detailed study of these corrections, see [104].

We now come to the crucial question, is there any property of the produced black holes that can resolve the number of dimensions? The cross-section is n-dependent, but the overall scale is set by $1/M_*^2$, so one would first have to measure M_* independently to good accuracy to obtain any resolution on n. Cross section ratios at different BH masses could be used, however, the range of energies that are clearly in the geometric regime and accessible to the LHC is not likely to be large. This leads us to the decay properties of black holes. One generically expects that black holes produced at colliders are formed in highly asymmetric states, with high angular momentum, and possibly a non-zero charge. However, they quickly shed their charge and angular momentum by emitting bulk graviton modes and soft brane modes, and relax to a simple Schwartzchild state; their decay then proceeds primarily by thermal

[1] We note that this is related to the other definitions in the literature by $M_* = (8\pi)^{-\frac{1}{n+2}} M_{\rm DL}$[69] $= [2(2\pi)^n]^{-1\frac{1}{n+2}} M_{\rm GT}$[86].

emission of Hawking radiation [112] until $M_{BH} \sim M_*$, where quantum gravity effects will mediate the final decay. The Hawking temperature is given by

$$T_H = \frac{(n+1)M_*}{4\pi}\left[\frac{\Gamma(\frac{n+3}{2})}{(n+2)\pi^{(n+3)/2}}\frac{M_{BH}}{M_*}\right]^{-1/(n+1)}. \tag{8.3}$$

From this we can see that, at fixed M_{BH}, higher dimensional BHs are hotter. Since the average multiplicity goes inversely with the temperature, a low dimensional BH will emit many quanta before losing all of it's energy. By contrast, the decay of a high dimension BH will have fewer final state particles, and each emitted quanta will carry a larger fraction of the BH energy. We will use this difference to obtain experimental resolution on n.

The previous argument suggests we examine the final state multiplicity, or the individual particle p_T distributions as a probe of n. The multiplicity is affected by two major sources of uncertainty: (a) contributions from initial and final state radiation that produce additional jets, and (b) the details of the final quantum gravity decay of the BH are unknown. In what follows we will assume that this decay is primarily 2-body. However, this is clearly model-dependent; we prefer observables that are independent of this assumption, disfavoring the multiplicity. By contrast, the p_T spectra of individual particles, particularly at high-p_T, will be mostly sensitive to the *initial* temperature of the BHs. There are many such distributions that one could consider. In particular, one would like to examine all possible distributions and see that the candidate BH states are coupling equally to each SM degree of freedom, verifying that these are gravitational phenomena [104]. For illustration we will focus here on the $\not{p}_T$ and individual jet p_T distributions for the BH final state.

To calculate these distributions, we have simulated BH events using a modified version of CHARYBDIS [99], linked to PYTHIA [150]. First, a large sample of BHs with masses above a critical value $M_{\rm min} = M_*$ is generated. From these we select events by cutting on the reconstructed invariant mass, $M_{\rm inv}$ of the event, defined by summing over all visible final state particles or jets with rapidity $|\eta| < 3$, and with $p_T \geq 50\,\text{GeV}$. We would like to select events where the BH mass is large enough that the event is in the geometrical regime, and quantum gravity corrections are small.

To do this, one would need to extract from the data an estimate of the size of M_*. While we have no fundamental model for the quantum gravity effects near threshold, we can assume that there will be a turn-on for BH production near M_*, and the cross-section will then asymptote to the geometric value. While this will not lead to a precision determination of M_*, it can clearly be used to set an optimum cut on $M_{\rm inv}$. In the context of a particular model of the threshold based on the action (8.2), we find that $M_{\rm inv} \geq 2M_*$ is a reasonable cut [104]. We include initial-state radiation in the simulations, since that can lead to a contamination of lower $\sqrt{\hat{s}}$ events in our sample. In the case of jets, for simplicity we turn off hadronization, and simply look at the parton-level characteristics.

To be specific, we generate a "data" set of $\sim 300k$ events with $n = 21$ and $M_* = 1\,\text{TeV}$. We use this size sample as a conservative lower estimate of BH production. If the cross section is within an order of magnitude of that in Fig. 8.2, the LHC will collect many millions of events, giving an increase in statistical power over that presented here. These "data" events are then compared to a number of template sets of events. We then ask at what confidence the template can be excluded by performing a χ^2 test using only the resulting $\not{p}_T$ distribution (shown in Fig. 8.2). We examine the range $2 \leq n \leq 21$, and $0.75 \leq M_* \leq 5\,\text{TeV}$. The lower bound on M_* comes from non-observation at the Tevatron, while the upper bound is set by demanding that the LHC be able to collect at least $50k$ events given the cross-section uncertainties. We then determine whether the CST region can be excluded at high confidence. For this test case, we find at least a 5σ exclusion for the entire CST region using the $\not{p}_T$ distribution alone, or $\sim 40\sigma$ using the jet-p_T spectrum. Though the statistical power in jets is much higher, it suffers from more systematic uncertainties. Fig. 8.3 shows the 3, 5, and 10σ exclusion contours in the (n, M_*) plane obtained using the $\not{p}_T$ distribution for this test case. If the LHC collects a few million events rather than the $300k$ sample used here, simple scaling tells us that the 5σ curve excludes $n \leq 20$, and the 10σ curve excludes $n \leq 11$.

We have shown that the CST region can be excluded if $n = 21$. What about other values of n? On changing the number of dimensions used in generating the"data", we find that for any $n \geq 15$ the CST region can be excluded by at least 5σ, with

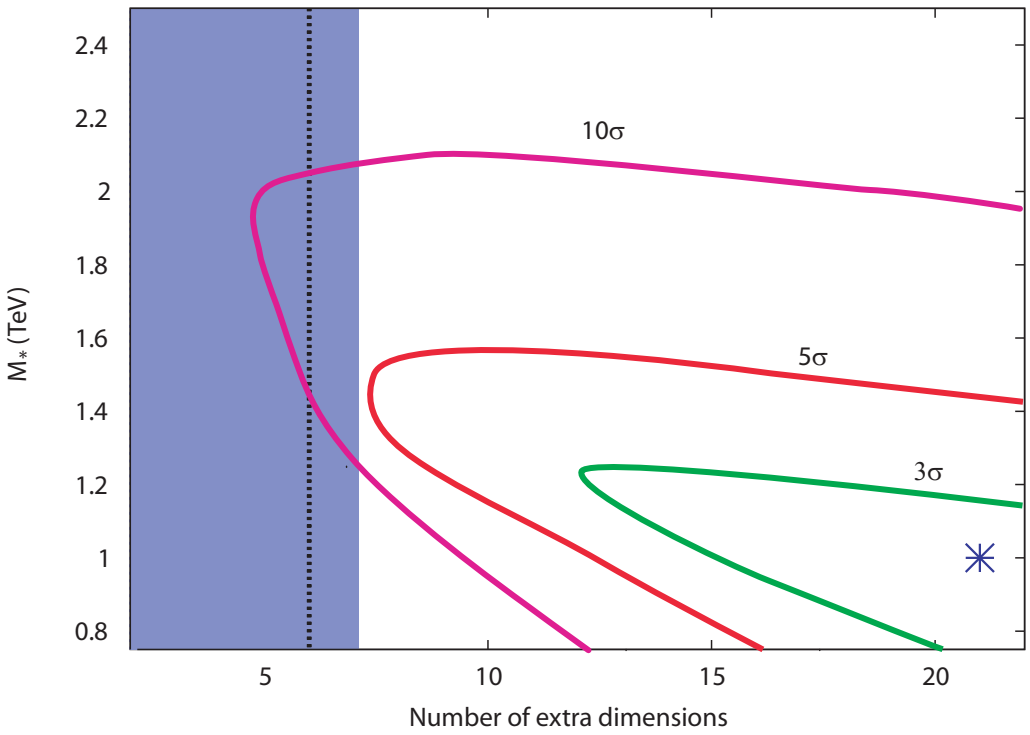

Figure 8.3: Exclusion curves in the (n, M_*) plane, assuming the data lies at the point $(21, 1\,\text{TeV})$. Points outside the curves are excluded at 3, 5, or 10σ.

$300k$ events. We would, of course, like to know in what region of the parameter space this type of definitive test can be performed. A more detailed study of the parameter space is in progress [104].

In conclusion, we have shown that if there exist many TeV sized extra dimensions, which solves the Hierarchy Problem, then there exists an observable that can rule out critical string theory.

Bibliography

[1] V. M. Abazov et al. Search for heavy particles decaying into electron positron pairs in p anti-p collisions. *Phys. Rev. Lett.*, 87:061802, 2001.

[2] F. Abe et al. Search for the decays b/d0 –¿ mu+ mu- and b/s0 –¿ mu+ mu- in p anti-p collisions at s**(1/2) = 1.8-tev. *Phys. Rev.*, D57:3811–3816, 1998.

[3] S. A. Abel, M. Masip, and J. Santiago. Flavour changing neutral currents in intersecting brane models. 2003.

[4] P. Achard et al. Search for single top production at lep. *Phys. Lett.*, B549:290–300, 2002.

[5] T. Affolder et al. Search for quark lepton compositeness and a heavy w' boson using the e nu channel in p anti-p collisions at s**(1/2) = 1.8-tev. *Phys. Rev. Lett.*, 87:231803, 2001.

[6] K. Agashe, N. G. Deshpande, and G. H. Wu. Universal extra dimensions and b –¿ s gamma. *Phys. Lett.*, B514:309–314, 2001.

[7] Kaustubh Agashe, Roberto Contino, and Alex Pomarol. The minimal composite Higgs model. 2004.

[8] Kaustubh Agashe, Roberto Contino, and Raman Sundrum. Top compositeness and precision unification. 2005.

[9] Kaustubh Agashe, Antonio Delgado, Michael J. May, and Raman Sundrum. RS1, custodial isospin and precision tests. *JHEP*, 08:050, 2003.

[10] Kaustubh Agashe and Geraldine Servant. Baryon number in warped GUTs: Model building and (dark matter related) phenomenology. 2004.

[11] Kaustubh Agashe and Geraldine Servant. Warped unification, proton stability and dark matter. *Phys. Rev. Lett.*, 93:231805, 2004.

[12] J. A. Aguilar-Saavedra et al. Tesla technical design report part iii: Physics at an e+e- linear collider. 2001.

[13] Guido Altarelli and Riccardo Barbieri. Vacuum polarization effects of new physics on electroweak processes. *Phys. Lett.*, B253:161–167, 1991.

[14] Guido Altarelli et al. Extended gauge models and precision electroweak data. *Phys. Lett.*, B318:139–147, 1993.

[15] K. Anikeev et al. B physics at the tevatron: Run ii and beyond. 2001.

[16] Ignatios Antoniadis. A possible new dimension at a few tev. *Phys. Lett.*, B246:377–384, 1990.

[17] Ignatios Antoniadis, Nima Arkani-Hamed, Savas Dimopoulos, and G. R. Dvali. New dimensions at a millimeter to a fermi and superstrings at a tev. *Phys. Lett.*, B436:257–263, 1998.

[18] Thomas Appelquist, Hsin-Chia Cheng, and Bogdan A. Dobrescu. Bounds on universal extra dimensions. *Phys. Rev.*, D64:035002, 2001.

[19] Philip C. Argyres, Savas Dimopoulos, and John March-Russell. Black holes and sub-millimeter dimensions. *Phys. Lett.*, B441:96–104, 1998.

[20] Nima Arkani-Hamed, Savas Dimopoulos, and G. R. Dvali. The hierarchy problem and new dimensions at a millimeter. *Phys. Lett.*, B429:263–272, 1998.

[21] Nima Arkani-Hamed, Savas Dimopoulos, and G. R. Dvali. Phenomenology, astrophysics and cosmology of theories with sub-millimeter dimensions and tev scale quantum gravity. *Phys. Rev.*, D59:086004, 1999.

[22] Nima Arkani-Hamed, Yuval Grossman, and Martin Schmaltz. Split fermions in extra dimensions and exponentially small cross-sections at future colliders. *Phys. Rev.*, D61:115004, 2000.

[23] Nima Arkani-Hamed and Martin Schmaltz. Hierarchies without symmetries from extra dimensions. *Phys. Rev.*, D61:033005, 2000.

[24] G. Azuelos et al. The beyond the standard model working group: Summary report. 2002.

[25] R. Barate et al. Search for the standard model higgs boson at lep. *Phys. Lett.*, B565:61–75, 2003.

[26] Riccardo Barbieri, Alex Pomarol, and Riccardo Rattazzi. Weakly coupled Higgsless theories and precision electroweak tests. *Phys. Lett.*, B591:141–149, 2004.

[27] Riccardo Barbieri, Alex Pomarol, Riccardo Rattazzi, and Alessandro Strumia. Electroweak symmetry breaking after LEP1 and LEP2. *Nucl. Phys.*, B703:127–146, 2004.

[28] Riccardo Barbieri and Alessandro Strumia. Cp violation in b decays and supersymmetry. *Nucl. Phys.*, B508:3–16, 1997.

[29] Andreas Birkedal, Konstantin Matchev, and Maxim Perelstein. Collider phenomenology of the Higgsless models. 2004.

[30] David G. Boulware and S. Deser. String generated gravity models. *Phys. Rev. Lett.*, 55:2656, 1985.

[31] G. C. Branco, Andre de Gouvea, and M. N. Rebelo. Split fermions in extra dimensions and cp violation. *Phys. Lett.*, B506:115–122, 2001.

[32] Gerhard Buchalla, Andrzej J. Buras, and Markus E. Lautenbacher. Weak decays beyond leading logarithms. *Rev. Mod. Phys.*, 68:1125–1144, 1996.

[33] Andrzej J. Buras, Anton Poschenrieder, Michael Spranger, and Andreas Weiler. The impact of universal extra dimensions on $b- > x_s$ gamma, $b- > x_s$ gluon, $b- > x_s mu^+ mu^-, k_l- > pi^0 e^+ e^-$, and epsilon'/epsilon. 2003.

[34] Andrzej J. Buras, Michael Spranger, and Andreas Weiler. The impact of universal extra dimensions on the unitarity triangle and rare k and b decays. *Nucl. Phys.*, B660:225–268, 2003.

[35] Gustavo Burdman and Yasunori Nomura. Holographic theories of electroweak symmetry breaking without a Higgs boson. *Phys. Rev.*, D69:115013, 2004.

[36] C. P. Burgess, Stephen Godfrey, Heinz Konig, David London, and Ivan Maksymyk. A global fit to extended oblique parameters. *Phys. Lett.*, B326:276–281, 1994.

[37] Giacomo Cacciapaglia, Csaba Csaki, Christophe Grojean, Matthew Reece, and John Terning. Top and bottom: A brane of their own. 2005.

[38] Giacomo Cacciapaglia, Csaba Csaki, Christophe Grojean, and John Terning. Oblique corrections from Higgsless models in warped space. *Phys. Rev.*, D70:075014, 2004.

[39] Elena Caceres, Vadim S. Kaplunovsky, and I. Michael Mandelberg. Large-volume string compactifications, revisited. *Nucl. Phys.*, B493:73–100, 1997.

[40] Marcela Carena, Antonio Delgado, Eduardo Ponton, Tim M. P. Tait, and C. E. M. Wagner. Warped fermions and precision tests. *Phys. Rev.*, D71:015010, 2005.

[41] Marcela Carena, Eduardo Ponton, Tim M. P. Tait, and C. E. M Wagner. Opaque branes in warped backgrounds. *Phys. Rev.*, D67:096006, 2003.

[42] Marcela Carena, Tim M. P. Tait, and C. E. M. Wagner. Branes and orbifolds are opaque. *Acta Phys. Polon.*, B33:2355, 2002.

[43] R. Casalbuoni, S. De Curtis, and D. Dominici. Moose models with vanishing S parameter. *Phys. Rev.*, D70:055010, 2004.

[44] Debrupa Chakraverty, Katri Huitu, and Anirban Kundu. Effects of universal extra dimensions on b0 - anti-b0 mixing. *Phys. Lett.*, B558:173–181, 2003.

[45] We-Fu Chang and John N. Ng. Cp violation in 5d split fermions scenario. *JHEP*, 12:077, 2002.

[46] Hsin-Chia Cheng, Jonathan L. Feng, and Konstantin T. Matchev. Kaluza-klein dark matter. *Phys. Rev. Lett.*, 89:211301, 2002.

[47] R. Sekhar Chivukula, Duane A. Dicus, Hong-Jian He, and Satyanarayan Nandi. Unitarity of the higher dimensional standard model. *Phys. Lett.*, B562:109–117, 2003.

[48] R. Sekhar Chivukula, Hong-Jian He, Masafumi Kurachi, Elizabeth H. Simmons, and Masaharu Tanabashi. Ideal fermion delocalization in Higgsless models. 2005.

[49] R. Sekhar Chivukula, Elizabeth H. Simmons, Hong-Jian He, Masafumi Kurachi, and Masaharu Tanabashi. The structure of corrections to electroweak interactions in Higgsless models. *Phys. Rev.*, D70:075008, 2004.

[50] R. Sekhar Chivukula, Elizabeth H. Simmons, Hong-Jian He, Masafumi Kurachi, and Masaharu Tanabashi. Universal non-oblique corrections in Higgsless models and beyond. *Phys. Lett.*, B603:210–218, 2004.

[51] R. Sekhar Chivukula, Elizabeth H. Simmons, Hong-Jian He, Masafumi Kurachi, and Masaharu Tanabashi. Deconstructed Higgsless models with one-site delocalization. 2005.

[52] D. Jeremy Copeland. personal communication.

[53] Csaba Csaki, Joshua Erlich, and John Terning. The effective lagrangian in the Randall-Sundrum model and electroweak physics. *Phys. Rev.*, D66:064021, 2002.

[54] Csaba Csaki, Christophe Grojean, Jay Hubisz, Yuri Shirman, and John Terning. Fermions on an interval: Quark and lepton masses without a Higgs. *Phys. Rev.*, D70:015012, 2004.

[55] Csaba Csaki, Christophe Grojean, Hitoshi Murayama, Luigi Pilo, and John Terning. Gauge theories on an interval: Unitarity without a Higgs. *Phys. Rev.*, D69:055006, 2004.

[56] Csaba Csaki, Christophe Grojean, Luigi Pilo, and John Terning. Towards a realistic model of Higgsless electroweak symmetry breaking. *Phys. Rev. Lett.*, 92:101802, 2004.

[57] Schuyler Cullen, Maxim Perelstein, and Michael E. Peskin. Tev strings and collider probes of large extra dimensions. *Phys. Rev.*, D62:055012, 2000.

[58] H. Davoudiasl, J. L. Hewett, B. Lillie, and T. G. Rizzo. Higgsless electroweak symmetry breaking in warped backgrounds: Constraints and signatures. *Phys. Rev.*, D70:015006, 2004.

[59] H. Davoudiasl, J. L. Hewett, B. Lillie, and T. G. Rizzo. Warped Higgsless models with IR-brane kinetic terms. *JHEP*, 05:015, 2004.

[60] H. Davoudiasl, J. L. Hewett, and T. G. Rizzo. Bulk gauge fields in the Randall-Sundrum model. *Phys. Lett.*, B473:43–49, 2000.

[61] H. Davoudiasl, J. L. Hewett, and T. G. Rizzo. Phenomenology of the Randall-Sundrum gauge hierarchy model. *Phys. Rev. Lett.*, 84:2080, 2000.

[62] H. Davoudiasl, J. L. Hewett, and T. G. Rizzo. Experimental probes of localized gravity: On and off the wall. *Phys. Rev.*, D63:075004, 2001.

[63] H. Davoudiasl, J. L. Hewett, and T. G. Rizzo. Brane localized curvature for warped gravitons. *JHEP*, 08:034, 2003.

[64] H. Davoudiasl, J. L. Hewett, and T. G. Rizzo. Brane localized kinetic terms in the Randall-Sundrum model. *Phys. Rev.*, D68:045002, 2003.

[65] H. Davoudiasl, J. L. Hewett, and T. G. Rizzo. Phenomenology on a slice of ads(5) x m**delta spacetime. *JHEP*, 04:001, 2003.

[66] F. del Aguila, M. Perez-Victoria, and J. Santiago. Bulk fields with general brane kinetic terms. *JHEP*, 02:051, 2003.

[67] F. Del Aguila and J. Santiago. Signals from extra dimensions decoupled from the compactification scale. *JHEP*, 03:010, 2002.

[68] A. Delgado, A. Pomarol, and M. Quiros. Electroweak and flavor physics in extensions of the standard model with large extra dimensions. *JHEP*, 01:030, 2000.

[69] Savas Dimopoulos and Greg Landsberg. Black holes at the lhc. *Phys. Rev. Lett.*, 87:161602, 2001.

[70] Bogdan A. Dobrescu and Erich Poppitz. Number of fermion generations derived from anomaly cancellation. *Phys. Rev. Lett.*, 87:031801, 2001.

[71] E. Dudas and J. Mourad. String theory predictions for future accelerators. *Nucl. Phys.*, B575:3–34, 2000.

[72] M. J. Duncan, Gordon L. Kane, and W. W. Repko. W W physics at future colliders. *Nucl. Phys.*, B272:517, 1986.

[73] G. R. Dvali, Gregory Gabadadze, and Mikhail A. Shifman. (quasi)localized gauge field on a brane: Dissipating cosmic radiation to extra dimensions? *Phys. Lett.*, B497:271–280, 2001.

[74] S. Eidelman et al. Review of particle physics. *Phys. Lett.*, B592:1, 2004.

[75] Jens Erler. Constraining electroweak physics. 2003.

[76] Nick Evans and Phil Membry. Higgless W unitarity from decoupling deconstruction. 2004.

[77] Harald Fritzsch and Zhi-zhong Xing. Mass and flavor mixing schemes of quarks and leptons. *Prog. Part. Nucl. Phys.*, 45:1–81, 2000.

[78] F. Gabbiani, E. Gabrielli, A. Masiero, and L. Silvestrini. A complete analysis of fcnc and cp constraints in general susy extensions of the standard model. *Nucl. Phys.*, B477:321–352, 1996.

[79] S. Gabriel, S. Nandi, and G. Seidl. 6D Higgsless standard model. 2004.

[80] Howard Georgi, Aaron K. Grant, and Girma Hailu. Brane couplings from bulk loops. *Phys. Lett.*, B506:207–214, 2001.

[81] Howard Georgi, Aaron K. Grant, and Girma Hailu. Chiral fermions, orbifolds, scalars and fat branes. *Phys. Rev.*, D63:064027, 2001.

[82] Tony Gherghetta and Alex Pomarol. Bulk fields and supersymmetry in a slice of ads. *Nucl. Phys.*, B586:141–162, 2000.

[83] Tony Gherghetta and Alex Pomarol. A warped supersymmetric standard model. *Nucl. Phys.*, B602:3–22, 2001.

[84] F. Gianotti et al. Physics potential and experimental challenges of the lhc luminosity upgrade. *Eur. Phys. J.*, C39:293–333, 2005.

[85] Steven B. Giddings and Vyacheslav S. Rychkov. Black holes from colliding wavepackets. *Phys. Rev.*, D70:104026, 2004.

[86] Steven B. Giddings and Scott Thomas. High energy colliders as black hole factories: The end of short distance physics. *Phys. Rev.*, D65:056010, 2002.

[87] Gian F. Giudice, Riccardo Rattazzi, and James D. Wells. Quantum gravity and extra dimensions at high-energy colliders. *Nucl. Phys.*, B544:3–38, 1999.

[88] R. Gregory and R. Laflamme. Black strings and p-branes are unstable. *Phys. Rev. Lett.*, 70:2837–2840, 1993.

[89] Yuval Grossman and Matthias Neubert. Neutrino masses and mixings in non-factorizable geometry. *Phys. Lett.*, B474:361–371, 2000.

[90] Yuval Grossman and Gilad Perez. Realistic construction of split fermion models. *Phys. Rev.*, D67:015011, 2003.

[91] LEP Electroweak Working Group. 2003.

[92] LEP Electroweak Working Group. A combination of preliminary electroweak measurements and constraints on the standard model. 2003.

[93] J. F. Gunion, J. Grifols, A. Mendez, B. Kayser, and Fredrick I. Olness. Higgs bosons in left-right symmetric models. *Phys. Rev.*, D40:1546, 1989.

[94] John F. Gunion, Howard E. Haber, Gordon L. Kane, and Sally Dawson. The higgs hunter's guide. SCIPP-89/13.

[95] K. Hagiwara et al. Review of particle physics. *Phys. Rev.*, D66:010001, 2002.

[96] Tao Han and JoAnne L. Hewett. Top charm associated production in high energy e+ e- collisions. *Phys. Rev.*, D60:074015, 1999.

[97] Tao Han, Joseph D. Lykken, and Ren-Jie Zhang. On kaluza-klein states from large extra dimensions. *Phys. Rev.*, D59:105006, 1999.

[98] C. M. Harris et al. Exploring higher dimensional black holes at the large hadron collider. 2004.

[99] C. M. Harris, P. Richardson, and B. R. Webber. Charybdis: A black hole event generator. *JHEP*, 08:033, 2003.

[100] J. L. Hewett, B. Lillie, and T. G. Rizzo. Monte carlo exploration of warped Higgsless models. *JHEP*, 10:014, 2004.

[101] J. L. Hewett, F. J. Petriello, and T. G. Rizzo. Precision measurements and fermion geography in the randall-sundrum model revisited. *JHEP*, 09:030, 2002.

[102] JoAnne Hewett and Maria Spiropulu. Particle physics probes of extra spacetime dimensions. *Ann. Rev. Nucl. Part. Sci.*, 52:397–424, 2002.

[103] JoAnne L. Hewett. Indirect collider signals for extra dimensions. *Phys. Rev. Lett.*, 82:4765–4768, 1999.

[104] JoAnne L. Hewett, Ben Lillie, and Thomas G. Rizzo. 2005. In progress.

[105] Johannes Hirn and Jan Stern. The role of spurions in Higgs-less electroweak effective theories. *Eur. Phys. J.*, C34:447–475, 2004.

[106] Petr Horava and Edward Witten. Eleven-dimensional supergravity on a manifold with boundary. *Nucl. Phys.*, B475:94–114, 1996.

[107] Petr Horava and Edward Witten. Heterotic and type i string dynamics from eleven dimensions. *Nucl. Phys.*, B460:506–524, 1996.

[108] Stephan J. Huber. Flavor violation and warped geometry. 2003.

[109] R. Jackiw and C. Rebbi. Solitons with fermion number 1/2. *Phys. Rev.*, D13:3398–3409, 1976.

[110] T. Jacobson, N. C. Tsamis, and R. P. Woodard. Tachyons and perturbative unitarity. *Phys. Rev.*, D38:1823, 1988.

[111] Nemanja Kaloper, John March-Russell, Glenn D. Starkman, and Mark Trodden. Compact hyperbolic extra dimensions: Branes, kaluza-klein modes and cosmology. *Phys. Rev. Lett.*, 85:928–931, 2000.

[112] Panagiota Kanti. Black holes in theories with large extra dimensions: A review. *Int. J. Mod. Phys.*, A19:4899–4951, 2004.

[113] David Elazzar Kaplan and Tim M. P. Tait. New tools for fermion masses from extra dimensions. *JHEP*, 11:051, 2001.

[114] Benjamin W. Lee, C. Quigg, and H. B. Thacker. Weak interactions at very high-energies: The role of the higgs boson mass. *Phys. Rev.*, D16:1519, 1977.

[115] Ben Lillie and JoAnne L. Hewett. Flavor constraints on split fermion models. *Phys. Rev.*, D68:116002, 2003.

[116] David Lovelock. The einstein tensor and its generalizations. *Journal of Mathematical Physics*, 12(3):498–501, 1971.

[117] Markus A. Luty and Raman Sundrum. Technicolor theories with negative values of the peskin- takeuchi electroweak parameter s. *Phys. Rev. Lett.*, 70:529, 1993.

[118] Joseph D. Lykken. Weak scale superstrings. *Phys. Rev.*, D54:3693–3697, 1996.

[119] I. Maksymyk, C. P. Burgess, and David London. Beyond s, t and u. *Phys. Rev.*, D50:529–535, 1994.

[120] Juan M. Maldacena. The large N limit of superconformal field theories and supergravity. *Adv. Theor. Math. Phys.*, 2:231–252, 1998.

[121] Alexander Maloney, Eva Silverstein, and Andrew Strominger. De sitter space in noncritical string theory. 2002.

[122] William J. Marciano. Fermi constants and 'new physics'. *Phys. Rev.*, D60:093006, 1999.

[123] Manuel Masip and Alex Pomarol. Effects of sm kaluza-klein excitations on electroweak observables. *Phys. Rev.*, D60:096005, 1999.

[124] Eugene A. Mirabelli, Maxim Perelstein, and Michael E. Peskin. Collider signatures of new large space dimensions. *Phys. Rev. Lett.*, 82:2236–2239, 1999.

[125] Eugene A. Mirabelli and Martin Schmaltz. Yukawa hierarchies from split fermions in extra dimensions. *Phys. Rev.*, D61:113011, 2000.

[126] R. N. Mohapatra. Unification and supersymmetry. the frontiers of quark - lepton physics. Berlin, Germany: Springer (1986) 309 P. (Contemporary Physics).

[127] Robert C. Myers. New dimensions for old strings. *Phys. Lett.*, B199:371, 1987.

[128] Yasunori Nomura. Higgsless theory of electroweak symmetry breaking from warped space. *JHEP*, 11:050, 2003.

[129] Thorsten Ohl and Christian Schwinn. Unitarity, BRST symmetry and Ward identities in orbifold gauge theories. *Phys. Rev.*, D70:045019, 2004.

[130] Michele Papucci. Nda and perturbativity in higgsless models. 2004.

[131] G. Passarino and M. J. G. Veltman. One loop corrections for e+ e- annihilation into mu+ mu- in the weinberg model. *Nucl. Phys.*, B160:151, 1979.

[132] Michael E. Peskin and Tatsu Takeuchi. A new constraint on a strongly interacting Higgs sector. *Phys. Rev. Lett.*, 65:964–967, 1990.

[133] Frank J. Petriello. Kaluza-klein effects on Higgs physics in universal extra dimensions. *JHEP*, 05:003, 2002.

[134] Alex Pomarol. Gauge bosons in a five-dimensional theory with localized gravity. *Phys. Lett.*, B486:153–157, 2000.

[135] Lisa Randall and Raman Sundrum. An alternative to compactification. *Phys. Rev. Lett.*, 83:4690–4693, 1999.

[136] Lisa Randall and Raman Sundrum. A large mass hierarchy from a small extra dimension. *Phys. Rev. Lett.*, 83:3370–3373, 1999.

[137] Gerhard Raven. sin(2beta): Status and prospects. 2003.

[138] Thomas G. Rizzo. Decays of heavy Higgs bosons. *Phys. Rev.*, D22:722, 1980.

[139] Thomas G. Rizzo. A(lr), negative s, and extended gauge models. *Phys. Rev.*, D50:2256–2264, 1994.

[140] Thomas G. Rizzo. An exploration of below threshold z' mass and coupling determinations at the nlc. *Phys. Rev.*, D55:5483–5493, 1997.

[141] Thomas G. Rizzo. More and more indirect signals for extra dimensions at more and more colliders. *Phys. Rev.*, D59:115010, 1999.

[142] Thomas G. Rizzo. Cartography with accelerators: Locating fermions in extra dimensions at future lepton colliders. *Phys. Rev.*, D64:015003, 2001.

[143] Thomas G. Rizzo. Kaluza-klein / z' differentiation at the lhc and linear collider. *JHEP*, 06:021, 2003.

[144] Thomas G. Rizzo and James D. Wells. Electroweak precision measurements and collider probes of the standard model with large extra dimensions. *Phys. Rev.*, D61:016007, 2000.

[145] Christian Schwinn. Higgsless fermion masses and unitarity. *Phys. Rev.*, D69:116005, 2004.

[146] R. Sekhar Chivukula, Duane A. Dicus, and Hong-Jian He. Unitarity of compactified five dimensional yang-mills theory. *Phys. Lett.*, B525:175–182, 2002.

[147] R. Sekhar Chivukula, Elizabeth H. Simmons, Hong-Jian He, Masafumi Kurachi, and Masaharu Tanabashi. Electroweak corrections and unitarity in linear moose models. 2004.

[148] Geraldine Servant and Tim M. P. Tait. Elastic scattering and direct detection of kaluza-klein dark matter. *New J. Phys.*, 4:99, 2002.

[149] Geraldine Servant and Tim M. P. Tait. Is the lightest kaluza-klein particle a viable dark matter candidate? *Nucl. Phys.*, B650:391–419, 2003.

[150] Torbjorn Sjostrand et al. High-energy-physics event generation with pythia 6.1. *Comput. Phys. Commun.*, 135:238–259, 2001.

[151] A. Soddu and N-K. Tran. Democratic mass matrices from five dimensions. 2003.

[152] Junichi Tanaka, Taiki Yamamura, Shoji Asai, and Junichi Kanzaki. Study of black holes with the atlas detector at the lhc. 2004.

[153] Brian Whitt. Spherically symmetric solutions of general second order gravity. *Phys. Rev.*, D38:3000, 1988.

[154] M. Wirbel, B. Stech, and Manfred Bauer. Exclusive semileptonic decays of heavy mesons. *Z. Phys.*, C29:637, 1985.

[155] Edward Witten. Strong coupling expansion of calabi-yau compactification. *Nucl. Phys.*, B471:135–158, 1996.

[156] Hirotaka Yoshino and Vyacheslav S. Rychkov. Improved analysis of black hole formation in high-energy particle collisions. 2005.

[157] Bruno Zumino. Gravity theories in more than four-dimensions. *Phys. Rept.*, 137:109, 1986.

[158] Barton Zwiebach. Curvature squared terms and string theories. *Phys. Lett.*, B156:315, 1985.